

Epigenetic mechanisms involved in the long-term proinflammatory effects of hyperuricemia



Oana-Medeea Badii

**RADBOD
UNIVERSITY
PRESS**

Radboud
Dissertation
Series

Epigenetic mechanisms involved in the long-term proinflammatory effects of hyperuricemia

Oana-Medeea Badii

The work presented in this thesis received financial support from a Competitiveness Operational Programme grant of the Romanian Ministry of European Funds (P 37 762, MySMIS 103587) and a grant of the Romanian Ministry of European Investments and Projects, PNRR-III-C9-2022-I8, CF 85/15.11.2022.

The work presented in this thesis is performed at the Department of Medical Genetics, University Iuliu Hațieganu, Cluj-Napoca, Romania and the Radboud Institute for Molecular Life Sciences and the Department of Internal Medicine, Radboud University Center, Nijmegen, the Netherlands.

Epigenetic mechanisms involved in the long-term proinflammatory effects of hyperuricemia

Oana-Medeea Badii

Radboud Dissertation Series

ISSN: 2950-2772 (Online); 2950-2780 (Print)

Published by RADBOUD UNIVERSITY PRESS
Postbus 9100, 6500 HA Nijmegen, The Netherlands
www.radbouduniversitypress.nl

Design: Proefschrift AIO | Annelies Lips
Cover: Proefschrift AIO | Guntra Laivacuma
Printing: DPN Rikken/Pumbo

ISBN: 9789465150543

DOI: 10.54195/9789465150543

Free download at: <https://doi.org/10.54195/9789465150543>

© 2025 Oana-Medeea Badii

**RADBOUD
UNIVERSITY
PRESS**



Radboudumc
university medical center

This is an Open Access book published under the terms of Creative Commons Attribution-Noncommercial-NoDerivatives International license (CC BY-NC-ND 4.0). This license allows reusers to copy and distribute the material in any medium or format in unadapted form only, for noncommercial purposes only, and only so long as attribution is given to the creator, see <http://creativecommons.org/licenses/by-nc-nd/4.0/>.

Epigenetic mechanisms involved in the long-term proinflammatory effects of hyperuricemia

Proefschrift ter verkrijging van de graad van doctor
aan de Radboud Universiteit Nijmegen
op gezag van de rector magnificus prof. dr. J.M. Sanders,
volgens besluit van het college voor promoties

en

ter verkrijging van de graad van doctor
aan de Universitatea de Medicină și Farmacie „Iuliu Hațieganu”
din Cluj-Napoca
op gezag van de rector prof. dr. Anca Dana Buzoianu
in het openbaar te verdedigen op
dinsdag 25 maart 2025
om 16.30 uur precies

door

Oana-Medeea Badii
geboren op 2 juli 1990
te Botoșani, Roemenië

Promotoren:

Prof. dr. L.A.B. Joosten (Universitatea de Medicină și Farmacie „Iuliu Hațieganu” din Cluj-Napoca, România)

Prof. dr. M.G. Netea

Copromotor:

Dr. T.O. Crișan

Manuscriptcommissie:

Prof. M.M.K. Mhlanga

Dr. M.I. Koenders

Prof. dr. N. Busso (Centre hospitalier universitaire vaudois, Zwitserland)

Epigenetic mechanisms involved in the long-term proinflammatory effects of hyperuricemia

Dissertation to obtain the degree of doctor
from Radboud University Nijmegen
on the authority of the Rector Magnificus prof. dr. J.M. Sanders,
according to the decision of the Doctorate Board

and

to obtain the degree of doctor
from Universitatea de Medicină și Farmacie „Iuliu Hațieganu” din Cluj-Napoca
on the authority of the Rector prof. dr. Anca Dana Buzoianu
to be defended in public on
Tuesday, March 25, 2025
at 4:30 PM

by

Oana-Medeea Badii

born on July 2, 1990

in Botoșani, Romania

PhD supervisors:

Prof. dr. L.A.B. Joosten (Universitatea de Medicină și Farmacie „Iuliu
Hațieganu” din Cluj-Napoca, Romania)

Prof. dr. M.G. Netea

PhD co-supervisor:

Dr. T.O. Crișan

Manuscript Committee:

Prof. M.M.K. Mhlanga

Dr. M.I. Koenders

Prof. dr. N. Busso (Centre hospitalier universitaire vaudois, Switzerland)

*To my mother
Dedic cartea mamei mele,
pe care o port mereu în gând.*

Table of contents

Chapter 1	General introduction and outline of the thesis	11
Chapter 2	Urate-induced epigenetic modifications in myeloid cells <i>Arthritis Res Ther. 2021 Jul 28;23(1):202.</i>	41
Chapter 3	Regulation of SOCS3-STAT3 in urate-induced inflammation in human myeloid cells <i>Joint Bone Spine. 2024;91(3):105698.</i>	101
Chapter 4	Downregulation of type I interferon signalling pathway by urate in primary human PBMCs <i>Immunology, 2024 Oct 1, doi: 10.1111/imm.13858. Epub ahead of print</i>	127
Chapter 5	Sex-specific differences in cytokine levels in patients with gout compared to controls <i>Gout, Urate, and Crystal Deposition Disease. 2024; 2(2):133-143.</i>	179
Chapter 6	Trained immunity and inflammation in rheumatic diseases. <i>Joint Bone Spine. 2022 Feb 24;89(4):105364.</i>	201
Chapter 7	Summary, general discussion, and perspectives	221
Appendices	Summary in English	240
	Nederlandse samenvatting	243
	List of publications	247
	Curriculum vitae	249
	Portfolio	250
	Research data management	251
	Acknowledgements	253



CHAPTER 1

General introduction and
outline of the thesis

1. Understanding the causes of gout

Uric acid is the final product derived from the purine catabolism in the liver of hominoids, such as humans and great apes. Urate is the ionized form of uric acid and exists in the bloodstream at physiological pH [1]. Elevated levels of serum urate are clinically defined as hyperuricemia. The prevalence of hyperuricemia can reach up to 21% in developed areas [2] and, although in most cases it remains asymptomatic, a prolonged state may lead to the formation of monosodium urate crystals (MSU), the precipitated form of uric acid [3]. When serum urate concentration exceeds the solubility threshold, it can trigger the formation of needle-shaped MSU crystals that accumulate in the joints and surrounding tissues, causing painful acute conditions known as gouty arthritis and tophaceous gout [4] [5]. MSU crystal build-up in the joints will activate resident macrophages, which are derived from the circulating monocytes, and recruit neutrophils, resulting in the production of pro-inflammatory cytokines, which will further promote inflammation in the affected area [6]. Furthermore, MSU crystal uptake by synoviocytes within the joints via phagocytosis can further exacerbate inflammatory responses, leading to synovial activation through the release of proinflammatory cytokines [7].

Gout is one of the oldest rheumatic conditions to be described, affecting approximately 1% of the world's population. It can reach up to 2.5-3.9% prevalence in developed countries [8] and increases with time in various populations [9]. Gout is accompanied by sudden, intense pain, along with joint swelling, redness, and inflammation, symptoms that describe the acute flare (**Figure 1**) [6]. The inflammatory processes in gout are initiated by the activation of the NLRP3 inflammasome-dependent secretion of interleukin-1 beta (IL-1 β) by macrophages responsible for clearing the MSU crystals. Conversely, interleukin-1 receptor antagonist (IL-1Ra) functions by binding to IL-1 receptor type 1 and blocking IL-1 β signalling by competitive inhibition [10]. The production of immune mediators will contribute to neutrophil recruitment, which will further help in the clearance of the MSU crystals and dampening of inflammatory processes [11]. During acute episodes of gouty arthritis, the flare can often resolve spontaneously due to the production of anti-inflammatory cytokines and the release of neutrophil extracellular traps (NETs) in the joints. Acute gout can progress to a chronic state, and if hyperuricemia is not effectively controlled, it can result in the formation of tophi, which are large nodule-like deposits of MSU crystals that can severely deform and debilitate the joints [12] [6]. The discovery that uric acid is the main constituent of the

tophi and that it is linked to the development of gout dates back more than a century to Sir Alfred Baring Garrod [13].

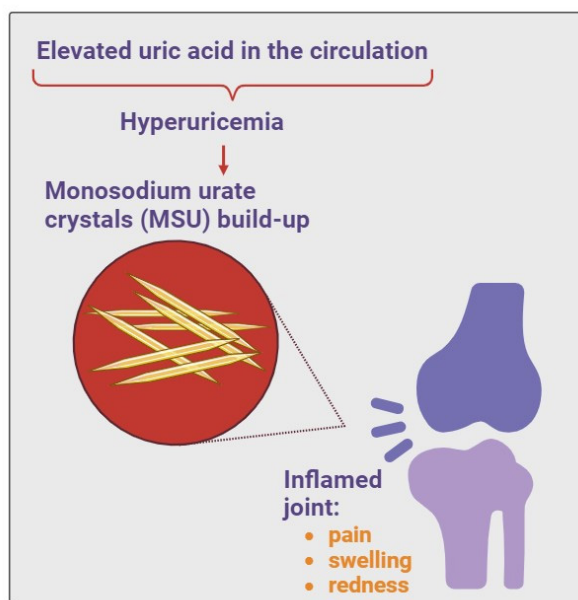


Figure 1. Gouty flare - urate crystals accumulate in a joint and trigger an inflammatory response characterized by severe joint pain, redness, and swelling in the affected area.

Given that the prevalence of gout is more frequent in men, it has traditionally been viewed as a disease that primarily affects men [8]. The prevalence of gout in both men and women becomes more uniformly distributed after the age of 60 [14]. This may be partially attributed to the effect of the hormone estradiol on the kidneys in pre-menopausal women, which is known to enhance the renal excretion of urate [15]. A study of urate levels in transsexual individuals undergoing cross-sex hormone treatment supports this premise [15]. However, it's noteworthy to highlight that the clinical profiles of patients with gout have been observed to differ according to sex [16].

Gout is often accompanied by additional medical conditions like metabolic syndrome, and cardiovascular and kidney disease [17]. Despite significant progress in our understanding of gout, urate-lowering therapy (ULT) and medication that relieves pain and reduces inflammation are still the mainstays of current management in order to prevent future flare-ups [18]. Other interventions such as lifestyle changes and dietary adjustments are

frequently combined with therapy since their stand-alone effectiveness is still debatable [6].

2. Hyperuricemia to gout

2.1 Sources of hyperuricemia

Uric acid, an organic heterocyclic compound, is the final product resulting from purine turnover, primarily in the liver. Uric acid is subsequently transported into the bloodstream where it exists in its ionized form as urate. Purines such as adenosine monophosphate (AMP) and guanosine monophosphate (GMP) are converted through a series of metabolic reactions into xanthine, which is further metabolized into uric acid by xanthine oxidase (**Figure 2**) [1]. Other tissues such as the intestines, muscles, kidneys, and vascular endothelium, which have xanthine oxidase activity, can also generate uric acid, but to a lesser extent [1]. Through the bloodstream, urate arrives at the kidneys, where is filtered out of the blood, and approximately two-thirds pass into the kidney tubules. Here, a portion is then secreted into the urine, while up to 90% is reabsorbed back into the bloodstream. The intestine also accounts for a small fraction of urate excretion [19].

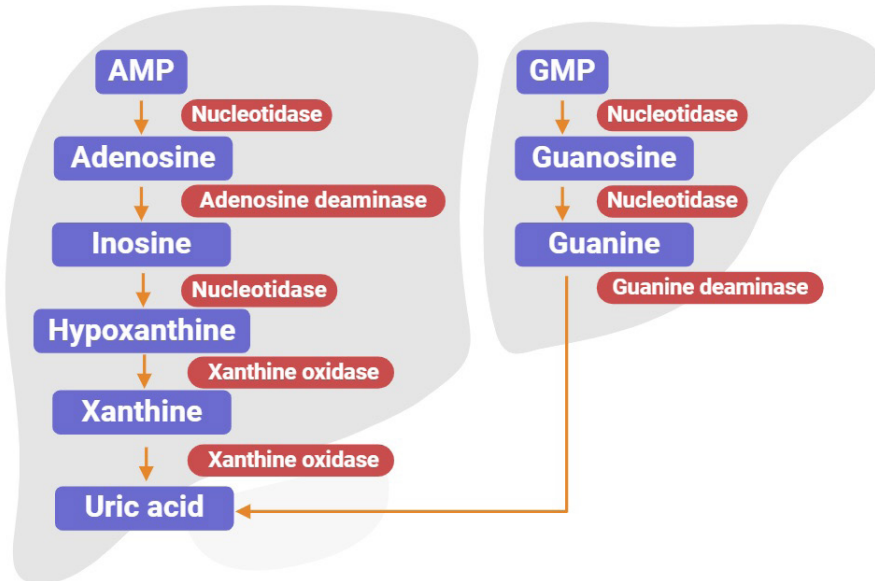


Figure 2. Uric acid metabolism in the human liver (adaptation from [1])

The enzyme urate oxidase (uricase) catalyzes the conversion of uric acid into allantoin, a water-soluble compound easier to excrete [20]. Humans and higher apes (e.g., gorillas and chimpanzees) lack uricase due to a sequence of mutations that occurred millions of years ago, sometime in the Miocene. Consequently, humans and higher primates have increased serum urate levels compared to other mammals due to the absence of uricase, a trait believed to have provided though some evolutionary advantages to humans [21]. One such proposed advantage was its antioxidant role as a scavenger of free radicals to mitigate oxidative stress. The complex antioxidant role of urate was explored by the renowned biochemist Bruce Ames in the 80s' [22] and later accepted as a fact, although his further studies indicate that urate has rather poor antioxidant properties in comparison with thiols and ascorbic acid [23]. For instance, superoxide cannot be scavenged by urate alone and requires the presence of ascorbic acid [23]. The urate-antioxidant theory has also later been challenged by evidence that elevated concentrations of urate are linked to oxidative stress-based conditions such as hypertension, cardiovascular disease, and diabetes [24] [25]. In addition, more recent research has shown that urate can exert pro-inflammatory effects within the intracellular space [26]. Another theory proposed that urate may have been involved in regulating blood pressure during a period when the diet of hominoids was low in salt since urate has the potential to stabilize blood pressure under low sodium intake [27]. The theory about the relationship between fructose and urate is well-supported by experimental data [28] and proposed that increased blood urate levels promote increased fat storage and this would have benefited the early apes during periods of food scarcity when their diet was primarily based on fruits [29]. In modern times, the loss of uricase has shifted from a mechanism to prevent starvation to a contributing factor in disease by promoting the accumulation of serum urate levels, leading to hyperuricemia.

Elevated concentrations of serum urate define hyperuricemia, a condition described by either an excess due to overproduction or a decreased excretion of urate. Moreover, excessive consumption of dietary purine or alcohol can exacerbate hyperuricemia. Medical conditions characterized by a high cell replacement rate or cell death, such as tumor lysis syndrome, can also contribute to hyperuricemia [18]. Genetic variation in genes that encode for urate production, metabolism, and renal excretion can significantly impact the development of hyperuricemia [30]. Polymorphisms in the *SLC2A9* or *ABCG2* genes, involved in urate transport and excretion, have been associated with hyperuricemia, among other risk factors, in genome-wide association studies (GWAS) [31].

Nevertheless, the involvement of urate in inflammatory responses extends beyond gout. In addition to being connected to the development of gout, high concentrations of serum urate are also associated with chronic low-grade inflammation and increased risk of several other inflammatory and metabolic diseases [25]. Uric acid is known to contribute to endothelial dysfunction via the production of reactive oxygen species (ROS) and increased inflammation [32], and this has subsequently been associated with the development of vascular diseases, such as hypertension and coronary artery disease [33]. In addition, endothelial dysfunction in the form of digital ulcers is linked to elevated levels of serum urate in patients with systemic sclerosis [34]. Individuals with hyperuricemia also face an increased risk of developing type 2 diabetes or chronic kidney disease and evidence suggests that elevated serum urate concentrations manifest before the onset of these diseases [35] [36] (**Figure 3**). A pro-inflammatory state associated with hyperuricemia might also pose an increased risk of infections. Several studies underline an association between high serum urate concentrations [37] or gout [38] and worsened outcomes in patients with Sars-CoV- 2 infection.

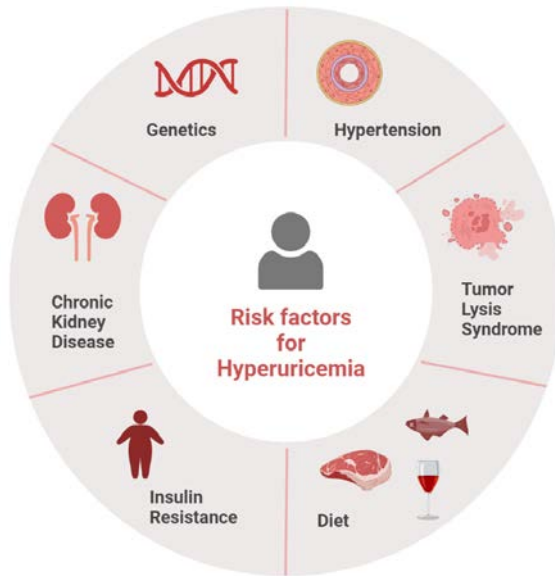


Figure 3. Risk factors for hyperuricemia include genetics -genetic factors can increase susceptibility to high urate levels; hypertension -is associated with increased risk of hyperuricemia; tumor lysis syndrome -can result in excessive uric acid production due to massive cell damage; diet -contributes to hyperuricemia; insulin resistance- can elevate uric acid levels, and chronic kidney disease -impaired kidney function can decrease uric acid excretion.

2.2 Soluble uric acid has immune modulatory roles

The innate immune system monitors the extracellular space for the presence of molecules that could endanger the host. These molecules, whether foreign or endogenous, possess the ability to signal injury within the host organism [39]. Damage-associated molecular patterns (DAMPs) have an endogenous origin, as a result of processes such as cellular breakdown and stress. DAMPs can bind to pattern-recognition receptors (PRRs) on the surface of immune cells to initiate a cascade of fast and strong inflammatory responses. On the other hand, Pathogen-Associated Molecular Patterns (PAMPs) are foreign molecules that include ligands such as lipopolysaccharides (LPS), viral RNA or DNA, and components of fungi cell walls like beta-glucan that can be recognized by Pattern Recognition Receptors (PRRs) [40]. On myeloid cells, expressed PRRs include the transmembrane Toll-like receptors (TLRs) and C-type lectin receptors, as well as intracellular receptors, such as nucleic acid sensors, Nod-like receptors, and inflammasomes [41]. Furthermore, an increasing number of recent studies have documented that altered levels of end products of metabolism can function as DAMPs - e.g., nucleic acids, oxidized low-density lipoproteins (ox-LDL), high mobility group box 1 (HMGB1) [42]. Urate, in both its soluble and crystalline form, has been proposed to function as a DAMP, therefore contributing to immune activation [25] [43].

2.2.1 Pro-inflammatory pathways

Soluble urate has the potential to induce sterile inflammation and stimulate the production of pro-inflammatory mediators such as IL-1 β and TNF [44]. The pro-inflammatory effects of urate on human macrophages may partially be mediated through URAT1, a protein involved in the transport of urate within the body [45]. Once intracellular, urate is sensed by the Naip1-Nlrp3 inflammasome platform in murine macrophages [46]. The mechanism through which urate may activate the NLRP3 inflammasome to further propagate inflammatory responses is by promoting mitochondrial reactive oxygen species (ROS) [46]. Although ROS plays an important role in cell signalling and regulation of immune responses, overproduction can have detrimental effects and result in activation of the NLRP3/NALP3 inflammasome and subsequent maturation of IL-1 β and IL-18 in the macrophages [47]. Recent evidence indicates that, in addition to MSU crystals, soluble urate stimulates the MyD88 pathway and activates the NLRP3 inflammasome through a mechanism that triggers the generation of reactive oxygen species (ROS) within the mitochondria [48]. The production of ROS by urate treatment in PBMCs may activate endoplasmic reticulum (ER) stress as well, but the mechanisms are not fully understood

and require further investigation [49]. *In vitro*, urate promotes inflammatory processes in human peripheral blood mononuclear cells (PBMCs). Pre-treatment of human monocytes of gout patients with urate results in elevated IL-1 β on a subsequent restimulation with a TLR agonist like lipopolysaccharide (LPS) [50]. A proposed mechanism may involve the inhibition of autophagy and the activation of NF- κ B and the mammalian target of rapamycin (mTOR), leading to increased IL-1 β cytokine production [26]. Protein phosphatase-2A (PP2A) is an enzyme that contributes to the regulation of various cellular processes, including the activation of immune cells. In gout, PP2A regulates the activation of monocytes by urate through the inhibition of the nuclear factor kappa B (NF- κ B) pathway [51]. These could constitute potential mechanisms that contribute to chronic inflammation in patients with gout. Although the inflammatory potential of soluble urate is increasingly recognized, its potential pathogenic involvement in various diseases still requires further investigation.

2.2.1.1 Urate-induced responses in immune cell types/tissues

The main cells involved in the inflammatory responses in gout are macrophages and neutrophils, which react to the monosodium urate (MSU) crystals to trigger an acute inflammatory reaction [52]. In addition, other immune cells such as T cells, mast cells, and synovial fibroblast may also amplify the immune response and contribute to the progression of gout [53].

Moreover, soluble urate can also trigger inflammatory activation in monocytes and various immune and non-immune cells, prompting the release of pro-inflammatory cytokines and further driving the inflammatory process. Human monocytes that have been exposed *in vitro* to urate show an increased production of IL-1 β cytokine and a decrease in IL-1Ra upon subsequent stimulation with MSU and TLR ligands [50]. Interestingly, in familial Mediterranean fever (FMF), a hereditary disorder marked by recurring bouts of inflammation, interleukin-1 receptor antagonist (IL1Ra) production is decreased due to activation of the PYRIN inflammasome in monocytes [54].

Neutrophils play an important role in the immune system's response to infection and inflammation as they are attracted to the site of an infection or injury where they can engulf invading microorganisms or host-derived endogenous molecules. Soluble urate has been shown to inhibit *in vitro* neutrophil migration, potentially hindering the immune system's ability to effectively respond to infection or injury. This inhibition is, at least in part, regulated by the activity of β 2 integrin, a protein found on the surface of

neutrophils that helps them adhere to other cells and tissues [55]. High serum urate concentrations pose a risk factor for atherosclerosis as well, a disease characterized by the build-up of plaques in the arteries and primarily regulated by macrophage and T cell activity. While the mechanism is complex and not fully understood, this might occur via the activation of AMPK (AMP-activated protein kinase), a protein that plays a role in regulating inflammation and glucose metabolism. Activation of AMPK by urate is thought to lead to inflammation and oxidative stress in the endothelial cells that line the blood vessels, which can contribute to the development of atherosclerosis [56]. While urate as a result of necrosis is considered a DAMP, it has also been found to stimulate the maturation of dendritic cells (DC) to enhance T-cell responses. Interestingly, when uric acid is administered at specific doses, has the potential to function as an immunoadjuvant, increasing the effectiveness of anti-tumor vaccines that rely on DC, and delaying tumor growth in mice [57]. Moreover, soluble urate can stimulate both CD4+ and CD8+ T cells even in the absence of antigen presentation, as shown by the overexpression of markers such as CD25 and CD70, later with a role in antibody production [58]. In addition, patients with hyperuricemia can present higher numbers of CD4+ T cells and increased IL-4 and IL-10 levels in circulation [59].

2.2.1.2 Urate-induced responses in non-immune cell types/tissues

In non-immune cells, urate can stimulate oxidative stress and activate the vascular renin-angiotensin system, which can contribute to endothelial dysfunction by promoting vascular smooth muscle cell proliferation and oxidative stress [32]. In addition, urate can stimulate the production of monocyte chemoattractant protein-1 (MCP-1) in vascular smooth muscle cells (VSMCs), a chemokine involved in regulating the migration and infiltration of monocytes and macrophages from the bloodstream to vascular endothelium. The process is mediated *in vitro* via p38 MAPK and the activation of NF- κ B and AP-1 (activator protein-1) [60].

2.2.2 Immune protective and antioxidant roles of urate

In the extracellular environment, urate can act as a scavenger of singlet oxygen and radicals such as peroxynitrite and hydroxyl radicals, whereas its intracellular role, particularly when present at elevated concentrations, points to pro-inflammatory effects [61]. Low concentrations of serum urate are associated with neurologic damage, such as increased prevalence of multiple sclerosis, suggesting a possible protective role of urate against neurodegeneration [62]. However, the causal relationship between low

urate concentrations (hypouricemia) and the onset of neurodegenerative disorders like Parkinson's disease has been questioned since clinical trials have not demonstrated positive effects from increasing urate levels [23]. The protective role of urate is under debate, also when considering that patients with xanthinuria, a genetic disorder resulting in the absence of xanthine oxidase that leads to the accumulation of urate precursors in the urine and the later formation of xanthine kidney stones, are rarely diagnosed with other complications [25].

Nonetheless, urate levels within the normal physiological ranges have been proposed to exert certain protective roles on the chondrocytes by inhibiting the production of pro-inflammatory cytokines like IL-1 and TNF in other conditions affecting the joints and cartilage, such as osteoarthritis (OA) and rheumatoid arthritis (RA) [63].

2.3 MSU crystals

Urate plays a pivotal role in the onset of gout and its associated inflammation. Persistent hyperuricemia can lead to the formation of monosodium urate (MSU) crystals in the joints and surrounding tissues. Other factors, such as temperature, pH, or sodium ions can influence urate solubility and favor its precipitation into crystals [64].

2.3.1 Inflammatory role

Several mechanisms contribute to the inflammatory response in gout and a well-characterized one involves the activation of the inflammasome, a multiprotein complex responsible for the processing and release of pro-inflammatory cytokine. Urate crystals uptake by tissue-resident macrophages stimulates the production of IL-1 β by activating the NLRP3 inflammasome complex [10]. In addition, they also stimulate the expression of several chemokines with a role in the recruitment of classical innate inflammatory cells, such as MIP-1 α , MIP-1 β , and MCP-1, through the activation of ERK1/2, which involves AP-1 nuclear translocation [65]. In monocytes, MSU crystals activate the complement system, resulting in the production of C5a, a potent mediator of chemotaxis. This, in turn, triggers the production of pro-inflammatory cytokine and the subsequent recruitment of immune cells like macrophages and neutrophils to the site of inflammation [66].

2.3.2 Regulation of IL-1

Interleukin 1 (IL-1) is mainly produced by monocytes and macrophages, but other cell types are capable of IL-1 secretion as well [67]. The IL-1 cytokine family encompasses 11 members, particularly IL-1 α and IL-1 β , both with pro-inflammatory properties, which play a central role in immune cell activation, inducing a cascade of inflammatory responses by binding to IL-1 receptors on target cells. IL-1 β induction by MSU crystals holds a pivotal role in the development of acute gout pathology, although other members have recently been identified as contributors to the pathogenesis [68]. The subsequent induction of IL-1 β pathway involves the activation of Toll-like receptors (TLR) / IL-1 receptor 1, continuing with the recruitment of adapter myeloid differentiation factor 88 (MyD88), the IL-1 receptor-associated kinases (IRAKs) and activation of transcription factor NF- κ B [69]. This will result in the synthesis of pro-IL-1 β , an inactive precursor that requires cleavage by caspase-1 to become biologically active IL-1 β . Once it is released in the extracellular space it can bind to IL-1 receptors IL-1R1 and IL-1R2. The anti-inflammatory IL-1Ra (Interleukin-1 Receptor Antagonist) is the natural inhibitor of IL-1 α and IL-1 β and also binds to IL-1R and blocks further signalling. IL-1R2 works as a decoy receptor to regulate IL-1 activity. IL-1 inhibitors, like anakinra, have demonstrated significant efficacy in decreasing the intensity of gout flares [68].

2.3.3 Inflammasome activation

Unlike IL-1 α , pro-IL-1 β is inactive, and cleavage by caspase-1 is mandatory to have the mature active form of IL-1 β [70]. Caspase-1 activity is in turn tightly controlled by the assembly of the NLRP3 inflammasome, a multiprotein complex that recognizes danger signals and engages in inflammatory responses [10]. Urate, in the form of MSU crystals, stimulates the inflammasome [71] [72] and facilitates the release of biologically active IL-1 β [10]. However, transcription of pro-IL-1 β , the precursor, needs to be induced by other stimuli, such as PRR ligands via activation of transcription factor NF- κ B [73] [74]. The release of IL-1 β attracts neutrophils and other immune cells to the site of action and elicits an inflammatory response in the injured tissue [75]. This creates a two-step paradigm for the activation of IL-1 β in which urate crystals are proven to exert inflammasome activation properties, but this effect needs synergistic stimuli in order to mount inflammation (**Figure 4**) [76]. In patients with gout, this synergistic effect is more pronounced and might be linked to increased maturation from pro-IL-1 β into its active counterpart, IL-1 β . Furthermore, MSU

crystal stimulation alone is insufficient to induce the production of other several cytokines such as IL-6 and TNF- α without additional TLR activation [76].

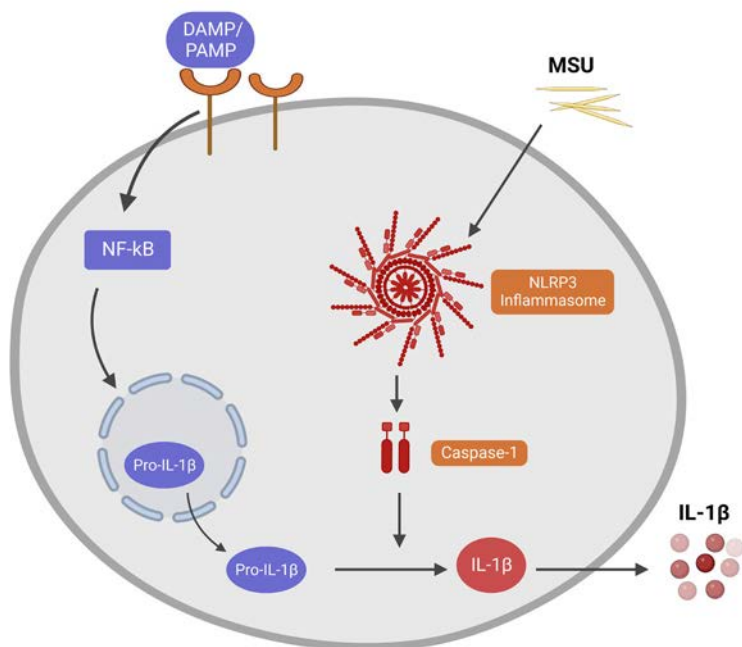


Figure 4. Proposed mechanism by which DAMPs/PAMPs trigger inflammation, activating transcription of pro-IL-1 β - in active form - via TLR ligands and NF- κ B pathway (first step). The biologically active form of IL-1 β results in the presence of caspase-1 which in turn requires activation by NLRP3 inflammasome (second step).

2.3.4 Inflammasome-independent effects

Autophagy is a cellular clearance process and can modulate cytokine production in human myeloid cells. The disruption of autophagic processes in human PBMCs results in enhanced IL-1 β production on a subsequent stimulation with TLR2/4 ligands through mechanisms that likely involve transcriptional regulation, as suggested by the unaltered inflammasome activity [77]. In accordance with this concept, urate-induced IL-1 synthesis can also take place through mechanisms that do not rely on the inflammasome activation pathway. In human lymphocytes, urate crystals can trigger an IL-1 β response by activating the purinergic receptor P2X7. This supports the idea that MSU crystals may play a role in specific adaptive immunity responses as well [78] and this aligns with studies in cancer therapy, that proposed certain

concentrations of uric acid as an adjuvant for DC-based vaccine against tumors [57]. Interestingly, the accumulation of monosodium urate (MSU) crystals in DNA-damaged tumor cells stimulates the production of a protein called NKG2D, which is a lectin-like type 2 transmembrane receptor, that can activate the immune system to further attack and kill the tumor cells. The activation of a protein called TGF-beta-activated kinase 1 (TAK1) seems to mediate this process [79]. In neutrophils, MSU crystals will induce the formation of neutrophil extracellular traps (NETs), with a role in resolving inflammation [80].

3. Innate immune memory; Implications for soluble urate and MSU crystals

Immunological memory is the main characteristic of the adaptive immune system that works by „remembering“ (T and B lymphocytes possess immune memory capacities) that it has previously encountered an antigen and can react more rapidly on subsequent exposure to the same stimulus. However, recent evidence shows that the innate immune system, considered less specific and short-term, can also build an immunological memory that relies on cellular processes like epigenetic reprogramming or metabolic changes that take place after stimulation with microbial ligands (PAMPs) or danger-associated molecule patterns (DAMPs) – a mechanism referred to as „trained immunity“ [81] (**Figure 5**).

At the beginning of the last decade, the group of Mihai G. Netea was strongly interested in innate immune mechanisms, especially from the point of view of pathogen recognition by pattern recognition receptors (PRR). Their main interest was to unveil how the innate immune system recognizes important human pathogens such as *Mycobacterium tuberculosis* and *Candida albicans*. Recent research shows that not only classical adaptive immunity but also the innate immunity arm of the host defense can adapt after an insult represented by an infection or vaccination and remain in such a state of enhanced function for a significant amount of time („trained immunity“) [82] [81]. The hallmark of trained immunity is the lack of specificity in the immune response and it is considered to be an old biological process that evolved for the protection of multicellular organisms lacking adaptive immune responses [83]. For instance, BCG vaccination triggers robust immune responses that are not limited to targeting only pathogens such as mycobacteria. The research suggests that

these non-specific effects of BCG don't arise from specific lymphocyte-mediated mechanisms, but rather from non-specific adaptation within the innate cells [84]. In line with this, the research on vaccines has yielded several epidemiological studies suggesting non-specific effects of vaccines beyond their target disease [85]. Vaccination with BCG results in enhanced innate immune responses through the production of pro-inflammatory cytokines such as IL-6, TNF- α , and IL-1 β , on a later *ex vivo* non-specific stimulation of monocytes. These changes were observed to be dependent on epigenetic modifications like histone methylation (H3K4me3) [86]. This persistent state of immunological memory can be induced by microbial stimuli such as *Candida albicans* or β -glucan (cell wall component of *C. albicans*) [87, 88], as well as sterile stimuli such as oxidized cholesterol or phospholipids [89, 90].

Although trained immunity suggests a protective role against infectious diseases, a dysregulated trained immunity might contribute to the pathogenesis of several autoimmune and inflammatory conditions [91]. When PBMCs from patients with gout and healthy controls were exposed 24h to soluble urate and restimulated with TLR2/4 agonists, it resulted in a shift in the pattern of cytokine production: IL-1 β was enhanced, while the production of its antagonist, IL-1Ra was reduced. The authors underline that soluble urate might be involved in a distinct inflammatory pathway as treatment with the crystal form of urate increased the IL-1Ra levels. The effect of soluble urate-priming was rescued using broad-spectrum histone methyltransferase inhibitors, indicating a possible link between epigenetic changes and inflammatory dysregulation [50]. In atherosclerosis, a chronic inflammatory disease of the arteries, trained immunity via metabolic changes may contribute to the persistent activation of immune cells within the arterial wall and promote the progression of plaque formation [92][93]. Similarly, in autoinflammatory diseases such as gout, trained immunity may play a role in the exaggerated inflammatory response to the crystals or high levels of serum urate through epigenetic rewiring processes [94].

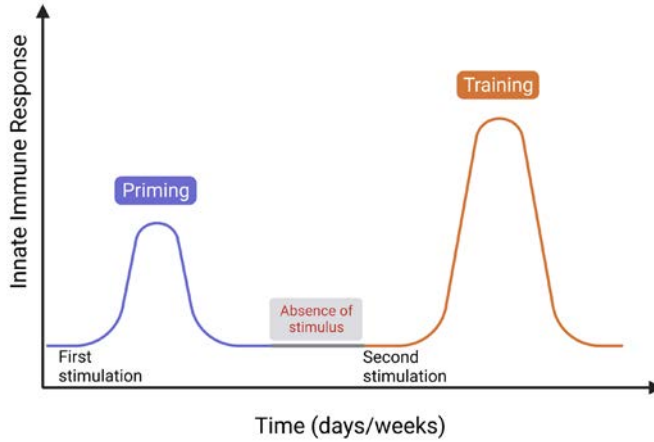


Figure 5. Schematic representation of trained immunity

3.1 Transcriptional reprogramming

Epigenetic modifications are essential for an organism's proper functioning, from governing the fate of induced pluripotent stem (iPS) cells and the development of embryos to X chromosome inactivation in mammals and regulation of gene expression by turning them “on” or “off”. Epigenetic alterations that include DNA methylation, histone modifications, and non-coding RNA-dependent cellular processes, constitute central regulators of gene expression by modulating gene accessibility for transcription [95]. Transcriptomics-focused RNA studies can now provide mechanistic information by uncovering specific genes that get activated or suppressed during disease states and which contribute to the fine-tuning of inflammatory cascades. Single-cell RNA sequencing of immune cells from both the synovial fluid and peripheral blood of patients with acute gout was able to reveal differences in cell subpopulations of classic monocytes, intermediate monocytes, pDCs, and naïve CD4 T cells when compared to healthy volunteers. Furthermore, the expression of genes such as interleukin-1 (IL-1), tumor necrosis factor-alpha (TNF- α), and transforming growth factor-beta1 (TGF- β 1) in patients with acute gout was associated with distinct cell-to-cell connections [53]. Another study validates an altered T cell population profile in patients with gout and, in addition, shows an increase in NK cell population [96]. These recent studies suggest that the clinical manifestation of gouty arthritis is likely to be more intricate and suggests a role in the pathology of gout that extends beyond the macrophages.

Additionally, high throughput RNA sequencing studies showed that various trained immunity programs are activated in human monocytes in response to different stimuli (such as beta-glucan, the Bacillus Calmette-Guérin vaccine, or soluble urate), indicating that they can develop distinct responses to previous inflammatory stimuli or infections [97]. Transcriptomics analysis of vitro urate-primed human monocytes reveals upregulation of genes involved in the NFκB signalling pathway and several other pro-inflammatory pathways (*IL1B* up and *IL1RN* down). This transcriptional dysregulation is consequently reflected by an altered immune profile as shown by the increased IL-1β and decreased IL-1Ra cytokine levels in vitro [26]. Furthermore, a targeted proteomic analysis of serum samples of patients with gout, asymptomatic hyperuricemia, and normouricemic controls, reveals an inflammatory signature driven by urate in both gout and hyperuricemia, with a more pronounced effect in hyperuricemia. These in vivo findings further support the presence of persistent immune activation linked to urate exposure [26]. Furthermore, epidemiological studies have identified sex-based differences in the clinical presentation of patients with gout, emphasizing the importance of exploring whether the mechanisms of inflammation might differ between women and men with gout as well [16].

3.2 Metabolic changes

Cellular processes rely on various metabolic changes in pathways that involve energy and molecule synthesis as well as the regulation of different biological functions. Cells of the innate immune system, such as macrophages and dendritic cells, may undergo alterations in the cellular metabolism that result in the development of an innate immune memory which is distinct from classic adaptive memory based on antibody generation. These metabolic changes in macrophages are marked by a shift towards upregulation of glycolysis (increased ATP generation) and pentose phosphate pathway and downregulation of oxidative phosphorylation and fatty acid oxidation pathway, which are characteristic of a pro-inflammatory phenotype. These changes occur to meet the growing need for energy to maintain immunological activation, which is marked by rapid cell proliferation, cell migration, and cytokine production [26]. For example, the upregulation of glycolysis not only promotes NLRP3 inflammasome activation [98] but also, the activation of the inflammasome and subsequent IL-1β release can directly modulate glycolysis in macrophages [99]. Transcriptomic study of monocyte-derived macrophages that have been exposed to monosodium urate crystals and LPS in vitro reveals distinct patterns of gene expression. The differences observed in cells treated only with MSU crystals involve the upregulation of genes involved in

lipid, amino acid, and carbohydrate metabolism, as well as the production of metabolites associated with glucose metabolism. In contrast, LPS stimulation primarily upregulated interferon genes. This was consistent with a distinct metabolic profile identified in the air pouch lavage samples of mice injected with MSU crystals as well [100].

3.3 Epigenetics modifications

In the context of trained immunity, epigenetic reprogramming refers to changes at the level of epigenetic marks, such as modifications to DNA methylation, histones, and non-coding RNA expression. These modifications can impact the gene expression profile of innate immune cells in response to certain stimuli, resulting in an increased immune response to subsequent stimulation. Even after the initial trigger is removed, the epigenetic modifications are documented to persist over long periods, indicating an underlying innate memory capacity [101]. Furthermore, recent research proposed that both, crystal and soluble urate, could prompt innate immune memory in monocytes and macrophages [44]. The promising aspect of the epigenetic foundation for gout and hyperuricemia-related inflammation is that epigenetic marks can be reversed. Studying the epigenetic basis of inflammation in gout opens new possibilities for personalized and targeted treatments that may improve the well-being and overall life quality of patients.

3.3.1 DNA methylation

DNA methylation involves the addition of a methyl group ($-CH_3$) to a cytosine nucleotide. DNA methyltransferases (DNMTs) are enzymes that catalyse the transfer of a methyl group to DNA, resulting in the methylation of cytosine residues. This process participates in genome stability, being vital for embryonic development and the good functioning of cellular processes. Additionally, DNA methylation is involved in the formation of chromatin via interactions with histones to modulate gene expression by modifying the accessibility of the DNA to transcription factors and other regulatory proteins. However, when these methylation patterns are altered, they can contribute to diseases including cancer and autoimmune disorders [102].

DNA methylation patterns are altered in monocytes of patients with gout, and the presence of several differentially methylated sites associated with IL-1 β signalling indicates that urate may induce inflammatory responses that are modulated at the epigenetic level [103]. Epigenetic therapies that target methylation patterns may be useful in identifying novel therapeutic options

for managing gout and reducing inflammation. An epigenome-wide analysis study (EWAS) identifies significant DNA methylation markers associated with serum urate levels, some of which are linked to known urate-related genes. Specifically, certain markers at the SLC2A9 gene, a known serum urate locus, have causal effects on urate levels and gout [104]. Furthermore, in patients with gout, DNA methylation patterns and various enriched pathways have been identified in relation to immune responses, inflammation, and osteoclastogenesis [105]. These findings provide valuable insight into the epigenomic changes associated with DNA methylation in patients with gout and hyperuricemia.

3.3.2 Histone posttranslational modifications

Histones are proteins located in the cell nuclei and are involved in the packaging and regulation of the DNA structure. The histones also control the accessibility of the chromatin for transcription factor binding, hence modulating gene expression. In monocytes, the initiation of trained immunity involves changes in these chromatin epigenetic markers that have a significant role in modulating gene expression patterns. Generally, the induction of gene transcription relies on the presence of open chromatin (euchromatin) structures that enable transcription factors to easily access and bind to promoter regions. On the other hand, when chromatin is densely packed (heterochromatin), its compact structure prevents transcription factors from accessing the DNA template. In establishing innate immune memory, the histone modifications that accumulate following training can include modifications such as H3K4me3 at gene promoters, as well as H3K4me1 and H3K27ac at enhancer regions. Some of these modifications continue to exist even after the initial stimuli have been removed [101].

Histone deacetylase (HDAC) regulates gene expression and HDAC inhibitors show promising potential as treatments for gouty arthritis in reducing inflammation. Butyrate inhibits class I HDAC and decreases the production of several cytokines in C16+MSU crystals-stimulated PBMCs [106]. Romidepsin, another HDAC 1/2 inhibitor, was also efficient in reducing cytokine production and mRNA levels of IL-1 β in stimulated PBMCs [107]. In mice, the knockout of HDAC3 prevented gouty inflammation induced by MSU crystals through the IL-6/STAT3 signalling pathway and promoted an anti-inflammatory phenotype in macrophages. These results were confirmed using a selective inhibitor of HDAC3, RGFP966, which suppressed IL-6 and TNF- α production [108]. Joint damage is an important clinical involvement in gout, and patients with chronic

tophaceous and erosive gout are characterized by increased development of osteoclasts, cells responsible for bone resorption and metabolism [109]. The HDAC6 inhibitor CKD-WID effectively suppressed in vitro MSU-induced osteoclast formation by inhibiting the calcineurin-NFAT pathway [110]. These studies on MSU crystals-induced inflammation might rely on epigenetic changes, but further research and clinical studies are still warranted to explore the full potential of HDAC inhibitors as therapeutic interventions for gout.

3.3.3 non-coding RNA (ncRNA)

Non-coding RNAs such as microRNAs (miRNAs) or long non-coding RNAs (lncRNAs) participate in both transcriptional and post-transcriptional regulation of gene expression [111]. MiRNAs are known for their ability to bind to mRNAs and block their translation to protein and subsequently can regulate immune function and control inflammatory responses [112]. In patients with gout and hyperuricemia, several miRNAs were found upregulated in the plasma, although their expression did not vary significantly between different stages of gout [113]. Synovial fluid mononuclear cells (SFMcs) of patients with gout, cultured in vitro with MSU crystals show upregulated levels of miR-155 and consequently, downregulation of SHIP-1 (Src homology-2 domain-containing inositol 5-phosphatase 1), a direct target. This in turn promoted proinflammatory cytokine production like IL-1 β and TNF- α [114]. Other microRNAs, like miR-488 and miR-920, may directly target the production of MSU-induced IL-1 β in patients with gouty arthritis and could be explored as therapeutic targets [115]. Many long non-coding RNAs (lncRNAs) can reside in the chromatin where they regulate gene expression by controlling protein binding and activity at certain DNA regions [111]. In PBMCs of patients with gout, several lncRNAs are differentially expressed in acute and inter-critical phase with a role in both inflammation and lipid metabolism associated with gout [116]. The knockdown lncRNA HOTAIR alleviates gouty arthritis through miR-20b upregulation and NLRP3 downregulation [117].

4. Objective and general outline of the thesis

This thesis will explore how the epigenetic and transcriptional reprogramming processes shape the memory of the innate immune system's cells in response to urate. The immune cells undergo dynamic epigenetic modifications as they evolve and face immunological challenges. The crystallization of urate, known as monosodium urate crystals, in joints and tissues, initiates a

proinflammatory state as seen in gouty arthritis. In gout, the acute attack is accompanied by systemic signs of inflammation, with fever, leucocytosis, and increased high-sensitivity CRP in the blood. However, the role of soluble urate extends beyond gout, contributing to other comorbidities such as metabolic syndrome, hypertension, and renal and cardiovascular diseases. Moreover, clinical research reveals different patient profiles between women and men with gout. The following research aims to provide new perspectives on the pathogenesis of gout and hyperuricemia, expanding our understanding of these conditions.

In **Chapter 2** of this manuscript, we investigate the impact of urate exposure on the production of proinflammatory cytokines in human cells at the epigenetic level. Our findings show that these effects persist even after removing urate and allowing the cells to rest *in vitro*. Furthermore, these effects can be reversed upon pharmacological inhibition of methylation *in vivo* in mice. We hypothesized that urate priming induces innate immune memory, and we investigated whether urate treatment can trigger epigenetic reprogramming in myeloid cells. Based on studies of our group linking metabolic stimuli to changes in histone marks at candidate gene promoter regions, we tested two initial histone mark candidates through ChIP-sequencing (H3K4me3 and H3K27ac). Moreover, we assessed DNA methylation status in 76 New Zealand Māori individuals with varying levels of serum urate. Our findings suggest that both mechanisms of epigenetic regulation are associated with urate exposure, providing potential new targets for further investigation into gout and urate-induced inflammation. To further investigate the mechanisms associated with urate-induced inflammation *in vitro*, **chapter 3** employs an immunological, transcriptomic, and epigenetic approach to investigate the role of the suppressor of cytokine signalling 3 (SOCS3) in urate-induced inflammation, using both healthy donors and patients. It has previously been shown *in vitro* that urate priming facilitates IL-1 β production in peripheral blood mononuclear cells and that a mechanism for the amplification of IL-1 β consists in the down-regulation of IL-1 receptor antagonist (IL-1Ra). In the present study, we extend these findings to individuals with hyperuricemia and patients with gout. We further show that *in vitro* urate priming would result in higher levels of SOCS3 due to the suppression of phosphorylated STAT3, accompanied by a reduction in IL-1Ra cytokine production. The observed shift in elevated SOCS3 and reduced pSTAT3 could play a role in urate-induced hyperinflammation since urate priming had no effect on PBMCs from patients with constitutively activated STAT3.

In **Chapter 4** we assess the modulation of the type 1 interferon pathway by urate priming in human myeloid cells. To this end, we analyse the type I interferon-related genes in the transcriptome of human primary cells in response to soluble urate *in vitro* and in correlation to serum urate levels in patients. We find that urate priming downregulates genes in the type 1 interferon-related pathways in both human monocytes and PBMCs. However, stimulation of PBMCs with INF- β does not rescue the pro-inflammatory effects of urate. Interestingly, we observed an inverse correlation between serum urate levels *in vivo* and *in vitro* stimulations. These findings suggest that the downregulation of IFN1 is most likely not the driving mechanism behind urate priming, but nevertheless, these results support a deficient IFN1 signalling, which could potentially lead to an increased vulnerability to viral infections in patients with hyperuricemia.

In **Chapter 5** we examine the differences in cytokine patterns between sexes, both in circulation and in stimulated peripheral blood mononuclear cells (PBMCs) of patients with gout and those without. Previous research has indicated that clinical manifestations of gout can vary between men and women. PBMCs of women with gout who were challenged *ex vivo* with various stimuli show higher production of IL-1 β , IL-1Ra, and TNF. However, circulating cytokines were higher in men with gout compared to men without gout. This data suggests the possibility of different mechanisms regulating inflammation in men and women with gout.

In **Chapter 6**, we discuss the current understanding of how innate immune cells can develop a form of immunological memory called trained immunity, through long-term immune adaptations that involve metabolic and epigenetic reprogramming, which leads to increased cytokine production. We present an overall review of the involvement of trained immunity in hyperuricemia and gout, and, finally, we expand the discussion to explore the role of trained immunity in other rheumatic diseases.

5. References

- [1] Maiuolo J, Oppedisano F, Gratteri S, et al. Regulation of uric acid metabolism and excretion. *Int J Cardiol* 2016; 213: 8–14.
- [2] Li L, Zhang Y, Zeng C. Update on the epidemiology, genetics, and therapeutic options of hyperuricemia. *Am J Transl Res* 2020; 12: 3167–81.
- [3] Bardin T, Richette P. Definition of hyperuricemia and gouty conditions. *Curr Opin Rheumatol* 2014; 26: 186–91.
- [4] Mandel NS, Mandel GS. Monosodium Urate Monohydrate, the Gout Culprit. *J Am Chem Soc.* 1976;98(8):2319–23.
- [5] Dalbeth N, Merriman TR, Stamp LK. Gout. *The Lancet.* 2016;388(10055):2039–52.
- [6] Dalbeth N, Choi HK, Joosten LAB, et al. Gout. *Nat Rev Dis Prim*; 2019;5(1):69.
- [7] Zamudio-Cuevas Y, Fernández-Torres J, Martínez-Nava GA, et al. Highlight Article: Phagocytosis of monosodium urate crystals by human synoviocytes induces inflammation. *Exp Biol Med* 2019; 244: 344–51.
- [8] Zhu Y, Pandya BJ, Choi HK. Prevalence of gout and hyperuricemia in the US general population: The National Health and Nutrition Examination Survey 2007–2008. *Arthritis Rheum* 2011; 63: 3136–41.
- [9] Elfshaw MM, Zleik N, Kvgic Z, et al. Changes in the Presentation of Incident Gout and the Risk of Subsequent Flares: A Population-based Study over 20 Years. *J Rheumatol* 2020; 47: 613–18.
- [10] Martinon F, Pétrilli V, Mayor A, et al. Gout-associated uric acid crystals activate the NALP3 inflammasome. *Nature* 2006; 440: 237–41.
- [11] Busso N, So A. Mechanisms of inflammation in gout. *Arthritis Res Ther* 2010; 12: 1–8.
- [12] Dalbeth N, Bardin T, Doherty M, et al. Discordant American College of Physicians and international rheumatology guidelines for gout management: Consensus statement of the Gout, Hyperuricemia and Crystal-Associated Disease Network (G-CAN). *Nat Rev Rheumatol* 2017; 13: 561–8.
- [13] Storey GD. Alfred Baring Garrod (1819–1907). *Rheumatology (Oxford)* 2001; 40: 1189–90.
- [14] Dirken-heukensfeldt KJM, Teunissen TAM. " Clinical features of women with gout arthritis. " A systematic review. 2010; 575–82.
- [15] Yahyaoui R, Esteva I, Haro-Mora JJ, et al. Effect of long-term administration of cross-sex hormone therapy on serum and urinary uric acid in transsexual persons. *J Clin Endocrinol Metab* 2008; 93: 2230–33.
- [16] te Kampe R, Janssen M, van Durme C, et al. Sex differences in the clinical profile among patients with gout: Cross-sectional analyses of an observational study. *J Rheumatol* 2021; 48: 286–292.
- [17] Singh JA, Gaffo A. Gout epidemiology and comorbidities. *Semin Arthritis Rheum* 2020; 50: S11–S16.
- [18] Richette P, Doherty M, Pascual E, et al. 2016 updated EULAR evidence-based recommendations for the management of gout. *Ann Rheum Dis* 2017; 76: 29–42.
- [19] Albertoni GA, Borges FT, Schor N. Uric Acid and Renal Function. *Dis Ren parenchyma* 2012; 267: 1045–6.

- [20] Kratzer JT, Lanaspas MA, Murphy MN, et al. Evolutionary history and metabolic insights of ancient mammalian uricases. *Proc Natl Acad Sci U S A*. 2014;111(10):3763-8.
- [21] Oda M, Satta Y, Takenaka O, et al. Loss of urate oxidase activity in hominoids and its evolutionary implications. *Mol Biol Evol* 2002; 19: 640-53.
- [22] Ames BN, Cathcart R, Schwiers E, et al. Uric acid provides an antioxidant defense in humans against oxidant- and radical-caused aging and cancer: a hypothesis. *Proc Natl Acad Sci* 1981; 78: 6858-62.
- [23] Seifar F, Dinasarapu AR, Jinnah HA. Uric Acid in Parkinson's Disease: What Is the Connection? *Mov Disord* 2022; 37: 2173-83.
- [24] Joosten LAB, Crişan TO, Bjornstad P, et al. Asymptomatic hyperuricaemia: a silent activator of the innate immune system. *Nat Rev Rheumatol* 2020; 16: 75-86.
- [25] Rock KL, Kataoka H, Lai JJ. Uric acid as a danger signal in gout and its comorbidities. *Nat Rev Rheumatol* 2013; 9: 13-23.
- [26] Crişan TO, Cleophas MCP, Novakovic B, et al. Uric acid priming in human monocytes is driven by the AKT-PRAS40 autophagy pathway. *Proc Natl Acad Sci U S A* 2017; 114(21):5485-90.
- [27] Watanabe S, Kang DH, Feng L, et al. Uric acid, hominoid evolution, and the pathogenesis of salt-sensitivity. *Hypertension* 2002; 40: 355-60.
- [28] Perez-Pozo SE, Schold J, Nakagawa T, et al. Excessive fructose intake induces the features of metabolic syndrome in healthy adult men: Role of uric acid in the hypertensive response. *Int J Obes* 2010; 34: 454-61.
- [29] Johnson RJ, Andrews P. Fructose, uricase, and the Back-to-Africa hypothesis. *Evol Anthropol* 2010; 19: 250-57.
- [30] Reginato AM, Mount DB, Yang I, et al. The genetics of hyperuricaemia and gout. *Nat Rev Rheumatol* 2012; 8: 610-21.
- [31] Dehghan A, Köttgen A, Yang Q, et al. Association of three genetic loci with uric acid concentration and risk of gout: a genome-wide association study. *Lancet* 2008; 372: 1953-61.
- [32] Yu M-A, Sánchez-Lozada LG, Johnson RJ, et al. Oxidative stress with an activation of the renin-angiotensin system in human vascular endothelial cells as a novel mechanism of uric acid-induced endothelial dysfunction. *J Hypertens* 2010; 28(6):1234-42.
- [33] Rahimi-Sakak F, Maroofi M, Rahmani J, et al. Serum uric acid and risk of cardiovascular mortality: A systematic review and dose-response meta-analysis of cohort studies of over a million participants. *BMC Cardiovasc Disord* 2019; 19: 1-8.
- [34] Kim E, Lee HN, Kim YK, et al. Increased serum uric acid levels are associated with digital ulcers in patients with systemic sclerosis. *Rheumatol Int* 2019; 39: 255-63.
- [35] Johnson RJ, Nakagawa T, Jalal D, et al. Uric acid and chronic kidney disease: Which is chasing which? *Nephrol Dial Transplant* 2013; 28: 2221-8.
- [36] Johnson RJ, Nakagawa T, Sanchez-Lozada LG, et al. Sugar, uric acid, and the etiology of diabetes and obesity. *Diabetes* 2013; 62: 3307-15.
- [37] Chen B, Lu C, Gu HQ, et al. Serum Uric Acid Concentrations and Risk of Adverse Outcomes in Patients With COVID-19. *Front Endocrinol (Lausanne)* 2021; 12: 1-8.

- [38] Topless RK, Gaffo A, Stamp LK, et al. Gout and the risk of COVID-19 diagnosis and death in the UK Biobank: a population-based study. *Lancet Rheumatol* 2022; 4: e274–e281.
- [39] Janeway CA. The immune system evolved to discriminate infectious nonself from noninfectious self. *Immunol Today* 1992; 13: 11–16.
- [40] Matzinger P. The danger model: A renewed sense of self. *Science* 2002; 296: 301–5.
- [41] Li D, Wu M. Pattern recognition receptors in health and diseases. *Signal Transduct Target Ther* 2021; 6: 1–24.
- [42] Chen GY, Nuñez G. Sterile inflammation: Sensing and reacting to damage. *Nat Rev Immunol* 2010; 10: 826–37.
- [43] Shi Y, Evans JE, Rock KL. Molecular identification of a danger signal that alerts the immune system to dying cells. *Nature* 2003; 425: 516–21.
- [44] Cabău G, Crișan TO, Klück V, et al. Urate-induced immune programming: Consequences for gouty arthritis and hyperuricemia. *Immunol Rev* 2020; 294: 92–105.
- [45] Martínez-Reyes CP, Manjarrez-Reyna AN, Méndez-García LA, et al. Uric acid has direct proinflammatory effects on human macrophages by increasing proinflammatory mediators and bacterial phagocytosis probably via URAT1. *Biomolecules* 2020; 10: 1–16.
- [46] Braga TT, Davanzo MR, Mendes D, et al. Sensing soluble uric acid by Naip1-Nlrp3 platform. *Cell Death Dis.* 2021;12(2):158.
- [47] Martinon F. Signaling by ROS drives inflammasome activation. *Eur J Immunol* 2010; 40: 616–19.
- [48] Braga TT, Forni MF, Correa-Costa M, et al. Soluble Uric Acid Activates the NLRP3 Inflammasome. *Sci Rep* 2017; 7: 1–14.
- [49] Ebrahimi R, Pasalar P, Shokri H, et al. Evidence for the effect of soluble uric acid in augmenting endoplasmic reticulum stress markers in human peripheral blood mononuclear cells. *J Physiol Biochem* 2022; 78: 343–53.
- [50] Crișan TO, Cleophas MCP, Oosting M, et al. Soluble uric acid primes TLR-induced proinflammatory cytokine production by human primary cells via inhibition of IL-1Ra. *Ann Rheum Dis* 2016; 75: 755–62.
- [51] ElSayed, S. Role of Protein Phosphatase-2A in Regulating Monocyte Activation by Soluble and Crystalline Uric Acid in Gout. [master's thesis]. Irvine, CA: Chapman University;
- [52] Dalbeth N, Haskard DO. Mechanisms of inflammation in gout. *Rheumatology* 2005; 44: 1090–6.
- [53] Chang JG, Tu SJ, Huang CM, et al. Single-cell RNA sequencing of immune cells in patients with acute gout. *Sci Rep* 2022; 12: 1–10.
- [54] Mortensen SB, Hansen ABE, Mogensen TH, et al. Pyrin Inflammasome Activation Abrogates Interleukin-1 Receptor Antagonist, Suggesting a New Mechanism Underlying Familial Mediterranean Fever Pathogenesis. *Arthritis Rheumatol* 2021; 73: 2116–26.
- [55] Ma Q, Immler R, Pruenster M, et al. Soluble uric acid inhibits $\beta 2$ integrin-mediated neutrophil recruitment in innate immunity. *Blood* 2022; 139: 3402–17.
- [56] Kimura Y, Yanagida T, Onda A, et al. Soluble uric acid promotes atherosclerosis via AMPK (AMP-activated protein kinase)-mediated inflammation. *Arterioscler Thromb Vasc Biol* 2019; 570–82.
- [57] Wang Y, Ma X, Su C, et al. Uric acid enhances the antitumor immunity of dendritic cell-based vaccine. *Sci Rep* 2015; 5: 1–11.

- [58] Webb R, Jeffries M, Sawalha AH. Uric acid directly promotes human T-cell activation. *Am J Med Sci* 2009; 337: 23–7.
- [59] Yu Q, Sun Z, Wang Y, et al. Hyperuricemia is accompanied by elevated peripheral CD4+ T cells. *Sci Rep* 2023; 13: 12537.
- [60] Kanellis J, Watanabe S, Li JH, et al. Uric acid stimulates monocyte chemoattractant protein-1 production in vascular smooth muscle cells via mitogen-activated protein kinase and cyclooxygenase-2. *Hypertension* 2003; 41: 1287–93.
- [61] Sautin YY, Johnson RJ. Uric acid: The oxidant-antioxidant paradox. In: *Nucleosides, Nucleotides and Nucleic Acids*. 2008;27(6):608–19.
- [62] Toncev G, Milicic B, Toncev S, et al. Serum uric acid levels in multiple sclerosis patients correlate with activity of disease and blood-brain barrier dysfunction. *Eur J Neurol* 2002; 9: 221–6.
- [63] Lai JH, Luo SF, Hung LF, et al. Physiological concentrations of soluble uric acid are chondroprotective and anti-inflammatory. *Sci Rep* 2017; 7: 1–12.
- [64] Chhana A, Lee G, Dalbeth N. Factors influencing the crystallization of monosodium urate: A systematic literature review Pathophysiology of musculoskeletal disorders. *BMC Musculoskelet Disord* 2015; 16: 1–11.
- [65] Jaramillo M, Godbout M, Naccache PH, et al. Signaling events involved in macrophage chemokine expression in response to monosodium urate crystals. *J Biol Chem* 2004; 279: 52797–805.
- [66] An LL, Mehta P, Xu L, et al. Complement C5a potentiates uric acid crystal-induced IL-1 β production. *Eur J Immunol* 2014; 44(12):3669–79.
- [67] Mantovani A, Dinarello CA, Molgora M, et al. Interleukin-1 and Related Cytokines in the Regulation of Inflammation and Immunity. *Immunity* 2019; 50: 778–95.
- [68] Klück V, Liu R, Joosten LAB. The role of interleukin-1 family members in hyperuricemia and gout. *Jt Bone Spine*. 2021;88(2):105092.
- [69] Chen CJ, Shi Y, Hearn A, et al. MyD88-dependent IL-1 receptor signaling is essential for gouty inflammation stimulated by monosodium urate crystals. *J Clin Invest* 2006; 116: 2262–71.
- [70] Brough D, Rothwell NJ. Caspase-1-dependent processing of pro-interleukin-1 β is cytosolic and precedes cell death. *J Cell Sci* 2007; 120: 772–81.
- [71] Hari A, Zhang Y, Tu Z, et al. Activation of NLRP3 inflammasome by crystalline structures via cell surface contact. *Sci Rep* 2014; 4:7281.
- [72] Joosten LAB, Netea MG, Mylona E, et al. Engagement of fatty acids with toll-like receptor 2 drives interleukin-1 β production via the ASC/caspase 1 pathway in monosodium urate monohydrate crystal-induced gouty arthritis. *Arthritis Rheum* 2010; 62: 3237–48.
- [73] Chung YH, Kim DH, Lee WW. Monosodium urate crystal-induced pro-interleukin-1 β production is post-transcriptionally regulated via the p38 signaling pathway in human monocytes. *Sci Rep*. 2016;6:34533.
- [74] Kinoshita T, Imamura R, Kushiyaama H, et al. NLRP3 Mediates NF- κ B activation and cytokine induction in microbially induced and sterile inflammation. *PLoS One*. 2015;10(3):e0119179.
- [75] Schorn C, Janko C, Krenn V, et al. Bonding the foe - NETting neutrophils immobilize the pro-inflammatory monosodium urate crystals. *Front Immunol*. 2012;3:376.

- [76] Mylona EE, Mouktaroudi M, Crisan TO, et al. Enhanced interleukin-1 β production of PBMCs from patients with gout after stimulation with Toll-like receptor-2 ligands and urate crystals. *Arthritis Res Ther* 2012; 14: R158.
- [77] Crisan TO, Plantinga TS, van de Veerdonk FL, et al. Inflammasome-independent modulation of cytokine response by autophagy in human cells. *PLoS One*. 2011;6(4):e18666.
- [78] Eleftheriadis T, Pissas G, Karioti A, et al. Uric acid induces caspase-1 activation, IL-1 β secretion and P2X7 receptor dependent proliferation in primary human lymphocytes. *Hippokratia* 2013; 17: 141–5.
- [79] Wang J, Liu K, Xiao T, et al. Uric acid accumulation in DNA-damaged tumor cells induces NKG2D ligand expression and antitumor immunity by activating TGF- β -activated kinase 1. *Oncoimmunology*. 2022;11(1):2016159.
- [80] Schorn C, Janko C, Latzko M, et al. Monosodium urate crystals induce extracellular DNA traps in neutrophils, eosinophils, and basophils but not in mononuclear cells. *Front Immunol* 2012; 3: 1–8.
- [81] Netea MG, Joosten LAB, Latz E, et al. Trained immunity: A program of innate immune memory in health and disease. *Science*. 2016;352(6284):aaf1098.
- [82] Netea MG, van der Meer JWM. Trained Immunity: An Ancient Way of Remembering. *Cell Host Microbe* 2017; 21: 297–300.
- [83] Crisan TO, Netea MG, Joosten LAB. Innate immune memory: Implications for host responses to damage-associated molecular patterns. *Eur J Immunol* 2016; 46: 817–28.
- [84] Bowdish DME, Loffredo MS, Mukhopadhyay S, et al. Macrophage receptors implicated in the 'adaptive' form of innate immunity. *Microbes Infect*. 2007;9(14–15):1680–7.
- [85] Benn CS, Netea MG, Selin LK, et al. A Small Jab - A Big Effect: Nonspecific Immunomodulation By Vaccines. *Trends in Immunology*. 2013;34(9):431–9.
- [86] Kleinnijenhuis J, Quintin J, Preijers F, et al. Bacille Calmette-Guérin induces NOD2-dependent nonspecific protection from reinfection via epigenetic reprogramming of monocytes. *Proc Natl Acad Sci U S A* 2012; 109: 17537–42.
- [87] Quintin J, Saeed S, Martens JHA, et al. Candida albicans infection affords protection against reinfection via functional reprogramming of monocytes. *Cell Host Microbe*. 2012;12(2):223–32.
- [88] Saeed S, Quintin J, Kerstens HHD, et al. Epigenetic programming of monocyte-to-macrophage differentiation and trained innate immunity. *Science*. 2014;345(6204):1251086.
- [89] Bekkering S, Quintin J, Joosten LAB, et al. Oxidized low-density lipoprotein induces long-term proinflammatory cytokine production and foam cell formation via epigenetic reprogramming of monocytes. *Arterioscler Thromb Vasc Biol*. 2014;34(8):1731–8.
- [90] Van Der Valk FM, Bekkering S, Kroon J, et al. Oxidized phospholipids on Lipoprotein(a) elicit arterial wall inflammation and an inflammatory monocyte response in humans. *Circulation*. 2016;134(8):611–24.
- [91] Ochando J, Mulder WJM, Madsen JC, et al. Trained immunity – basic concepts and contributions to immunopathology. *Nat Rev Nephrol* 2023; 19: 23–37.
- [92] Groh LA, Ferreira A V., Helder L, et al. oxLDL-Induced Trained Immunity Is Dependent on Mitochondrial Metabolic Reprogramming. *Immunometabolism*. 2021;3(3):e210025.
- [93] Schnack L, Sohrabi Y, Lagache SMM, et al. Mechanisms of trained innate immunity in oxLDL primed human coronary smooth muscle cells. *Front Immunol* 2019; 10: 1–12.

- [94] Renaudin F, Orliaguet L, Castelli F, et al. Gout and pseudo-gout-related crystals promote GLUT1-mediated glycolysis that governs NLRP3 and interleukin-1 β activation on macrophages. *Ann Rheum Dis* 2020; 79: 1506–14.
- [95] Jaenisch R, Bird A. Epigenetic regulation of gene expression: How the genome integrates intrinsic and environmental signals. *Nat Genet* 2003; 33: 245–54.
- [96] Wang M, Chen W, Zhang X, et al. Single-Cell Analysis in Blood Reveals Distinct Immune Cell Profiles in Gouty Arthritis. *J Immunol* 2023; 210: 745–52.
- [97] Zhang B, Moorlag SJCFM, Dominguez-Andres J, et al. Single-cell RNA sequencing reveals induction of distinct trained-immunity programs in human monocytes. *J Clin Invest.* 2022;132(7):e147719.
- [98] Xie M, Yu Y, Kang R, et al. PKM2-Dependent glycolysis promotes NLRP3 and AIM2 inflammasome activation. *Nat Commun* 2016; 7: 1–13.
- [99] Finucane OM, Sugrue J, Rubio-Araiz A, et al. The NLRP3 inflammasome modulates glycolysis by increasing PFKFB3 in an IL-1 β -dependent manner in macrophages. *Sci Rep* 2019; 9: 1–10.
- [100] Cobo I, Cheng A, Murillo-Saich J, et al. Monosodium urate crystals regulate a unique JNK-dependent macrophage metabolic and inflammatory response. *Cell Rep* 2022; 38: 110489.
- [101] Fanucchi S, Domínguez-Andrés J, Joosten LAB, et al. The Intersection of Epigenetics and Metabolism in Trained Immunity. *Immunity* 2021; 54: 32–43.
- [102] Greenberg MVC, Bourc'his D. The diverse roles of DNA methylation in mammalian development and disease. *Nat Rev Mol Cell Biol* 2019; 20: 590–607.
- [103] Tseng CC, Liao WT, Wong MC, et al. Cell lineage-specific methylome and genome alterations in gout. *Aging (Albany NY)* 2021; 13: 3843–63.
- [104] Tin A, Schlosser P, Matias-Garcia PR, et al. Epigenome-wide association study of serum urate reveals insights into urate co-regulation and the SLC2A9 locus. *Nat Commun* 2021; 12: 1–18.
- [105] Wang Z, Zhao Y, Phipps-Green A, et al. Differential DNA Methylation of Networked Signaling, Transcriptional, Innate and Adaptive Immunity, and Osteoclastogenesis Genes and Pathways in Gout. *Arthritis Rheumatol.* 2020;72(5):802–14.
- [106] Cleophas MCP, Crişan TO, Lemmers H, et al. Suppression of monosodium urate crystal-induced cytokine production by butyrate is mediated by the inhibition of class I histone deacetylases. *Ann Rheum Dis* 2016; 75: 593–600.
- [107] Cleophas MCP, Crişan TO, Klück V, et al. Romidepsin suppresses monosodium urate crystal-induced cytokine production through upregulation of suppressor of cytokine signaling 1 expression. *Arthritis Res Ther.* 2019;21(1):50.
- [108] Yang Q Bin, Zhang MY, Yang L, et al. Deficiency of histone deacetylases 3 in macrophage alleviates monosodium urate crystals-induced gouty inflammation in mice. *Arthritis Res Ther* 2024; 26: 1–12.
- [109] Dalbeth N, Smith T, Nicolson B, et al. Enhanced osteoclastogenesis in patients with tophaceous gout: Urate crystals promote osteoclast development through interactions with stromal cells. *Arthritis Rheum* 2008; 58: 1854–65.
- [110] Kim SK, Choe JY, Kim JW, et al. Histone Deacetylase 6 Inhibitor CKD-WID Suppressed Monosodium Urate-Induced Osteoclast Formation by Blocking Calcineurin-NFAT Pathway in RAW 264.7 Cells. *Pharmaceuticals (Basel).* 2023;16(3):446.
- [111] Esteller M. Non-coding RNAs in human disease. *Nat Rev Genet* 2011; 12: 861–74.

- [112] Wang Y, Xu D, Wang B, et al. Could MicroRNAs be regulators of gout pathogenesis? *Cell Physiol Biochem* 2015; 36: 2085–92.
- [113] Bohatá J, Horváthová V, Pavlíková M, et al. Circulating microRNA alternations in primary hyperuricemia and gout. *Arthritis Res Ther* 2021; 23: 1–11.
- [114] Jin HM, Kim TJ, Choi JH, et al. MicroRNA-155 as a proinflammatory regulator via SHIP-1 down-regulation in acute gouty arthritis. *Arthritis Res Ther* 2014; 16: 1–9.
- [115] Zhou W, Wang Y, Wu R, et al. MicroRNA-488 and -920 regulate the production of proinflammatory cytokines in acute gouty arthritis. *Arthritis Res Ther* 2017; 19: 1–11.
- [116] Qing YF, Zheng JX, Tang YP, et al. LncRNAs Landscape in the patients of primary gout by microarray analysis. *PLoS One* 2021; 16: 1–17.
- [117] Liu YF, Xing GL, Chen Z, et al. Long non-coding RNA HOTAIR knockdown alleviates gouty arthritis through miR-20b upregulation and NLRP3 downregulation. *Cell Cycle* 2021; 20: 332–44.

CHAPTER 2

Urate-induced epigenetic modifications in myeloid cells

Badii, M.* , Gaal, O. I.* , Cleophas, M. C., Klück, V., Davar, R., Habibi, E., Keating, S. T., Novakovic, B., Helsen, M. M., Dalbeth, N., Stamp, L. K., Macartney-Coxson, D., Phipps-Green, A. J., Stunnenberg, H. G., Dinarello, C. A., Merriman, T. R., Netea, M. G., Crişan, T. O.# , & Joosten, L. A. B#.

*These authors contributed equally to this work

#These authors share senior authorship

Arthritis Res Ther. 2021 Jul 28;23(1):202.

Summary

Hyperuricemia is a metabolic condition central to gout pathogenesis. Urate exposure primes human monocytes towards a higher capacity to produce and release IL-1 β . In this study we assessed the epigenetic processes associated to urate-mediated hyper-responsiveness. Freshly isolated human peripheral blood mononuclear cells or enriched monocytes were pre-treated with solubilized urate and stimulated with LPS with or without monosodium urate (MSU) crystals. Cytokine production was determined by ELISA. Histone epigenetic marks were assessed by sequencing immunoprecipitated chromatin. Mice were injected intraarticularly with MSU crystals and palmitate after inhibition of uricase and urate administration in the presence or absence of methylthioadenosine. DNA methylation was assessed by methylation array in whole blood of 76 participants with normouricemia or hyperuricemia. High concentrations of urate enhanced the inflammatory response *in vitro* in human cells and *in vivo* in mice, and broad-spectrum methylation inhibitors reversed this effect. Assessment of histone 3 lysine 4 trimethylation (H3K4me3) and histone 3 lysine 27 acetylation (H3K27ac) revealed differences in urate-primed monocytes compared to controls. Differentially methylated regions (e.g. HLA-G, IFITM3, PRKAB2) were found in people with hyperuricemia compared to normouricemia in genes relevant for inflammatory cytokine signalling. Urate alters the epigenetic landscape in selected human monocytes or whole blood of people with hyperuricemia compared to normouricemia. Both histone modifications and DNA methylation show differences depending on urate exposure. Subject to replication and validation, epigenetic changes in myeloid cells may be a therapeutic target in gout.

Introduction

Urate is the end-point metabolite in purine catabolism in humans and is regarded as an alarmin released from disintegrating cells at times of stress or cell death[1][2]. Higher urate concentration in the serum defines the condition of hyperuricemia, at which point monosodium urate (MSU) crystals can precipitate in peripheral tissues and cause an inflammatory response. Gout is caused by persistent hyperuricemia, a painful inflammatory arthritis caused by deposition of (MSU) crystals in the synovial cavity[3]. MSU crystals have been shown to induce IL-1 β release through activation of the NLRP3 inflammasome[4]. They recruit ASC (Inflammasome Adaptor Protein Apoptosis-Associated Speck-Like Protein Containing CARD) at the inflammasome formation site through the polymerization of tubulin[5]. MSU crystals alone are insufficient for a gout flare and second signals are required to act in synergy with MSU crystals. Such second signals can be pathogen-related ligands such as lipopolysaccharide (LPS), [6] or Pam3Cys[7], or sterile stimuli such as fatty acids (e.g. stearate)[8], or the C5a component of the complement[9].

Despite a widely accepted pathogenesis model for gout stemming from long-lasting hyperuricemia that determines the formation of MSU crystals, many questions remain to address the clinical observations of urate-related inflammation[10]. The reasons why not all people with hyperuricemia develop gout, or why some people with MSU crystals in synovial fluid do not show signs of inflammation[11], remain unknown. Genome-wide association studies have identified hundreds of genomic loci associated with serum urate levels and gout [12][13][14][15]. However, little progress has been made in understanding the genetic control of the progression from hyperuricemia to gout[16]. Large-scale genetic studies are likely to pinpoint additional factors that specifically lead to gout in people with hyperuricemia. Environmental factors (e.g. dietary triggers)[17] can also contribute to inflammation in people with hyperuricemia. Moreover, epidemiological studies suggest that MSU crystals and soluble urate itself also play a role in signalling danger in diseases other than gout: from the low-grade inflammation in aging[18], to common metabolic disorders[19], and cancer[20].

We previously described the priming effects of high concentrations of soluble urate on primary human peripheral blood mononuclear cells (PBMC)s and monocytes, where a shift in cytokine production towards elevated IL-1 β concomitant with reduced IL-1Ra could be observed [21]. In addition, we

reported that PBMCs of individuals with hyperuricemia produce higher amounts of pro-inflammatory cytokines than normouricemic controls after *ex vivo* stimulation[21]. This can be reproduced *in vitro* by pre-treating cells with increasing urate doses followed by washout and re-stimulation with toll-like receptor ligands and MSU crystals. Interestingly, the high proinflammatory capacity coincided with a reduction in IL-1 receptor antagonist (IL-1Ra) production[21], which is at least in part mediated by AKT phosphorylation and autophagy repression in primary human monocytes[22]. Several stimuli exert long-term effects on innate immunity through epigenetic modifications (a process termed trained immunity)[23]. This persistent state of immunological memory can be induced by microbial stimuli such as *Candida albicans* or β -glucan (cell wall component of *C. albicans*) [24, 25], as well as sterile stimuli such as oxidized cholesterol or phospholipids[26, 27].

A recent study performed in patients with gout highlights several differentially methylated loci (DML) with relevance to inflammation (28). DMLs were found in known gout risk genes and candidate genes (eg.: *SLC2A9*, *ABCC9*), transcription factor genes (*NFATC2* and *MEF2C*) and their regulated gene networks in leukocytes. Pathway analysis of DML suggests gout patients have altered DNA methylation levels of genes involved in both innate and adaptive immunity pathways, with a strong signature for Th17 differentiation and osteoclastogenesis[28].

In the present study, we hypothesize that urate drives persistent proinflammatory effects through epigenetically mediated innate immune memory and that hyperuricemic individuals could have altered epigenetic landscapes in immune cells compared to normouricemic people. We use complementary approaches aimed to establish the molecular basis of urate-mediated proinflammatory status of human monocytes. We show that exposure to urate can have persistent effects *in vitro*, which is consistent with previous data showing that monocytes of gout patients retain their capacity to produce more cytokines in the absence of hyperuricemia[7, 21]. We identify post-translational histone modifications and DNA methylation as molecular substrates for the effects of hyperuricemia.

Materials and methods

A detailed version of this section is provided in Supplementary Material.

Participants

Urate priming experiments were performed in 85 Dutch volunteers from the Human Functional Genomics Project (<http://www.humanfunctionalgenomics.org>) [29]. Experiments were approved by the Ethical Committee of Radboud University Nijmegen (nr. 42561.091.12). The DNA methylation study was performed in 76 individuals (Table S1) of New Zealand Māori ancestry and was approved by the New Zealand Lower South Health and Disability Ethics Committee (MEC/05/10/130). Patients or the public were not involved in the design, conduct, reporting, or dissemination of our research.

PBMC and monocyte isolation

Human PBMCs were separated using Ficoll-Paque (Pharmacia Biotech). Monocytes were enriched using hyperosmotic Percoll solution [30], and were subsequently purified by negative selection using magnetic beads (Miltenyi Biotec).

Stimulation experiments

Experiments were performed in culture medium containing RPMI 1640, supplemented with 50 µg/mL gentamicin, 2 mM L-glutamine, 1 mM pyruvate and 10% human pooled serum following an *in vitro* urate priming protocol described extensively elsewhere [22].

Cytokine measurements

Cytokine concentrations were determined in cell culture supernatants using ELISA.

Animal model

Male 10–12 weeks old C57Bl/6J mice were purchased from Jackson Laboratories (Bar Harbor, Maine, USA). Uricase was inhibited using oxonic acid and urate was administered according to a previously described protocol [22].

ChIP sequencing preparation and analysis

DNA-histone crosslinking was performed using 1% formaldehyde followed by 1.25 mol/L glycine. Chromatin was sonicated using a Diagenode Bioruptor UCD-300 and immunoprecipitated using H3K27ac or H3K4me3 antibodies (Diagenode) and protein A/G magnetic beads. DNA was purified using QIAGEN Qiaquick

MinElute PCR purification Kit. Illumina library preparation was done as previously described[31]. Sequencing was performed using Illumina HiSeq 2000.

DNA methylation analysis

Genomic DNA was isolated from the peripheral blood white cells of 76 individuals of Aotearoa New Zealand Māori ancestry with varying serum urate levels. Genome-wide methylation analysis was performed using Illumina InfiniumMethylationEPIC BeadChips[32].

Statistical analysis

Cytokine data were analyzed in GraphPad Prism version 8 using Friedmann or Wilcoxon signed rank test. ChIP sequencing and DNA methylation data were analysed using R.

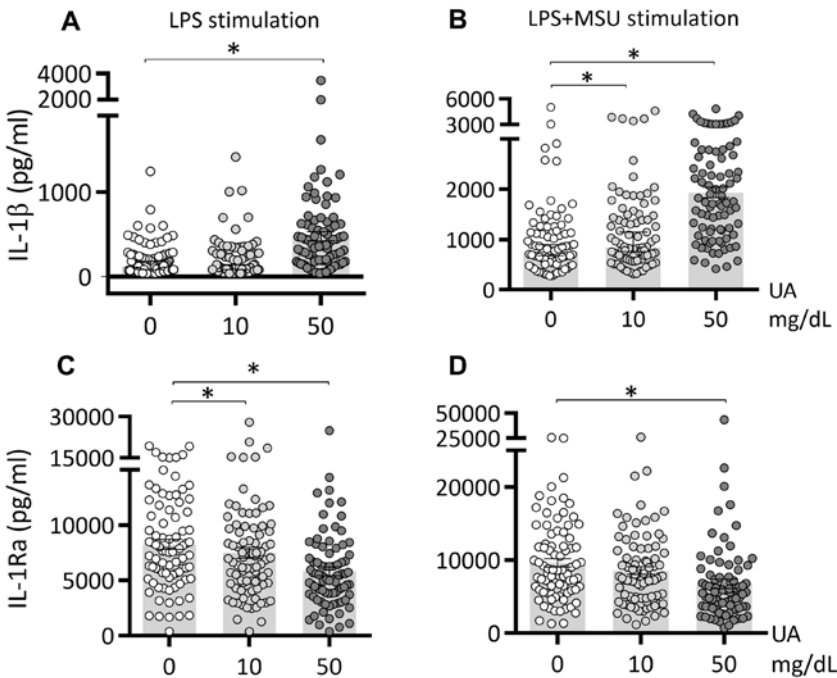


Figure 1. IL-1 β and IL-1Ra production after urate priming of PBMCs *in vitro*. Freshly isolated PBMCs from 85 healthy volunteers were exposed to culture medium (RPMI 1640 supplemented with 10% human pooled serum) in the presence or absence of urate (UA) 10 or 50 mg/dL. After 24 hours, urate was removed, and cells were stimulated with LPS 10 ng/mL in the presence or absence of MSU crystals (300 μ g/mL). IL-1 β (A-B) and IL-1Ra (C-D) were measured in the supernatants of cells, data are representative of 3 independent experiments using a total of 85 different healthy volunteers of the 200FG cohort, graphs depict means \pm SEM. UA, uric acid/urate. *, Friedman test and post-hoc analysis $p < 0.05$.

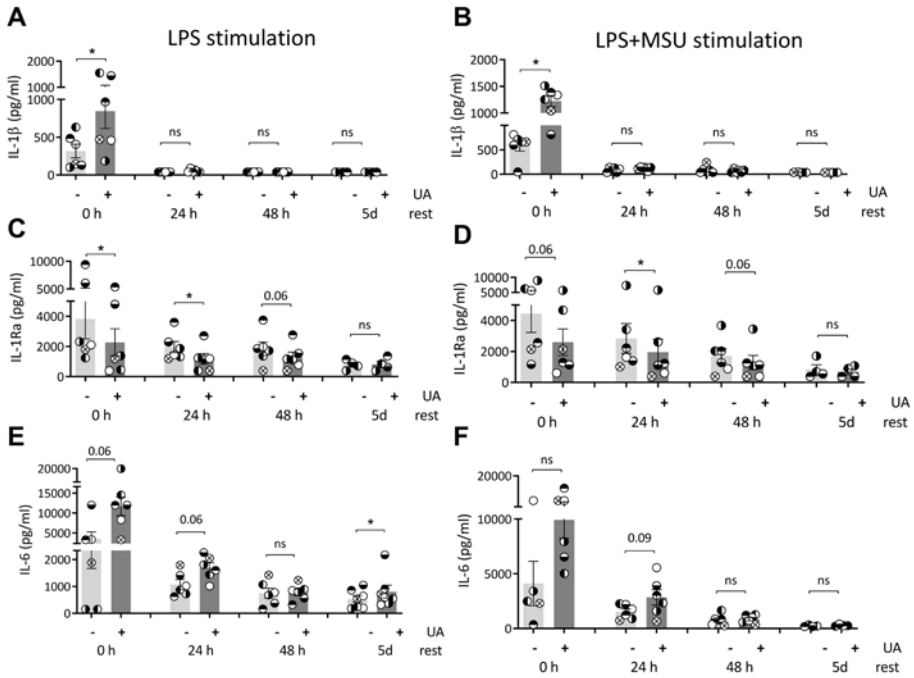


Figure 2. Persistence of urate priming effects *in vitro*. Freshly isolated PBMCs from 6 healthy volunteers were exposed to culture medium (RPMI 1640 supplemented with 10% human pooled serum) in the presence or absence of urate (UA) 50 mg/dL. After 24 hours, urate was removed, and cells were stimulated with LPS 10 ng/mL in the presence or absence of MSU crystals (300µg/mL). The second stimulation was performed at different times after urate washout: immediately (0 h resting time), or after increasing number of days of resting in 10% serum RPMI (24 hours, 48 hours, 5 days). IL-1β (A-B), IL-1Ra (C-D) and IL-6 (E-F) were measured in the supernatants of cells, data are representative for 3 independent experiments and 6 different volunteers, graphs depict individual values with paired samples shown in identical symbols, bars and error bars represent means \pm SEM. UA, uric acid/urate 50 mg/dL. *, Wilcoxon $p < 0.05$.

Results

Urate treatment of human PBMCs *in vitro* results in a specific and persistent cytokine production phenotype

We tested the effects of urate solubilized in culture medium at high concentration (50 mg/dL) or at concentrations similar to *in vivo* hyperuricemia (10 mg/dL). Both concentrations of soluble urate primed the cells to produce higher IL-1β and lower IL-1Ra production (Fig.1A-D). Next, we investigated whether these priming effects persisted beyond the 24h period of urate

priming. Cells were incubated for 24h with urate, washed and thereafter subjected to increasing resting times (up to 5 days) in culture medium before stimulation with LPS (10 ng/mL) and MSU crystals (300 µg/mL). While IL-1 β production capacity was strongly diminished after 48h of culture (Fig.2A-B – 24 h resting periods and onwards), persistent effects were observed for reduction of IL-1Ra (Fig.2C-D) and for induction of IL-6 (Fig.2E-F).

Pharmacological inhibition of methyl-transferases inhibits urate effects in an *in vivo* murine model of gout

The broad protein methyl-transferase inhibitor methylthioadenosine (5'-S-methyl-5'-thioadenosine, MTA) was previously shown to inhibit the cytokine production induced by urate *in vitro* [21]. To provide validation in an *in vivo* model, mice were administered exogenous urate in addition to oxonic acid (uricase inhibitor). Acute gout was induced by intraarticular injections with MSU crystals and palmitate (C16:0). Inflammation was significantly enhanced in the oxonic acid group compared with controls as observed by macroscopically scored inflammation (Fig. 3A). Addition of MTA inhibited this effect on the enhanced joint inflammation and histology at 24h post intraarticular injections (Fig.3A-C).

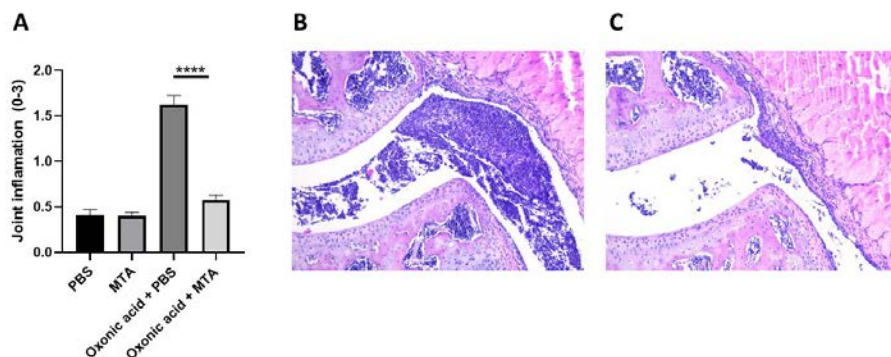


Figure 3. Methyl transferase inhibition limits gout inflammation in mice. Macroscopic (Panel A) scores of the knees in mice treated with vehicle control or oxonic acid + urate in the presence or absence of methyl transferase inhibitor MTA (methyl-thio-adenosine) followed by intraarticular injection of MSU+C16:0. Inflammation was scored at 24 h. Histology (H&E staining) of joints treated with MSU+C16:0 in oxonic acid + urate mice (panel B) and in the presence of MTA (panel C).

Histone 3 Lysine 4 trimethylation (H3K4me3) or Histone 3 Lysine 27 acetylation (H3K27ac) are mildly affected by urate treatment of human monocytes *in vitro*

To test whether specific histone modifications are associated with the persistent effects of urate priming, we used chromatin immunoprecipitation coupled with massively parallel sequencing (ChIP-seq) to profile the enrichment of H3 histones trimethylated at lysine 4 (H3K4me3) and H3 histones acetylated at lysine 27 (H3K27ac), two transcriptionally permissive chromatin modifications previously associated with long-term effects of sterile stimuli[26].

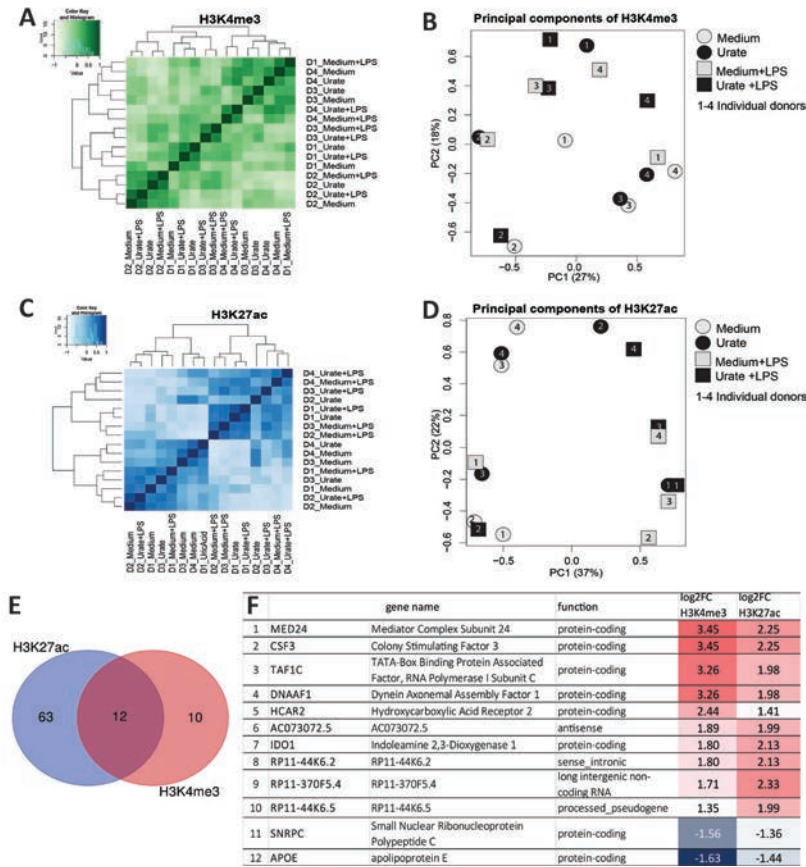


Figure 4. ChIP sequencing in urate-stimulated monocytes reveals no urate-dependent clustering based on phenotype for H3K4 trimethylation and H3K27 acetylation. Cluster and principal component analysis of datasets obtained on ChIP sequencing for H3K4me3 (A and B) or H3K27ac (C and D) in 4 different donors (labelled D1-4) and 4 different conditions (Medium, Urate, Medium+LPS, Urate+LPS). Venn diagram of regions showing differential enrichment of either H3K27ac or H3K4me3 in urate primed cells (E) and list of overlapping genes based on histone marks at promoter regions, including log 2 fold change values for each of the two histone marks (F).

The ChIP-seq analysis was based on all dynamic genes that were identified by comparing all samples to each other. After filtering the data based on these cutoffs, no clustering of stimulated samples was evident to indicate that urate induced genome-wide significant differences on these two histone marks (Fig. 4A-D, Fig. S1). Nevertheless, some individual genes, exhibited nominally-significant evidence for variability for H3K4me3 (Table S2) or H3K27ac (Table S3) enrichment at promoter regions. Of these, 12 genes (MED24, CSF3, TAF1C, DNAAF1, HCAR2, ACO73072.5, IDO1, RP11-44K6.2, RP11-370F5.4, RP11-44K6.5, SNRPC, and APOE) displayed variability for both histone modifications in urate-primed cells compared to control conditions (Fig. 4E-F).

DNA methylation profiling reveals candidates for effects of serum urate levels *in vivo* in humans.

DNA methylation could also function as a basis for urate imprinting as it is a stable epigenetic mark, often associated with long-term gene silencing. In the Aotearoa New Zealand Māori participants, DNA methylation was determined and assessed in whole blood samples of hyperuricemic and normouricemic volunteers. Approximately 850K CpG sites were studied among the two groups and revealed 223 differentially methylated probes (difference in DNA methylation of at least 5%) (Fig. 5). 23 regions that exhibited significant differential methylation across the two groups of participants were found both in intergenic or intragenic regions of specific genes, one notable example being *HLA-G* (Fig. B-C). Individual differentially methylated probes and differentially methylated regions are listed in Table S4 and Table S5, respectively. An expanded list of candidates was revealed by data analysis of DNA methylation without cell composition correction (detailed information is provided in the supporting information material, Fig. S2, Tables S6 and S7).

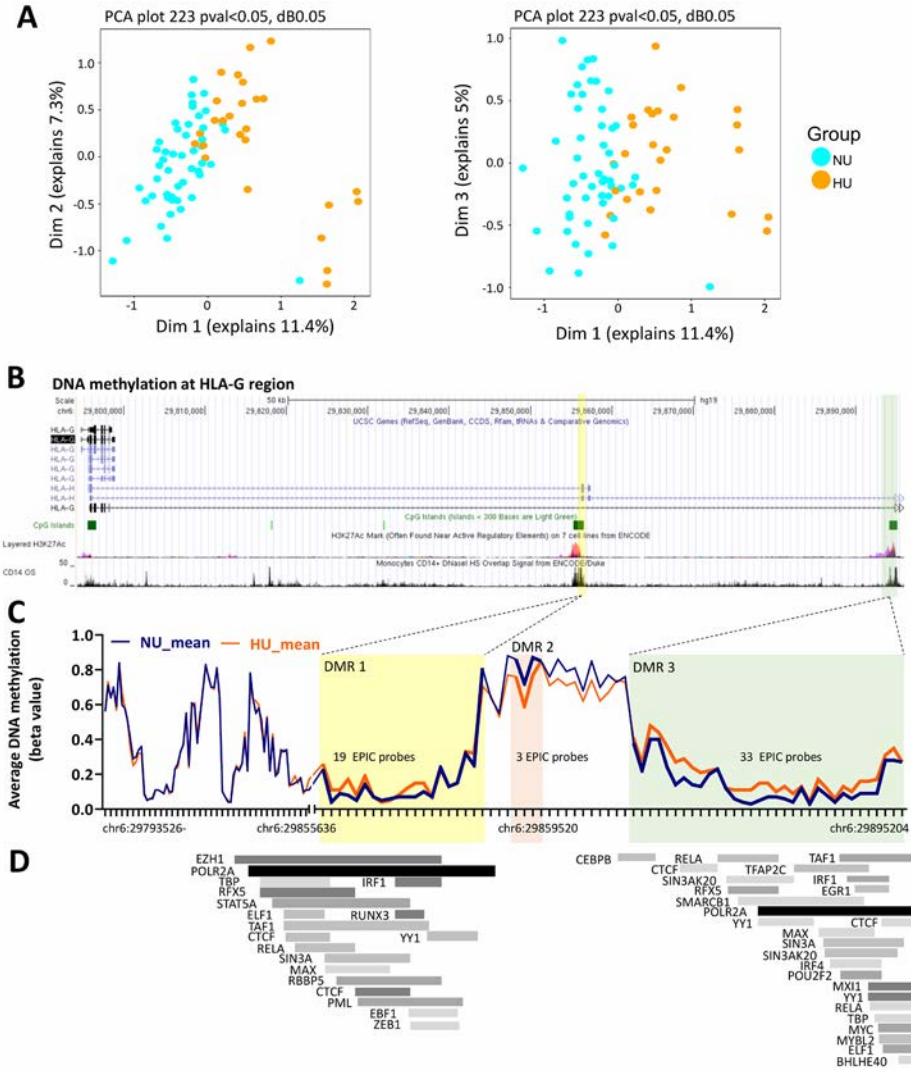


Figure 5. Differential DNA methylation in hyperuricemic versus normouricemic people. Principal component analysis of whole blood DNA methylation data obtained using Illumina InfiniumMethylationEPIC BeadChips in whole blood of 26 people with hyperuricemia compared to 50 normouricemic individuals (A). Differentially methylated regions (DMRs) at the *HLA-G* locus (B) and average DNA methylation levels (beta values) for all CpG probes found within *HLA-G* (ticks on the x axis represent individual probes and DNA chromosome position is indicated) (C). Transcription factors known to bind at the highlighted DMR1 and DMR3 regions according to the transcription factor ChIP-seq clusters from ENCODE with factorbook motifs (D).

Discussion

In this study, we assess the effects of exposing PBMCs of 85 healthy participants to soluble urate at concentrations of 10 mg/dL or 50 mg/dL *in vitro*. We show that both concentrations induce a higher IL-1 β release and a lower IL-1Ra production in response to subsequent stimulation with LPS or LPS+MSU crystals (Fig.1). We also describe persistent effects of the treatment with soluble urate in primary myeloid cells that were treated with urate for 24h, followed by medium removal and stimulation for another 24h with LPS or LPS+MSU crystals (in the absence of urate). The behavior of monocytes after priming for 24h with urate has been described previously, demonstrating that the cytokine production capacity of the cells switches to higher IL-1 β production and lower IL-1Ra basal concentrations[21], by activating AKT-PRAS40 and inhibiting autophagy[22]. Here, we demonstrate similar effects of urate at 10 mg/dL as high dose urate stimulations (50 mg/dL). Moreover, even after extended resting times between priming and restimulation, modified cytokine levels persisted in primary cells exposed to urate. IL-1Ra remained downregulated after 48h resting time (Fig.2 C-D). The increase in IL-6 remained present at all timepoints, although statistically significant differences were only observed after 5 days of rest in between stimulations (Fig.2 E-F). This may be due to the limited number of donors and high variability. Significant differences have been previously shown for IL-6 in past reports on urate priming, with direct stimulation at the end of the first 24h of urate exposure [33][21]. Other reports have shown that innate immune memory induced by β -glucan, BCG or oxidized LDL particles is best observed after 5 days resting intervals compared to 1 day rest or 3 days rest, possibly in connection with immunometabolism changes (glycolysis induction associated to innate immune memory) [34] IL-1 β induction upon stimulation was, however, markedly reduced at later incubation time points in all conditions (Fig.1A-B). As opposed to monocytes which express constitutively active caspase-1, in macrophages, the production of IL-1 β is more stringently regulated and needs two signals for active IL-1 β release: a PRR signal leading to proIL-1 β transcription and translation and an inflammasome activator which leads to the proteolysis of proIL-1 β into active IL-1 β [35]. Our results are in accordance with the restricted IL-1 β production in differentiated macrophages after longer *in vitro* culture of primary monocytes, due to inflammasome (caspase-1) inactivation[35].

Broad protein methylation inhibitor MTA was shown to reverse the urate effect *in vitro*[21]. Here we show reversal of inflammation in an *in vivo* model of gout in mice (Fig. 3). The pharmacological inhibition of the uricase enzyme using oxonic acid is a commonly used model to assess hyperuricemia in animal models where the uricase gene functionality is maintained[36, 37]. Previously, we have reported that oxonic acid and urate treatment in mice enhances inflammation triggered by intraarticular injections of palmitate and MSU crystals[22]. In the current study we show that this effect is reversible in mice that were subjected to MTA treatment prior to intraarticular injections, providing evidence that epigenetic modulators could be potential therapeutic agents for the proinflammatory effects associated to urate exposure. Given the broad effects of MTA it cannot be excluded that other processes, such as transcription factor methylation, are at play in urate priming.

To further decipher the involvement of histone marks in urate priming and persistence of effects, a genome-wide approach was undertaken in the pursuit of assessing epigenetic modifications globally. Two histone marks were analysed in the setting of urate priming: trimethylation of lysine 4 of histone 3 (H3K4me3) and acetylation of lysine 27 of histone 3 (H3K27ac). Both marks are associated with activation of gene expression across different cell types[38], have been previously studied in relation to other trained immunity stimuli in recent reports[25, 39], and are known to be present at the promoters of *IL1B* and *IL1RN* in monocytes[40]. The ChIPseq data (Fig. 4) shows lack of sample clustering based on urate exposure, indicating absence of genome wide effects for H3K4me3 and H3K27ac in this experiment. Nevertheless, given the small number of participants, targeted approaches at validating the hits which showed evidence of variability are likely to provide new understanding of urate-induced epigenetic effects. Target genes that are relevant for urate-mediated effects were identified in the histone modification datasets. The *IL1B* and *IL1A* genes encoding the IL-1 β and IL-1 α proinflammatory cytokines show enrichment of the H3K27ac epigenetic mark, which is consistent with previously shown induction of these cytokines by urate *in vitro* [21]. Twelve genes showed concordant variance in both H3K4me3 and H3K27ac (Fig. 4 E-F). Enrichment of both histone marks was highest for *MED24* (mediator complex subunit 24), *CSF3* (colony stimulating factor 3), *TAF1C* (TATA-box binding protein associated factor, RNA polymerase I subunit C), *DNAAF1* (dynein axonemal assembly factor 1), while both marks were downregulated for *APOE* (apolipoprotein E). APOE has been previously associated to gout and hyperuricemia as a potential link with hypertriglyceridaemia, a common

finding in patients with gout[41]. APOE has also been reported to coat MSU crystals and inhibit MSU-induced inflammatory signalling[42], therefore, the finding that urate exposure can lead to a reduction in H3K4me3 and H3K27ac (and, consequently, reduced chromatin accessibility) at the *APOE* locus, suggests, that this effect could be a point of study for the progression from hyperuricemia to gout. The validation of H3K27ac or H3K4me3 enrichment in response to lower concentrations of urate or in patients with hyperuricemia would be a useful next step. The fact that no differences are observed for LPS stimulation in our dataset is intriguing and could be attributable to the in vitro differentiation of the monocytes into macrophages in the presence of serum-supplemented culture medium. Serum is known to downregulate CD14 expression and to induce the release of CD14 in the extracellular space [43]. Moreover, in vitro culture of monocytes for 24h in standard conditions is reported to lead to the irreversible loss of MD2 activity [44]. Taken together these data suggest that serum-derived macrophages are less responsive to LPS due to CD14 and MD2 downregulation in standard culture conditions, which may explain the lack of significant alteration in the studied histone marks in response to the short 4 h stimulation with LPS.

We also studied the possibility of DNA methylation involvement in the proinflammatory effects associated to hyperuricemia in a sample set of New Zealand Māori ancestry [28]. The Māori population has 2-3-fold higher risk of gout compared to the population of European descent[45], likely contributed to by genetic susceptibility alleles that have increased in prevalence during the Pacific ancestral migrations, through mechanisms that are still debated[46]. By comparing DNA methylation status in hyperuricemic versus normouricemic volunteers within this cohort, 223 differentially methylated probes and 23 differentially methylated regions were identified in the vicinity of genes. Interestingly, three DMRs were found to be present at the *HLA-G* locus (human leukocyte associated antigen, class I, G) (Fig.5). Two of the *HLA-G* DMRs coincided with H3K27ac enrichment peaks (Fig.5B), CD14+ monocyte DNase I accessibility peaks (Fig.5B) and binding sites for several transcription factors (Fig.5D) (www.encodeproject.org), which is indicative of potential functional effects of the DNA methylation variance observed at these sites. *HLA-G* is a HLA-class Ib molecule with immunomodulatory properties across several tissues, which has recently been suggested to limit the progression of autoimmune and autoinflammatory disorders (extensively reviewed in[47]) and could be a promising target to study in gout.

Other candidates highlighted by the presence of two DMPs in the vicinity of the gene (Table S4) were *IFITM3* (Interferon Induced Transmembrane Protein 3) or *PRKAB2* (AMP-Activated Protein Kinase Subunit Beta 2, AMPK- β 2). Genes in the interferon signalling pathway have previously been reported to be differentially expressed (upregulated) in whole blood of healthy individuals administered rasburicase compared to placebo,[48]. In monocytes pre-treated with urate, transcriptomic analysis revealed downregulation of genes associated to GO term "Influenza A", which includes several interferon signalling related genes[22]. Moreover, type I interferons are known to inhibit STAT1 signalling and inflammasome activation[49], hence, urate-induced downregulation of interferon signalling could play a role in escalating IL-1 production and release. AMPK- β 2 is a regulatory subunit of AMP-activated protein kinase (AMPK). AMPK activation was shown to limit MSU crystal-induced IL-1 β production and to drive anti-inflammatory macrophage M2 polarisation[50]. DNA hypomethylation at the *PRKAG2* gene body (AMPK Subunit Gamma 2) was reported in gout patients compared to controls [50]. Furthermore, *PRKAG2* is one of the loci associated with hyperuricemia [12] and gout [51]. Our data suggest that urate exposure could modulate AMPK and interferon signalling pathways via DNA methylation in hyperuricemic people.

This report has the limitation of having studied a small number of donors for the assessment of genome-wide epigenetic modifications (monocytes of 4 donors and stimulations for ChIP sequencing, or 26 versus 50 volunteers for the DNA methylation study). Variation in histone modification or DNA methylation in no gene were found to be experimentally wide significant between urate-exposed and control. Nevertheless, there is evidence of variation correlated to urate exposure for all these epigenetic mechanisms in candidate genes. Further studies using larger sample sizes or targeted approaches based on these initial candidates are needed in order to find statistically significant effects. Since this report describes consequences of higher than normal urate levels, we cannot exclude that any of these effects could also be driven by the precipitated form of urate. For the *in vitro* experiments, using polarized light microscopy, we were not able to observe urate crystals formed during the 24 hours of exposure time for the described experimental conditions. Validating the changes in the histone mark landscape at lower concentrations of urate or in patients with hyperuricemia would be an important next step. Finally, the current study lacks mRNA data to show transcriptional regulation of cytokine genes in response to urate after differential resting periods. A previous report by our group showed that the gene expression of *IL1B*, *IL1RN* and *IL6* follows

the same trend as the protein levels at 24h [22]. Further assessment of the transcriptome of samples at later time-points after the initial encounter with urate would help understand the extent of persistence of the transcriptional programme induced by urate.

Conclusions

We have generated datasets involving epigenomic and functional immunological experiments to investigate potential major mechanisms involved in the urate priming of myeloid cells. Based on complementary methods we show that epigenetic changes are likely to play a role in mediating the persistent effects of urate exposure on innate immune cells. Our study shows that high levels of urate can persistently alter the cytokine production capacity of primary PBMCs *in vitro*, leading to increased IL-1 β and IL-6 production and reduced levels of IL-1 receptor antagonist (IL-1Ra). Uricase inhibition in mice led to higher inflammation scores upon intraarticular injection of MSU crystals and palmitate, and this effect was reversed by methyl transferase inhibition. We present here evidence that histone modifications (H3K4me3 or H3K27ac) and DNA methylation show differences in response to high urate exposure and provide potential candidates of differentially regulated targets. The differences in epigenetic regulation may provide new understanding and possibility for intervention in urate-dependent inflammatory responses as well as in the progression from hyperuricemia to gout.

Ethics approval and consent to participate

In-vitro experiments were approved by the Ethical Committee of Radboud University Nijmegen (nr. 42561.091.12). The animal experiments were approved by The Institutional Animal Care and Use Committees of the University of Colorado Denver, Aurora, CO (protocol #0035). The DNA methylation study was approved by the New Zealand Lower South Health and Disability Ethics Committee (MEC/05/10/130). All participants provided written informed consent. All experiments were conducted according to the principles of the Declaration of Helsinki.

References

- [1] Shi Y, Evans JE, Rock KL (2003) Molecular identification of a danger signal that alerts the immune system to dying cells. *Nature* 425:516–521
- [2] Kono H, Chen CJ, Ontiveros F, Rock KL (2010) Uric acid promotes an acute inflammatory response to sterile cell death in mice. *J Clin Invest* 120(6):1939–49.
- [3] Mandel NS, Mandel GS. Monosodium Urate Monohydrate, the Gout Culprit. *J Am Chem Soc* 1976; 14;98(8):2319–23.
- [4] Martinon F, Pétrilli V, Mayor A, et al. Gout-associated uric acid crystals activate the NALP3 inflammasome. *Nature* 2006; 440:237–241
- [5] Misawa T, Takahama M, Kozaki T, et al. Microtubule-driven spatial arrangement of mitochondria promotes activation of the NLRP3 inflammasome. *Nat Immunol* 2013; 14(5):454–60.
- [6] Giamarellos-Bourboulis EJ, Mouktaroudi M, Bodar E, Van Der Ven J, Kullberg BJ, Netea MG, Van Der Meer JWM. Crystals of monosodium urate monohydrate enhance lipopolysaccharide-induced release of interleukin 1 β by mononuclear cells through a caspase 1-mediated process. *Ann Rheum Dis* 2009; 68(2):273–8.
- [7] Mylona EE, Mouktaroudi M, Crisan TO, et al. Enhanced interleukin-1 β production of PBMCs from patients with gout after stimulation with Toll-like receptor-2 ligands and urate crystals. *Arthritis Res Ther* 2012; 4;14(4):R158.
- [8] Joosten LAB, Netea MG, Mylona E, et al. Engagement of fatty acids with toll-like receptor 2 drives interleukin-1 β production via the ASC/caspase 1 pathway in monosodium urate monohydrate crystal-induced gouty arthritis. *Arthritis Rheum* 2010; 62(11):3237–48.
- [9] An LL, Mehta P, Xu L, et al. Complement C5a potentiates uric acid crystal-induced IL-1 β production. *Eur J Immunol* 2014; 44(12):3669–79.
- [10] Dalbeth N, Merriman TR, Stamp LK. Gout. *Lancet* 2016; 388(10055):2039–52.
- [11] Pascual E. Persistence of monosodium urate crystals and low-grade inflammation in the synovial fluid of patients with untreated gout. *Arthritis Rheum* 1991; 34(2):141–5.
- [12] Köttgen A, Albrecht E, Teumer A, et al. Genome-wide association analyses identify 18 new loci associated with serum urate concentrations. *Nat Genet* 2013; 45:145–154.
- [13] Nakatochi M, Kanai M, Nakayama A, et al. Genome-wide meta-analysis identifies multiple novel loci associated with serum uric acid levels in Japanese individuals. *Commun Biol* 2019; 2:115.
- [14] Boocock J, Leask M, Okada Y, et al. Genomic dissection of 43 serum urate-associated loci provides multiple insights into molecular mechanisms of urate control. *Hum Mol Genet* 2020; 29(6):923–43.
- [15] Tin A, Marten J, Halperin Kuhns VL, et al. Target genes, variants, tissues and transcriptional pathways influencing human serum urate levels. *Nat Genet* 2019; 51(10):1459–74.
- [16] Dalbeth N, Stamp LK, Merriman TR. The genetics of gout: Towards personalised medicine? *BMC Med* 2017; 15(1):108.
- [17] Flynn TJ, Cadzow M, Dalbeth N, et al Positive association of tomato consumption with serum urate: Support for tomato consumption as an anecdotal trigger of gout flares. *BMC Musculoskelet Disord* 2015; 16:196.
- [18] Feldman N, Rotter-Maskowitz A, Okun E. DAMPs as mediators of sterile inflammation in aging-related pathologies. *Ageing Res Rev* 2015; 24(Pt A):29–39.

- [19] Athyros VG, Mikhailidis DP. Uric acid, chronic kidney disease and type 2 diabetes: A cluster of vascular risk factors. *J Diabetes Complications* 2014; 28(2):122-3.
- [20] Eisenbacher JL, Schrezenmeier H, Jahrsdörfer B, et al. S100A4 and Uric Acid Promote Mesenchymal Stromal Cell Induction of IL-10 + /IDO + Lymphocytes. *J Immunol* 2014; 192(12):6102-10.
- [21] Crişan TO, Cleophas MCP, Oosting M, et al. Soluble uric acid primes TLR-induced proinflammatory cytokine production by human primary cells via inhibition of IL-1Ra. *Ann Rheum Dis* 2016; 75:755-762
- [22] Crişan TO, Cleophas MCP, Novakovic B, et al. Uric acid priming in human monocytes is driven by the AKT-PRAS40 autophagy pathway. *Proc Natl Acad Sci U S A* 2017; 114(21):5485-90.
- [23] Netea MG, Quintin J, Van Der Meer JWM. Trained immunity: A memory for innate host defense. *Cell Host Microbe* 2011; 9(5):355-61.
- [24] Quintin J, Saeed S, Martens JHA, et al. *Candida albicans* infection affords protection against reinfection via functional reprogramming of monocytes. *Cell Host Microbe* 2012; 12(2):223-32.
- [25] Saeed S, Quintin J, Kerstens HHD, et al. Epigenetic programming of monocyte-to-macrophage differentiation and trained innate immunity. *Science* 2014; 345(6204):1251086.
- [26] Bekkering S, Quintin J, Joosten LAB, et al. Oxidized low-density lipoprotein induces long-term proinflammatory cytokine production and foam cell formation via epigenetic reprogramming of monocytes. *Arterioscler Thromb Vasc Biol* 2014; 34(8):1731-8.
- [27] Van Der Valk FM, Bekkering S, Kroon J, et al. Oxidized phospholipids on Lipoprotein(a) elicit arterial wall inflammation and an inflammatory monocyte response in humans. *Circulation* 2016; 134(8):611-24.
- [28] Wang Z, Zhao Y, Phipps-Green A, et al. Differential DNA Methylation of Networked Signaling, Transcriptional, Innate and Adaptive Immunity, and Osteoclastogenesis Genes and Pathways in Gout. *Arthritis Rheumatol* 2020; 72(5):802-14.
- [29] Li Y, Oosting M, Deelen P, et al. Inter-individual variability and genetic influences on cytokine responses to bacteria and fungi. *Nat Med* 2016; 22(8):952-60.
- [30] Repnik U, Knezevic M, Jeras M. Simple and cost-effective isolation of monocytes from buffy coats. *J Immunol Methods* 2003; 278(1-2):283-92.
- [31] Novakovic B, Habibi E, Wang SY, et al. β -Glucan Reverses the Epigenetic State of LPS-Induced Immunological Tolerance. *Cell* 2016; 167(5):1354-1368.e14.
- [32] Pidsley R, Zotenko E, Peters TJ, et al. Critical evaluation of the Illumina MethylationEPIC BeadChip microarray for whole-genome DNA methylation profiling. *Genome Biol* 2016; 17(1):208.
- [33] Crişan TO, Cleophas MCP, Novakovic B, et al. Uric acid priming in human monocytes is driven by the AKT-PRAS40 autophagy pathway. *Proc Natl Acad Sci* 2017; 114: 5485-90.
- [34] Bekkering S, Blok BA, Joosten LAB, et al. In Vitro experimental model of trained innate immunity in human primary monocytes. *Clin Vaccine Immunol* 2016; 23:926-933.
- [35] Netea MG, Nold-Petry CA, Nold MF, et al. Differential requirement for the activation of the inflammasome for processing and release of IL-1 β in monocytes and macrophages. *Blood* 2009; 113(10):2324-35.
- [36] Dankers ACA, Mutsaers HAM, Dijkman HBPM, et al. Hyperuricemia influences tryptophan metabolism via inhibition of multidrug resistance protein 4 (MRP4) and breast cancer resistance protein (BCRP). *Biochim Biophys Acta - Mol Basis Dis* 2013; 1832(10):1715-22.

- [37] Patschan D, Patschan S, Gobe GG, et al. Uric acid heralds ischemic tissue injury to mobilize endothelial progenitor cells. *J Am Soc Nephrol* 2007; 18(5):1516-24.
- [38] Heintzman ND, Hon GC, Hawkins RD, et al. Histone modifications at human enhancers reflect global cell-type-specific gene expression. *Nature* 2009; 459(7243):108-12.
- [39] Cheng SC, Quintin J, Cramer RA, et al. MTOR- and HIF-1 α -mediated aerobic glycolysis as metabolic basis for trained immunity. *Science* 2014; 346(6210):aaa1503.
- [40] Yates A, Akanni W, Amode MR, et al. Ensembl 2016. *Nucleic Acids Res* 2016; 44(D1):D710-6.
- [41] Moriwaki Y, Yamamoto T, Takahashi S, et al. Apolipoprotein E phenotypes in patients with gout: Relation with hypertriglyceridaemia. *Ann Rheum Dis* 1995; 54(5):351-4.
- [42] Terkeltaub RA, Dyer CA, Martin J, et al. Apolipoprotein (Apo) E inhibits the capacity of monosodium urate crystals to stimulate neutrophils. Characterization of intraarticular Apo E and demonstration of Apo E binding to urate crystals in vivo. *J Clin Invest* 1991; 87(1):20-6.
- [43] Ruppert J, Schtitt C, Ostermeier D, Peters JH CD14. 281-286
- [44] Kennedy MN, Mullen GED, Leifer CA, et al. A complex of soluble MD-2 and lipopolysaccharide serves as an activating ligand for toll-like receptor 4. *J Biol Chem* 2004; 279:34698-704.
- [45] Dalbeth N, Dowell T, Gerard C, et al. Gout in aotearoa New Zealand: The equity crisis continues in plain sight. *N. Z. Med. J* 2018; 131(1485):8-12.
- [46] Gosling AL, Buckley HR, Matisoo-Smith E, et al. Pacific Populations, Metabolic Disease and "Just-So Stories": A Critique of the "Thrifty Genotype" Hypothesis in Oceania. *Ann Hum Genet* 2015; 79(6):470-80.
- [47] Morandi F, Rizzo R, Fainardi E, et al. Recent advances in our understanding of HLA-G biology: Lessons from a wide spectrum of human diseases. *J Immunol Res* 2016;;2016:4326495.
- [48] Tanaka T, Milaneschi Y, Zhang Y, et al. A double blind placebo controlled randomized trial of the effect of acute uric acid changes on inflammatory markers in humans: A pilot study. *PLoS One* 2017; 12(8):e0181100.
- [49] Dasgupta B, Ju JS, Sasaki Y, et al. The AMPK 2 Subunit Is Required for Energy Homeostasis during Metabolic Stress. *Mol Cell Biol* 2012; 32(14):2837-48.
- [50] Wang Y, Viollet B, Terkeltaub R, et al. AMP-activated protein kinase suppresses urate crystal-induced inflammation and transduces colchicine effects in macrophages. *Ann Rheum Dis* 2016; 75:286-94.
- [51] Phipps-Green AJ, Merriman ME, Topless R, et al. Twenty-eight loci that influence serum urate levels: Analysis of association with gout. *Ann Rheum Dis* 2016; 75(1):124-30.

Supplementary material

Materials and methods

Participants

Venous blood was drawn from the cubital vein of Dutch participants without gout into EDTA tubes. Urate priming experiments were performed in freshly isolated PBMCs of 85 healthy volunteers of Dutch nationality from the 200 Functional Genomics (200FG) cohort in the Human Functional Genomics Project (<http://www.humanfunctionalgenomics.org>) [1]. Experiments requiring large amounts of cells were performed using cells isolated from buffy coats after overnight storage at room temperature (Sanquin blood bank, Nijmegen, The Netherlands). Stimulation experiments were approved by the Ethical Committee of Radboud University Nijmegen (nr. 42561.091.12) and were conducted according to the principles of the Declaration of Helsinki. The DNA methylation study was approved by the New Zealand Lower South Health and Disability Ethics Committee (MEC/05/10/130). The study included 76 individuals of New Zealand Māori ancestry (Table S1), 36 men and 40 women, with a range of serum urate values (average 0.37 mmol/L, +/- standard deviation 0.12 mmol/L, range 0.6 mmol/L), who for further analysis were segregated into a hyperuricemia group (0.42 mmol/L or higher) (n=26) or a normouricemia (n=50) group. All participants provided written informed consent. Patients or the public were not involved in the design, conduct, reporting, or dissemination of our research.

Reagents

Urate, lipopolysaccharide (LPS, *E. coli* serotype 055:B5), and 5'-S-methyl-5'-thioadenosine (methylthioadenosine, MTA) were purchased from Sigma. LPS was subjected to ultra-purification before cell culture experiments. Monosodium urate (MSU) crystals were prepared inhouse as previously described[2].

PBMC and monocyte isolation

Human PBMCs were separated using Ficoll-Paque (Pharmacia Biotech) and suspended in culture medium RPMI (Roswell Park Memorial Institute 1640). Monocytes were enriched using hyperosmotic Percol solution[3] and were subsequently purified by negative selection using the Pan Monocyte Isolation kit (Miltenyi Biotec) according to the manufacturer's instructions. This led to a cell suspension containing monocytes with 85-95% purity.

Stimulation experiments

Experiments were performed in culture medium containing RPMI 1640, supplemented with 50 µg/mL gentamicin, 2 mM L-glutamine, 1 mM pyruvate and 10% human pooled serum following an *in vitro* urate priming protocol described extensively elsewhere[4]. For ChIP-seq experiments, 5x10⁶ human monocytes were seeded in Petri dishes (Corning) and were primed for 20 hours followed by addition of medium or LPS 10 ng/mL for another 4 h. Cells from all donors used for ChIP-seq were also used in a separate experiment conducted in parallel for RNA-seq assessment and for control experiments to test if the expected urate priming phenotype was present. The experimental setup, purity of cells and cytokine control experiments were as previously described[4]. For the *in vitro* experiments, using polarized light microscopy, we were not able to observe urate crystals formed during the 24 hours of exposure time for the described experimental conditions.

Cytokine measurements

Cytokine concentrations were determined in supernatants of cell culture using specific sandwich ELISA kits for interleukin-1β (IL-1β), IL-1Ra (receptor antagonist) (R&D Systems), and IL-6 (Sanquin) according to the manufacturer's instructions.

Animal model

Male 10–12 week-old C57Bl/6J mice were purchased from Jackson Laboratories (Bar Harbor, Maine, USA), a total of five males were selected per group. The experiments were approved by The Institutional Animal Care and Use Committees of the University of Colorado Denver, Aurora, CO (protocol #0035) and were conducted according to the principles of the Declaration of Helsinki. Uricase was inhibited using oxonic acid and urate was administered in order to increase serum urate levels according to a previously described protocol[4]. At Day 0, mice were given oxonic acid orally 140 mg/kg, 2 times/day (in the morning and in the evening). Each administration was followed after 2 hours by urate 4 mg/kg, intraperitoneally, in the presence of MTA 30 mg/kg or equivalent volumes of vehicle control. At Day 1, the same treatment as Day 0 was performed, together with induction of gouty arthritis at noon. Gouty arthritis was induced by intra-articular injection (i.a.) of 300 µg MSU crystals and 200 µM palmitic acid (C16) in a volume of 10 µl phosphate buffered saline (PBS) as previously described in both the right and left knee joints of each mouse [2–5]. 24h after injection, mice were sacrificed, knees were macroscopically scored for joint thickness after removal of skin resulting

in 10 joints in total, 5 mice per group (scores ranging from 0 to 3), followed by harvesting of joints for histology (only the right knee joint of the mice). Histology was performed as previously described[2].

ChIP sequencing preparation and analysis

Immediately after cell isolation and after stimulation, samples were subjected to DNA-histone crosslinking by treatment with 1% formaldehyde for 10 minutes followed by treatment with 1.25 mol/L glycine for another 3 minutes. For cultured cells, floating medium and cells were removed followed by three cycles of scraping and recovering adherent fixated cells ($2.4\text{--}4.8 \times 10^6$ cells could be recovered from 5×10^6 plated monocytes). Samples were stored at 4°C in PBS containing complete phosphate inhibitor cocktail until sonicated and subjected to chromatin immunoprecipitation as previously described[6]. Briefly, fixed cell preparations were sonicated using a Diagenode Bioruptor UCD-300 for 3x 10min (30s on; 30s off). 67µl of chromatin (1 million cells) was incubated with 229µl dilution buffer, 3µl protease inhibitor cocktail and 0.5–1µg of H3K27ac or H3K4me3 antibodies (Diagenode) and incubated overnight at 4°C with rotation. Protein A/G magnetic beads were washed in dilution buffer with 0.15% SDS and 0.1% BSA, added to the chromatin/antibody mix and rotated for 60 min at 4°C. Beads were washed with 400µl of buffer for 5min at 4°C with five rounds of washes. Chromatin was eluted using an elution buffer for 20min. Supernatant was collected, 8µl 5M NaCl, 3µl proteinase K were added and samples were incubated for 4hr at 65°C. Finally, samples were purified using QIAGEN; Qiaquick MinElute PCR purification Kit and eluted in 20µl EB. Detailed protocols can be found on the Blueprint website (http://www.blueprint-epigenome.eu/UserFiles/file/Protocols/Histone_ChIP_May2013.pdf).

Illumina library preparation was done as previously described[6], using the Kapa Hyper Prep Kit. Samples were purified using the QIAquick MinElute PCR purification kit and 300bp fragments selected using E-gel. Correct size selection was confirmed by BioAnalyzer analysis. Sequencing was performed using Illumina HiSeq 2000 machines and generated 43bp single end reads. Sequence reads were aligned to human genome assembly hg19 (NCBI version 37) using bwa. Duplicate reads were removed after alignment with Picard tools. For peak calling the BAM files were first filtered to remove the reads with mapping quality less than 15, followed by fragment size modeling (<https://code.google.com/archive/p/phantompeakqualtools/>) and MACS2 (<https://github.com/taoliu/MACS/>) was used to call the peaks. For each histone mark dataset, the data

were normalized using the R package DESeq2 and then pair-wise comparisons were performed (fold change 3, adjusted p-value < 0.05 and reads per kilo base per million mapped reads ≥ 2) to determine the differentially expressed genes per condition. The results from all possible pairwise comparisons (within each condition and similar time points across all conditions per mark) were pooled and merged to define the dynamic set of enriched regions.

DNA methylation analysis

Genomic DNA was isolated from peripheral blood of 76 individuals of New Zealand Māori ancestry with varying serum urate levels. Genome-wide methylation analysis was performed using Illumina InfiniumMethylationEPIC BeadChips (referred to from now as 'EPIC array') [7]. The EPIC array measures DNA methylation level at more than 850,000 CpG sites (referred to as 'EPIC probes'), and covers all gene promoters, gene bodies and ENCODE-assigned distal regulatory elements [8].

Raw IDAT files were processed and analysed using the MissMethyl and minfi packages for R [9, 10], both available from Bioconductor [11]. Samples were checked for quality, with all samples remaining for analysis (all with a mean detection p-value of < 0.01). A total of 50 controls and 26 hyperuricemia samples were used for analysis.

Data were normalized for both within and between array technical variation using SWAN (Subset-quantile Within Array Normalization) [12]. A total of 798,740 probes were used for analysis after removal of poor probes, probes that overlap SNPs with MAF > 0%, and cross hybridising probes. Cell composition was determined using the estimateCellCounts tool, with the 'Blood' reference data used for adult peripheral blood analysis [13]. Differential methylation analysis by linear regression modelling was performed using limma [14]. Differential methylation analysis with and without cell composition correction was performed.

Differentially methylated probes (DMPs) were identified as those having a p-value of < 0.05 and a change in methylation (delta beta or $\Delta\beta$) of $\geq 5\%$. Differentially methylated regions (DMRs) were identified using the DMRcate tool [15].

Statistical analysis

Cytokine data were analysed using GraphPad Prism version 8. The differences were analysed using Friedmann or Wilcoxon signed rank test after testing

for distribution normality. Data were considered statistically significant at a $p\text{-value} < 0.05$. Data is shown as individual or cumulative results of levels obtained in all volunteers (means \pm SEM). ChIP sequencing and DNA methylation data were analysed using R.

Results

ChIP-Seq analysis in freshly isolated monocytes at day 0 displays a marked clustering feature compared to all stimulated samples obtained at day 1.

To assess whether the ChIP-seq data showed differences in freshly isolated monocytes compared to cultured monocytes, samples before and after culturing conditions were included in the analysis. The data was reanalysed with an extra negative control sample for each of the four donors, which was prepared from freshly isolated monocytes, at day 0, before culture. The analyses performed using day 0 samples and day 1 samples (with the 4 conditions described – RPMI or urate primed cells stimulated with either control medium or LPS) revealed distinct features of the samples obtained at day 0 compared to all samples obtained at day 1.

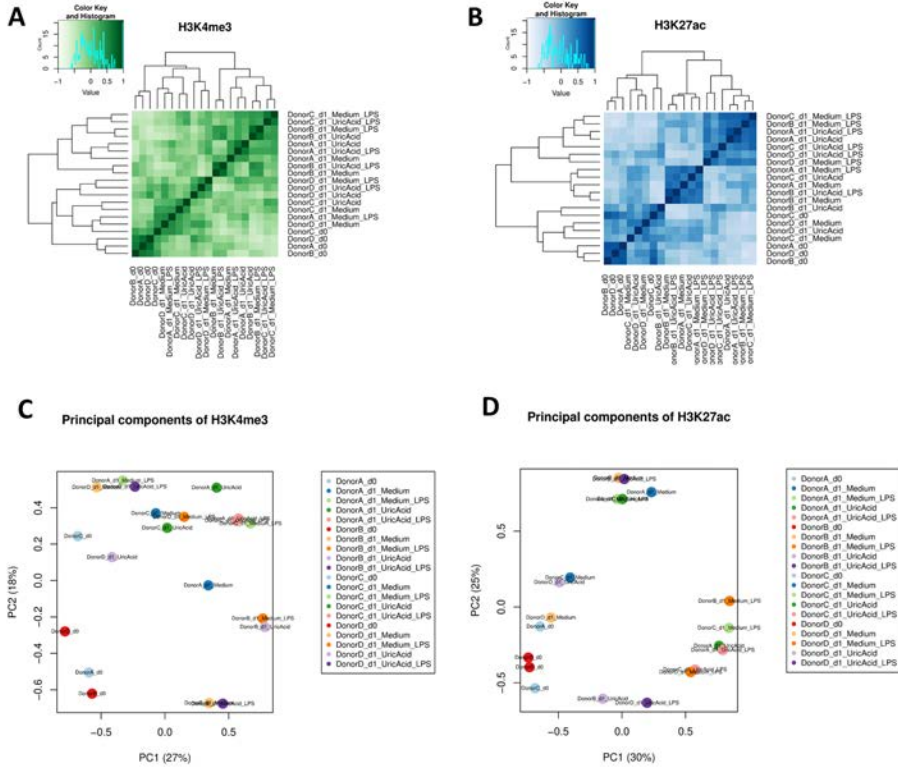


Figure S1. ChIP-Seq analysis in freshly isolated monocytes at day 0 (d0), without culturing, reveals distinct clustering features compared to all stimulated samples obtained at day 1 (d1). Cluster and principal component analysis of datasets obtained on ChIP sequencing for H3K4me3 (A and C) or H3K27ac (B and D) in 4 different donors (labelled D1-4) and 4 different conditions (Medium, Urate, Medium+LPS, Urate+LPS).

DNA methylation profiling without cell composition correction reveals an expanded list of candidates for effects of urate in vivo in humans.

To obtain additional information regarding the DNA methylation patterns associated to hyperuricemia, DNA methylation data were also analysed without correction for cell composition. This second analysis revealed 676 differentially methylated probes (which consisted of a difference in DNA methylation of at least 5%) and 55 differentially methylated regions (Tables S6 and S7, respectively). The *HLA-G* locus was consistently identified by both types of analyses. Regions that depicted significant differential methylation over the two groups of patients were found in intergenic or intragenic regions of certain genes, of which a list of candidate genes are shown in Fig.6A. One interesting example with possible roles for the modulation of the IL-1 β /IL-1Ra

pathway is *SOCS3*, which exhibited three significantly differentially methylated CpG probes that were found intragenically (Fig.S2) and which showed higher methylation in hyperuricemic compared to normouricemic patients (Fig.S2 D). Publicly available data from the ENCODE database show that this region includes transcription factor binding sites that could be influenced by variable methylation and chromatin accessibility (Fig.S2 E).

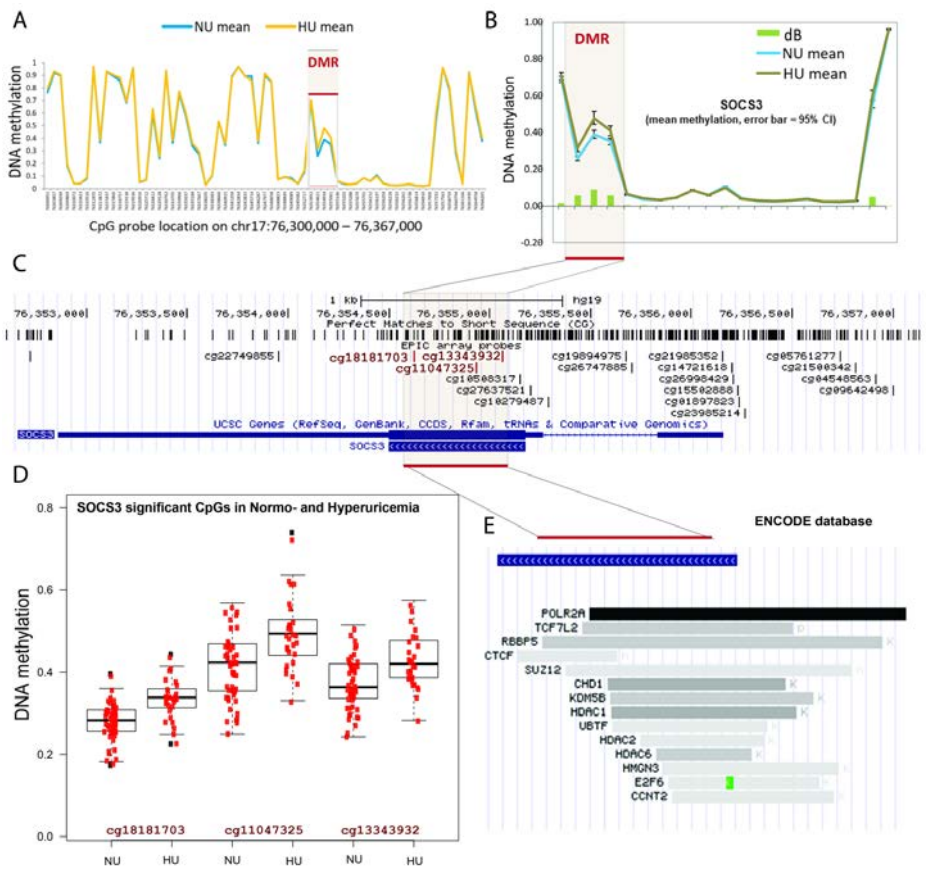


Figure S2. Differential DNA methylation analysis (without cell composition correction) in hyperuricemic versus normouricemic people. DNA methylation levels (A) and absolute change in mean methylation between hyperuricemic (HU) and normouricemic (NU) people (B). UCSC genome browser snapshot of 3 intragenic probes located at the *SOCS3* locus (C). Individual methylation levels in NU compared to HU people for the 3 highlighted *SOCS3* probes (D). Transcription factors known to bind at the highlighted DMR region according to the transcription factor ChIP-seq clusters from ENCODE with factorbook motifs (E).

Discussion

Recently, the use of the cell composition correction (Houseman correction,[16]) for whole blood DNA methylation data was challenged due to the possible violation of the no multicollinearity assumption in statistical regression models[17]. This possibility is of particular relevance for studies in which the assessed outcomes are represented by inflammatory phenotypes, because inflammation can be associated to cell-type composition variation[17]. For this reason, in this study, DNA methylation was determined and assessed between hyperuricemic and normouricemic volunteers by using both cell composition correction (as described in the main text of this manuscript) and no correction for cell composition. While this analysis identified 163 differentially methylated probes and 10 differentially methylated regions which were common for the targets identified by the two types of analyses (data not shown), new targets were also revealed. One example is *SOCS3* (suppressor of cytokine signalling 3), a regulator of STAT3 signalling with broad roles in cytokine signalling[18, 19], mostly associated with negative feedback inhibition of proinflammatory cytokines[20, 21]. Our data show higher DNA methylation in hyperuricemic individuals at 3 neighbouring *SOCS3* intragenic regions (Fig.S2). Since the functionality of this higher methylation status is not known, future validation studies are necessary to show whether *SOCS3* levels are indeed modified in the context of urate exposure *in vitro* or *in vivo*. If *SOCS3* levels are diminished, this could typically coincide with less STAT3 inhibition and promotion of proinflammatory cytokines production[20, 21]. However, *SOCS3* has been shown to have the dual role of upregulating TLR4 induced cytokines by TGF β inhibition[22]. Therefore, the possible consequences of *SOCS3* regulation in the context of urate priming are an interesting pathway to be tested and further validated in patients.

Supplementary tables

Table S1. Patient characteristics for DNA methylation study.

Group	Subjects	Age	Sex	BMI	Serum urate	Gout
HU	n = 26	Min.:20.00	F = 7	Min.:30.40	Min.:0.4200	n = 15
		1st Qu.:41.00	M = 19	1st Qu.:33.92	1st Qu.:0.4425	
		Median :47.50		Median:37.20	Median :0.4800	
		Mean:47.88		Mean:39.74	Mean:0.4919	
		3rd Qu.:59.50		3rd Qu.:42.06	3rd Qu.:0.5200	
		Max.:70.00		Max.:66.90	Max.:0.6700	
NU	n = 50	Min.:25.00	F = 33	Min.:27.01	Min.:0.0700	n = 14
		1st Qu.:42.25	M = 17	1st Qu.:32.06	1st Qu.:0.2725	
		Median :52.00		Median :35.66	Median :0.3300	
		Mean:51.52		Mean:36.74	Mean:0.3104	
		3rd Qu.:62.00		3rd Qu.:39.66	3rd Qu.:0.3800	
		Max.:83.00		Max.:56.25	Max.:0.4100	

NU=Normouricaemia, HU=Hyperuricaemia; Serum urate levels = mmol/L; NU <0.42mmol/L, HU> 0.42mmol/L.

Table S2. Genes showing enrichment of histone modification H3K4me3.

ENSEMBL gene ID	gene name	function	chr	Log 2 Fold change	p-val
ENSG00000008838	MED24	protein_coding	chr17	3,4531	0,0036
ENSG00000108342	CSF3	protein_coding	chr17	3,4531	0,0036
ENSG00000103168	TAF1C	protein_coding	chr16	3,2611	0,0016
ENSG00000154099	DNAAF1	protein_coding	chr16	3,2611	0,0016
ENSG00000182782	HCAR2	protein_coding	chr12	2,7893	0,0035
ENSG00000255398	HCAR3	protein_coding	chr12	2,4391	0,0051
ENSG00000256249	RP11-324E6.6	lincRNA	chr12	2,4391	0,0051
ENSG00000166278	C2	protein_coding	chr6	2,1957	0,0172
ENSG00000179428	AC073072.5	antisense	chr7	1,8949	0,0109
ENSG00000131203	IDO1	protein_coding	chr8	1,7988	0,0162
ENSG00000253838	RP11-44K6.2	sense_intronic	chr8	1,7988	0,0162
ENSG00000171855	IFNB1	protein_coding	chr9	1,7420	0,0444
ENSG00000203364	RP11-370F5.4	lincRNA	chr9	1,7082	0,0317
ENSG00000115009	CCL20	protein_coding	chr2	1,4683	0,0118
ENSG00000229172	AC073065.3	pseudogene	chr2	1,4683	0,0118
ENSG00000253320	KB-1507C5.2	protein_coding	chr8	1,4589	0,0305
ENSG00000237568	RP4-620F22.2	antisense	chr1	1,3998	0,0438
ENSG00000140379	BCL2A1	protein_coding	chr15	1,3622	0,0187
ENSG00000253790	RP11-44K6.5	pseudogene	chr8	1,3460	0,0384
ENSG00000095970	TREM2	protein_coding	chr6	-1,4660	0,0192
ENSG00000124562	SNRPC	protein_coding	chr6	-1,5600	0,0009
ENSG00000130203	APOE	protein_coding	chr19	-1,6253	0,0146

Table S3. Genes showing enrichment of histone modification H3K27ac.

ENSEMBL gene ID	gene name	function	chr	Log 2 Fold change	p-val
ENSG00000240481	Metazoa_SRP	misc_RNA	chr9	2,6607	0,0494
ENSG00000169184	MN1	protein_coding	chr22	2,4834	0,0083
ENSG00000203364	RP11-370F5.4	lincRNA	chr9	2,3311	0,0298
ENSG00000231525	AC002486.2	processed_pseudogene	chr7	2,3170	0,0237
ENSG00000240624	RP11-45P15.2	processed_pseudogene	chr14	2,2890	0,0334
ENSG00000234496	MRPS21P1	processed_pseudogene	chr1	2,2565	0,0380
ENSG00000008838	MED24	protein_coding	chr17	2,2487	0,0314
ENSG00000108342	CSF3	protein_coding	chr17	2,2487	0,0314
ENSG00000238793	SNORD124	snoRNA	chr17	2,2487	0,0314
ENSG00000131203	IDO1	protein_coding	chr8	2,1271	0,0298
ENSG00000253838	RP11-44K6.2	sense_intronic	chr8	2,1271	0,0298
ENSG00000101460	MAP1LC3A	protein_coding	chr20	2,1127	0,0241
ENSG00000101464	PIGU	protein_coding	chr20	2,1127	0,0241
ENSG00000134460	IL2RA	protein_coding	chr10	2,0580	0,0362
ENSG00000251922	SNORA14	snoRNA	chr10	2,0580	0,0362
ENSG00000105855	ITGB8	retained_intron	chr7	2,0193	0,0351
ENSG00000248719	RP11-377G16.2	antisense	chr4	2,0036	0,0298
ENSG00000179428	AC073072.5	antisense	chr7	1,9881	0,0318
ENSG00000188676	IDO2	processed_transcript	chr8	1,9871	0,0482
ENSG00000253790	RP11-44K6.5	processed_pseudogene	chr8	1,9871	0,0482
ENSG00000103168	TAF1C	protein_coding	chr16	1,9753	0,0227
ENSG00000154099	DNAAF1	retained_intron	chr16	1,9753	0,0227
ENSG00000115008	IL1A	protein_coding	chr2	1,9373	0,0193
ENSG00000125538	IL1B	protein_coding	chr2	1,9373	0,0193
ENSG00000221541	AC079753.1	miRNA	chr2	1,9373	0,0193
ENSG00000244104	Metazoa_SRP	misc_RNA	chr12	1,8827	0,0098
ENSG00000234869	RP3-439F8.1	antisense	chr22	1,8560	0,0305
ENSG00000129277	CCL4	protein_coding	chr17	1,8478	0,0370
ENSG00000263488	Metazoa_SRP	misc_RNA	chr17	1,8478	0,0370
ENSG00000264684	MIR4773-2	miRNA	chr2	1,8258	0,0384
ENSG00000234956	RP11-356I2.1	lincRNA	chr6	1,8221	0,0219
ENSG00000232591	RP5-1031D4.2	lincRNA	chr10	1,7670	0,0050
ENSG00000250762	RP1-313L4.4	unprocessed_pseudogene	chr1	1,7670	0,0408
ENSG00000259090	RP11-173D9.5	processed_pseudogene	chr14	1,7077	0,0378
ENSG00000128271	ADORA2A	processed_transcript	chr22	1,6242	0,0166
ENSG00000178803	ADORA2A-AS1	protein_coding	chr22	1,6242	0,0166
ENSG00000258555	SPECC1L	nonsense_mediated_decay	chr22	1,6242	0,0166
ENSG00000168260	C14orf183	protein_coding	chr14	1,5943	0,0289
ENSG00000251792	Y_RNA	misc_RNA	chr14	1,5943	0,0289

Table S3. Continued

ENSEMBL gene ID	gene name	function	chr	Log 2 Fold change	p-val
ENSG00000110047	EHD1	protein_coding	chr11	1,5784	0,0121
ENSG00000226169	RP11-375H17.1	antisense	chr22	1,5761	0,0165
ENSG00000251230	RP11-701P16.5	processed_transcript	chr4	1,5183	0,0464
ENSG00000266698	MIR3945	miRNA	chr4	1,5183	0,0464
ENSG00000235842	RP11-356I2.2	processed_transcript	chr6	1,5052	0,0469
ENSG00000160325	CACFD1	protein_coding	chr9	1,5017	0,0153
ENSG00000160326	SLC2A6	protein_coding	chr9	1,5017	0,0153
ENSG00000227898	RP13-100B2.4	antisense	chr9	1,5017	0,0153
ENSG00000228923	AP000355.2	antisense	chr22	1,4950	0,0496
ENSG00000254693	RP11-58K22.5	antisense	chr11	1,4674	0,0285
ENSG00000227269	RP11-96L7.2	lincRNA	chr9	1,4561	0,0494
ENSG00000240235	Metazoa_SRP	misc_RNA	chr9	1,4561	0,0165
ENSG00000268621	AC006262.5	lincRNA	chr19	1,4445	0,0308
ENSG00000181577	C6orf223	retained_intron	chr6	1,4410	0,0011
ENSG00000238486	snoU13	snoRNA	chr19	1,4326	0,0351
ENSG00000173578	XCR1	protein_coding	chr3	1,4309	0,0429
ENSG00000182782	HCAR2	protein_coding	chr12	1,4093	0,0343
ENSG00000184588	PDE4B	protein_coding	chr1	1,3800	0,0432
ENSG00000169429	IL8	protein_coding	chr4	1,3583	0,0207
ENSG00000228277	AC112518.3	lincRNA	chr4	1,3583	0,0207
ENSG00000101337	TM9SF4	protein_coding	chr20	1,3472	0,0054
ENSG00000232759	AC002480.3	processed_transcript	chr7	-1,3221	0,0487
ENSG00000223009	AL138930.1	miRNA	chr1	-1,3501	0,0027
ENSG00000235007	RP11-344B5.4	lincRNA	chr9	-1,3508	0,0467
ENSG00000124562	SNRPC	protein_coding	chr6	-1,3638	0,0133
ENSG00000232131	RP1-293L8.5	antisense	chr6	-1,4102	0,0082
ENSG00000130203	APOE	protein_coding	chr19	-1,4381	0,0177
ENSG00000267009	RP11-120M18.2	processed_transcript	chr17	-1,4398	0,0217
ENSG00000110079	MS4A4A	protein_coding	chr11	-1,4508	0,0047
ENSG00000260872	RP11-680G24.5	antisense	chr16	-1,4750	0,0065
ENSG00000170323	FABP4	protein_coding	chr8	-1,4973	0,0092
ENSG00000141293	SKAP1	protein_coding	chr17	-1,5263	0,0231
ENSG00000269843	CTC-490E21.10	lincRNA	chr19	-1,5742	0,0419
ENSG00000197849	OR8G7P	unprocessed_pseudogene	chr11	-1,6011	0,0004
ENSG00000255298	OR8G1	unprocessed_pseudogene	chr11	-1,6011	0,0004
ENSG00000204872	AC092653.5	unprocessed_pseudogene	chr2	-1,6486	0,0430
ENSG00000230490	RP11-141M1.3	lincRNA	chr13	-1,6965	0,0169
ENSG00000217746	RP1-303A1.1	processed_pseudogene	chr6	-1,6984	0,0112
ENSG00000235899	RP11-345L23.1	antisense	chr6	-1,9337	0,0001

Table S4. Differentially methylated probes in whole blood of people with hyperuricemia compared to normouricemic people with cell composition correction

Nr.	probe ID	nearest gene (distance in bp)	chr	NU_mean	HU_mean	dB	P.Value
1	cg20482334	FASN (+7677)	chr17	0.715	0.858	0.143	0.0098
2	cg21224286	LRTM2 (-19517)	chr12	0.474	0.611	0.137	0.0016
3	cg12859507	LRTM2 (-19470)	chr12	0.289	0.415	0.126	0.0022
4	cg21022775	AREG (+28658)	chr4	0.685	0.810	0.126	0.0408
5	cg20347269	P2RX1 (+11637)	chr17	0.498	0.623	0.124	0.0003
6	cg18850127	POU6F2 (+152900)	chr7	0.484	0.608	0.124	0.0231
7	cg24751894	HLA-G (+99386)	chr6	0.144	0.266	0.123	0.0071
8	cg18786623	HLA-G (+99295)	chr6	0.239	0.361	0.121	0.0066
9	cg15212455	POU6F2 (+152942)	chr7	0.545	0.662	0.117	0.0153
10	cg15070894	HLA-G (+99407)	chr6	0.180	0.291	0.111	0.0072
11	cg04520169	HLA-G (+99440)	chr6	0.138	0.240	0.103	0.0300
12	cg08951186	ZNF469 (-203509)	chr16	0.531	0.631	0.101	0.0295
13	cg26175789	EVA1A (-25045)	chr2	0.385	0.485	0.100	0.0173
14	cg07973162	UGT2B17 (-1006)	chr4	0.409	0.504	0.095	0.0179
15	cg08231349	HLA-G (+99889)	chr6	0.051	0.146	0.095	0.0043
16	cg03806328	ARHGAP32 (-67539)	chr11	0.588	0.683	0.095	0.0226
17	cg13365324	UGT2B17 (-1229)	chr4	0.427	0.521	0.094	0.0163
18	cg07952421	UGT2B17 (-1357)	chr4	0.525	0.618	0.092	0.0152
19	cg10388667	MRPL53 (+2528)	chr2	0.687	0.779	0.092	0.0049
20	cg24239165	C17orf82 (+7542)	chr17	0.580	0.672	0.091	0.0001
21	cg20302533	POU6F2 (+153166)	chr7	0.266	0.355	0.089	0.0375
22	cg22772380	ZNF12 (-484)	chr7	0.445	0.533	0.088	0.0321
23	cg14381313	ZNF469 (-225540)	chr16	0.493	0.579	0.085	0.0364
24	cg26353469	HLA-G (+61215)	chr6	0.085	0.170	0.085	0.0404
25	cg14904295	PEG3 (+3535)	chr19	0.291	0.375	0.084	0.0262
26	cg03660162	MAF (+721526)	chr16	0.710	0.793	0.083	0.0229
27	cg21332948	AGPAT3 (-21173)	chr21	0.674	0.758	0.083	0.0428
28	cg07346359	OPTC (+26398)	chr1	0.422	0.505	0.083	0.0122
29	cg03995122	HLA-G (+99887)	chr6	0.030	0.113	0.083	0.0183
30	cg21549632	HLA-G (+61532)	chr6	0.066	0.148	0.082	0.0128
31	cg15671450	HLA-G (+100361)	chr6	0.089	0.168	0.079	0.0497
32	cg16302021	HLA-G (+99189)	chr6	0.404	0.481	0.078	0.0230
33	cg00409917	HLA-G (+99924)	chr6	0.074	0.152	0.077	0.0068
34	cg00901687	MYCBPAP (-475)	chr17	0.453	0.529	0.076	0.0250
35	cg23237314	HLA-G (+99442)	chr6	0.130	0.206	0.076	0.0401
36	cg19823512	OPTC (+26455)	chr1	0.305	0.380	0.075	0.0388
37	cg09597767	IFITM3 (-4866)	chr11	0.700	0.772	0.072	0.0036

Table S4. Continued

Nr.	probe ID	nearest gene (distance in bp)	chr	NU_mean	HU_mean	dB	P.Value
38	cg21323039	MATN1 (+3484)	chr1	0.792	0.863	0.072	0.0063
39	cg01336390	HLA-G (+100304)	chr6	0.087	0.159	0.072	0.0118
40	cg26028489	LMO3 (+85999)	chr12	0.478	0.550	0.072	0.0297
41	cg17341345	CCNH (-574)	chr5	0.505	0.575	0.071	0.0151
42	cg26054541	GSDMC (+815502)	chr8	0.691	0.761	0.070	0.0034
43	cg22968327	NUP93 (+59405)	chr16	0.258	0.327	0.069	0.0406
44	cg14449180	HLA-G (+99864)	chr6	0.040	0.109	0.069	0.0293
45	cg10632656	UGT2B17 (-1349)	chr4	0.274	0.343	0.069	0.0171
46	cg06223984	UGT2B17 (-7507)	chr4	0.561	0.629	0.068	0.0230
47	cg13597893	UBE2E3 (-272789)	chr2	0.493	0.561	0.068	0.0121
48	cg03071500	IFITM3 (-4915)	chr11	0.562	0.629	0.067	0.0012
49	cg10193107	HSPB1 (-7591)	chr7	0.481	0.547	0.067	0.0378
50	cg00738934	PKIA (-432095)	chr8	0.487	0.554	0.067	0.0010
51	cg21665744	POU6F2 (+153516)	chr7	0.631	0.697	0.066	0.0211
52	cg15931205	HLA-G (+100065)	chr6	0.060	0.126	0.066	0.0121
53	cg18191116	STON2 (+241)	chr14	0.502	0.568	0.065	0.0475
54	cg09549987	SPAG11B (+644)	chr8	0.310	0.374	0.064	0.0091
55	cg22253032	PRSS1 (-37378)	chr7	0.431	0.495	0.063	0.0012
56	cg21862992	MRPL21 (+12905)	chr11	0.404	0.467	0.063	0.0418
57	cg15598217	ZZEF1 (+44435)	chr17	0.524	0.587	0.063	0.0237
58	cg00135841	USP18 (+104683)	chr22	0.762	0.825	0.063	0.0423
59	cg11440486	MYCBPAP (-529)	chr17	0.462	0.524	0.062	0.0347
60	cg00186468	CCNH (-393)	chr5	0.248	0.310	0.062	0.0095
61	cg11449146	GAS2 (+62304)	chr11	0.555	0.617	0.062	0.0034
62	cg20111217	MYCBPAP (-481)	chr17	0.542	0.604	0.062	0.0171
63	cg27584762	CCNH (-291)	chr5	0.207	0.269	0.062	0.0202
64	cg19748509	HLA-G (+116023)	chr6	0.070	0.131	0.061	0.0152
65	cg01617603	UGT2B17 (+15538)	chr4	0.243	0.304	0.061	0.0116
66	cg03249561	FCAR (+14427)	chr19	0.674	0.734	0.060	0.0275
67	cg04815973	STOML1 (+17521)	chr15	0.251	0.311	0.060	0.0453
68	cg06112835	MRPL21 (+12495)	chr11	0.293	0.352	0.059	0.0399
69	cg19481811	UGT2B17 (+563)	chr4	0.587	0.646	0.059	0.0314
70	cg15218522	SBSPON (-75679)	chr8	0.333	0.392	0.059	0.0225
71	cg21894124	FBRSL1 (-161448)	chr12	0.146	0.205	0.059	0.0018
72	cg11994053	VEZT (+100370)	chr12	0.740	0.799	0.059	0.0034
73	cg04184807	GAPVD1 (+207038)	chr9	0.672	0.731	0.059	0.0386
74	cg17453273	ITSN2 (-61147)	chr2	0.116	0.174	0.059	0.0135

Table S4. Continued

Nr.	probe ID	nearest gene (distance in bp)	chr	NU_mean	HU_mean	dB	P.Value
75	cg09274344	SOX8 (+46882)	chr16	0.313	0.372	0.059	0.0211
76	cg01062395	HLA-G (+60881)	chr6	0.110	0.169	0.058	0.0212
77	cg09874992	SDC3 (+67000)	chr1	0.372	0.430	0.057	0.0026
78	cg08743428	ROBO2 (+678273)	chr3	0.456	0.513	0.057	0.0070
79	cg18976649	LMX1A (+213468)	chr1	0.718	0.774	0.056	0.0011
80	cg14453346	TSPAN33 (+19652)	chr7	0.807	0.862	0.056	0.0389
81	cg21733854	ZSCAN22 (-615)	chr19	0.517	0.571	0.055	0.0387
82	cg19727165	DHFR1 (-114061)	chr3	0.608	0.663	0.055	0.0077
83	cg07398106	LDHC (+318)	chr11	0.450	0.505	0.054	0.0182
84	cg20476087	CGREF1 (-126)	chr2	0.117	0.171	0.054	0.0018
85	cg21705926	DNAJB6 (+276978)	chr7	0.483	0.537	0.054	0.0385
86	cg14080482	NONE	chr6	0.383	0.438	0.054	0.0182
87	cg10773881	GGA1 (+15331)	chr22	0.115	0.170	0.054	0.0314
88	cg26942295	PDZD2 (+49191)	chr5	0.494	0.548	0.054	0.0249
89	cg13719529	C11orf44 (+4653)	chr11	0.513	0.567	0.054	0.0379
90	cg19445457	OR52N5 (+451)	chr11	0.531	0.584	0.054	0.0197
91	cg09142843	ARHGAP18 (+389699)	chr6	0.737	0.790	0.053	0.0264
92	cg13910785	HLA-DRB1 (+7776)	chr6	0.283	0.336	0.053	0.0040
93	cg23917496	UACA (+300798)	chr15	0.379	0.432	0.053	0.0416
94	cg15853715	C14orf39 (-2535)	chr14	0.447	0.500	0.053	0.0059
95	cg12884719	SIPA1L2 (+451040)	chr1	0.420	0.473	0.053	0.0053
96	cg22083892	KCNJ8 (-907)	chr12	0.341	0.394	0.053	0.0215
97	cg26637898	PAPD7 (+44310)	chr5	0.804	0.857	0.053	0.0396
98	cg14332815	LDHC (-290)	chr11	0.403	0.456	0.053	0.0267
99	cg13056653	UCP1 (-49011)	chr4	0.519	0.572	0.053	0.0220
100	cg13048967	CXCR1 (+1595)	chr2	0.624	0.676	0.052	0.0150
101	cg03278639	DNAJB8 (+50966)	chr3	0.672	0.724	0.052	0.0003
102	cg23999422	SIRT6 (+9135)	chr19	0.228	0.280	0.052	0.0024
103	cg03518414	TOPAZ1 (-104724)	chr3	0.424	0.476	0.052	0.0270
104	cg07040013	GLRX3 (+164891)	chr10	0.351	0.402	0.052	0.0056
105	cg06012695	TRIM27 (+121173)	chr6	0.296	0.347	0.051	0.0015
106	cg15236555	HS1BP3 (+7072)	chr2	0.319	0.370	0.051	0.0178
107	cg23155965	TTC40 (-22088)	chr10	0.788	0.839	0.051	0.0060
108	cg01521378	ZNRD1 (-40965)	chr6	0.713	0.764	0.051	0.0288
109	cg06902219	HLA-G (+61539)	chr6	0.102	0.152	0.051	0.0144
110	cg15279541	PDCD2 (-142631)	chr6	0.426	0.477	0.051	0.0297
111	cg24931191	STAC (-172977)	chr3	0.264	0.315	0.051	0.0063

Table S4. Continued

Nr.	probe ID	nearest gene (distance in bp)	chr	NU_mean	HU_mean	dB	P.Value
112	cg03742947	HLA-G (+61520)	chr6	0.067	0.118	0.051	0.0407
113	cg21234506	BCL2A1 (+656)	chr15	0.388	0.438	0.051	0.0477
114	cg19107429	FAM86B2 (+21475)	chr8	0.646	0.696	0.050	0.0196
115	cg05707985	PRSS1 (-26980)	chr7	0.294	0.344	0.050	0.0093
116	cg11395062	HS3ST3B1 (-64543)	chr17	0.710	0.760	0.050	0.0388
117	cg13503915	SIGLEC5 (-640)	chr19	0.638	0.588	-0.050	0.0199
118	cg21158434	CLSTN3 (+8365)	chr12	0.700	0.650	-0.050	0.0359
119	cg12709009	DLL1 (+41979)	chr6	0.622	0.571	-0.050	0.0028
120	cg18838701	TNNI3 (+488)	chr19	0.309	0.259	-0.050	0.0094
121	cg17707095	MPC1 (-197056)	chr6	0.653	0.602	-0.051	0.0494
122	cg14222229	HIST2H3PS2 (+262795)	chr1	0.326	0.275	-0.051	0.0111
123	cg15797131	IRS2 (+54603)	chr13	0.547	0.496	-0.051	0.0403
124	cg11524065	ZCCHC8 (+21993)	chr12	0.832	0.781	-0.051	0.0084
125	cg10218876	TNNT1 (+97)	chr19	0.245	0.193	-0.051	0.0007
126	cg04737881	TENM3 (-103639)	chr4	0.326	0.275	-0.051	0.0295
127	cg00143193	SMYD3 (+519171)	chr1	0.753	0.702	-0.051	0.0490
128	cg04161902	BAI2 (+1728)	chr1	0.732	0.681	-0.051	0.0004
129	cg12463722	OR4D1 (+6)	chr17	0.730	0.678	-0.052	0.0225
130	cg24045276	NCF2 (+7621)	chr1	0.654	0.603	-0.052	0.0133
131	cg20212775	SPON2 (+1980)	chr4	0.639	0.587	-0.052	0.0057
132	cg26965779	HLA-G (+59334)	chr6	0.507	0.455	-0.052	0.0088
133	cg12847536	ARHGEF10 (+50045)	chr8	0.636	0.584	-0.052	0.0441
134	cg22027267	COBL (-160023)	chr7	0.751	0.699	-0.052	0.0094
135	cg22898160	NDRG4 (-1339)	chr16	0.662	0.609	-0.053	0.0207
136	cg08121925	FXR1 (-42049)	chr3	0.324	0.271	-0.053	0.0020
137	cg03321588	FAM208A (-70669)	chr3	0.462	0.409	-0.053	0.0398
138	cg20660297	KRR1 (-903)	chr12	0.532	0.479	-0.053	0.0054
139	cg07510085	IL15RA (+18184)	chr10	0.721	0.667	-0.054	0.0079
140	cg05010260	NAT16 (+3266)	chr7	0.610	0.556	-0.054	0.0070
141	cg15324331	SVIL (-60404)	chr10	0.652	0.598	-0.054	0.0054
142	cg20304530	NTRK3 (+297163)	chr15	0.798	0.744	-0.054	0.0158
143	cg01540595	LHX8 (-3159)	chr1	0.468	0.413	-0.054	0.0113
144	cg01799458	HOXB13 (+1736)	chr17	0.569	0.514	-0.055	0.0353
145	cg00590063	B3GNT3 (+12877)	chr19	0.336	0.281	-0.055	0.0457
146	cg11016221	PTGES (+9679)	chr9	0.411	0.356	-0.055	0.0416
147	cg08071329	DLL1 (+43704)	chr6	0.739	0.683	-0.056	0.0096
148	cg19504245	TNNT1 (+102)	chr19	0.294	0.238	-0.056	0.0031

Table S4. Continued

Nr.	probe ID	nearest gene (distance in bp)	chr	NU_mean	HU_mean	dB	P.Value
149	cg09810149	NFU1 (-27150)	chr2	0.655	0.599	-0.056	0.0295
150	cg20336352	HERC4 (-13229)	chr10	0.757	0.701	-0.056	0.0032
151	cg16603012	APRT (-1242)	chr16	0.660	0.604	-0.057	0.0037
152	cg19902553	JPH3 (+49910)	chr16	0.241	0.184	-0.057	0.0394
153	cg08124399	DDX43 (+398)	chr6	0.730	0.672	-0.057	0.0469
154	cg27516945	ZNF528 (-603)	chr19	0.669	0.611	-0.057	0.0010
155	cg08122831	ERBB4 (-294015)	chr2	0.767	0.710	-0.057	0.0356
156	cg06968712	MS4A15 (+10431)	chr11	0.553	0.495	-0.058	0.0024
157	cg18423549	MTRNR2L1 (-278559)	chr17	0.394	0.336	-0.058	0.0050
158	cg09602542	GGT6 (-36137)	chr17	0.840	0.782	-0.058	0.0176
159	cg15199034	ADAMTS1 (-42681)	chr21	0.701	0.642	-0.058	0.0003
160	cg17240725	ABHD11 (+3841)	chr7	0.393	0.335	-0.058	0.0207
161	cg25122629	EML6 (-14857)	chr2	0.360	0.301	-0.059	0.0009
162	cg05176970	GLOD4 (-38693)	chr17	0.654	0.593	-0.060	0.0009
163	cg24441899	FOXK1 (-477568)	chr7	0.561	0.501	-0.060	0.0112
164	cg18503693	FAM155A (+595468)	chr13	0.618	0.557	-0.061	0.0356
165	cg15925527	WRAP73 (+6530)	chr1	0.733	0.672	-0.062	0.0462
166	cg10491108	TST (+6245)	chr22	0.640	0.578	-0.062	0.0352
167	cg22647161	TMPO (-223043)	chr12	0.591	0.529	-0.062	0.0407
168	cg10432947	NAT8L (+1203)	chr4	0.578	0.516	-0.062	0.0000
169	cg09430341	CCDC17 (-481)	chr1	0.762	0.700	-0.062	0.0129
170	cg22871949	NOM1 (-6814)	chr7	0.639	0.577	-0.062	0.0119
171	cg08617160	MIER2 (-520)	chr19	0.542	0.479	-0.062	0.0042
172	cg07442889	SIGLEC5 (-914)	chr19	0.694	0.631	-0.063	0.0029
173	cg21158163	CDH4 (-284904)	chr20	0.809	0.746	-0.063	0.0057
174	cg17014757	CHI3L1 (-221)	chr1	0.393	0.330	-0.064	0.0183
175	cg22526555	KCNJ15 (-49635)	chr21	0.771	0.706	-0.065	0.0002
176	cg19708055	C6orf123 (+151983)	chr6	0.647	0.581	-0.065	0.0174
177	cg16814483	PRKAB2 (+94049)	chr1	0.500	0.435	-0.066	0.0400
178	cg10852875	IRX2 (+214079)	chr5	0.589	0.523	-0.066	0.0000
179	cg10292709	MCPH1 (-435562)	chr8	0.715	0.649	-0.066	0.0065
180	cg14248883	SERP2 (+30700)	chr13	0.736	0.670	-0.066	0.0095
181	cg12159505	DDX56 (+8747)	chr7	0.770	0.704	-0.066	0.0021
182	cg17959580	ELFN2 (-1113)	chr22	0.648	0.581	-0.067	0.0419
183	cg23441030	CACYBP (-59405)	chr1	0.712	0.645	-0.067	0.0089
184	cg15634083	HLA-B (+86056)	chr6	0.204	0.137	-0.067	0.0107
185	cg09189601	UGT2B15 (+22315)	chr4	0.480	0.410	-0.070	0.0264
186	cg20478239	COBL (-159980)	chr7	0.691	0.620	-0.071	0.0010

Table S4. Continued

Nr.	probe ID	nearest gene (distance in bp)	chr	NU_mean	HU_mean	dB	P.Value
187	cg16754099	THEM6 (+1615)	chr8	0.560	0.488	-0.072	0.0005
188	cg05056638	NEFM (+30300)	chr8	0.598	0.525	-0.073	0.0411
189	cg07569483	NLRP9 (-8089)	chr19	0.634	0.558	-0.076	0.0014
190	cg01880147	FCGR3B (-8389)	chr1	0.702	0.625	-0.077	0.0010
191	cg00256329	GLOD4 (-38794)	chr17	0.692	0.614	-0.078	0.0014
192	cg24480926	SFSWAP (-276103)	chr12	0.629	0.550	-0.079	0.0430
193	cg18220841	BANP (+156623)	chr16	0.551	0.472	-0.080	0.0446
194	cg05758861	BAI1 (+50033)	chr8	0.756	0.675	-0.081	0.0117
195	cg22445217	QKI (+585402)	chr6	0.690	0.609	-0.081	0.0020
196	cg18325044	HLA-G (+74145)	chr6	0.812	0.730	-0.081	0.0086
197	cg09105440	THEM6 (+1617)	chr8	0.549	0.468	-0.082	0.0015
198	cg13784004	MYO5B (+24730)	chr18	0.564	0.482	-0.082	0.0069
199	cg03526459	PRKAB2 (+94183)	chr1	0.630	0.546	-0.084	0.0482
200	cg06451157	HLA-G (+73540)	chr6	0.792	0.706	-0.085	0.0169
201	cg10805896	PLXNA4 (-88990)	chr7	0.439	0.350	-0.089	0.0411
202	cg19729930	BOLA3 (+17249)	chr2	0.596	0.506	-0.090	0.0119
203	cg00639946	NONE	chr19	0.499	0.408	-0.091	0.0215
204	cg10804687	HLA-G (+64765)	chr6	0.858	0.765	-0.093	0.0458
205	cg09163930	PDGFRB (+1459)	chr5	0.505	0.409	-0.096	0.0166
206	cg10474018	HLA-G (+65261)	chr6	0.871	0.774	-0.097	0.0043
207	cg01017244	BOLA3 (+17594)	chr2	0.717	0.620	-0.097	0.0097
208	cg26127187	HLA-G (+62040)	chr6	0.807	0.708	-0.099	0.0158
209	cg20891558	BOLA3 (+17270)	chr2	0.565	0.466	-0.099	0.0048
210	cg15514307	PPP2CA (-20989)	chr5	0.743	0.644	-0.099	0.0120
211	cg14018363	HLA-G (+116510)	chr6	0.504	0.404	-0.100	0.0137
212	cg06454464	TSNARE1 (+56622)	chr8	0.833	0.732	-0.101	0.0139
213	cg19077165	TCEB3CL2 (-2555)	chr18	0.744	0.637	-0.106	0.0054
214	cg26649688	HLA-G (+63605)	chr6	0.882	0.774	-0.108	0.0088
215	cg18423635	HLA-G (+75181)	chr6	0.853	0.744	-0.109	0.0345
216	cg24179288	HLA-G (+72530)	chr6	0.860	0.745	-0.115	0.0140
217	cg03395495	GOLGA6L4 (-83129)	chr15	0.706	0.582	-0.124	0.0495
218	cg15825968	SFSWAP (-276155)	chr12	0.614	0.489	-0.125	0.0011
219	cg20381372	ZFP14 (+68693)	chr19	0.571	0.445	-0.126	0.0116
220	cg12046183	HLA-G (+65074)	chr6	0.723	0.594	-0.129	0.0033
221	cg25817503	AFAP1 (+153311)	chr4	0.596	0.463	-0.133	0.0030
222	cg05890377	BOLA3 (+17408)	chr2	0.604	0.465	-0.139	0.0167
223	cg13393919	GPBAR1 (-10899)	chr2	0.788	0.602	-0.187	0.0009

Table S5. Differentially methylated regions in whole blood of people with hyperuricemia compared to normouricemic people with cell composition correction

Nr.	nearest gene	DMR chr	DMR start	DMR end	length	probes in dmr
1	HLA-G	chr6	29893273	29895204	1932	33
2	HLA-G	chr6	29855890	29856564	675	19
3	LDHC	chr11	18433500	18434354	855	10
4	DOC2A	chr16	30023028	30024074	1047	10
5	TNNT1	chr19	55660514	55661528	1015	10
6	DLL1	chr6	170553133	170555857	2725	10
7	IRX2	chr5	2537210	2537834	625	8
8	TNNI3	chr19	55667533	55669059	1527	6
9	FXR1	chr3	180587900	180588228	329	6
10	NAT8L	chr4	2061923	2063566	1644	6
11	C6orf123	chr6	168045268	168046457	1190	6
12	MYCBPAP	chr17	48585216	48585470	255	5
13	BOLA3	chr2	74357527	74358223	697	5
14	DLL1	chr6	170557102	170558102	1001	5
15	NOM1	chr7	156735260	156735656	397	5
16	BAI1	chr8	143580770	143581481	712	5
17	UGT2B17	chr4	69435250	69435601	352	4
18	THEM6	chr8	143809371	143810237	867	4
19	FBRSL1	chr12	132904540	132904796	257	3
20	ERBB4	chr2	213697579	213698158	580	3
21	KCNJ15	chr21	39578742	39579277	536	3
22	HLA-G	chr6	29859520	29860016	497	3
23	POU6F2	chr7	39170497	39170763	267	3

Table S6. Differentially methylated probes in whole blood of people with hyperuricemia compared to normouricemic people without cell composition correction

Nr.	probe ID	nearest gene (distance in bp)	chr	NU_mean	HU_mean	dB	P.Value
1	cg07334023	IL2RB (-9994)	chr22	0.487	0.668	0.182	0.0090
2	cg02821156	ANKH (+54827)	chr5	0.566	0.738	0.173	0.0045
3	cg20482334	FASN (+7677)	chr17	0.713	0.857	0.144	0.0011
4	cg21224286	LRTM2 (-19517)	chr12	0.476	0.613	0.137	0.0003
5	cg13632935	RPL12 (+6177)	chr9	0.495	0.624	0.129	0.0413
6	cg07412545	GPR88 (+232)	chr1	0.472	0.599	0.127	0.0256
7	cg12859507	LRTM2 (-19470)	chr12	0.293	0.420	0.127	0.0000
8	cg18850127	POU6F2 (+152900)	chr7	0.479	0.604	0.125	0.0003
9	cg21022775	AREG (+28658)	chr4	0.688	0.813	0.124	0.0035
10	cg20347269	P2RX1 (+11637)	chr17	0.501	0.625	0.124	0.0127
11	cg24751894	HLA-G (+99386)	chr6	0.146	0.269	0.123	0.0037
12	cg26294610	MUT (+158454)	chr6	0.525	0.647	0.122	0.0287
13	cg18786623	HLA-G (+99295)	chr6	0.243	0.363	0.121	0.0025
14	cg16515087	EFCAB6 (-22809)	chr22	0.315	0.435	0.119	0.0000
15	cg12432526	TMEM105 (-50229)	chr17	0.316	0.432	0.117	0.0149
16	cg15212455	POU6F2 (+152942)	chr7	0.551	0.666	0.116	0.0010
17	cg06405219	MTURN (+44710)	chr7	0.267	0.381	0.114	0.0446
18	cg15070894	HLA-G (+99407)	chr6	0.183	0.294	0.111	0.0084
19	cg06223162	GPR88 (-5)	chr1	0.350	0.459	0.109	0.0261
20	cg07297153	REPIN1 (-2012)	chr7	0.655	0.763	0.108	0.0085
21	cg00956193	ZNF770 (-95077)	chr15	0.450	0.557	0.107	0.0054
22	cg13093842	NLRP7 (-23)	chr19	0.600	0.706	0.106	0.0068
23	cg04520169	HLA-G (+99440)	chr6	0.137	0.239	0.102	0.0067
24	cg02249577	SGMS1 (-51036)	chr10	0.682	0.783	0.101	0.0054
25	cg07655261	NANOG (+6526)	chr12	0.490	0.591	0.101	0.0110
26	cg03447150	SEMA5A (+662041)	chr5	0.546	0.646	0.100	0.0244
27	cg08951186	ZNF469 (-203509)	chr16	0.536	0.635	0.100	0.0087
28	cg24680439	TTC40 (-22379)	chr10	0.505	0.604	0.099	0.0260
29	cg26175789	EVA1A (-25045)	chr2	0.391	0.490	0.099	0.0062
30	cg06013395	EPHB3 (+1141)	chr3	0.668	0.766	0.099	0.0072
31	cg18060330	BTNL2 (-1162)	chr6	0.589	0.686	0.097	0.0147
32	cg08778598	LPCAT1 (-70488)	chr5	0.168	0.263	0.096	0.0188
33	cg07973162	UGT2B17 (-1006)	chr4	0.413	0.509	0.096	0.0200
34	cg06221963	KCNN3 (+2943)	chr1	0.298	0.394	0.096	0.0028
35	cg13166535	LOXL4 (-28710)	chr10	0.459	0.554	0.095	0.0240

Table S6. Continued

Nr.	probe ID	nearest gene (distance in bp)	chr	NU_mean	HU_mean	dB	P.Value
36	cg08231349	HLA-G (+99889)	chr6	0.052	0.146	0.095	0.0006
37	cg07748963	LPHN2 (+361581)	chr1	0.316	0.411	0.095	0.0299
38	cg13365324	UGT2B17 (-1229)	chr4	0.431	0.525	0.094	0.0290
39	cg12088417	RPTOR (+55649)	chr17	0.754	0.848	0.094	0.0411
40	cg03806328	ARHGAP32 (-67539)	chr11	0.594	0.687	0.094	0.0015
41	cg07952421	UGT2B17 (-1357)	chr4	0.529	0.622	0.093	0.0183
42	cg24239165	C17orf82 (+7542)	chr17	0.583	0.675	0.092	0.0221
43	cg09359103	KCNN3 (+2847)	chr1	0.240	0.331	0.092	0.0022
44	cg17370981	ATP4B (+918)	chr13	0.445	0.535	0.090	0.0344
45	cg10388667	MRPL53 (+2528)	chr2	0.692	0.782	0.090	0.0171
46	cg06871764	BTNL2 (-1191)	chr6	0.518	0.607	0.089	0.0077
47	cg27219185	BTBD3 (-511455)	chr20	0.453	0.542	0.089	0.0463
48	cg20302533	POU6F2 (+153166)	chr7	0.263	0.352	0.089	0.0004
49	cg27175123	SEL1L (-121914)	chr14	0.617	0.706	0.089	0.0020
50	cg18806707	EPDR1 (+38254)	chr7	0.326	0.414	0.088	0.0122
51	cg22742493	SLC25A38 (-6194)	chr3	0.525	0.613	0.088	0.0276
52	cg22772380	ZNF12 (-484)	chr7	0.450	0.538	0.088	0.0010
53	cg18734446	GNDF (-38184)	chr5	0.653	0.739	0.086	0.0073
54	cg14381313	ZNF469 (-225540)	chr16	0.496	0.581	0.085	0.0098
55	cg26353469	HLA-G (+61215)	chr6	0.086	0.171	0.085	0.0007
56	cg02947374	ZNF469 (-226413)	chr16	0.561	0.645	0.084	0.0208
57	cg15727171	NONE	chr9	0.241	0.325	0.084	0.0019
58	cg04485391	ZMIZ1 (-327344)	chr10	0.526	0.610	0.084	0.0161
59	cg14904295	PEG3 (+3535)	chr19	0.295	0.379	0.083	0.0037
60	cg03660162	MAF (+721526)	chr16	0.713	0.796	0.083	0.0207
61	cg07346359	OPTC (+26398)	chr1	0.427	0.509	0.083	0.0005
62	cg21549632	HLA-G (+61532)	chr6	0.066	0.149	0.083	0.0004
63	cg03995122	HLA-G (+99887)	chr6	0.030	0.112	0.082	0.0008
64	cg13132497	LYSMD4 (-195527)	chr15	0.464	0.544	0.080	0.0321
65	cg00621508	SLC17A2 (+4745)	chr6	0.603	0.684	0.080	0.0250
66	cg20744362	BRD1 (+168288)	chr22	0.473	0.553	0.080	0.0235
67	cg18768136	ASAH2 (-87699)	chr10	0.436	0.516	0.080	0.0009
68	cg07113537	DAZL (+3439)	chr3	0.137	0.217	0.080	0.0001
69	cg25835058	TMEM51 (-71271)	chr1	0.422	0.502	0.080	0.0109
70	cg00935887	CXXC11 (+32120)	chr2	0.446	0.526	0.079	0.0178
71	cg15671450	HLA-G (+100361)	chr6	0.090	0.170	0.079	0.0107

Table S6. Continued

Nr.	probe ID	nearest gene (distance in bp)	chr	NU_mean	HU_mean	dB	P.Value
72	cg06014707	PI15 (-69154)	chr8	0.571	0.650	0.079	0.0028
73	cg10983929	FAM90A1 (+213)	chr12	0.445	0.523	0.079	0.0047
74	cg15681295	TTC40 (-22198)	chr10	0.497	0.575	0.079	0.0070
75	cg08363235	ASAH2 (-168462)	chr10	0.454	0.533	0.078	0.0007
76	cg00413089	WDR60 (+101717)	chr7	0.294	0.372	0.078	0.0223
77	cg16302021	HLA-G (+99189)	chr6	0.409	0.486	0.077	0.0016
78	cg19196320	DEFB115 (-322339)	chr20	0.573	0.650	0.077	0.0158
79	cg00409917	HLA-G (+99924)	chr6	0.074	0.150	0.077	0.0025
80	cg23237314	HLA-G (+99442)	chr6	0.132	0.209	0.076	0.0176
81	cg18896979	CXXC11 (+32294)	chr2	0.455	0.531	0.076	0.0177
82	cg19783563	SPACA7 (-45022)	chr13	0.323	0.399	0.076	0.0022
83	cg19823512	OPTC (+26455)	chr1	0.308	0.383	0.075	0.0011
84	cg14091258	DNAJB6 (+276948)	chr7	0.512	0.587	0.075	0.0067
85	cg05237260	CNTNAP3B (+717097)	chr9	0.291	0.366	0.075	0.0053
86	cg16906964	AJAP1 (-54934)	chr1	0.412	0.487	0.075	0.0040
87	cg00845968	ZMIZ1 (-318760)	chr10	0.578	0.653	0.075	0.0085
88	cg14859874	HAX1 (-6722)	chr1	0.091	0.166	0.075	0.0066
89	cg05181157	SNAPC1 (+47084)	chr14	0.615	0.689	0.075	0.0275
90	cg01918803	PSG2 (-36757)	chr19	0.538	0.613	0.074	0.0013
91	cg02048733	CBLB (-480477)	chr3	0.456	0.530	0.074	0.0016
92	cg01719566	FAM90A1 (-83)	chr12	0.470	0.544	0.074	0.0135
93	cg02033694	NPIP11 (+118553)	chr16	0.284	0.358	0.074	0.0002
94	cg09928274	ELSPBP1 (+3822)	chr19	0.764	0.837	0.073	0.0313
95	cg17155018	TRAF3IP2 (-25618)	chr6	0.519	0.592	0.073	0.0060
96	cg24236953	FGFR2 (+41563)	chr10	0.496	0.569	0.073	0.0324
97	cg17291189	SLC2A14 (+25003)	chr12	0.346	0.418	0.073	0.0066
98	cg09597767	IFITM3 (-4866)	chr11	0.698	0.770	0.072	0.0037
99	cg13266242	HLA-G (+39740)	chr6	0.551	0.623	0.072	0.0014
100	cg01336390	HLA-G (+100304)	chr6	0.086	0.158	0.072	0.0048
101	cg15532640	GLT1D1 (+216486)	chr12	0.305	0.376	0.071	0.0382
102	cg03410772	ZNRD1 (-59026)	chr6	0.665	0.736	0.071	0.0000
103	cg25539628	ENSG00000182319 (+55525)	chr8	0.300	0.371	0.071	0.0004
104	cg15780967	PPP2R5E (+76068)	chr14	0.580	0.651	0.071	0.0377
105	cg20744163	PPIF (-107393)	chr10	0.665	0.736	0.071	0.0413
106	cg26028489	LMO3 (+85999)	chr12	0.485	0.556	0.071	0.0027

Table S6. Continued

Nr.	probe ID	nearest gene (distance in bp)	chr	NU_mean	HU_mean	dB	P.Value
107	cg25877386	DHX37 (-1348)	chr12	0.755	0.825	0.071	0.0361
108	cg17341345	CCNH (-574)	chr5	0.510	0.580	0.071	0.0116
109	cg16223220	HLA-G (+61159)	chr6	0.042	0.112	0.071	0.0017
110	cg09646655	ZFP37 (-2357)	chr9	0.481	0.551	0.070	0.0102
111	cg10632656	UGT2B17 (-1349)	chr4	0.278	0.348	0.070	0.0192
112	cg00661861	GPRIN2 (-3909)	chr10	0.591	0.660	0.069	0.0381
113	cg12038583	ZNF727 (-476334)	chr7	0.484	0.554	0.069	0.0181
114	cg05202858	FGF12 (+352912)	chr3	0.408	0.477	0.069	0.0330
115	cg22968327	NUP93 (+59405)	chr16	0.262	0.331	0.069	0.0178
116	cg14449180	HLA-G (+99864)	chr6	0.039	0.108	0.069	0.0021
117	cg08993878	TMPO (-758029)	chr12	0.355	0.424	0.069	0.0301
118	cg05246613	SH3RF3 (+9250)	chr2	0.302	0.370	0.069	0.0088
119	cg17746638	ENSG00000233024 (-7835)	chr16	0.541	0.609	0.069	0.0219
120	cg09199338	AGA (-311227)	chr4	0.270	0.338	0.069	0.0003
121	cg07318398	NT5C3B (-587)	chr17	0.338	0.406	0.068	0.0043
122	cg03977382	CNTN5 (+672992)	chr11	0.574	0.643	0.068	0.0085
123	cg15411272	HLA-G (+100432)	chr6	0.284	0.352	0.068	0.0392
124	cg01499815	HLA-G (+100319)	chr6	0.087	0.156	0.068	0.0028
125	cg08422420	LPCAT1 (-70642)	chr5	0.145	0.213	0.068	0.0205
126	cg26274304	NCAPG2 (+942)	chr7	0.273	0.341	0.068	0.0042
127	cg24289952	ZNF80 (+14382)	chr3	0.474	0.542	0.068	0.0331
128	cg21963583	MRPL21 (+12452)	chr11	0.399	0.467	0.068	0.0303
129	cg21138405	IRF1 (-1318)	chr5	0.226	0.294	0.068	0.0247
130	cg09801012	ASAH2 (-127080)	chr10	0.644	0.712	0.067	0.0049
131	cg13597893	UBE2E3 (-272789)	chr2	0.498	0.565	0.067	0.0009
132	cg11047325	SOC3S (+1224)	chr17	0.481	0.548	0.067	0.0042
133	cg14372705	GSC2 (-3235)	chr22	0.490	0.557	0.067	0.0470
134	cg23703303	SPAG11A (+14714)	chr8	0.545	0.611	0.067	0.0107
135	cg03071500	IFITM3 (-4915)	chr11	0.559	0.626	0.067	0.0227
136	cg05187965	TMEM72 (+117)	chr10	0.553	0.619	0.067	0.0142
137	cg15878909	FAM90A1 (-73)	chr12	0.399	0.465	0.066	0.0240
138	cg00255919	IRF1 (-1429)	chr5	0.234	0.300	0.066	0.0153
139	cg25952247	LHX3 (+2131)	chr9	0.413	0.479	0.066	0.0099
140	cg11406274	HLA-G (+61809)	chr6	0.253	0.319	0.066	0.0040
141	cg10621924	POU6F2 (+153473)	chr7	0.692	0.758	0.066	0.0016

Table S6. Continued

Nr.	probe ID	nearest gene (distance in bp)	chr	NU_mean	HU_mean	dB	P.Value
142	cg03181300	HIST1H2AD (+3476)	chr6	0.220	0.285	0.066	0.0288
143	cg04034577	AGXT (+28480)	chr2	0.418	0.484	0.066	0.0177
144	cg27149073	LPCAT1 (-70239)	chr5	0.134	0.199	0.066	0.0077
145	cg04972766	NONE	chr5	0.466	0.531	0.066	0.0003
146	cg03607220	HLA-DRB5 (-28200)	chr6	0.564	0.629	0.066	0.0440
147	cg21257293	ZFP37 (-5722)	chr9	0.393	0.459	0.066	0.0484
148	cg08835755	NKX1-1 (-114199)	chr4	0.474	0.540	0.065	0.0191
149	cg08009379	COBL (+125847)	chr7	0.331	0.396	0.065	0.0001
150	cg12744031	WDR60 (+101916)	chr7	0.318	0.383	0.065	0.0460
151	cg15931205	HLA-G (+100065)	chr6	0.060	0.125	0.065	0.0003
152	cg23490161	SDHA (+97)	chr5	0.136	0.201	0.065	0.0240
153	cg21665744	POU6F2 (+153516)	chr7	0.637	0.701	0.065	0.0083
154	cg18191116	STON2 (+241)	chr14	0.508	0.572	0.065	0.0093
155	cg20696345	HS1BP3 (+39466)	chr2	0.415	0.480	0.065	0.0137
156	cg16666458	FAM126A (+72462)	chr7	0.588	0.652	0.065	0.0005
157	cg18146737	GFI1 (+2811)	chr1	0.705	0.769	0.064	0.0432
158	cg05090351	CTBP2 (-134704)	chr10	0.461	0.525	0.064	0.0096
159	cg22253032	PRSS1 (-37378)	chr7	0.436	0.500	0.064	0.0005
160	cg08757828	CPT1A (-28717)	chr11	0.290	0.354	0.064	0.0227
161	cg03877706	NCAM2 (+202000)	chr21	0.544	0.607	0.063	0.0111
162	cg15011775	RARB (+13136)	chr3	0.505	0.569	0.063	0.0020
163	cg06025105	RSPH1 (+21549)	chr21	0.701	0.764	0.063	0.0476
164	cg27421994	NAB1 (+9952)	chr2	0.363	0.426	0.063	0.0027
165	cg02748618	ATPAF2 (+10470)	chr17	0.370	0.433	0.063	0.0016
166	cg19954471	SPACA7 (+66683)	chr13	0.406	0.469	0.063	0.0009
167	cg00186468	CCNH (-393)	chr5	0.250	0.313	0.063	0.0011
168	cg17184855	HLA-G (+595)	chr6	0.607	0.670	0.063	0.0008
169	cg21862992	MRPL21 (+12905)	chr11	0.409	0.471	0.063	0.0432
170	cg10077346	BCKDHB (+104095)	chr6	0.481	0.543	0.063	0.0333
171	cg06752595	ALDH5A1 (-1115)	chr6	0.530	0.592	0.062	0.0464
172	cg27584762	CCNH (-291)	chr5	0.208	0.271	0.062	0.0022
173	cg05332308	CDH8 (-372226)	chr16	0.439	0.501	0.062	0.0047
174	cg04535902	GFI1 (+2179)	chr1	0.632	0.694	0.062	0.0248
175	cg25897043	ITGB1 (-95701)	chr10	0.511	0.573	0.062	0.0057
176	cg27209610	ST3GAL5 (-102063)	chr2	0.454	0.516	0.062	0.0041
177	cg14223671	GNG13 (-7249)	chr16	0.142	0.205	0.062	0.0065

Table S6. Continued

Nr.	probe ID	nearest gene (distance in bp)	chr	NU_mean	HU_mean	dB	P.Value
178	cg15598217	ZZEF1 (+44435)	chr17	0.530	0.592	0.062	0.0058
179	cg01668281	CLDN14 (-62894)	chr21	0.272	0.334	0.062	0.0016
180	cg01324550	HOXB5 (-4777)	chr17	0.355	0.417	0.062	0.0016
181	cg11365170	SEMA6A (+77177)	chr5	0.590	0.652	0.062	0.0015
182	cg27618398	DCLK1 (-27638)	chr13	0.647	0.709	0.062	0.0458
183	cg00135841	USP18 (+104683)	chr22	0.766	0.828	0.062	0.0110
184	cg19748509	HLA-G (+116023)	chr6	0.071	0.133	0.062	0.0014
185	cg03551406	MT1X (-580)	chr16	0.444	0.506	0.062	0.0006
186	cg01617603	UGT2B17 (+15538)	chr4	0.247	0.309	0.062	0.0185
187	cg11449146	GAS2 (+62304)	chr11	0.560	0.622	0.061	0.0026
188	cg00369056	NPIPA7 (+490096)	chr16	0.658	0.719	0.061	0.0223
189	cg19684894	C1orf222 (+11284)	chr1	0.097	0.158	0.061	0.0379
190	cg10031873	ALG10B (-166540)	chr12	0.732	0.793	0.061	0.0003
191	cg27540865	CEP170 (+364418)	chr1	0.189	0.250	0.061	0.0056
192	cg12439472	DNAJC15 (-31940)	chr13	0.497	0.558	0.061	0.0182
193	cg02556954	ETF1 (+30412)	chr5	0.483	0.544	0.061	0.0010
194	cg27119318	WRB (+7405)	chr21	0.171	0.232	0.061	0.0033
195	cg24699985	C1orf174 (-276752)	chr1	0.462	0.522	0.060	0.0024
196	cg16680214	KCNN3 (+2773)	chr1	0.181	0.241	0.060	0.0004
197	cg03249561	FCAR (+14427)	chr19	0.678	0.738	0.060	0.0371
198	cg12545480	SYT14 (-12090)	chr1	0.405	0.465	0.060	0.0309
199	cg23248910	FGFR2 (+87847)	chr10	0.469	0.529	0.060	0.0177
200	cg11351709	TDRP (-333843)	chr8	0.418	0.478	0.060	0.0271
201	cg19061000	GALC (+182752)	chr14	0.560	0.620	0.060	0.0045
202	cg03618918	ITLN1 (-10138)	chr1	0.653	0.713	0.060	0.0004
203	cg16681436	EGFL8 (+2860)	chr6	0.694	0.753	0.060	0.0209
204	cg02447462	CFD (+1619)	chr19	0.403	0.462	0.060	0.0175
205	cg19686152	TMOD3 (-285)	chr15	0.458	0.517	0.060	0.0484
206	cg24960960	LPCAT1 (-70587)	chr5	0.171	0.230	0.059	0.0169
207	cg15218522	SBSPON (-75679)	chr8	0.339	0.398	0.059	0.0137
208	cg02850689	PLCH2 (-7551)	chr1	0.439	0.499	0.059	0.0026
209	cg21167402	LPCAT1 (-70585)	chr5	0.217	0.277	0.059	0.0214
210	cg02015053	EIF3J (+24728)	chr15	0.412	0.471	0.059	0.0039
211	cg22872376	MAGEL2 (-2568)	chr15	0.310	0.369	0.059	0.0015
212	cg06611532	RASA3 (-1936)	chr13	0.436	0.495	0.059	0.0423
213	cg03589715	SLC8A3 (-34563)	chr14	0.620	0.679	0.059	0.0256

Table S6. Continued

Nr.	probe ID	nearest gene (distance in bp)	chr	NU_mean	HU_mean	dB	P.Value
214	cg01719179	NPIPB11 (+118657)	chr16	0.221	0.280	0.059	0.0004
215	cg05037738	ATP13A3 (-1381)	chr3	0.531	0.590	0.059	0.0149
216	cg21894124	FBRSL1 (-161448)	chr12	0.148	0.207	0.059	0.0006
217	cg06112835	MRPL21 (+12495)	chr11	0.298	0.357	0.059	0.0296
218	cg13488542	MPHOSPH6 (+17514)	chr16	0.669	0.728	0.059	0.0152
219	cg08835956	POU6F2 (+153437)	chr7	0.639	0.698	0.059	0.0086
220	cg07962847	ACTR3B (+531378)	chr7	0.390	0.449	0.059	0.0233
221	cg14079719	IPCEF1 (+100117)	chr6	0.420	0.479	0.059	0.0088
222	cg20370296	ZNF251 (+69043)	chr8	0.352	0.411	0.059	0.0184
223	cg03785755	HIST1H2AD (+2677)	chr6	0.360	0.419	0.059	0.0038
224	cg05845204	RBM39 (+12594)	chr20	0.733	0.792	0.059	0.0182
225	cg09274344	SOX8 (+46882)	chr16	0.315	0.373	0.059	0.0136
226	cg15111296	CXXC1 (-33327)	chr18	0.545	0.603	0.058	0.0466
227	cg24126361	SLC25A37 (+12029)	chr8	0.499	0.558	0.058	0.0423
228	cg01062395	HLA-G (+60881)	chr6	0.111	0.170	0.058	0.0060
229	cg05875302	CXXC11 (+32901)	chr2	0.695	0.753	0.058	0.0023
230	cg17590488	NEBL (-132505)	chr10	0.447	0.505	0.058	0.0089
231	cg26188685	HDC (+17954)	chr15	0.220	0.278	0.058	0.0021
232	cg20748132	SCARB1 (+130686)	chr12	0.474	0.532	0.058	0.0075
233	cg11851257	TAC4 (+21973)	chr17	0.579	0.637	0.058	0.0014
234	cg05636112	KYNU (+47533)	chr2	0.488	0.546	0.058	0.0196
235	cg11284736	ENSG00000166503 (+50062)	chr15	0.603	0.661	0.058	0.0003
236	cg09239700	IRF4 (+58348)	chr6	0.604	0.662	0.058	0.0033
237	cg07872519	ABCB1 (-301)	chr7	0.459	0.517	0.057	0.0021
238	cg01889129	PDZD8 (-63910)	chr10	0.505	0.562	0.057	0.0063
239	cg15534755	TAGLN (-2730)	chr11	0.574	0.631	0.057	0.0161
240	cg05900440	TTC30A (+19814)	chr2	0.441	0.498	0.057	0.0145
241	cg10814153	ODF3L2 (+10)	chr19	0.578	0.635	0.057	0.0103
242	cg09874992	SDC3 (+67000)	chr1	0.376	0.434	0.057	0.0044
243	cg12798157	AKR7A3 (+15025)	chr1	0.185	0.242	0.057	0.0159
244	cg05452645	PRDM8 (+11224)	chr4	0.348	0.405	0.057	0.0426
245	cg14643763	STK35 (+71468)	chr20	0.387	0.444	0.057	0.0146
246	cg13126979	EME2 (+970)	chr16	0.232	0.289	0.057	0.0045
247	cg01876548	ZNF608 (-45746)	chr5	0.560	0.617	0.057	0.0068
248	cg03594447	PLA2G5 (-36957)	chr1	0.292	0.348	0.057	0.0016

Table S6. Continued

Nr.	probe ID	nearest gene (distance in bp)	chr	NU_mean	HU_mean	dB	P.Value
249	cg08121845	NONE	chr3	0.261	0.318	0.057	0.0017
250	cg04124281	MTHFS (-747)	chr15	0.229	0.286	0.057	0.0047
251	cg03701930	ADARB2 (-201767)	chr10	0.144	0.200	0.057	0.0014
252	cg07324633	LPCAT1 (-44578)	chr5	0.431	0.488	0.057	0.0012
253	cg23420995	DCLK1 (-2777)	chr13	0.171	0.227	0.057	0.0010
254	cg18181703	SOCS3 (+1537)	chr17	0.307	0.363	0.057	0.0004
255	cg19167230	NONE	chr4	0.344	0.401	0.056	0.0015
256	cg11861562	TAGLN (-2809)	chr11	0.540	0.596	0.056	0.0135
257	cg27029450	BRD1 (+120378)	chr22	0.339	0.396	0.056	0.0013
258	cg18943014	ZNF92 (+89579)	chr7	0.375	0.431	0.056	0.0018
259	cg20681948	ASCL1 (-9167)	chr12	0.373	0.429	0.056	0.0034
260	cg15817705	CAMK1G (-350999)	chr1	0.537	0.594	0.056	0.0018
261	cg16884706	TAS1R2 (+66273)	chr1	0.462	0.518	0.056	0.0011
262	cg07782112	CHAC2 (-887087)	chr2	0.391	0.447	0.056	0.0229
263	cg17309085	CNTN5 (+672975)	chr11	0.681	0.737	0.056	0.0096
264	cg14864167	PDE7A (+3005)	chr8	0.388	0.444	0.056	0.0014
265	cg22872396	SCN9A (+9830)	chr2	0.507	0.562	0.055	0.0150
266	cg11807280	MEIS1 (-7888)	chr2	0.296	0.352	0.055	0.0036
267	cg17361885	MXRA7 (+6038)	chr17	0.669	0.725	0.055	0.0438
268	cg13363596	CLDN14 (-62926)	chr21	0.394	0.449	0.055	0.0036
269	cg10773881	GGA1 (+15331)	chr22	0.118	0.173	0.055	0.0000
270	cg23962358	CPZ (+79985)	chr4	0.402	0.457	0.055	0.0099
271	cg18737081	PPIF (-107427)	chr10	0.624	0.679	0.055	0.0280
272	cg04118610	LPHN3 (+639168)	chr4	0.106	0.161	0.055	0.0309
273	cg00417819	SYT3 (+33140)	chr19	0.579	0.633	0.055	0.0009
274	cg13294652	OBSCN (+20917)	chr1	0.353	0.408	0.055	0.0158
275	cg23299919	DNAJB6 (+276437)	chr7	0.335	0.389	0.055	0.0185
276	cg13470831	SALL3 (-59897)	chr18	0.504	0.558	0.054	0.0058
277	cg10464773	QKI (+335832)	chr6	0.479	0.534	0.054	0.0121
278	cg20476087	CGREF1 (-126)	chr2	0.115	0.170	0.054	0.0002
279	cg27404186	CXXC11 (+31941)	chr2	0.661	0.716	0.054	0.0133
280	cg08206881	LPIN1 (+499637)	chr2	0.124	0.178	0.054	0.0167
281	cg01176694	MKL2 (+208587)	chr16	0.440	0.495	0.054	0.0009
282	cg12019814	RAD21 (+25858)	chr8	0.376	0.431	0.054	0.0015
283	cg26942295	PDZD2 (+49191)	chr5	0.498	0.552	0.054	0.0125
284	cg02407415	GNG13 (-6722)	chr16	0.207	0.261	0.054	0.0429

Table S6. Continued

Nr.	probe ID	nearest gene (distance in bp)	chr	NU_mean	HU_mean	dB	P.Value
285	cg23340194	USP14 (-3299)	chr18	0.484	0.538	0.054	0.0390
286	cg14827090	BEGAIN (+42983)	chr14	0.520	0.574	0.054	0.0233
287	cg25711786	ETF1 (+24486)	chr5	0.417	0.471	0.054	0.0018
288	cg14080482	NONE	chr6	0.389	0.443	0.054	0.0004
289	cg08937153	CEBPD (+146838)	chr8	0.609	0.663	0.054	0.0010
290	cg21705926	DNAJB6 (+276978)	chr7	0.488	0.542	0.054	0.0285
291	cg11124651	NONE	chr19	0.655	0.709	0.054	0.0132
292	cg17565702	KIFC2 (-138)	chr8	0.457	0.511	0.054	0.0029
293	cg19727165	DHFRL1 (-114061)	chr3	0.613	0.667	0.054	0.0436
294	cg14088970	ENGASE (+140423)	chr17	0.342	0.396	0.054	0.0094
295	cg21733854	ZSCAN22 (-615)	chr19	0.523	0.577	0.054	0.0078
296	cg00242965	MRPL21 (+12319)	chr11	0.271	0.325	0.054	0.0396
297	cg18449879	CYP4F11 (+591)	chr19	0.487	0.540	0.054	0.0169
298	cg23917496	UACA (+300798)	chr15	0.383	0.437	0.054	0.0276
299	cg19852147	WWOX (+662174)	chr16	0.311	0.365	0.054	0.0061
300	cg25282559	NONE	chr14	0.468	0.522	0.054	0.0011
301	cg24693741	DYM (+101009)	chr18	0.237	0.290	0.054	0.0009
302	cg12607525	ATXN7L3 (-11412)	chr17	0.559	0.613	0.054	0.0042
303	cg05333568	C1orf65 (+80)	chr1	0.256	0.309	0.053	0.0035
304	cg12884719	SIPA1L2 (+451040)	chr1	0.424	0.477	0.053	0.0066
305	cg10358342	NOBOX (-307)	chr7	0.315	0.368	0.053	0.0004
306	cg19445457	OR52N5 (+451)	chr11	0.536	0.589	0.053	0.0110
307	cg01256539	PRR16 (+2004)	chr5	0.510	0.563	0.053	0.0116
308	cg09142843	ARHGAP18 (+389699)	chr6	0.740	0.793	0.053	0.0448
309	cg13056744	HLA-G (+100185)	chr6	0.118	0.171	0.053	0.0073
310	cg06588529	ECI2 (-18261)	chr6	0.655	0.708	0.053	0.0232
311	cg00666877	CEP112 (+190945)	chr17	0.553	0.606	0.053	0.0028
312	cg11706815	MBD3L1 (+59748)	chr19	0.396	0.449	0.053	0.0274
313	cg03362483	LDLRAP1 (-23383)	chr1	0.352	0.405	0.053	0.0095
314	cg15853715	C14orf39 (-2535)	chr14	0.452	0.505	0.053	0.0060
315	cg25556464	STOML1 (+17620)	chr15	0.551	0.603	0.053	0.0113
316	cg22083892	KCNJ8 (-907)	chr12	0.347	0.400	0.053	0.0172
317	cg19684207	WRB (+7517)	chr21	0.165	0.217	0.052	0.0050
318	cg03904042	NECAB3 (+6723)	chr20	0.213	0.266	0.052	0.0364
319	cg25220979	IGF2BP1 (+17499)	chr17	0.481	0.533	0.052	0.0002
320	cg18018313	IRS1 (+7283)	chr2	0.322	0.374	0.052	0.0005

Table S6. Continued

Nr.	probe ID	nearest gene (distance in bp)	chr	NU_mean	HU_mean	dB	P.Value
321	cg12700863	IRX4 (-244322)	chr5	0.516	0.568	0.052	0.0047
322	cg19318330	SIK1 (+64136)	chr21	0.285	0.338	0.052	0.0059
323	cg13434361	PRSS16 (-18100)	chr6	0.620	0.672	0.052	0.0337
324	cg09125754	POTEF (-8533)	chr2	0.377	0.429	0.052	0.0386
325	cg10130564	TAGLN (-2740)	chr11	0.602	0.654	0.052	0.0456
326	cg23245007	TNK2 (-59895)	chr3	0.580	0.633	0.052	0.0161
327	cg08045932	BHLHE23 (-21594)	chr20	0.419	0.471	0.052	0.0310
328	cg05760951	SPATA31A5 (+453801)	chr9	0.225	0.278	0.052	0.0051
329	cg24531534	R3HCC1 (+16742)	chr8	0.313	0.366	0.052	0.0320
330	cg10609241	MTHFD1 (+29577)	chr14	0.669	0.721	0.052	0.0014
331	cg08975641	COL5A2 (+85053)	chr2	0.500	0.552	0.052	0.0426
332	cg25452172	CYP27B1 (-1718)	chr12	0.568	0.620	0.052	0.0002
333	cg10341310	MTFR1 (+25233)	chr8	0.452	0.503	0.052	0.0053
334	cg16543056	ZFP42 (-236815)	chr4	0.443	0.495	0.052	0.0013
335	cg13343932	SOC3 (+1097)	chr17	0.440	0.492	0.052	0.0129
336	cg09790280	TMEM229A (-316698)	chr7	0.574	0.625	0.052	0.0076
337	cg11232815	ATP6V0E2 (+176593)	chr7	0.431	0.482	0.052	0.0378
338	cg02830496	SLC25A51 (-25460)	chr9	0.299	0.350	0.052	0.0197
339	cg06012695	TRIM27 (+121173)	chr6	0.300	0.351	0.052	0.0045
340	cg02260461	USH2A (+35690)	chr1	0.467	0.519	0.051	0.0016
341	cg02027518	NDST3 (-201083)	chr4	0.530	0.581	0.051	0.0003
342	cg13048967	CXCR1 (+1595)	chr2	0.629	0.681	0.051	0.0017
343	cg07490070	ANKRD23 (+4307)	chr2	0.159	0.210	0.051	0.0049
344	cg25664381	STX18 (-33719)	chr4	0.228	0.280	0.051	0.0041
345	cg24589936	MTX1 (+2106)	chr1	0.410	0.462	0.051	0.0489
346	cg06531573	GNG13 (-6844)	chr16	0.180	0.232	0.051	0.0220
347	cg23155965	TTC40 (-22088)	chr10	0.786	0.837	0.051	0.0057
348	cg01124420	EDAR (+310)	chr2	0.401	0.453	0.051	0.0034
349	cg23999422	SIRT6 (+9135)	chr19	0.225	0.276	0.051	0.0005
350	cg12761472	CEP85L (-685)	chr6	0.586	0.637	0.051	0.0014
351	cg20746451	SMARCAD1 (-1059)	chr4	0.593	0.644	0.051	0.0478
352	cg24931191	STAC (-172977)	chr3	0.269	0.319	0.051	0.0044
353	cg08695253	ODF3L2 (+4)	chr19	0.473	0.524	0.051	0.0096
354	cg03742947	HLA-G (+61520)	chr6	0.068	0.119	0.051	0.0080
355	cg25883179	GABRG2 (+256684)	chr5	0.665	0.715	0.051	0.0003
356	cg12552320	SLC25A21 (+176861)	chr14	0.434	0.484	0.051	0.0015

Table S6. Continued

Nr.	probe ID	nearest gene (distance in bp)	chr	NU_mean	HU_mean	dB	P.Value
357	cg05707985	PRSS1 (-26980)	chr7	0.299	0.350	0.051	0.0288
358	cg04492858	PPP2R2D (-189169)	chr10	0.244	0.295	0.051	0.0085
359	cg10848692	TCL1A (-121392)	chr14	0.250	0.301	0.051	0.0010
360	cg15441605	TYRP1 (+121209)	chr9	0.538	0.589	0.051	0.0024
361	cg06902219	HLA-G (+61539)	chr6	0.100	0.151	0.051	0.0026
362	cg03307118	MAP1LC3B2 (-41193)	chr12	0.663	0.713	0.051	0.0162
363	cg12219752	FAM189A2 (+56037)	chr9	0.534	0.585	0.051	0.0288
364	cg09775918	NONE	chr9	0.360	0.410	0.051	0.0399
365	cg03226871	MAP3K2 (+17083)	chr2	0.515	0.565	0.051	0.0033
366	cg22499139	HLA-G (-35038)	chr6	0.643	0.693	0.051	0.0065
367	cg22542685	ZNF624 (+36608)	chr17	0.562	0.612	0.051	0.0117
368	cg16875568	ITGBL1 (+68145)	chr13	0.453	0.503	0.050	0.0277
369	cg18087694	RFPL4A (-1134)	chr19	0.319	0.370	0.050	0.0119
370	cg03626024	WSCD2 (-1183)	chr12	0.452	0.502	0.050	0.0019
371	cg21234506	BCL2A1 (+656)	chr15	0.394	0.445	0.050	0.0008
372	cg09680926	CHD2 (-13636)	chr15	0.413	0.464	0.050	0.0005
373	cg09004254	RNF157 (-34042)	chr17	0.578	0.628	0.050	0.0148
374	cg07583744	AUTS2 (+294919)	chr7	0.313	0.363	0.050	0.0254
375	cg05284887	GJA5 (+12178)	chr1	0.527	0.578	0.050	0.0046
376	cg22943590	MEIS1 (-13735)	chr2	0.458	0.508	0.050	0.0387
377	cg15221739	GPR98 (+381941)	chr5	0.267	0.318	0.050	0.0027
378	cg20787634	UQCRB (+7604)	chr8	0.592	0.642	0.050	0.0128
379	cg09906620	CCNB2 (-21939)	chr15	0.786	0.736	-0.050	0.0063
380	cg00919702	C1QL3 (+2653)	chr10	0.719	0.669	-0.050	0.0231
381	cg23223755	LHFPL4 (-1364)	chr3	0.625	0.575	-0.050	0.0024
382	cg02512888	CAMK1D (+66264)	chr10	0.637	0.587	-0.050	0.0007
383	cg26985140	SLC23A2 (-848)	chr20	0.710	0.660	-0.050	0.0019
384	cg14222229	HIST2H3PS2 (+262795)	chr1	0.322	0.272	-0.050	0.0115
385	cg09166973	PRDM9 (-151)	chr5	0.707	0.656	-0.050	0.0146
386	cg05250352	POR (+27235)	chr7	0.695	0.645	-0.050	0.0010
387	cg27019757	PDCD4 (+18771)	chr10	0.715	0.665	-0.050	0.0041
388	cg11541587	TPGS2 (-123951)	chr18	0.779	0.728	-0.051	0.0014
389	cg13795666	DDX59 (+20818)	chr1	0.685	0.634	-0.051	0.0075
390	cg24821564	KIR2DL1 (-591)	chr19	0.774	0.723	-0.051	0.0270
391	cg04161902	BAI2 (+1728)	chr1	0.736	0.686	-0.051	0.0043

Table S6. Continued

Nr.	probe ID	nearest gene (distance in bp)	chr	NU_mean	HU_mean	dB	P.Value
392	cg00804338	TFDP1 (+179)	chr13	0.166	0.115	-0.051	0.0038
393	cg10085053	NARS2 (-5329)	chr11	0.692	0.641	-0.051	0.0105
394	cg09886641	SPESP1 (+180)	chr15	0.741	0.690	-0.051	0.0018
395	cg00496389	OTOP1 (+88771)	chr4	0.748	0.697	-0.051	0.0139
396	cg23609713	TRIM27 (+153477)	chr6	0.585	0.534	-0.051	0.0045
397	cg11524065	ZCCHC8 (+21993)	chr12	0.834	0.783	-0.051	0.0402
398	cg10218876	TNNT1 (+97)	chr19	0.243	0.192	-0.051	0.0443
399	cg12463722	OR4D1 (+6)	chr17	0.734	0.682	-0.051	0.0002
400	cg23492448	RPL38 (-113727)	chr17	0.598	0.547	-0.051	0.0134
401	cg06820102	ZBTB38 (-2263)	chr3	0.665	0.614	-0.051	0.0003
402	cg15547703	CSTB (+3154)	chr21	0.590	0.539	-0.051	0.0018
403	cg10556772	HLA-G (+679)	chr6	0.406	0.354	-0.051	0.0065
404	cg24836607	ASZ1 (-176)	chr7	0.679	0.627	-0.051	0.0096
405	cg26259926	LRRRC24 (-3573)	chr8	0.655	0.604	-0.051	0.0294
406	cg03203155	SCAND3 (-154692)	chr6	0.681	0.630	-0.052	0.0152
407	cg10082647	C12orf23 (-645)	chr12	0.690	0.638	-0.052	0.0049
408	cg14841443	RGS9 (+92958)	chr17	0.543	0.492	-0.052	0.0457
409	cg02109003	HSBP1 (-106440)	chr16	0.552	0.500	-0.052	0.0051
410	cg24045276	NCF2 (+7621)	chr1	0.658	0.606	-0.052	0.0035
411	cg20212775	SPON2 (+1980)	chr4	0.643	0.591	-0.052	0.0008
412	cg09598512	XYLB (-17726)	chr3	0.602	0.550	-0.052	0.0254
413	cg20050113	SLC9A2 (+696)	chr2	0.387	0.334	-0.052	0.0092
414	cg17623013	FAM81B (+81020)	chr5	0.856	0.804	-0.052	0.0172
415	cg08121925	FXR1 (-42049)	chr3	0.319	0.267	-0.052	0.0009
416	cg23522194	CABP5 (-17880)	chr19	0.786	0.734	-0.052	0.0452
417	cg02675179	ACSM1 (+16505)	chr16	0.518	0.466	-0.052	0.0093
418	cg12847536	ARHGEF10 (+50045)	chr8	0.641	0.589	-0.052	0.0147
419	cg22898160	NDRG4 (-1339)	chr16	0.666	0.614	-0.052	0.0018
420	cg08087268	CHGA (+16658)	chr14	0.619	0.567	-0.052	0.0218
421	cg26209990	LEP (+29922)	chr7	0.682	0.630	-0.052	0.0289
422	cg13518079	EBF4 (+1549)	chr20	0.438	0.386	-0.052	0.0205
423	cg17241353	CBLN4 (+712513)	chr20	0.672	0.620	-0.052	0.0026
424	cg02663317	ARNTL2 (-40043)	chr12	0.671	0.619	-0.053	0.0018
425	cg18193195	SUOX (-10774)	chr12	0.709	0.657	-0.053	0.0237
426	cg22027267	COBL (-160023)	chr7	0.749	0.696	-0.053	0.0047
427	cg11546683	CPPED1 (+187159)	chr16	0.787	0.734	-0.053	0.0140

Table S6. Continued

Nr.	probe ID	nearest gene (distance in bp)	chr	NU_mean	HU_mean	dB	P.Value
428	cg22079902	PRDM9 (-80)	chr5	0.592	0.539	-0.053	0.0193
429	cg19162470	FAN1 (-3185)	chr15	0.663	0.610	-0.053	0.0170
430	cg22762992	DDX18 (+44152)	chr2	0.657	0.604	-0.053	0.0384
431	cg09209787	PROX1 (-10179)	chr1	0.519	0.466	-0.053	0.0015
432	cg03971051	KLHL35 (-11281)	chr11	0.816	0.762	-0.053	0.0280
433	cg01066472	LHX8 (-3090)	chr1	0.431	0.378	-0.053	0.0216
434	cg24920126	RPP40 (-82986)	chr6	0.693	0.639	-0.053	0.0167
435	cg15846771	ZDHHC11 (-4165)	chr5	0.542	0.488	-0.053	0.0039
436	cg07531550	FRG1 (-209348)	chr4	0.661	0.607	-0.053	0.0402
437	cg21556998	STRBP (+44032)	chr9	0.686	0.632	-0.054	0.0003
438	cg20304530	NTRK3 (+297163)	chr15	0.801	0.747	-0.054	0.0018
439	cg13476778	FRMD6 (-1261)	chr14	0.555	0.501	-0.054	0.0191
440	cg14771877	C17orf99 (-1396)	chr17	0.712	0.658	-0.054	0.0133
441	cg18211633	RHOF (+26559)	chr12	0.669	0.615	-0.054	0.0081
442	cg20660297	KRR1 (-903)	chr12	0.538	0.484	-0.054	0.0169
443	cg09053901	SHANK2 (+8174)	chr11	0.821	0.767	-0.054	0.0041
444	cg05010260	NAT16 (+3266)	chr7	0.615	0.561	-0.054	0.0054
445	cg27585222	ACTR3 (+90194)	chr2	0.649	0.595	-0.054	0.0108
446	cg04678955	DEFB115 (-321336)	chr20	0.512	0.458	-0.054	0.0336
447	cg00561395	ATXN10 (+46358)	chr22	0.693	0.638	-0.054	0.0045
448	cg17850273	KIF21A (+74994)	chr12	0.649	0.595	-0.054	0.0049
449	cg01540595	LHX8 (-3159)	chr1	0.474	0.420	-0.054	0.0071
450	cg03779490	SNX9 (-174754)	chr6	0.551	0.496	-0.055	0.0162
451	cg00590063	B3GNT3 (+12877)	chr19	0.332	0.277	-0.055	0.0255
452	cg03499324	PSMD5 (-858)	chr9	0.741	0.686	-0.055	0.0352
453	cg00105415	EGR2 (-3162)	chr10	0.669	0.615	-0.055	0.0021
454	cg09048334	FGD2 (+39218)	chr6	0.432	0.377	-0.055	0.0455
455	cg23425970	HS6ST1 (-244)	chr2	0.242	0.187	-0.055	0.0172
456	cg15620114	SLC16A12 (-1145)	chr10	0.768	0.713	-0.055	0.0053
457	cg01799458	HOXB13 (+1736)	chr17	0.573	0.518	-0.055	0.0048
458	cg25890575	DNAJB6 (+240283)	chr7	0.788	0.733	-0.055	0.0343
459	cg02655397	TMEM262 (-3138)	chr11	0.731	0.675	-0.056	0.0009
460	cg11016221	PTGES (+9679)	chr9	0.415	0.359	-0.056	0.0123
461	cg05874329	CYP11B1 (+17565)	chr8	0.625	0.569	-0.056	0.0018
462	cg13375654	DOC2A (-1283)	chr16	0.454	0.398	-0.056	0.0084
463	cg05663294	DUSP10 (-236921)	chr1	0.594	0.538	-0.056	0.0027

Table S6. Continued

Nr.	probe ID	nearest gene (distance in bp)	chr	NU_mean	HU_mean	dB	P.Value
464	cg16506114	EPHA6 (-37633)	chr3	0.638	0.581	-0.057	0.0020
465	cg14551984	SGOL2 (+8923)	chr2	0.726	0.669	-0.057	0.0018
466	cg05208483	CSPG4 (+30148)	chr15	0.797	0.740	-0.057	0.0362
467	cg11206167	SEPP1 (-112187)	chr5	0.767	0.710	-0.057	0.0328
468	cg08310558	SLFN13 (-10935)	chr17	0.851	0.794	-0.057	0.0233
469	cg05343328	ING1 (+98215)	chr13	0.649	0.593	-0.057	0.0172
470	cg16603012	APRT (-1242)	chr16	0.658	0.602	-0.057	0.0195
471	cg20336352	HERC4 (-13229)	chr10	0.761	0.704	-0.057	0.0157
472	cg08145067	PIP5K1C (+12301)	chr19	0.329	0.272	-0.057	0.0112
473	cg03264585	MTRNR2L1 (-229467)	chr17	0.646	0.589	-0.057	0.0031
474	cg02996355	STON2 (+14373)	chr14	0.278	0.221	-0.057	0.0105
475	cg00816676	MTRNR2L7 (-78458)	chr10	0.731	0.674	-0.057	0.0018
476	cg02661831	PHF3 (+41346)	chr6	0.676	0.619	-0.057	0.0105
477	cg26137217	TAF4 (+309977)	chr20	0.600	0.543	-0.057	0.0090
478	cg08122831	ERBB4 (-294015)	chr2	0.770	0.713	-0.057	0.0002
479	cg18844029	TRIM27 (+6749)	chr6	0.753	0.696	-0.057	0.0131
480	cg08124399	DDX43 (+398)	chr6	0.733	0.676	-0.057	0.0257
481	cg10831285	B3GNT3 (+13009)	chr19	0.319	0.261	-0.058	0.0009
482	cg11643285	OXNAD1 (+104962)	chr3	0.814	0.757	-0.058	0.0042
483	cg24727089	TXNL1 (+46082)	chr18	0.663	0.606	-0.058	0.0082
484	cg27516945	ZNF528 (-603)	chr19	0.673	0.616	-0.058	0.0114
485	cg14361252	ING1 (+98129)	chr13	0.593	0.536	-0.058	0.0223
486	cg05275595	TEX101 (-47774)	chr19	0.374	0.316	-0.058	0.0430
487	cg07938212	BICD1 (+13201)	chr12	0.637	0.579	-0.058	0.0007
488	cg06968712	MS4A15 (+10431)	chr11	0.558	0.500	-0.058	0.0059
489	cg15199034	ADAMTS1 (-42681)	chr21	0.705	0.647	-0.058	0.0024
490	cg09602542	GGT6 (-36137)	chr17	0.839	0.780	-0.059	0.0025
491	cg18423549	MTRNR2L1 (-278559)	chr17	0.398	0.339	-0.059	0.0210
492	cg06650819	ACTL6A (+2784)	chr3	0.495	0.436	-0.059	0.0309
493	cg04272684	OVCH1 (-21212)	chr12	0.676	0.617	-0.059	0.0173
494	cg27393610	TMEM116 (+6954)	chr12	0.889	0.831	-0.059	0.0015
495	cg17240725	ABHD11 (+3841)	chr7	0.398	0.339	-0.059	0.0110
496	cg16294255	MMEL1 (+1855)	chr1	0.507	0.448	-0.059	0.0057
497	cg03116837	ZNF596 (+34320)	chr8	0.453	0.394	-0.059	0.0257
498	cg20493661	KIR3DL1 (+15456)	chr19	0.590	0.531	-0.059	0.0093
499	cg02878510	SERTAD4 (-32407)	chr1	0.654	0.595	-0.059	0.0063

Table S6. Continued

Nr.	probe ID	nearest gene (distance in bp)	chr	NU_mean	HU_mean	dB	P.Value
500	cg03218402	TAS2R13 (+26087)	chr12	0.818	0.759	-0.059	0.0196
501	cg06015275	HSBP1 (-66549)	chr16	0.603	0.544	-0.059	0.0175
502	cg27427514	HES1 (+68104)	chr3	0.199	0.139	-0.060	0.0083
503	cg25122629	EML6 (-14857)	chr2	0.366	0.306	-0.060	0.0045
504	cg13729548	CHGA (+16513)	chr14	0.742	0.682	-0.060	0.0204
505	cg04601780	ENSG00000264813 (+10162)	chr17	0.474	0.413	-0.060	0.0182
506	cg06520296	ZNF703 (-202288)	chr8	0.569	0.509	-0.060	0.0155
507	cg14554415	SPESP1 (+150)	chr15	0.636	0.576	-0.060	0.0107
508	cg06513015	ERV3-1 (+7785)	chr7	0.784	0.723	-0.060	0.0016
509	cg07256649	HOPX (+68186)	chr4	0.828	0.768	-0.060	0.0408
510	cg08030235	EEPD1 (-95569)	chr7	0.726	0.665	-0.060	0.0104
511	cg05471900	IL1F10 (-1191)	chr2	0.704	0.643	-0.061	0.0035
512	cg00167275	GLUD1 (+35)	chr10	0.165	0.104	-0.061	0.0008
513	cg10846356	CALCB (-726)	chr11	0.643	0.581	-0.061	0.0042
514	cg15936068	DDX43 (+407)	chr6	0.751	0.689	-0.061	0.0312
515	cg18503693	FAM155A (+595468)	chr13	0.623	0.561	-0.062	0.0131
516	cg10491108	TST (+6245)	chr22	0.645	0.583	-0.062	0.0384
517	cg22647161	TMPO (-223043)	chr12	0.595	0.533	-0.062	0.0017
518	cg26111308	TVP23B (+14743)	chr17	0.524	0.462	-0.062	0.0173
519	cg00464738	HLA-G (+35493)	chr6	0.784	0.722	-0.062	0.0009
520	cg10432947	NAT8L (+1203)	chr4	0.583	0.521	-0.062	0.0061
521	cg09430341	CCDC17 (-481)	chr1	0.766	0.703	-0.063	0.0054
522	cg08617160	MIER2 (-520)	chr19	0.537	0.475	-0.063	0.0058
523	cg22871949	NOM1 (-6814)	chr7	0.641	0.578	-0.063	0.0007
524	cg22545206	DDX18 (+45274)	chr2	0.523	0.460	-0.063	0.0084
525	cg07442889	SIGLEC5 (-914)	chr19	0.698	0.635	-0.063	0.0207
526	cg12060669	R3HCC1 (+33863)	chr8	0.323	0.259	-0.064	0.0443
527	cg17014647	GMPR (+192496)	chr6	0.603	0.539	-0.064	0.0011
528	cg22599254	BCAR3 (+126150)	chr1	0.863	0.799	-0.064	0.0027
529	cg09419670	PSMD5 (-405)	chr9	0.215	0.151	-0.064	0.0388
530	cg06940110	DDX18 (+44205)	chr2	0.498	0.434	-0.064	0.0201
531	cg11092486	RPP40 (-83324)	chr6	0.547	0.482	-0.064	0.0252
532	cg17014757	CHI3L1 (-221)	chr1	0.398	0.334	-0.064	0.0256
533	cg15838333	PCNXL4 (-4189)	chr14	0.684	0.619	-0.065	0.0211
534	cg05915609	PRSS22 (+3716)	chr16	0.650	0.585	-0.065	0.0105

Table S6. Continued

Nr.	probe ID	nearest gene (distance in bp)	chr	NU_mean	HU_mean	dB	P.Value
535	cg22526555	KCNJ15 (-49635)	chr21	0.774	0.709	-0.065	0.0026
536	cg26011615	BATF3 (+34020)	chr1	0.692	0.627	-0.065	0.0003
537	cg19708055	C6orf123 (+151983)	chr6	0.644	0.578	-0.065	0.0027
538	cg14248883	SERP2 (+30700)	chr13	0.739	0.674	-0.065	0.0053
539	cg10852875	IRX2 (+214079)	chr5	0.586	0.521	-0.066	0.0030
540	cg08219700	IMPAD1 (-149624)	chr8	0.485	0.419	-0.066	0.0201
541	cg10292709	MCPH1 (-435562)	chr8	0.719	0.653	-0.066	0.0091
542	cg00073565	ZFPM2 (+131789)	chr8	0.562	0.496	-0.066	0.0279
543	cg03994477	FKBP4 (-75225)	chr12	0.556	0.489	-0.066	0.0007
544	cg27565337	RASA3 (+42024)	chr13	0.543	0.476	-0.067	0.0274
545	cg04580344	KIAA0408 (-16487)	chr6	0.728	0.661	-0.067	0.0053
546	cg06068545	SMYD2 (+81413)	chr1	0.161	0.094	-0.067	0.0219
547	cg15634083	HLA-B (+86056)	chr6	0.203	0.136	-0.067	0.0041
548	cg23441030	CACYBP (-59405)	chr1	0.716	0.648	-0.067	0.0001
549	cg06143315	CXXC11 (+138431)	chr2	0.769	0.702	-0.067	0.0201
550	cg19097082	ZBTB44 (-16742)	chr11	0.732	0.664	-0.068	0.0024
551	cg10907232	FAM49B (+44722)	chr8	0.790	0.722	-0.068	0.0012
552	cg16048001	PPP1R12B (+30298)	chr1	0.787	0.719	-0.068	0.0017
553	cg10756719	NKX6-1 (+118018)	chr4	0.736	0.668	-0.068	0.0001
554	cg08557536	ZNF112 (-689)	chr19	0.516	0.447	-0.069	0.0045
555	cg09798387	DEFB115 (-321358)	chr20	0.382	0.313	-0.069	0.0059
556	cg04974804	HTR1D (-594)	chr1	0.733	0.664	-0.070	0.0022
557	cg02603861	NONE	chr14	0.418	0.348	-0.070	0.0053
558	cg00783857	SYT2 (+104642)	chr1	0.782	0.712	-0.070	0.0015
559	cg18174881	MIS18BP1 (-749)	chr14	0.710	0.640	-0.070	0.0006
560	cg02825122	ZHX2 (-97192)	chr8	0.784	0.714	-0.071	0.0139
561	cg20478239	COBL (-159980)	chr7	0.696	0.625	-0.071	0.0044
562	cg12011299	ADH4 (-99)	chr4	0.609	0.537	-0.071	0.0121
563	cg11494091	GH2 (-233)	chr17	0.711	0.640	-0.072	0.0156
564	cg03804706	SYT2 (+115163)	chr1	0.775	0.703	-0.072	0.0007
565	cg00191853	SPAG1 (+7078)	chr8	0.506	0.434	-0.072	0.0277
566	cg27562174	ADH4 (+2)	chr4	0.740	0.667	-0.073	0.0203
567	cg06083423	RHOU (+244657)	chr1	0.690	0.617	-0.073	0.0112
568	cg05056638	NEFM (+30300)	chr8	0.595	0.522	-0.073	0.0026
569	cg05697751	DUSP16 (+4582)	chr12	0.786	0.713	-0.073	0.0056
570	cg17765025	SUCLG1 (+581435)	chr2	0.747	0.674	-0.073	0.0027

Table S6. Continued

Nr.	probe ID	nearest gene (distance in bp)	chr	NU_mean	HU_mean	dB	P.Value
571	cg24008280	PLD5 (-288775)	chr1	0.643	0.569	-0.073	0.0213
572	cg09027495	TBC1D2B (+210643)	chr15	0.735	0.661	-0.073	0.0022
573	cg04603290	TNFSF14 (+9947)	chr19	0.624	0.550	-0.074	0.0017
574	cg06489993	CALM3 (-21497)	chr19	0.640	0.566	-0.074	0.0190
575	cg21720175	MAF (-53056)	chr16	0.537	0.462	-0.074	0.0343
576	cg14393316	CAMSAP1 (+86740)	chr9	0.780	0.705	-0.075	0.0010
577	cg13912224	MCM3 (-22449)	chr6	0.497	0.422	-0.075	0.0386
578	cg18325044	HLA-G (+74145)	chr6	0.814	0.739	-0.076	0.0051
579	cg16270721	EXOSC5 (-9704)	chr19	0.401	0.325	-0.076	0.0361
580	cg11061773	TSC22D2 (-156570)	chr3	0.760	0.683	-0.076	0.0188
581	cg11685843	ADAM29 (+509663)	chr4	0.628	0.551	-0.076	0.0015
582	cg07569483	NLRP9 (-8089)	chr19	0.638	0.562	-0.076	0.0388
583	cg01813171	HLA-G (-32746)	chr6	0.720	0.643	-0.077	0.0173
584	cg08414882	BCM01 (-15730)	chr16	0.595	0.517	-0.077	0.0095
585	cg03911306	DAZL (-1998)	chr3	0.727	0.650	-0.077	0.0021
586	cg01880147	FCGR3B (-8389)	chr1	0.706	0.628	-0.078	0.0264
587	cg22629375	OSCAR (+6096)	chr19	0.539	0.461	-0.078	0.0362
588	cg10661558	LIPI (+136111)	chr21	0.732	0.654	-0.078	0.0002
589	cg24480926	SFSWAP (-276103)	chr12	0.633	0.555	-0.078	0.0002
590	cg24213669	DDX18 (+44351)	chr2	0.472	0.393	-0.079	0.0029
591	cg16324669	CDK11A (-8318)	chr1	0.847	0.768	-0.079	0.0448
592	cg17056703	SYCP2L (+65575)	chr6	0.792	0.712	-0.079	0.0133
593	cg07753967	DEFB115 (-233815)	chr20	0.287	0.208	-0.080	0.0401
594	cg03787837	HLA-DQA1 (+252)	chr6	0.477	0.397	-0.080	0.0306
595	cg20811988	DEFB115 (-233543)	chr20	0.273	0.193	-0.080	0.0118
596	cg18220841	BANP (+156623)	chr16	0.553	0.473	-0.080	0.0236
597	cg22223119	STK24 (+78568)	chr13	0.542	0.462	-0.080	0.0080
598	cg07195891	CLEC4C (+1997)	chr12	0.729	0.648	-0.080	0.0117
599	cg10871684	PLB1 (-44639)	chr2	0.859	0.779	-0.081	0.0147
600	cg22445217	QKI (+585402)	chr6	0.695	0.614	-0.081	0.0104
601	cg05758861	BAI1 (+50033)	chr8	0.754	0.673	-0.081	0.0001
602	cg22744079	PLRG1 (+60727)	chr4	0.614	0.532	-0.081	0.0009
603	cg15563854	TLE1 (-59)	chr9	0.200	0.118	-0.082	0.0004
604	cg20390711	KIAA0408 (-16148)	chr6	0.733	0.651	-0.083	0.0009
605	cg14079463	KIAA0408 (-16454)	chr6	0.563	0.481	-0.083	0.0227
606	cg09829303	CALD1 (-44627)	chr7	0.674	0.591	-0.083	0.0004

Table S6. Continued

Nr.	probe ID	nearest gene (distance in bp)	chr	NU_mean	HU_mean	dB	P.Value
607	cg09516963	DYRK2 (-56)	chr12	0.320	0.237	-0.083	0.0017
608	cg22457256	AZGP1 (-1085)	chr7	0.662	0.579	-0.083	0.0010
609	cg22032020	MEF2A (+15666)	chr15	0.721	0.637	-0.083	0.0420
610	cg13469777	ZNRD1 (-50410)	chr6	0.676	0.591	-0.085	0.0141
611	cg06451157	HLA-G (+73540)	chr6	0.795	0.709	-0.085	0.0013
612	cg02783661	KDM5A (-3573)	chr12	0.614	0.529	-0.085	0.0117
613	cg24433124	IER3 (-43638)	chr6	0.611	0.524	-0.086	0.0383
614	cg04692312	DEFB115 (-326651)	chr20	0.278	0.191	-0.087	0.0028
615	cg18349077	TMEM87B (+30103)	chr2	0.524	0.436	-0.088	0.0122
616	cg23904161	ING1 (+98212)	chr13	0.542	0.452	-0.090	0.0135
617	cg27286337	NKX6-2 (+44276)	chr10	0.607	0.518	-0.090	0.0327
618	cg19729930	BOLA3 (+17249)	chr2	0.599	0.509	-0.090	0.0096
619	cg10805896	PLXNA4 (-88990)	chr7	0.444	0.354	-0.090	0.0033
620	cg13139335	C8orf37 (-333487)	chr8	0.465	0.374	-0.091	0.0173
621	cg11581472	SLC25A12 (+83511)	chr2	0.767	0.675	-0.091	0.0014
622	cg20926353	TLE1 (+862)	chr9	0.299	0.206	-0.093	0.0007
623	cg10804687	HLA-G (+64765)	chr6	0.860	0.766	-0.094	0.0061
624	cg00063654	OXNAD1 (+106372)	chr3	0.712	0.618	-0.094	0.0003
625	cg22425359	IRX2 (+335898)	chr5	0.810	0.716	-0.095	0.0061
626	cg22945019	RASGRP3 (-174836)	chr2	0.739	0.644	-0.095	0.0263
627	cg01966510	ZSCAN2 (-68809)	chr15	0.619	0.523	-0.096	0.0007
628	cg01017244	BOLA3 (+17594)	chr2	0.720	0.624	-0.096	0.0037
629	cg10892585	ZNF138 (+43878)	chr7	0.773	0.676	-0.097	0.0012
630	cg23024343	DUS4L (-2653)	chr7	0.605	0.508	-0.097	0.0321
631	cg12060786	HSPA1B (+8207)	chr6	0.267	0.170	-0.097	0.0184
632	cg10474018	HLA-G (+65261)	chr6	0.873	0.775	-0.098	0.0011
633	cg00399683	DPP6 (-640390)	chr7	0.698	0.600	-0.098	0.0027
634	cg15514307	PPP2CA (-20989)	chr5	0.746	0.647	-0.099	0.0185
635	cg20891558	BOLA3 (+17270)	chr2	0.569	0.470	-0.099	0.0141
636	cg21717724	PSMD5 (+748)	chr9	0.604	0.504	-0.099	0.0138
637	cg26127187	HLA-G (+62040)	chr6	0.810	0.710	-0.100	0.0008
638	cg11955727	SUCLG1 (+581058)	chr2	0.783	0.683	-0.100	0.0007
639	cg06454464	TSNARE1 (+56622)	chr8	0.834	0.733	-0.101	0.0288
640	cg19899561	BDH2 (-38226)	chr4	0.832	0.731	-0.102	0.0213
641	cg14018363	HLA-G (+116510)	chr6	0.509	0.407	-0.102	0.0044
642	cg15482884	PNO1 (+38423)	chr2	0.576	0.474	-0.103	0.0198

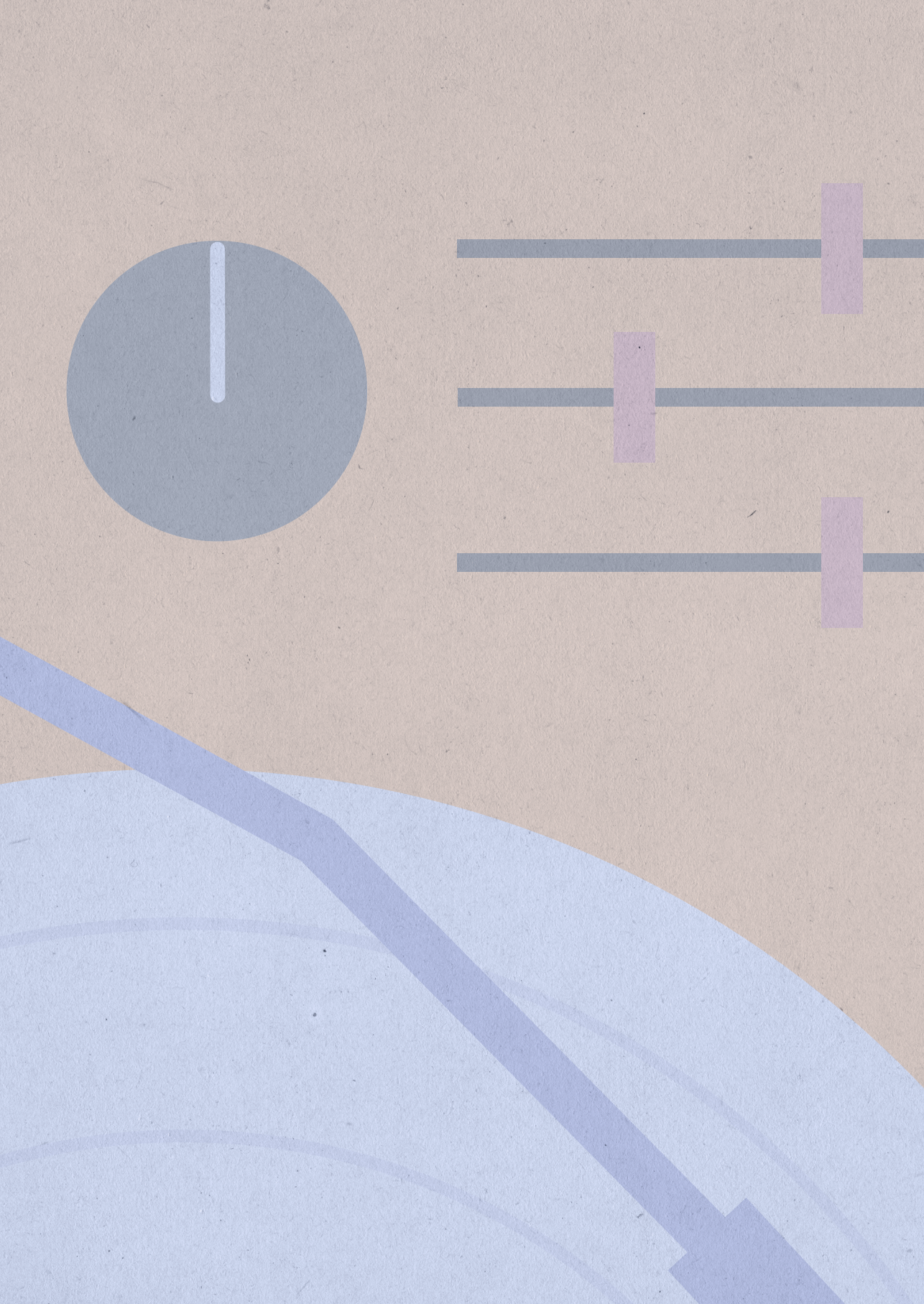
Table S6. Continued

Nr.	probe ID	nearest gene (distance in bp)	chr	NU_mean	HU_mean	dB	P.Value
643	cg12949927	ZNF138 (+43874)	chr7	0.750	0.647	-0.103	0.0009
644	cg00157199	DEFB115 (-293845)	chr20	0.439	0.336	-0.104	0.0037
645	cg26844603	TMEM87B (+30108)	chr2	0.631	0.528	-0.104	0.0107
646	cg14815891	DEFB115 (-233564)	chr20	0.290	0.186	-0.104	0.0217
647	cg20578893	HLA-G (+75305)	chr6	0.774	0.669	-0.105	0.0005
648	cg04057469	RFTN1 (+82369)	chr3	0.710	0.604	-0.106	0.0001
649	cg19077165	TCEB3CL2 (-2555)	chr18	0.747	0.640	-0.107	0.0002
650	cg26649688	HLA-G (+63605)	chr6	0.883	0.776	-0.107	0.0004
651	cg26964592	HLA-DMB (+4226)	chr6	0.566	0.457	-0.109	0.0046
652	cg18423635	HLA-G (+75181)	chr6	0.855	0.746	-0.109	0.0003
653	cg09104915	SHANK2 (-8851)	chr11	0.632	0.520	-0.112	0.0020
654	cg03126799	R3HCC1 (+33566)	chr8	0.657	0.545	-0.112	0.0254
655	cg24819596	ST3GAL5 (-18877)	chr2	0.765	0.649	-0.116	0.0008
656	cg09670175	KCNA6 (+5127)	chr12	0.734	0.618	-0.116	0.0230
657	cg12182020	NONE	chr3	0.415	0.298	-0.117	0.0297
658	cg15228509	CEP170 (+343635)	chr1	0.573	0.454	-0.119	0.0008
659	cg24179288	HLA-G (+72530)	chr6	0.866	0.747	-0.119	0.0002
660	cg00151744	AKAP13 (-32444)	chr15	0.576	0.456	-0.120	0.0012
661	cg03395495	GOLGA6L4 (-83129)	chr15	0.709	0.586	-0.123	0.0000
662	cg15825968	SFSWAP (-276155)	chr12	0.618	0.494	-0.125	0.0000
663	cg12927252	UPP2 (+18697)	chr2	0.715	0.590	-0.126	0.0305
664	cg20381372	ZFP14 (+68693)	chr19	0.574	0.448	-0.127	0.0266
665	cg17232014	HEBP1 (+14)	chr12	0.310	0.183	-0.127	0.0006
666	cg00727777	MYOM2 (+344659)	chr8	0.612	0.485	-0.128	0.0048
667	cg12046183	HLA-G (+65074)	chr6	0.727	0.597	-0.130	0.0013
668	cg13149459	PPP1R12B (+107853)	chr1	0.753	0.622	-0.131	0.0005
669	cg25817503	AFAP1 (+153311)	chr4	0.599	0.466	-0.133	0.0054
670	cg25343008	SYT2 (+142351)	chr1	0.701	0.564	-0.137	0.0004
671	cg05890377	BOLA3 (+17408)	chr2	0.601	0.461	-0.140	0.0014
672	cg13685349	STON2 (+14501)	chr14	0.736	0.586	-0.151	0.0047
673	cg17939448	FAM47E-STBD1 (-26347)	chr4	0.517	0.360	-0.157	0.0043
674	cg26919182	SYT2 (+90349)	chr1	0.720	0.541	-0.179	0.0004
675	cg13393919	GPBAR1 (-10899)	chr2	0.791	0.605	-0.186	0.0000
676	cg04462931	ZNF138 (+45259)	chr7	0.690	0.502	-0.188	0.0006

References

- [1] Li Y, Oosting M, Deelen P, et al. Inter-individual variability and genetic influences on cytokine responses to bacteria and fungi. *Nat Med* 2016; 22(10):1192.
- [2] Joosten LAB, Netea MG, Mylona E, et al. Engagement of fatty acids with toll-like receptor 2 drives interleukin-1 β production via the ASC/caspase 1 pathway in monosodium urate monohydrate crystal-induced gouty arthritis. *Arthritis Rheum* 2010; 62(11):3237-48.
- [3] Repnik U, Knezevic M, Jeras M. Simple and cost-effective isolation of monocytes from buffy coats. *J Immunol Methods* 2003; 278(1-2):283-92.
- [4] Crişan TO, Cleophas MCP, Novakovic B, et al. Uric acid priming in human monocytes is driven by the AKT-PRAS40 autophagy pathway. *Proc Natl Acad Sci U S A* 2017; 114(21):5485-90.
- [5] Joosten LAB, Crisan TO, Azam T, et al. Alpha-1-anti-trypsin-Fc fusion protein ameliorates gouty arthritis by reducing release and extracellular processing of IL-1 β and by the induction of endogenous IL-1Ra. *Ann Rheum Dis* 2016; 75(6):1219-27.
- [6] Novakovic B, Habibi E, Wang SY, et al. β -Glucan Reverses the Epigenetic State of LPS-Induced Immunological Tolerance. *Cell* 2016; 167(5):1354-1368.e14.
- [7] Martino D, Neeland M, Dang T, et al. Epigenetic dysregulation of naive CD4⁺ T-cell activation genes in childhood food allergy. *Nat Commun* 2018; 9(1):3308.
- [8] Pidsley R, Zotenko E, Peters TJ, et al. Critical evaluation of the Illumina MethylationEPIC BeadChip microarray for whole-genome DNA methylation profiling. *Genome Biol* 2016; 17(1):208.
- [9] Phipson B, Maksimovic J, Oshlack A (2016) MissMethyl: An R package for analyzing data from Illumina's HumanMethylation450 platform. *Bioinformatics*. <https://doi.org/10.1093/bioinformatics/btv560>
- [10] Aryee MJ, Jaffe AE, Corrada-Bravo H, et al. Minfi: A flexible and comprehensive Bioconductor package for the analysis of Infinium DNA methylation microarrays. *Bioinformatics* 2014; 30(10):1363-9.
- [11] Gentleman RC, Carey VJ, Bates DM, et al. Bioconductor: open software development for computational biology and bioinformatics. *Genome Biol* 2004; 5(10):R80.
- [12] Maksimovic J, Gordon L, Oshlack A. SWAN: Subset-quantile within array normalization for illumina infinium HumanMethylation450 BeadChips. *Genome Biol* 2012; 13(6):R44.
- [13] Houseman EA, Molitor J, Marsit CJ. Reference-free cell mixture adjustments in analysis of DNA methylation data. *Bioinformatics* 2014; 30(10):1431-9.
- [14] Ritchie ME, Phipson B, Wu D, et al. limma powers differential expression analyses for RNA-sequencing and microarray studies. *Nucleic Acids Res* 2015; 43(7):e47.
- [15] Peters TJ, Buckley MJ, Statham AL, et al. De novo identification of differentially methylated regions in the human genome. *Epigenetics and Chromatin* 2015; 8:6.
- [16] Houseman EA, Accomando WP, Koestler DC, et al. DNA methylation arrays as surrogate measures of cell mixture distribution. *BMC Bioinformatics* 2012; 13:86.
- [17] Barton SJ, Melton PE, Titcombe P, et al. In Epigenomic Studies, Including Cell-Type Adjustments in Regression Models Can Introduce Multicollinearity, Resulting in Apparent Reversal of Direction of Association. *Front Genet* 2019; 10:816.
- [18] Mahony R, Ahmed S, Diskin C, et al. SOCS3 revisited: a broad regulator of disease, now ready for therapeutic use? *Cell Mol Life Sci* 2016; 73(17):3323-36.

- [19] Yoshimura A, Suzuki M, Sakaguchi R, et al. SOCS, inflammation, and autoimmunity. *Front Immunol* 2012; 3:20.
- [20] Yan C, Ward PA, Wang X, et al. Myeloid depletion of SOCS3 enhances LPS-induced acute lung injury through CCAAT/enhancer binding protein δ pathway. *FASEB J* 2013; 27(8):2967-76.
- [21] Yoshimura A, Yasukawa H. JAK's SOCS: A Mechanism of Inhibition. *Immunity* 2012; 36(2):157-9.
- [22] Liu X, Zhang Y, Yu Y, et al. SOCS3 promotes TLR4 response in macrophages by feedback inhibiting TGF- β 1/Smad3 signaling. *Mol Immunol* 2008; 45(5):1405-13.
- [23] Ruppert J, Schtitt C, Ostermeier D, Peters JH CD14. 281-286
- [24] Kennedy MN, Mullen GED, Leifer CA, et al. A complex of soluble MD-2 and lipopolysaccharide serves as an activating ligand for toll-like receptor 4. *J Biol Chem* 2004; 279:34698-704.



CHAPTER 3

Regulation of SOCS3-STAT3 in urate-induced inflammation in human myeloid cells

Badii, M.* , Klück, V.* , Gaal, O., Cabău, G., Hotea, I., Nica, V., Mirea, A. M., Bojan, A., Zdrenghea, M., HINT Consortium, Novakovic, B., Merriman, T. R., Liu, Z., Li, Y., Xu, C. J., Pamfil, C., Rednic, S., Popp, R. A., Crişan, T. O.# , & Joosten, L. A. B#.

*These authors contributed equally to this work

#These authors share senior authorship

Joint Bone Spine. 2024;91(3):105698.

Summary

Hyperuricaemia is necessary for gout. High urate concentrations have been linked to inflammation in mononuclear cells via epigenetic modifications. In this study, we explore the role of the suppressor of cytokine signalling 3 (SOCS3) in urate-induced inflammation. Peripheral blood mononuclear cells (PBMCs) from gout patients, hyperuricemic and normouricemic individuals were cultured for 24h with varying concentrations of urate, followed by 24h restimulation with LPS or LPS+MSU. Transcriptomic profiling was performed using RNA-Sequencing. DNA methylation was assessed using an EPIC array. Phosphorylation of STAT3 was determined by flow cytometry. Cytokine responses were also assessed in PBMCs from patients with JAK2V617F mutation. PBMCs pre-treated with soluble urate produced more IL-1 β and IL-6 and less IL-1Ra after LPS stimulation. *In vitro*, urate treatment enhanced *SOCS3* expression in control monocytes but no DNA methylation changes were observed at the *SOCS3* gene. A dose-dependent reduction in phosphorylated STAT3 concomitant with a decrease in IL-1Ra was observed with increasing concentrations of urate. PBMCs with constitutively activated STAT3 (JAK2V617F mutation) could not be primed by urate. *In vitro*, urate exposure reveals increased *SOCS3* expression. *In vitro*, urate priming, and subsequent stimulation resulted in suppressed STAT3 phosphorylation along with decreased IL-1Ra production. There was no evidence that DNA methylation constitutes a regulatory mechanism of *SOCS3*. Elevated *SOCS3* and reduced pSTAT3 could play a role in urate-induced hyperinflammation since urate priming had no effect in PBMCs from patients with constitutively activated STAT3.

Introduction

Hyperuricemia is the necessary basis of gout and is defined as serum urate concentrations above the saturation threshold [1]. Urate results from the metabolism of purines and is primarily excreted via the kidney [2]. More recently, hyperuricemia has been associated with an increased risk for metabolic syndrome, diabetes, chronic kidney diseases, and even with increased all-cause and cardiovascular mortality rates [3–6]. High urate levels lead to pro-inflammatory regulation in mononuclear cells, with increased interleukin (IL)-1 β and IL-6 expression and, intriguingly, a shift towards reduced levels of the IL-1 receptor antagonist (IL-1Ra), the natural inhibitor of IL-1 [7]. These changes are mediated via epigenetic reprogramming, leading to differentially expressed genes [8], however, the signalling pathways involved remain to be elucidated.

The Suppressor of Cytokine Signalling (SOCS) family of proteins is induced by various cytokines, such as interleukins, interferons, and haematopoietic growth factors [9], but also by TLR-ligands such as lipopolysaccharide (LPS) [10]. The SOCS family comprises 8 proteins (SOCS1–7) and CIS (cytokine-inducible SH2-domain containing) that contain a Src Homology 2 (SH2) domain and a C-terminal SOCS-box domain [11]. SOCS1 and SOCS3 contain an additional short motif known as KIR (kinase inhibitory region), allowing them to directly modulate JAK catalytic activity and therefore suppress signalling by acting in a negative feedback loop [9]. SOCS3 is upregulated in monosodium urate (MSU) crystal-stimulated monocyte-derived macrophages [12]. SOCS3, potentially in the IL-1 signalling pathway, could play a role in the regulation of urate-dependent inflammation [13], given that cytokine signalling is negatively regulated by the activation of the JAK-STAT-SOCS transduction pathway [14]. Nonetheless, SOCS1/SOCS3 proteins are involved in a wide range of biological processes, including immunity and development, as deficiency of the *Socs3* gene in mice leads to placental defects and embryonic lethality [15].

SOCS3 acts as a negative feedback regulator of signal transducer and activator of transcription 1 and 3 (STAT1 and STAT3). STAT3 tyrosine phosphorylation plays an important role in IL-1 β and IL-6 production in response to LPS-induced inflammation [16]. Pro-inflammatory cytokines such as IL-1 β and TNF can trigger a cytokine amplification loop via IL-6/STAT3 to promote sustained inflammation and joint destruction [17]. On the other hand, STAT3 is also involved in the transcription of anti-inflammatory cytokines, such as IL-1Ra, as was demonstrated in monocytes stimulated by both IL-10 and LPS [18].

Based on these findings, we hypothesize that SOCS3-STAT3 signalling may hold relevance in relation to inflammation in gout and to cytokine production profiles in response to urate. Here we systematically investigate the involvement of the SOCS3/STAT3 pathway in urate-induced inflammation in human myeloid cells by combining immunological, transcriptomic, and epigenetic data from both healthy donors and patients.

Material and methods

A detailed version of this section is provided in Supplementary Material

Participants

Study participants in Romania were recruited at the Rheumatology Department of the Iuliu Hațieganu University of Medicine and Pharmacy and the Department of Haematology, Oncological Institute „Prof. Dr. Ion Chiricuță” in Cluj-Napoca. In the Netherlands, blood was drawn from healthy volunteers at the Radboud University Medical Center. Peripheral blood was drawn from the cubital vein on EDTA tubes under sterile conditions. The study was approved by the Ethical Committee of the institutions and the experiments were in accordance with the Declaration of Helsinki. All participants gave written informed consent before inclusion.

Cell preparation and culture conditions

Peripheral blood mononuclear cells (PBMCs) were isolated using Ficoll-Paque (GE Healthcare) density gradient centrifugation. PBMCs were cultured at 5×10^5 /well in a 96-well plate, flat bottom. Percoll monocyte enrichment was obtained by gradient centrifugation of PBMCs using a Percoll hyperosmotic density gradient solution. Percoll monocytes were cultured at 10^5 /well in a 96-well plate, flat bottom. Monocytes were isolated using a Pan Monocyte Isolation Kit and further cultured at 2×10^6 /well in a 6-well plate.

Cells were counted by Coulter Counter method and plated in Dutch Modified RPMI 1640 medium (Sigma) supplemented with 50 µg/mL gentamycin (Sigma), 2 mM GlutaMAX (Gibco), and 1 mM pyruvate (Gibco) and 10% human pooled serum. Cytokine responses to mimic hyperuricemia *in vitro* were induced by incubating the cells with varying doses of soluble urate (50 and 12.5 mg/dL) followed by restimulation of remaining adherent cells with LPS (10 ng/mL) or LPS (10 ng/mL) + MSU crystals (300 µg/mL). Urate concentrations were chosen based on previous studies [7][8]. This protocol consists of 24 hour pre-

treatment with soluble urate, followed by removal of media containing urate and restimulation for additional 24 hours with pattern recognition receptor agonists (in this case LPS with/without MSU crystals). While 24h treatment with urate alone (which we refer to as “priming”) does not typically induce IL-1 β or IL-6 cytokine production but does lower basal IL-1Ra production, a subsequent stimulation results in significant changes in proinflammatory cytokine production (in line with a silent effect of urate pre-exposure in priming the cells towards a proinflammatory state only visible upon secondary stimulation) [7]. Cells were incubated at 37 °C 5% CO₂. Cytokine levels were measured in culture supernatants. Treated cells were stored at -80 °C in TRIzol Reagent (Invitrogen) for further gene expression analysis.

Cytokine measurements

Cytokine measurements were carried out in conditioned media from the experiments using ELISA kits for IL-1 β , IL-1Ra, and IL-6 (R&D Systems, Minneapolis). Absorbance at 450 nm was measured with Synergy HTX Multi mode reader from Bio-Teck.

Intracellular phospho-STAT3 expression

Adherent monocytes were detached from the culture plates using Versene (Gibco). Cells were fixed and permeabilized with Cytofix/Cytoperm solution (eBioscience) and stained intracellularly with pSTAT3 antibody (Y705- PE; eBioscience). Cells were measured using an FC500 flow cytometer (Beckman Coulter) and gated on the monocytic cell population based on forward and side scatter plot.

RNA isolation and Quantitative PCR analysis

Percoll monocytes were cultured with urate for 24h at 37 °C. RNA was isolated using a phase separation method with TRIzol RNA isolation reagent (Life Technologies) and chloroform (VWR Life Science) in a 5:1 ratio. Subsequently, the RNA was precipitated with isopropanol (PanReac AppliChem). Reverse transcription into cDNA was performed using a cDNA synthesis kit (High-Capacity cDNA Reverse Transcription Kits, Applied Biosystems). Quantitative PCR was based on SYBR Green fluorescence (SYBR Green PCR master mix, Applied Biosystems) and a relative standard curve of 1:2 ratio in a final volume of 10 μ l on the StepOnePlus™ Real-Time PCR System.

Transcriptomic analysis

RNA-Sequencing for stimulated PBMCs was performed by Beijing Genomics Institute, Beijing, China. The integrity of the RNA was assessed using an Agilent

2100 BioAnalyzer. SOAPnuke (v1.5.2) was used for the initial quality control assessment. The clean reads were aligned to UniGene with Bowtie2 (v.2.2.5). RSEM (v.1.2.12) was used to estimate read counts. The resulting read counts were normalized using the R package (Version: R4.0.4.) DESeq2 (Version: DESeq2_1.34.0) along with the median of ratios method for downstream targeted gene expression statistical analysis.

DNA isolation and Whole Methylation Assay

Genomic DNA of 3 tested conditions (0, 10, and 50 mg/dL soluble urate) from 8 healthy volunteers (1 male, 7 females) was isolated using a Promega kit and was quantified using NanoDrop. Whole genome-wide DNA methylation profiles were measured using Infinium® MethylationEPIC array (~850,000 CpG sites). The DNA methylation values were gained from the raw IDAT files using the minfi package in R (v.4.0.3) [19], followed by sample- and probe-based quality control (QC). Stratified quantile normalization was subsequently implemented [20]. DNA methylation differential analysis between treated groups was performed in R using a Robust Linear Regression model, with sex as a covariate.

Statistical analysis

Statistical analysis was performed using GraphPad version 9.0.0 (GraphPad Software, La Jolla California USA) and R software. Considering data distribution, statistical evaluation was performed using One-Way ANOVA or Kruskal-Wallis when testing for at least 3 groups, and Student t-test or Mann-Whitney, when comparing 2 groups. Values of $P < 0.05$ were considered statistically significant.

Results

Increased pro-inflammatory cytokine production in human PBMCs after priming with urate

To evaluate the effect of soluble urate on human primary cells, we assessed cytokine production by PBMCs in the three groups of individuals: with normouricemia, asymptomatic hyperuricemia, and gout. After 24h priming with 12.5 and 50 mg/dL urate, the medium was removed, and the cells followed a subsequent 24h stimulation with LPS 10 ng/mL. A urate dose-dependent effect was observed in priming the cells to produce higher levels of IL-1 β and IL-6 and lower IL-1Ra production in all groups (Figure 1A-C), suggesting the

involvement of urate in inflammatory cytokine production, not only in controls but also in hyperuricemia and gout. In the normouricemia and gout group, IL-1 β and IL-6 production was significantly increased for both doses of urate. Possibly due to a lower number of donors and high variability, urate priming resulted in a significantly elevated production of IL-1 β and IL-6 only with the higher dose for the hyperuricaemia group, and IL-1Ra production was significantly decreased with the highest urate concentration across all groups (Figure 1A-C).

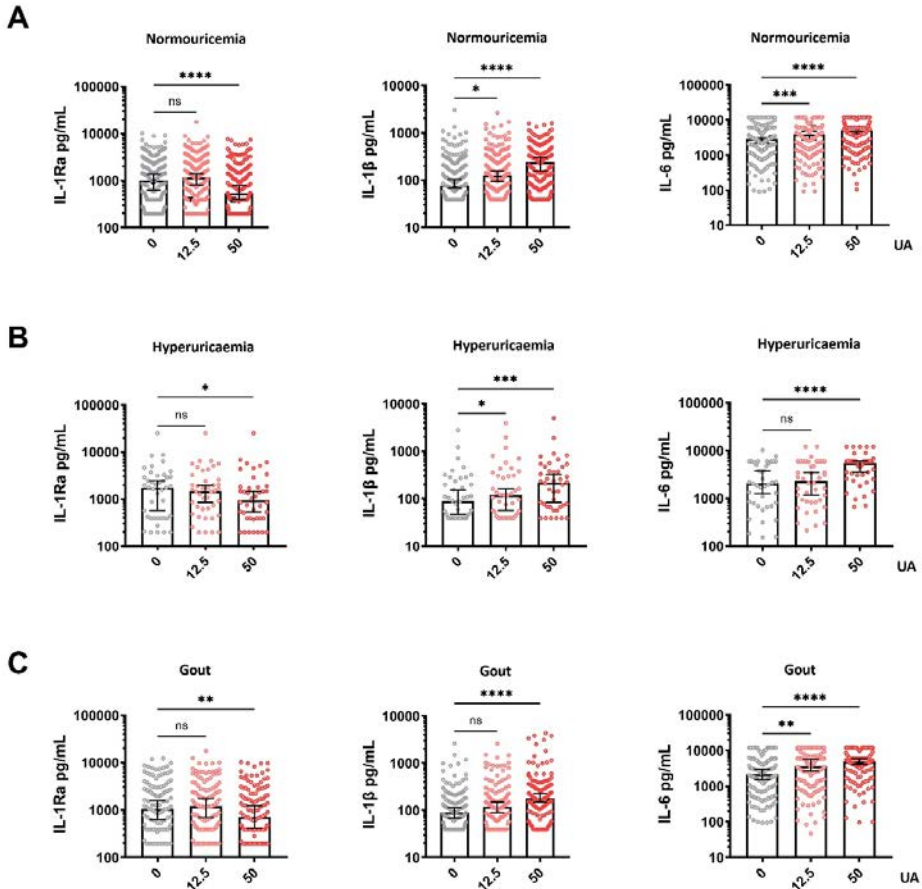


Figure 1. *In vitro*, urate priming of human PBMCs shows increased levels of IL-1 β concomitant with the decreased levels of IL-1Ra on a second restimulation with LPS. Cytokine production of IL-1Ra, IL-1, and IL-6 in supernatants of peripheral blood mononuclear cells (PBMCs) from patients with gout (n=126) (C), hyperuricaemia (n=42) (B) and normouricemia (n=192) (A) that have been primed for 24h with soluble urate in 10% serum and restimulated for additional 24h with LPS 10 ng/mL; Friedman test with Dunn's multiple comparisons test (*p<0.05; **p<0.01; ***p<0.001; ****p<0.0001); Data represents Median + 95% CI and it is shown on a log10 scale.

***SOCS3* expression enhanced by urate *in vitro* in human myeloid cells**

To evaluate the role of STAT3-*SOCS3* signalling in the urate-induced hyperinflammatory phenotype, firstly, *SOCS3* expression levels were assessed in a transcriptomic dataset available to our group from PBMCs of patients with gout, which were primed with urate and subsequently stimulated with LPS. The increase of *SOCS3* gene expression was urate dose-dependent and statistically significant for the highest dose, although a trend for the low dose can also be noted (Figure 2A). To test whether the increase in *SOCS3* expression is also present upon initial 24h priming with urate, monocytes from healthy volunteers were treated with urate alone for 24h, and *SOCS3* gene expression and IL-1Ra concentrations were assessed. Similar to the effect seen in post-LPS stimulation, *SOCS3* expression was also induced with urate treatment only (Figure 2B). In line with the previously described effect of urate reducing IL-1Ra, this increase in *SOCS3* expression was accompanied by a reduction in IL-1Ra cytokine production (Figure 2C).

DNA methylation of *SOCS3* gene shows no changes after 24h treatment of urate

Since urate-induced inflammation is associated with epigenetic modifications and *SOCS3* was previously reported to contain a differentially methylated region in hyperuricemic people [21], we explored whether the differential expression of *SOCS3* could be explained by differences in DNA methylation. We quantified genome-wide DNA methylation in monocytes treated 24h with a control medium (RPMI), a concentration close to *in vivo* hyperuricemia (10 mg/dL), and a high concentration of soluble urate (50 mg/dL) in 10% serum. Urate treatment resulted in reduced IL-1Ra production for both concentrations, thus confirming the priming phenotype (Supplementary Figure 1A). There were no significant differences in methylation levels (presented as β -values) across treatments (Figure 2D), although the observed pattern at cg18181703, cg11047325, and cg13343932 is consistent with what was previously described in whole blood from hyperuricemic individuals [8]. In addition, the 24h urate treatment did not induce substantial modifications in the samples as seen in the multidimensional scaling plot (Supplementary Figure 1B). The EWAS results (model 1: linear regression of Methylation (M value) \sim (Control/Uric acid) + sex) in *SOCS3* regions revealed that cg21985352 is the top differentially methylated site.

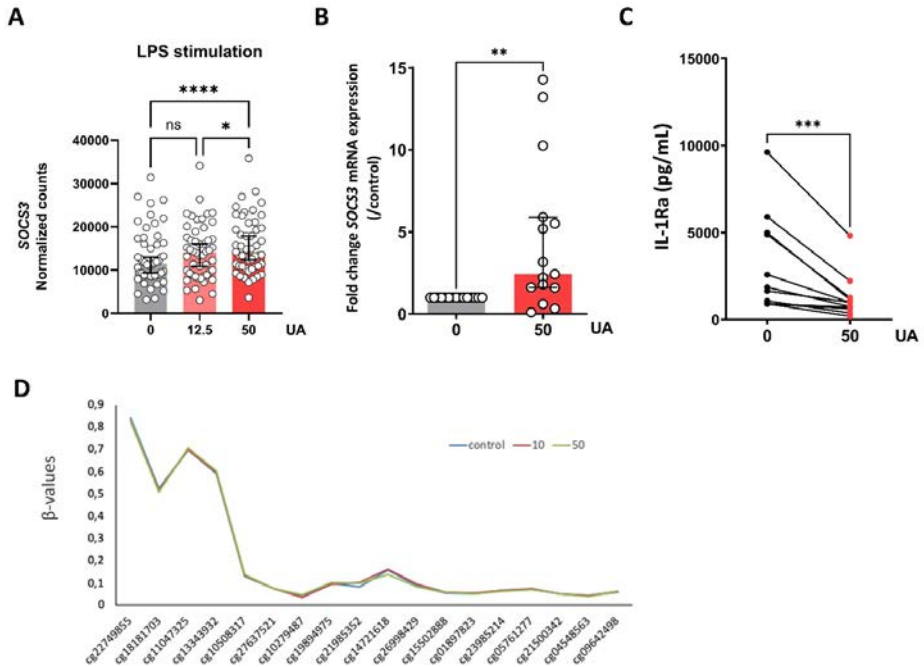


Figure 2. *SOCS3* is elevated by urate in myeloid cells. *SOCS3* normalized counts in PBMCs of gout patients that have been treated for 24h with culture medium (RPMI), urate 12.5 mg/dL or 50 mg/dL in 10% serum, followed by removal of medium and restimulation with LPS 10 ng/mL (Friedman test with Dunn's multiple comparisons test) **(A)**. *SOCS3* mRNA in a Percoll enriched monocyte fraction after 24h treatment (priming) with culture medium (RPMI) or urate 50 mg/dL in 10% serum (Wilcoxon test) **(B)** and corresponding IL-1Ra cytokine production (Wilcoxon test) **(C)**. DNA methylation β -values at *SOCS3* gene body in a pure population of monocytes from healthy volunteers ($n=8$) that were cultured for 24h with culture medium RPMI (blue line), urate 10 mg/dL (red line) or 50 mg/dL (green line) in 10% serum **(D)**. Data presented as Median with 95% CI (* $p < 0.05$; ** $p < 0.01$; *** $p < 0.001$; **** $p < 0.0001$).

STAT3 phosphorylation is inhibited in urate priming

To functionally validate *SOCS3* upregulation observed in gout patients and healthy volunteers, downstream levels of STAT3 phosphorylation were assessed. Freshly isolated PBMCs were exposed to soluble urate (10mg/dL and 50mg/dL), washed, and subsequently stimulated with LPS (10ng/mL) with or without MSU crystals (300 μ g/mL). Phosphorylation levels of STAT3 were determined by intracellular staining and flow cytometry. A dose-dependent reduction in phosphorylated STAT3 levels was observed with increasing concentration of urate on both LPS (Figure 3A) and LPS + MSU (Figure 3B) restimulation. These results were paralleled by a decrease in IL-1Ra (Figure 3C-D).

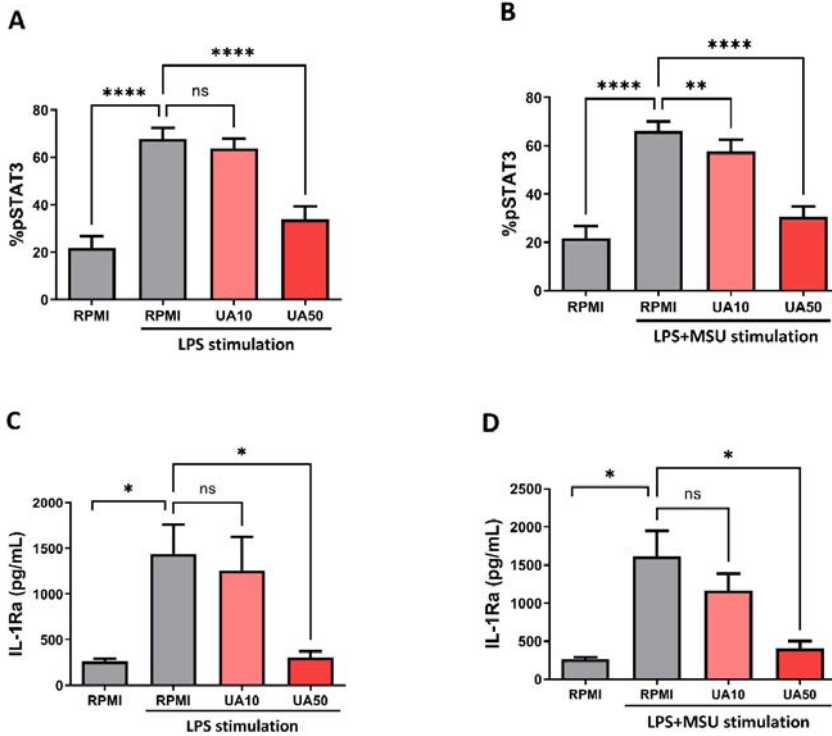


Figure 3. STAT3 involvement in urate priming. *In vitro* urate priming of human monocytes (Percoll) shows a decrease of phosphorylated STAT3 on LPS 10 ng/mL **(A)** and LPS 10ng/mL + MSU crystals 300ug/mL restimulation **(B)** (n=8) One-way ANOVA, Dunnett's multiple comparisons test (control column RPMI+LPS/LPS-MSU restimulation), Data presented as Mean \pm SEM; IL-1Ra cytokine production is decreased on LPS 10 ng/mL **(C)** and LPS 10ng/mL + MSU 300ug/mL restimulation (n=5) **(D)**, Paired t-test RPMI with RPMI + LPS/LPS+MSU restimulation, Data presented as Mean \pm SEM; One-way ANOVA on restimulated columns ((control column RPMI), Dunnett's multiple comparisons test, Data presented as Mean \pm SEM (* p <0.05; ** p <0.01; *** p <0.001; **** p <0.0001).

Urate priming is reversed in untreated patients with positive JAK2 V617F mutation

A *JAK2V617F* somatic mutation can be found in several myeloproliferative neoplasms and results in the constitutive activation of several signalling molecules, including STAT3 [22]. To investigate the involvement of STAT3 in urate priming, we pre-exposed PBMCs of patients with this mutation, who were not currently on any treatment, with two doses of soluble urate for 24h in 10% serum. Following the removal of culture media containing urate, the cells were restimulated with LPS 10 ng/mL and MSU crystals (300 μ g/mL). The

levels of IL-1 β (Figure 4A) and IL-6 (Figure 4B) were measured in supernatant. Intriguingly, our observations indicate that urate priming in PBMCs of patients with sustained STAT3 activation had no significant effect on the cytokine production in these cells, regardless of the urate concentration (Figure 4A-B).

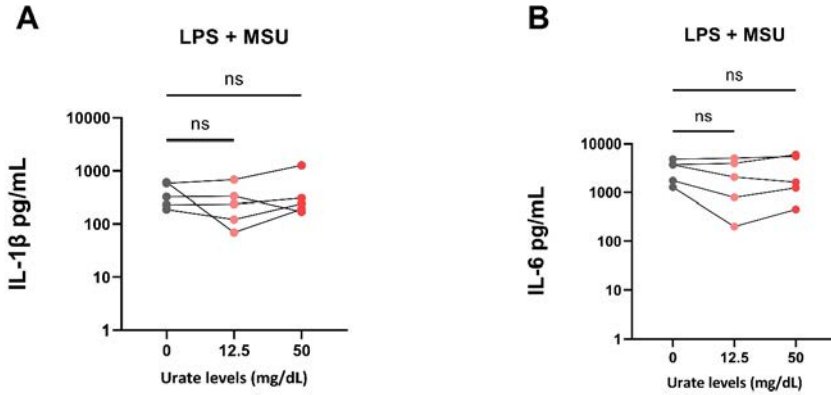


Figure 4. PBMCs from patients with the JAK2V617F somatic mutation (not receiving treatment) could not be primed by urate. IL-1 β (A) and IL-6 (B) production in supernatants of PBMCs of five JAK2 V617F positive patients subjected to the urate priming protocol: 24h priming with soluble urate (either no, 12,5 or 50mg/dL) and subsequent restimulation with LPS (10ng/mL) and MSU crystals (300 μ g/mL). One-Way ANOVA with Dunnett's multiple comparisons test. Cytokine production is presented on a log10 scale.

Discussion

Elevated serum uric acid levels, clinically referred to as hyperuricemia, can result in monosodium urate (MSU) crystal deposition and trigger the onset of gout. Previously published data shows that human myeloid cells that are pre-treated *in vitro* with soluble urate (also referred to as "primed") display an inflammatory profile characterized by increased pro-inflammatory IL-1 β and reduced anti-inflammatory IL-1Ra production in response to a later stimulation with LPS [7]. In our present study, we confirmed the urate priming effect in PBMCs of normouricemic volunteers, hyperuricemic individuals, and patients with gout [23]. Additionally, we report that *in vitro* urate priming leads to increased levels of *SOCS3* gene transcription in myeloid cells. This elevation leads to suppression of phosphorylated STAT3 and, in parallel, decreased production of IL-1Ra. This shift in increased *SOCS3* and decreased STAT3 is essential in the urate-induced pro-inflammatory phenotype as demonstrated

in PBMCs of patients with a mutation leading to STAT3 activation, where the urate-induced pro-inflammatory phenotype could not be observed. We conclude that STAT3 suppression due to the upregulation of SOCS3 may be linked to the decreased production of anti-inflammatory cytokine IL-1Ra in urate proinflammatory priming.

Previously, it was demonstrated that urate-primed monocytes produce increased pro-inflammatory cytokines by activation of the AKT-PRAS40 pathway and inhibition of autophagy [7]. The present study extends the mechanistic information related to soluble urate priming to show a role for SOCS3 via suppression of STAT3 in this urate-induced shift towards a pro-inflammatory phenotype. In general, SOCS3 is a potent intracellular cytokine negative regulator, mainly inhibiting IL-6 [13], but also IL-1 signalling [24], and plays an important role in regulating immune responses [9]. While SOCS3 does not directly inhibit IL-1, SOCS3 protects β -pancreatic cells against IL-1 β toxicity suggesting a cross-talk between SOCS3/IL-1 β pathway signalling [25]. Both IL-1 β and IL-6 can induce SOCS3 expression [26]. The expression level of *SOCS3* is found low in macrophages under baseline conditions and its induction requires exposure to inflammatory triggers such as LPS [27]. Although the generic effect of STAT3 on the IL-6-triggered pathway is anti-inflammatory, Murray proposed that the IL-6R, in the presence of SOCS3, generates a signal that suppresses the expression of anti-inflammatory genes [28].

Several studies on rats have demonstrated the involvement of the STAT3-SOCS3 pathway in hyperuricaemia. Hyperuricemia and hyperlipidaemia induced by fructose activate the NLRP3 inflammasome to promote the secretion of IL-1 β and IL-18, resulting in renal inflammation in rats. Pro-inflammatory cytokines cause dephosphorylation of key factors involved in renal leptin and insulin signalling transduction leading to increased renal STAT3 phosphorylation and SOCS3 expression, as well as the decreased phosphorylation of Akt and ERK1/2 [29]. On the other hand, in rat ischemic brain tissue, hyperuricaemia leads to the activation of IL-6/STAT3 signalling pathway and induces SOCS3 expression, conferring neuroprotection [30].

Interestingly, our results showed not only upregulation of *SOCS3* after LPS stimulation (Figure 2A) but also after urate treatment alone (Figure 2B). The upregulation of SOCS3 solely by urate coincided with lower production of IL-1Ra (Figure 2C). Possibly, the upregulation of SOCS3 has a pro-inflammatory effect in this context by suppressing phosphorylated STAT3 and IL-1Ra. This

is in line with previous studies, demonstrating STAT3 phosphorylation is essential not only for IL-1 β and IL-6 induction [31] but also for IL-1Ra as STAT3 is recruited to the IL-1Ra promoter in LPS plus IL-10 stimulated monocytes [18].

A prolonged state of hyperuricemia (high levels of serum urate) can progress to the formation and deposition of MSU crystals which, together with the triggering of TLRs, can lead to a gout flare [32]. SOCS proteins, including SOCS1 and SOCS3, regulate immune responses from TLR-induced stimuli in innate immune cells such as macrophages [33] and monocytes [34]. These responses are relevant in the first step of IL-1 β induction in gout flares [35]. Gout attacks usually resolve spontaneously to a full recovery over the course of 7 to 14 days, and although the molecular basis of this mechanism is not fully elucidated, some reports show it is associated with upregulation of intracellular CIS and SOCS3 expression in monocyte-derived macrophages [12]. In addition, MSU crystals may enhance *SOCS3* expression in human osteoclast precursors to inhibit JAK-STAT signalling by IL-6 and suppress osteoclastogenesis [36]. Also, in synovial fluid mononuclear cells from patients with a gout flare, *SOCS3* expression was elevated [37]. Orji *et al.* [38] propose that *SOCS3* may be involved in the resolution of gout flares as *SOCS3* expression is upregulated in PBMCs during a flare, and this inversely correlates with flare duration. The authors observed upregulation of *SOCS3* compared to normouricaemic non-gout patients with serum urate <360 $\mu\text{mol/l}$ (6 mg/dL) [38]. SOCS1, like SOCS3, was previously suggested to play a role in the inhibition of MSU crystal-induced inflammation. In a study by Cleophas *et al.*, monocytes were stimulated with MSU crystals and C16, a saturated fatty acid known to bind to TLR2, to mimic a gout flare. Thereafter, cells were treated with romidepsin, a potent HDAC inhibitor resulting in upregulation of SOCS1, which could further target inflammatory signalling molecules for proteasomal degradation, thereby inhibiting inflammation. The inhibition of the proteasome reversed the cytokine-suppressive effects of romidepsin [39]. Therefore, SOCS proteins may hold an important role in regulating and controlling inflammation in gout, by dampening excessive inflammatory response and consequently mitigating the intensity of flares.

Our results suggest that when human myeloid cells are subjected to *in vitro* urate priming, both phosphorylated STAT3 and IL-1Ra are downregulated leading to a pro-inflammatory phenotype (Figure 3A-B). In order to investigate the involvement of STAT3 in urate priming, we evaluated the priming capacity of PBMCs from patients positive for the *JAK2 V617F* somatic mutation, who

are characterized by constitutive STAT3 activation [22]. Interestingly, these patients showed unchanged levels of IL-1 β and IL-6 upon urate pretreatment (Figure 4A-B), suggesting that the inhibition of phosphorylated STAT3 may play an essential role in urate-induced pro-inflammatory phenotype.

As previous studies suggest a role for epigenetic modifications in urate-primed inflammation, we specifically assessed DNA methylation in the *SOCS3* gene. A study by Wang *et al.* highlights differential methylated loci (DML) in known gout risk genes from past GWAS (e.g. *SLC2A9*, *ABCC9*, *IL23R*), TF-gene regulatory networks in leukocytes such as *NFATC2* and *MEF2C*, and in signalling (*PRKAG2* involved in AMPK pathway), and transcriptional pathways involved in bridging innate to adaptive immunity (e.g. *STAT2*, *IRF1*, *NFATC2*, and *NFATC3*) [40]. Recently published data in individuals of Aotearoa NZ Māori ancestry revealed differential DNA methylation at three neighbouring CG sites within the *SOCS3* gene body in the whole blood of hyperuricemic individuals compared to normouricemic controls in an analysis without cell composition correction [8]. These differences were lost after correction for cell-type composition. Of note, inflammation could also change cell-type proportions and CpG methylation may be associated with these changes, complicating the interpretation of these findings. In the present study, interrogation of DNA methylation in a pure population of monocytes treated with soluble urate revealed no significant DMLs in *SOCS3* (Figure 2D). This could be related to possible hyperuricemia-induced cell proportion changes or that, at least in part, DNA methylation variability in *SOCS3* might be accounted for neutrophils [41]. Another possibility is that the *in vitro* stimulation conditions were insufficient to drive DNA methylation; 24-hour exposure to urate may not be comparable to long-term hyperuricemia *in vivo*.

Other limitations of this study include the limited number of patients with *JAK2V617F* mutations. More patients, including patients on targeted anti-JAK2 therapy, could give a more robust indication of the role of STAT3 in the urate-induced hyperinflammatory phenotype. Moreover, not all types of experiments could be performed for all patients due to logistic reasons. In addition, a direct link between phosphorylated STAT3 and the transcription of IL-1Ra would strengthen our hypothesis that hyperinflammation after urate treatment is due to inhibition of the anti-inflammatory cytokine IL-1Ra.

Conclusion

Urate-induced inflammation is characterized by elevated levels of pro-inflammatory IL-1 β and reduced levels of anti-inflammatory IL-1Ra. Urate leads to increased SOCS3 expression *in vitro* and suppressed STAT3 phosphorylation along with decreased IL-1Ra. This regulation of SOCS3 in response to urate is not dependent on DNA methylation in monocytes *in vitro*. Nevertheless, elevated SOCS3 and reduced pSTAT3 could play a relevant role in urate-induced hyperinflammation since urate priming had no effect in PBMCs from patients with continuously activated STAT3. Together, these findings add to the elucidation of intracellular mechanisms involved in the urate-induced hyperinflammatory phenotype.

Ethics approval and consent to participate

In-vitro experiments were approved by the Ethical Committee of the „Iuliu Hațieganu” University of Medicine and Pharmacy, Cluj-Napoca (approval no. 425/2016) and by the Ethical Committee of the Radboud University Medical Center (no. NL32357.091.10; registration number 2010/104). All participants provided written informed consent before inclusion. All experiments were conducted according to the principles of the Declaration of Helsinki.

Acknowledgements

This work is supported by a Competitiveness Operational Program Grant of the Romanian Ministry of European Funds (HINT, ID P_37_762; MySMIS 103587 to L.A.B.J.).

References

- [1] Dalbeth N, Bardin T, Doherty M, et al. Discordant American College of Physicians and international rheumatology guidelines for gout management: Consensus statement of the Gout, Hyperuricemia and Crystal-Associated Disease Network (G-CAN). *Nat Rev Rheumatol* 2017; 13:561–8.
- [2] Kahn K, Serfozo P, Tipton PA. Identification of the true product of the urate oxidase reaction. *J Am Chem Soc* 1997;119:5435–42.
- [3] Kim YS, Guevara JP, Kim KM, et al. Hyperuricemia and coronary heart disease: A systematic review and meta-analysis. *Arthritis Care Res (Hoboken)* 2010;62:170–80.
- [4] Stamp LK, Frampton C, Drake J, et al. Associations of Gout and Baseline Serum Urate Level With Cardiovascular Outcomes: Analysis of the Coronary Disease Cohort Study. *Arthritis Rheumatol* 2019;71:1733–8.
- [5] Disveld IJM, Zoakman S, Jansen TLTA, et al. Crystal-proven gout patients have an increased mortality due to cardiovascular diseases, cancer, and infectious diseases especially when having tophi and/or high serum uric acid levels: a prospective cohort study. *Clin Rheumatol* 2019;38:1385–91.
- [6] Athyros VG, Mikhailidis DP. Uric acid, chronic kidney disease and type 2 diabetes: A cluster of vascular risk factors. *J Diabetes Complications* 2014;28:122–3.
- [7] Crişan TO, Cleophas MCP, Novakovic B, et al. Uric acid priming in human monocytes is driven by the AKT-PRAS40 autophagy pathway. *Proc Natl Acad Sci* 2017;114:5485–90.
- [8] Badii M, Gaal OI, Cleophas MC, et al. Urate-induced epigenetic modifications in myeloid cells. *Arthritis Res Ther* 2021;23:1–11.
- [9] Alexander WS. Suppressors of cytokine signalling (SOCS) in the immune system. *Nat Rev Immunol* 2002;2:410–6.
- [10] Qin H, Roberts KL, Niyongere SA, et al. Molecular Mechanism of Lipopolysaccharide-Induced SOCS-3 Gene Expression in Macrophages and Microglia. *J Immunol* 2007;179:5966–76.
- [11] Hilton DJ, Richardson RT, Alexander WS, et al. Twenty proteins containing a C-terminal SOCS box form five structural classes. *Proc Natl Acad Sci U S A* 1998;95:114–9.
- [12] Chen YH, Hsieh SC, Chen WY, et al. Spontaneous resolution of acute gouty arthritis is associated with rapid induction of the anti-inflammatory factors TGF β 1, IL-10 and soluble TNF receptors and the intracellular cytokine negative regulators CIS and SOCS3. *Ann Rheum Dis* 2011;70:1655–63.
- [13] Croker BA, Krebs DL, Zhang JG, et al. SOCS3 negatively regulates IL-6 signaling in vivo. *Nat Immunol* 2003;4:540–5.
- [14] Babon JJ, Kershaw NJ, Murphy JM, et al. Suppression of Cytokine Signaling by SOCS3: Characterization of the Mode of Inhibition and the Basis of Its Specificity. *Immunity* 2012;36: 239–50.
- [15] Roberts AW, Robb L, Rakar S, et al. Placental defects and embryonic lethality in mice lacking suppressor of cytokine signaling 3. *Proc Natl Acad Sci U S A* 2001;98:9324–9.
- [16] Samavati L, Rastogi R, Du W, et al. STAT3 tyrosine phosphorylation is critical for interleukin 1 beta and interleukin-6 production in response to lipopolysaccharide and live bacteria. *Mol Immunol* 2009;46:1867–77.

- [17] Mori T, Miyamoto T, Yoshida H, et al. IL-1 β and TNF-initiated IL-6-STAT3 pathway is critical in mediating inflammatory cytokines and RANKL expression in inflammatory arthritis. *Int Immunol* 2011;23:701–12.
- [18] Tamassia N, Castellucci M, Rossato M, et al. Uncovering an IL-10-dependent NF- κ B recruitment to the IL-1 α promoter that is impaired in STAT3 functionally defective patients. *FASEB J* 2010;24:1365–75.
- [19] Aryee MJ, Jaffe AE, Corrada-Bravo H, et al. Minfi: A flexible and comprehensive Bioconductor package for the analysis of Infinium DNA methylation microarrays. *Bioinformatics* 2014;30:1363–9.
- [20] Touleimat N, Tost J. Complete pipeline for Infinium® Human Methylation 450K BeadChip data processing using subset quantile normalization for accurate DNA methylation estimation. *Epigenomics* 2012;4:325–341.
- [21] Cabău G, Crişan TO, Klück V, et al. Urate-induced immune programming: Consequences for gouty arthritis and hyperuricemia. *Immunol Rev* 2020;294:92–105.
- [22] Li R, Sun N, Chen X, et al. JAK2V617F Mutation Promoted IL-6 Production and Glycolysis via Mediating PKM1 Stabilization in Macrophages. *Front Immunol* 2021;11:1–12.
- [23] Crişan TO, Cleophas MCP, Oosting M, et al. Soluble uric acid primes TLR-induced proinflammatory cytokine production by human primary cells via inhibition of IL-1Ra. *Ann Rheum Dis* 2016;75:755–62.
- [24] Frobøse H, Rønn SG, Heding PE, et al. Suppressor of cytokine signaling-3 inhibits interleukin-1 signaling by targeting the TRAF-6/TAK1 complex. *Mol Endocrinol* 2006;20:1587–96.
- [25] Karlsen AE, Heding PE, Frobøse H, et al. Suppressor of cytokine signalling (SOCS)-3 protects beta cells against IL-1 β -mediated toxicity through inhibition of multiple nuclear factor- κ B-regulated proapoptotic pathways. *Diabetologia* 2004;47:1998–2011.
- [26] Tengesdal IW, Dinarello A, Powers NE, et al. Tumor NLRP3-Derived IL-1 β Drives the IL-6/STAT3 Axis Resulting in Sustained MDSC-Mediated Immunosuppression. *Front Immunol* 2021;12:661323.
- [27] Liu Y, Stewart KN, Bishop E, et al. Unique Expression of Suppressor of Cytokine Signaling 3 Is Essential for Classical Macrophage Activation in Rodents In Vitro and In Vivo. *J Immunol* 2008;180:6270–8.
- [28] Murray PJ. The JAK-STAT Signaling Pathway: Input and Output Integration. *J Immunol* 2007;178:2623–9.
- [29] Hu QH, Zhang X, Pan Y, et al. Allopurinol, quercetin and rutin ameliorate renal NLRP3 inflammasome activation and lipid accumulation in fructose-fed rats. *Biochem Pharmacol* 2012; 84:113–25.
- [30] Aliena-Valero A, Rius-Pérez S, Baixauli-Martín J, et al. Uric Acid Neuroprotection Associated to IL-6/STAT3 Signaling Pathway Activation in Rat Ischemic Stroke. *Mol Neurobiol* 2021;58:408–23.
- [31] Oike T, Kanagawa H, Sato Y, et al. IL-6, IL-17 and Stat3 are required for auto-inflammatory syndrome development in mouse. *Sci Rep* 2018;8:15783.
- [32] Dalbeth N, Choi HK, Joosten LAB, et al. Gout. *Nat Rev Dis Prim* 2019;5:69.

- [33] Qin H, Holdbrooks AT, Liu Y, et al. SOCS3 Deficiency Promotes M1 Macrophage Polarization and Inflammation. *J Immunol* 2012;189:3439–48.
- [34] Rastmanesh MM, Bluysen HAR, Joles JA, et al. Increased expression of SOCS3 in monocytes and SOCS1 in lymphocytes correlates with progressive loss of renal function and cardiovascular risk factors in chronic kidney disease. *Eur J Pharmacol* 2008;593:99–104.
- [35] Baetz A, Frey M, Heeg K, et al. Suppressor of cytokine signaling (SOCS) proteins indirectly regulate Toll-like receptor signaling in innate immune cells. *J Biol Chem* 2004;279:54708–15.
- [36] Cunningham CC, Corr EM, McCarthy GM, et al. Intra-articular basic calcium phosphate and monosodium urate crystals inhibit anti-osteoclastogenic cytokine signalling. *Osteoarthritis Cartilage* 2016;24:2141–52.
- [37] Liu L, Xue Y, Zhu Y, et al. Interleukin 37 limits monosodium urate crystal-induced innate immune responses in human and murine models of gout. *Arthritis Res Ther* 2016;18:268.
- [38] Orji OC, López-Domínguez MB, Sandoval-Plata G, et al. Upregulated expression of FFAR2 and SOCS3 genes is associated with Gout. *Rheumatology (Oxford)* 2023;62:977–83.
- [39] Cleophas MCP, Crişan TO, Klück V, et al. Romidepsin suppresses monosodium urate crystal-induced cytokine production through upregulation of suppressor of cytokine signaling 1 expression. *Arthritis Res Ther* 2019;21:50.
- [40] Wang Z, Zhao Y, Phipps-Green A, et al. Differential DNA Methylation of Networked Signaling, Transcriptional, Innate and Adaptive Immunity, and Osteoclastogenesis Genes and Pathways in Gout. *Arthritis Rheumatol* 2020;72:802–14.
- [41] Banks KM, Lan Y, Evans T. Tet Proteins Regulate Neutrophil Granulation in Zebrafish through Demethylation of socs3b mRNA. *Cell Rep* 2021;34:108632.

Supplementary material

Materials and methods

Participants

Study participants were recruited at the Rheumatology Department of the Iuliu Hațieganu University of Medicine and Pharmacy, Cluj-Napoca, Romania. The participants comprised patients with diagnosed gout (n= 126), hyperuricemic controls (n= 42) and normouricemic volunteers (n= 192) (the HINT study, hint-cluj.ro). All participants gave written informed consent before inclusion. Peripheral blood was drawn from the cubital vein on EDTA tubes under sterile conditions. The current study was approved by the Ethical Committee of the „Iuliu Hațieganu” University of Medicine and Pharmacy, Cluj-Napoca (approval no. 425/2016). Participants in the gout cohort were included based on at least one clinically diagnosed gout flare and either proven presence of MSU crystals in the synovial fluid or a score of at least 8 according to the American College of Rheumatology / European League Against Rheumatism (ACR/EULAR). Participants in the hyperuricemic group were included based on serum urate concentration ≥ 7 mg/dL and absence of gout.

Blood samples from patients with positive *JAK2V617F* somatic mutation were drawn at the Department of Haematology, Oncological Institute „Prof. Dr. Ion Chiricuță”, in Cluj-Napoca, Romania. Detection and quantification were done by real-time PCR using IVD Abaanalitica kit on a LightCycler 480 platform.

In the Netherlands, blood drawn from healthy volunteers was approved by the Ethical Committee of the Radboud University Medical Center (no. NL32357.091.10; registration number 2010/104). All patients with gout gave informed consent to use leftover blood for research purposes. The experiments were in accordance with the Declaration of Helsinki.

Cell preparation and culture conditions

Peripheral blood mononuclear cells (PBMCs) were isolated by means of Ficoll-Paque (GE Healthcare) density gradient centrifugation and washed 3 times with phosphate-buffered saline (PBS) at 4 °C. PBMCs were cultured at 5×10^5 /well in a 96-well plate, flat bottom. Percoll monocyte enrichment were obtained by gradient centrifugation of PBMCs using Percoll hyperosmotic density gradient solution. For preparation of 100 ml Percoll solution there were used: 48.5 mL Percoll (GE Healthcare), 41.5 mL sterile water (Sterile water for

irrigation, Versol) and 10 mL 1.6M NaCl. Percoll monocytes were cultured at 10^5 /well in a 96-well plate, flat bottom. Monocytes were isolated using a Pan Monocyte Isolation Kit and further cultured in a 6-well plate (2×10^6 /well) with soluble urate for 24h (50 and 10 mg/dL) and RPMI for control.

Cells were counted by Coulter Counter method and plated in Dutch Modified RPMI 1640 medium (Sigma) supplemented with 50 μ g/mL gentamycin (Sigma), 2 mM GlutaMAX (Gibco) and 1 mM pyruvate (Gibco) and 10% human pooled serum. Each condition was performed in replicate wells and supernatants (conditioned media) were pooled before measurement and stored at -20°C until performing of ELISA. Cytokine responses to mimic hyperuricemia *in vitro* were induced by incubating the cells with a high dose of soluble urate and a more *in vivo* relevant dose (50, 12.5, or 10mg/dL). Working dilutions were prepared in the cell-culture medium. Urate concentrations were chosen based on previous studies [1]. Cells were incubated for 24h at 37°C 5% CO_2 , followed by removal of culture medium along with washing of urate, and restimulation of remaining adherent cells for an additional 24h with LPS 10 ng/mL or LPS 10 ng/mL + MSU crystals 300 μ g/mL and RPMI for contamination control. Cytokine levels were measured in culture supernatants at 24h and 48h. Uric acid and LPS (*E. coli* serotype 055:b5), suitable for cell culture, were purchased from Sigma. LPS was ultra-purified before cell culture experiments. MSU crystals were prepared as previously described [2]. Treated cells were stored at -80°C in TRIzol Reagent (Invitrogen) for further gene expression.

Cytokine measurements

Cytokine measurements were carried out in conditioned media from experiments collected at 24h and 48h by means of enzyme-linked immunosorbent assay with ELISA kits for IL-1 β , IL-1Ra, IL-6 according to the manufacturer's instructions (R&D Systems, Minneapolis). Absorbance at 450 nm was measured with Synergy HTX Multi mode reader from Bio-Teck. The lowest range of detection was 39 pg/mL for IL-1 β ; 390 pg/mL for IL-1Ra and 94 pg/mL for IL-6. Samples were diluted prior to assay 10-fold for IL-1 β and IL-1Ra and 20-fold for IL-6.

Intracellular phospho-STAT3 expression

Following the protocol for urate priming described above, the remaining adherent cells were detached from the culture plates using Versene (Gibco). Cells were fixed and permeabilized with Cytofix/Cytoperm solution (eBioscience) according to the manufacturer's recommendations. Cells

were stained intracellularly with pSTAT3 antibody (Y705- PE; eBioscience) according to the manufacturer's recommendations. Cells were measured using an FC500 flow cytometer (Beckman Coulter). Cells were gated on the monocytic cell population based on forward and side scatter plot.

RNA isolation and Quantitative PCR analysis

Percoll monocytes were cultured with urate for 24h at 37 °C. Supernatants were collected for cytokine measurements to check for the possibility of contamination and a volume of 50ul of TRIzol to lyse the cells was added to the wells and stored at -80 °C until RNA isolation. RNA was isolated using a phase separation method with TRIzol RNA isolation reagent (Life Technologies) and chloroform (VWR Life Science) in a 5:1 ratio. Subsequently, the RNA was precipitated with isopropanol (PanReac AppliChem). Reverse transcription into cDNA was performed using cDNA synthesis kit (High-Capacity cDNA Reverse Transcription Kits, Applied Biosystems). Quantitative PCR was based on SYBR Green fluorescence (SYBR Green PCR master mix, Applied Biosystems) and a relative standard curve of 1:2 ratio in a final volume of 10 ul on the StepOnePlus™ Real-Time PCR System. *SOCS3* expression values from the samples were normalized by dividing them by the values obtained for *B2M* house-keeping gene. Primers used: *SOCS3* Fw 5' TGCGCCTCAAGACCTTCAG 3' and *SOCS3* Rv 5' GAGCTGTCGCGGATCAGAAA 3'; *B2M* Fw 5' ATGAGTATGCCTGCCGTGTG 3' and *B2M* Rv 5' CCAAATGCGGCATCTTCAAAC 3'.

Transcriptomic analysis

*The current study uses transcriptomic data generated by the HINT Project (Hyperuricemia-induced Inflammation: Targeting the central role of uric acid in rheumatic and cardiovascular diseases, ID P 37 762; MySMIS 103587) implemented in Cluj-Napoca Romania at the Iuliu Hațieganu University of Medicine and Pharmacy. The study aimed to describe inflammation associated with gout and urate using a systems biology approach, and therefore, relatively large datasets were available to assess differences in gene expression.

PBMCs were isolated by density gradient centrifugation method using Ficoll-Paque PLUS (Sigma Aldrich) from the whole blood of patients with gout. PBMCs after *in vitro* stimulations were stored at -80 °C in TRIzol reagent (Invitrogen) and outsourced for RNA-Seq analysis (Beijing Genomics Institute, Beijing, China). The integrity of the RNA was assessed using Agilent 2100 Bio.

The mRNA was captured from total RNA using Oligo dT magnetic beads. Fragmented target RNA was reverse transcribed to cDNA using random N6 primers followed by end-repair and a tailing for adaptor ligation. PCR amplification was used to enrich purified ligation products. The next step consisted of denaturation and cyclization of ssDNA by splint oligos and DNA ligase generating DNA nanoballs (DNBs). Sequencing of DNBs was performed on the DNBseq platform.

Raw data was generated by removing reads mapped to rRNAs. Clean reads were generated using SOAPnuke software (version v1.5.2) by removing reads with adaptors, reads with unknown bases >10% and low-quality reads, defined as reads with a quality score less than 15 in over 50% bases. Clean reads were further mapped to the reference UniGene using Bowtie2. Read counts were estimated with RSEM (v.1.2.12) and normalized using the R package (Version: R4.0.4.) DESeq2 (Version: DESeq2_1.24.0) along with median of ratios method for downstream targeted gene expression statistical analysis.

DNA isolation and Whole Methylation Assay

Genomic DNA of 3 tested conditions (0, 10 and 50 mg/dL soluble urate) from 8 healthy volunteers (1 male, 7 females) was isolated using the Promega kit according to the manufacturer's instructions and was quantified using NanoDrop. Samples that passed A260/280 ratio equal or above 1.7 were selected (all passed). A total of 750 ng of DNA was sent for methylation array.

Whole genome-wide DNA methylation profiles was measured using Infinium® MethylationEPIC array (~850,000 CpG sites). The DNA methylation values were gained from the raw IDAT files using the minfi package in R (v.4.0.3) [3], followed by sample- and probe-based quality control (QC). As for the sample QC, if 1% or more of the probes of a sample have a detection p-value > 1%, we excluded the sample. We also checked whether the samples were mixed up by using predicted gender information. There were no bad or mixed-up samples in this dataset. As for the probes QC, we filtered the bad quality probes with a detection *P-value* > 0.01 (n=2698), cross-reactive probes (n=42779), polymorphic probes (n=9769) [4], and probes in the sex chromosome (n=19470). After probes QC steps, 71660 probes were removed, 787214 probes and 24 samples were left for the downstream analyses. We subsequently implemented stratified quantile normalization [5]. DNA methylation differential analysis between treated groups was performed in R using a Robust Linear Regression model, with sex as covariates.

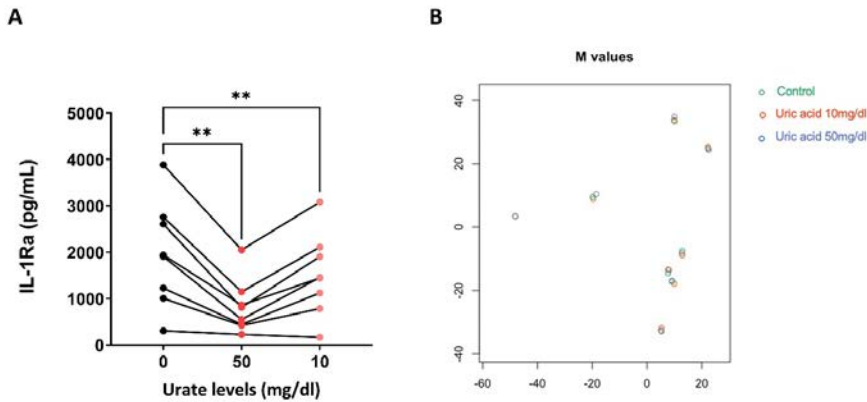
Statistical analysis

Statistical analysis was performed using Graphpad version 9.0.0 (GraphPad Software, La Jolla California USA) and R software (4.0.3, 4.0.4 version and 4.2.1). Considering data distribution, statistical evaluation was performed using One-Way ANOVA or Kruskal-Wallis when testing for at least 3 groups, and Student t-test or Mann-Whitney, when comparing 2 groups. Values of $P < 0.05$ were considered statistically significant.

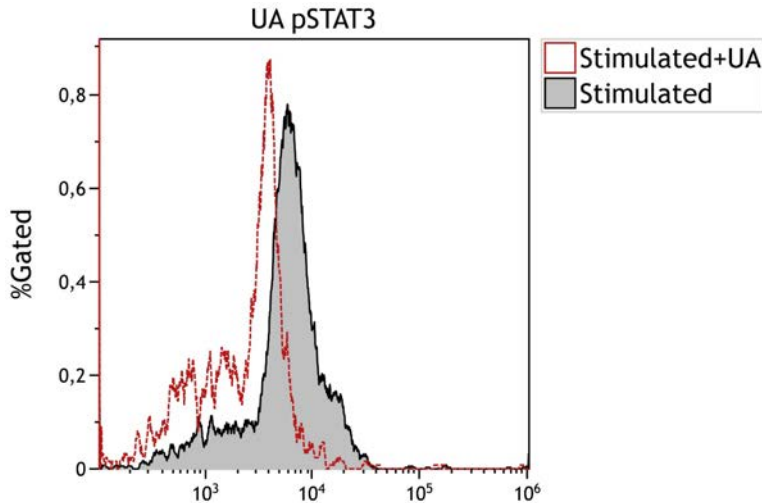
References

- [1] Crişan TO, Cleophas MCP, Novakovic B, et al. Uric acid priming in human monocytes is driven by the AKT-PRAS40 autophagy pathway. *Proc Natl Acad Sci* 2017;114:5485-90.
- [2] Joosten LAB, Netea MG, Mylona E, et al. Engagement of fatty acids with toll-like receptor 2 drives interleukin-1 β production via the ASC/caspase 1 pathway in monosodium urate monohydrate crystal-induced gouty arthritis. *Arthritis Rheum* 2010;62:3237-48.
- [3] Aryee MJ, Jaffe AE, Corrada-Bravo H, et al. Minfi: A flexible and comprehensive Bioconductor package for the analysis of Infinium DNA methylation microarrays. *Bioinformatics* 2014;30:1363-9.
- [4] Pidsley R, Zotenko E, Peters TJ, et al. Critical evaluation of the Illumina MethylationEPIC BeadChip microarray for whole-genome DNA methylation profiling. *Genome Biol* 2016;17:208.
- [5] Touleimat N, Tost J. Complete pipeline for Infinium® Human Methylation 450K BeadChip data processing using subset quantile normalization for accurate DNA methylation estimation. *Epigenomics* 2012;4:325-41.

Supplementary Figures



Supplementary Figure 1. *In-vitro* urate-primed monocytes for EPIC methylation array. (A) IL-1Ra cytokine production in monocytes treated for 24h with urate (10mg/dL, 50 mg/dL) and RPMI medium for control in 10% serum; One Way Anova; Dunnett's multiple comparisons test (* $p < 0.05$, ** $p < 0.01$); (B) Multidimensional scaling plot of 24h treated samples with urate (10mg/dL, 50 mg/dL) and RPMI medium for control in 10% serum ($n=8$), x- and y-axis represent abstract dimensions that capture the relationships and distance based on dissimilarities between the treated samples.



Supplementary Figure 2. Staining of STAT3 on urate-primed monocytes following stimulation with LPS. The filled grey histogram shows the level of staining in the monocytes pre-exposed to medium RPMI and LPS stimulated, while the red line corresponds to stimulated cells pre-exposed to urate 50 mg/dL.

CHAPTER 4

Downregulation of type I interferon signalling pathway by urate in primary human PBMCs

Medeea Badii*, Valentin Nica*, Ancuța Straton, Brenda Kischkel, Orsolya Gaal, Georgiana Cabău, Viola Klück, Ioana Hotea, HINT Consortium, Boris Novakovic, Cristina Pamfil, Simona Rednic, Mihai G. Netea, Radu A. Popp, Leo A. B. Joosten# and Tania O. Crișan#

*These authors contributed equally to this work

#These authors share senior authorship

Immunology, 2024 Oct 1, doi: 10.1111/imm.13858. Epub ahead of print

Summary

Type I interferons (IFN1) mediate innate responses to microbial stimuli and regulate interleukin (IL)-1 and IL-1 receptor antagonist (Ra) production in human cells. This study explores interferon-stimulated gene (ISG) alterations in the transcriptome of patients with gout and stimulated human primary cells *in vitro* in relation to serum urate concentrations. Peripheral blood mononuclear cells (PBMCs) and monocytes of patients with gout were primed *in vitro* with soluble urate, followed by lipopolysaccharide (LPS) stimulation. Separately, PBMCs were stimulated with various toll-like receptor (TLR) ligands. RNA sequencing and IL-1Ra cytokine measurement were performed. STAT1 phosphorylation was assessed in urate-treated monocytes. Cytokine responses to IFN- β were evaluated in PBMCs cultured with or without urate and restimulated with LPS and monosodium urate (MSU) crystals. Transcriptomics revealed suppressed IFN-related signalling pathways in urate-exposed PBMCs or monocytes which was supported by diminishment of phosphorylated STAT1. The stimulation of PBMCs with IFN- β did not modify the urate-induced inflammation. Interestingly, *in vivo*, serum urate concentrations were inversely correlated to *in vitro* ISG expression upon stimulations with TLR ligands. These findings support a deficient IFN1 signalling in the presence of elevated serum urate concentrations, which could translate to increased susceptibility to infections.

Introduction

Hyperuricemia, defined as elevated serum urate concentration above the saturation threshold, is mostly an asymptomatic condition but constitutes a prerequisite for gouty arthritis [1]. Normal serum urate concentrations in humans have been reported to range from 2 [2] and 6.8 mg/dL [3]. Individuals with hyperuricemia are also prone to develop other comorbidities such as hypertension, acute and chronic kidney disease, metabolic syndrome, and diabetes mellitus [4], and most studies indicate that hyperuricemia precedes the onset of these diseases [5] [6] [7]. Priming human monocytes with soluble urate increased the responsiveness of the immune cells to a second stimulation with TLR2/4 ligands [8]. Urate priming increases IL-6 and IL-1 β production, whereas IL-1Ra is decreased [8], and the process is mediated by the activation of the AKT-PRAS40 pathway and suppression of autophagy [9].

Several studies link hyperuricemia or gout to type I interferon (IFN1) pathway modulation. Serum urate concentrations are influenced by a combination of genetic traits and environmental factors, such as increased production or reduced excretion [10] [11]. DNA methylation changes, especially in *SLC2A9*, directly influence serum urate concentrations and are associated with urate transport and regulation of IFN1 [12]. In individuals with hyperuricemia, genome-wide DNA methylation analysis shows variations at loci such as *HLA-G*, *PRKAB2*, and *IFITM3*, indicating that urate might impact AMPK and IFN1 pathways [13]. In patients with gout, DNA methylation alterations were identified in transcription factors (TFs) involved in interferon signal transduction [14]. *In vitro*, monosodium urate (MSU) crystals transcriptionally reprogram macrophages, influencing SCL transporters and AP-1 activation, without affecting interferon regulatory factors (IRFs) or interferon genes, unlike LPS stimulation [15]. Meanwhile, transcriptome sequencing of human monocytes treated *in vitro* with the soluble form of urate shows that genes involved in IFN1-related signalling pathways are suppressed [9]. In support of this, a clinical study assessing the inflammatory effects of soluble urate found that genes belonging to the type I IFN signalling pathway were upregulated in patients receiving rasburicase to lower uric acid levels [16].

The induction of IFN1 and ISGs is essential for the host's immune response to microbial pathogens, particularly viruses [17], but also bacteria, parasites, and fungi [18]. IFN1, such as IFN- α and IFN- β , are induced by the engagement of Toll-like receptors such as TLR3 [19], TLR4 [20], TLR7/8, and TLR9 [21] [22],

acting locally in an autocrine and paracrine manner. They induce immune responses by binding the IFNAR1/IFNAR2 receptor and activating the JAK-STAT pathway. Downstream IFNAR, canonical signalling leads to the formation of STAT1 dimers, STAT3 dimers, and the ISGF3 complex, which translocate to the nucleus to regulate the expression of ISGs [23] [24]. Interestingly, IFN1 also antagonize inflammatory responses, especially through the regulation of IL-1 bioactivity. IFN1 can induce the expression of the IL-1 receptor antagonist (IL-1Ra) in monocytes [25] and PBMCs [26]. Furthermore, IFN1 have been documented to dampen IL-1 β production *in vitro* [27] and *in vivo* [28], indicating their ability to suppress IL-1-mediated inflammation.

The primary objective of this study is to assess the interaction between elevated urate concentrations and IFN1-related pathways. We propose that IFN1 downregulation might serve as a mechanism that explains the altered IL-1 β and IL-1Ra production observed in urate priming *in vitro*. We analyse the transcriptomic changes following urate exposure in human primary cells of patients with gout and healthy donors. Additionally, we examine ISG expression in peripheral blood mononuclear cells (PBMCs) of patients with gout and hyperuricemia upon TLR ligand stimulation.

Materials and methods

A detailed version of this section is provided in Supplementary Material.

Participants

The study included patients with diagnosed gout ($n = 52$, median serum urate 6.60 mg/dL), along with healthy volunteers for *in vitro* validation experiments.

This study was approved by the Ethical Committees of the „Iuliu Hațieganu” University of Medicine and Pharmacy or Radboud University Medical Center.

Cell preparation and culture conditions

PBMCs were isolated using Ficoll-Paque (GE Healthcare) from fresh whole blood and used immediately for *in vitro* experiments. The urate priming experiments were conducted using RPMI culture medium supplemented with 10% human pooled serum. 5×10^5 PBMCs were primed for 24h with medium RPMI, urate (50 mg/dL), IFN- β (100 IU/mL), or urate+IFN- β , followed by stimulation with LPS (10ng/mL) or LPS (10ng/mL) + MSU (300ug/mL). The priming experiment

for RNA-Seq involved 24h priming with urate 12.5 and 50 mg/dL followed by 24h restimulation with LPS 10 ng/mL. In separate experiments, PBMCs were stimulated for 24h with Poly: IC (10 ug/mL), CpG (1 ug/mL), and heat-killed *C.albicans* (10⁶ col/mL) without serum supplementation.

Cytokine measurements

IL-1 β , IL-1Ra, and IL-6 were measured using ELISA (R&D Systems, Minneapolis). The lowest range of detection was 39 pg/mL for IL-1 β , 390 pg/mL for IL-1Ra, and 94 pg/mL for IL-6.

Intracellular phospho-STAT1 expression

PBMCs from healthy volunteers were primed for 24h with urate 50 mg/dL and restimulated for 4h with LPS 10 ng/mL + MSU (300ug/mL). Cells were stained intracellularly with pSTAT1 antibody (PE anti-STAT1 Phospho (Ser727) Antibody) and measured using an FC500 flow cytometer (Beckman Coulter). The identification and selection of monocytic cell populations were carried out using a series of gating steps as described in Supplementary Material.

Transcriptomic profiling

RNA-sequencing of stimulated PBMCs was performed with the DNBseq technology (Beijing Genomics Institute, Beijing, China). Publicly available data [9] was used for urate-exposed monocytes.

Statistical analysis

The statistical analysis was performed using GraphPad version 9.0 (GraphPad Software, La Jolla California USA) and R version 4.2.2 (R Foundation for Statistical Computing, Vienna, Austria. URL <https://www.R-project.org/>).

The schematic representations were created using Biorender.

Results

IFN1 signalling pathway is down-regulated in PBMCs of patients with gout upon urate pre-treatment and LPS restimulation

To investigate alterations in gene transcription due to urate priming, PBMCs (n = 52) isolated from patients with gout were primed with RPMI medium, a high concentration (50 mg/dL), or a low concentration (12.5 mg/dL) of soluble urate for 24h. Following the removal and washing of urate, the cells

were restimulated for 24h with LPS 10 ng/mL. Cells were supplemented with 10% serum in all experiments (**Figure 1a**). Following differential expression analysis, up- and down-regulated genes (**Table S1**) were analysed separately. Pathway enrichment analysis of the differentially expressed genes (DEGs) with decreased transcription level (adjusted p-value < 0.05 and log2 FoldChange < -1) reveals significant Gene Ontology Biological Processes (GOBP) terms associated with the type I interferon signalling pathways, immune responses to virus and bacteria, and pathways that involve complement activation (**Table S2**, **Figure 1b**). Upregulated DEGs were enriched for GOBP terms such as cell response to bacteria, cell chemotaxis, and migration (**Table S3**).

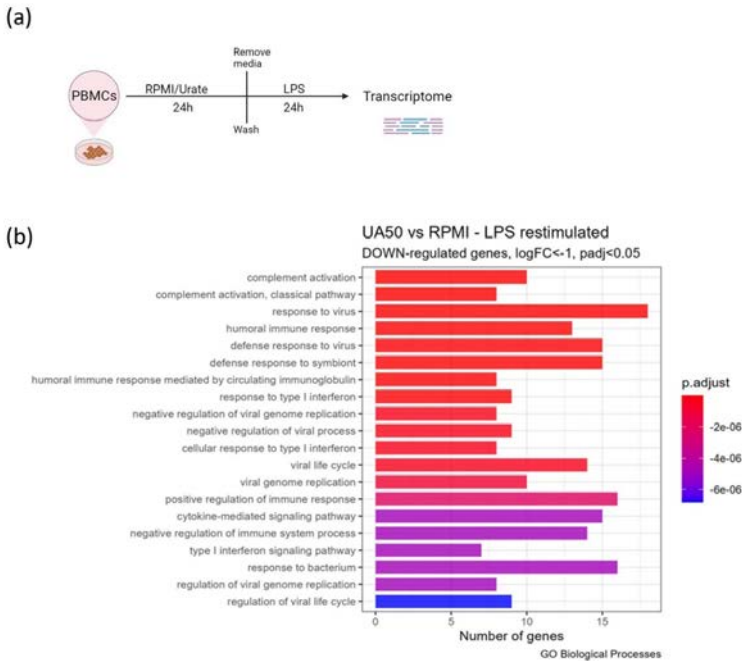
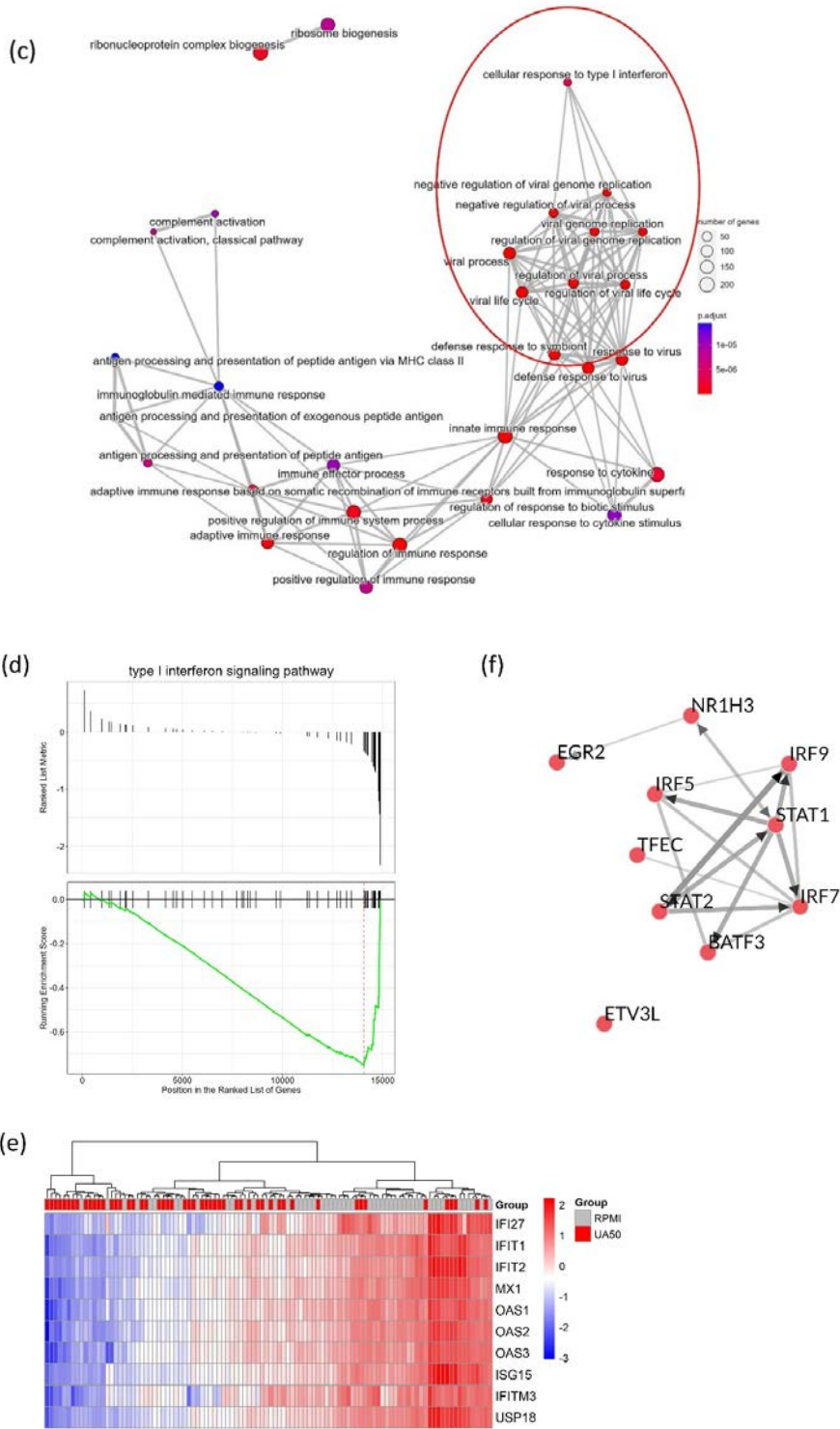


> **Figure 1. RNA-Seq reveals downregulation of type I interferon signalling pathways in human PBMCs upon urate priming.** Schematic representation of *in-vitro* experiments used for transcriptomic analysis (n = 52) (**a**); Pathway enrichment analysis of down-regulated genes at $\text{padj} < 0.05$ and $\text{log2FC} < -1$ using Gene Ontology - Biological processes (top 20 terms) (**b**). Enrichment map of GO Biological Processes terms of down-regulated genes at $\text{padj} < 0.05$ and $\text{log2FC} < -1$ (**c**). Curve of Gene Set Enrichment Analysis (GSEA) enrichment scores for type I interferon signalling pathways ($\text{padj} = 2.42022\text{E-}05$; $\text{NES} = -2,128$) (**d**). Heatmap of differentially expressed genes (down-regulated) that overlap the GO BP terms „response to type I interferon, „cellular response to type I interferon“ and „type I interferon signalling pathway“ (variance stabilized normalized counts corrected for batch effect); The relative value for each gene is shown by the colour intensity of the Z score, with red indicating up-regulated and blue indicating downregulated genes (**e**). Network Visualizations with ChEA3 of transcription factors (TFs) according to the similarity in their co-expression patterns using differentially expressed gene set of urate 50 mg/dL + LPS 10 ng/mL at $\text{padj} < 0.05$; $\text{logFC} < -1$ (**f**).



The enrichment map of GOBP visually represents clusters of enriched terms to show close relationships and associations between terms related to type I interferons and viral processes, indicating that they contain common genes (**Figure 1c**). GSEA analysis revealed a significant enrichment of IFN1 gene sets in the down-regulated genes, with a p-adjusted value of $2.42\text{E-}05$ and a negative enrichment score (NES) of -2.128 for the "type I interferon signalling pathway." (**Figure 1d, Table S4**). Several of these terms, such as "response to virus", "response to type I interferon" or "type I interferon signalling pathway", were associated with downregulated gene transcription (e.g. *IFI27*, *IFIT1*, *IFIT2*, *IFITM3*, *ISG15*, *MX1*, *OAS1*, *OAS2*, *OAS3*, *USP18*) (**Figure 1e**) upon urate 50 mg/dL priming in PBMCs. TF over-representation analysis of down-regulated DEGs in urate-primed PBMC identified a predicted TF co-expression network of the top 10 TFs (STAT1, STAT2, NR1H3, BATF3, TFEC, IRF9, ETV3L, IRF5, IRF7, and EGR2) (**Figure 1f, Table S5**).

DEG analysis of PBMCs primed with urate (12.5 mg/dL) and restimulated with LPS reveals decreased expression of genes belonging to IFN1, albeit to a lesser extent than the higher dose of urate (**Table S6**). GSEA using Reactome (**Table S7**) and GO Biological Processes (**Table S8**) helped uncover biologically relevant pathway alterations, even in the presence of minimal or no significant changes in individual gene expression. Notably, terms related to "interferon responses" and "viral regulation" were associated with down-regulated gene expression, even at a lower dose of urate (**Figure S1**). The effect size differs dose-dependently between urate 50 mg/dL and 12.5 mg/dL, with consistent changes in gene expression in response to both conditions (**Figure S2**).

Downregulation of the IFN1 pathway in human monocytes treated with urate

To investigate the specific regulation of IFN1-related pathways by urate alone, we analysed the previously published dataset described by Crisan et al. [9] in which monocytes isolated from healthy volunteers were primed with RPMI or a high dose of urate (50 mg/dL) for 20 h (**Figure 2a**). GOBP gene enrichment analysis of urate down-regulated genes identified enrichment for virus-regulated pathways (**Figure 2b, Table S9**). Among the genes associated with these terms are *IFIT1*, *MX1*, *OAS1*, *OAS2*, *OAS*, *ISG15*, *IFITM3*, *RSAD2*, and *USP18*. These genes also overlapped with the terms from the pathway analysis conducted on PBMCs. When examining the same set of genes depicted in **Figure 1f**, we observe a stronger grouping on the samples that received urate treatment only (**Figure 2c**). Within

the down-regulated gene set, we identified significant enrichment for key TFs of IFN1, such as STAT1, IRF5, and IRF9 (Figure 2d, Table S10).

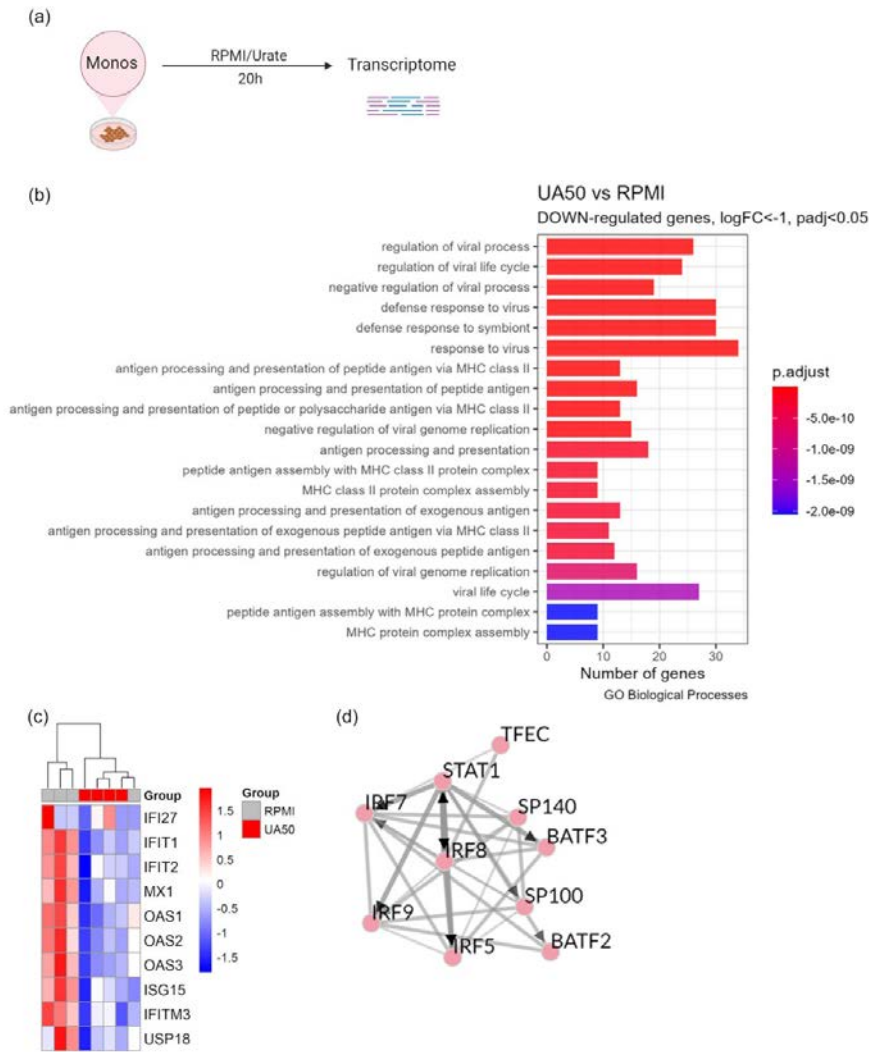


Figure 2. RNA-Seq confirms downregulation of type I interferon in primary human monocytes. Schematic representation of *in-vitro* experiments used for transcriptomic analysis ($n = 4$) (a); Pathway analysis of down-regulated differentially-expressed genes at $p_{adj} < 0.05$ and $\log_2FC < -1$ for GO Biological processes (top 20 terms) (b). Heatmap of Interferon Stimulated Genes treated with urate 50 mg/dL and RPMI medium for control. The relative value for each gene is shown by the colour intensity of the Z score, with red indicating up-regulated and blue indicating down-regulated genes (c). Network Visualizations with ChEA3 of transcription factors according to the similarity in their co-expression patterns using differentially expressed gene set of urate 50 mg/dL at $p_{adj} < 0.05$; $\log_2FC < -1$ (d).

STAT1 phosphorylation is decreased upon urate treatment

To assess at the protein level whether the signal transduction pathway associated with ISGs is altered in response to urate, PBMCs from healthy volunteers ($n = 5$, two independent experiments) were primed for 24h with urate 50 mg/dL or RPMI medium and were restimulated with LPS 10 ng/mL + MSU 300 ug/mL for an additional 4h (**Figure 3a**). At the end of the experiment, the cells were stained for intracellular phosphorylated STAT1 and extracellular markers to differentiate monocytic cell populations (**Figure S3, Table S11**). Urate treatment alone decreased STAT1 phosphorylation in HLA-DR⁺ or classical monocytes (left subpanel **Figure 3b,c**). Although not statistically significant, there is a noticeable difference in reduced phosphorylated STAT1 levels in urate 50 mg/dL treated and LPS+MSU restimulated HLA-DR⁺ (**Figure 3b,c**) and classical (**Figure 3c**) monocytes ($p=0.0625$). These observations were not possible for intermediate and non-classical monocytes, most likely because the population numbers were too low (**Figure S3**). The classic pathway for IFN1 involves the formation of the STAT1/STAT2/IRF9 complex, known as the ISGF3 complex, which translocates to the nucleus to bind to ISRE and induce the expression of antiviral ISGs [18]. We examined the transcriptome data for PBMCs primed with 50 and 12 mg/dL urate and observed a dose-dependent decrease in the expression of genes integral to the ISGF3 complex (**Figure S4**). These results complement the TF enrichment analysis shown in Figure 1 and Figure 2.

Induction of the IFN1 pathway with IFN- β did not reverse the pro-inflammatory effect in urate

Given that urate treatment leads to the transcriptional suppression of ISGs, we subsequently aimed to explore whether we could reverse the priming effect induced by urate by stimulating the IFN1 pathway *in vitro* using human recombinant interferons. To accomplish this, PBMCs were cultured for 24h with urate 50 mg/dL in the presence or absence of IFN- β 100 IU/mL followed by 24h restimulation with LPS 10 ng/mL + MSU 300 ug/mL (**Figure 4a**). Treatment with urate alone resulted in increased IL-1 β and IL-6 concentrations, along with a decrease in IL-1Ra, characteristic of the urate priming phenotype as described previously [9]. Although treatment with IFN- β alone significantly induced IL-1Ra production in the first 24h, the production of IL-1Ra, IL-1 β , and IL-6 after restimulation was not affected by the addition of IFN- β recombinant protein in the presence of urate (**Figure 4b**).

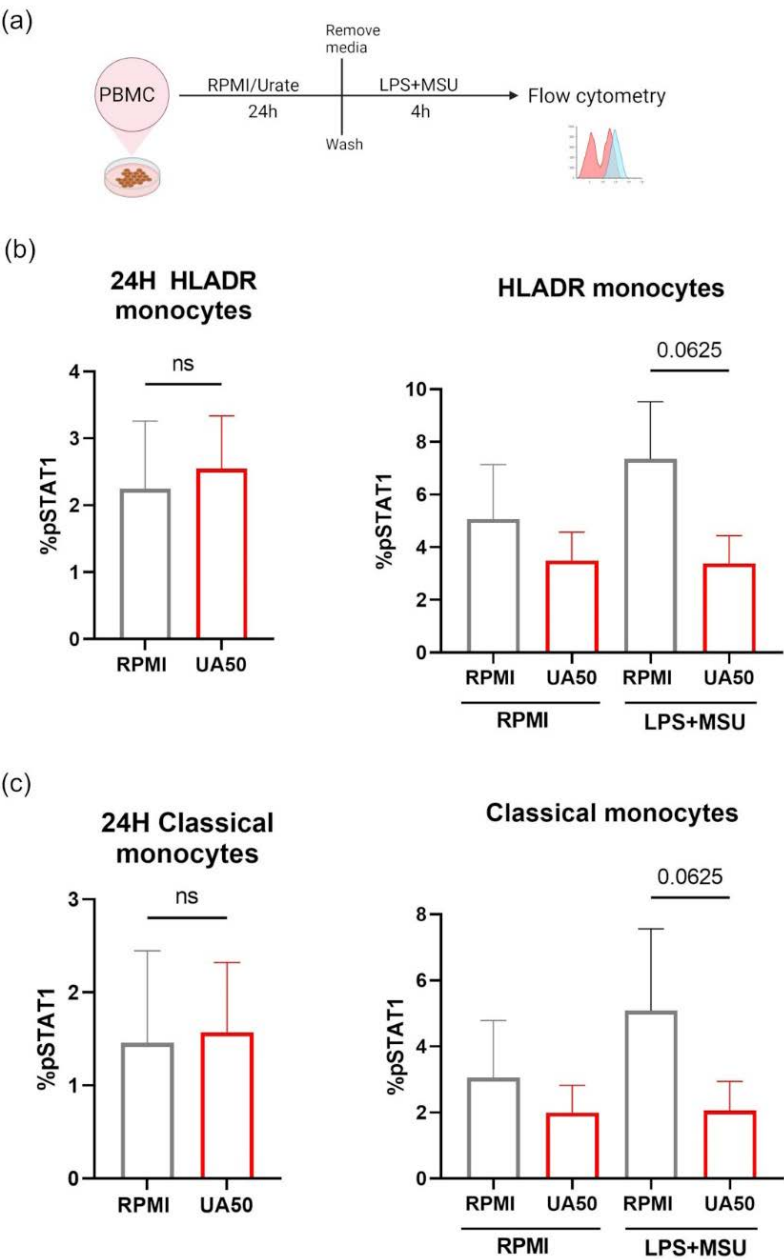


Figure 3. Phosphorylated STAT1 is decreased upon urate treatment in monocytes. Schematic representation of *invitro* experiments used for flow cytometry experiment; PBMCs primed *in vitro* with urate 50 mg/dL for 24h and restimulated with LPS 10 ng/mL + MSU crystals 300 ug/mL for 4h (a). Phosphorylated STAT1 in gated HLA-DR+ monocytes (b) and classical monocytes (c) (n= 5); Wilcoxon test; Data presented as Mean with SEM and representative of two independent experiments.

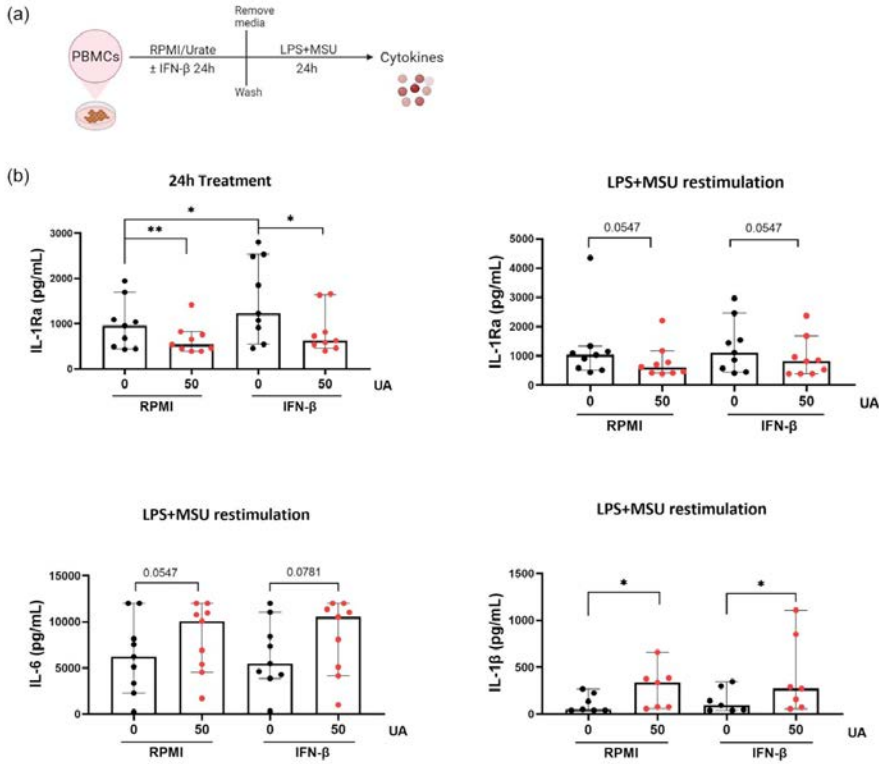


Figure 4. Cytokine production given by IFN- β stimulation in the presence of urate. Schematic representation of *invitro* experiments used for cytokine measurements ($n = 9$) (a). Coincubation of IFN- β (100 IU/mL) with urate (50 mg/dL) followed by restimulation with LPS (10 ng/mL) + MSU (300 ug/mL) in PBMCs of healthy volunteers (b). IL-1Ra, IL-1 β , and IL-6 cytokine production in supernatants from at least three independent experiments; Wilcoxon test; Data presented as Median with 95% CI.

ISGs in stimulated PBMCs are inversely correlated with the circulating serum urate levels

We next sought to expand upon these observations by investigating the potential impact of urate on infection responses in individuals with hyperuricemia. For this purpose, PBMCs isolated from patients with gout (serum urate range: min (3.8 mg/dL), median (6.60 mg/dL), max (11.2 mg/dL) were treated *in vitro* for 24h with various TLR ligands to mimic a context of microbial infection. RNA sequencing and cytokine measurement were performed (**Figure 5a**). The expression of ISGs in PBMCs stimulated with viral-like ligands such as Poly: IC and CpG were negatively correlated with circulating serum urate concentrations. A similar effect was observed in PBMCs stimulated with

C. albicans (**Figure 5b,c; Table S12**), indicating that the downregulation of ISGs in the presence of urate is exerted on the broad antimicrobial ISG response and not restricted only to viral ligand stimulation. IL-1Ra cytokine production in PBMCs stimulated with Poly: IC, CpG, and *C. albicans* was likewise observed to have an inverse correlation with serum urate concentrations (**Figure 5d**).

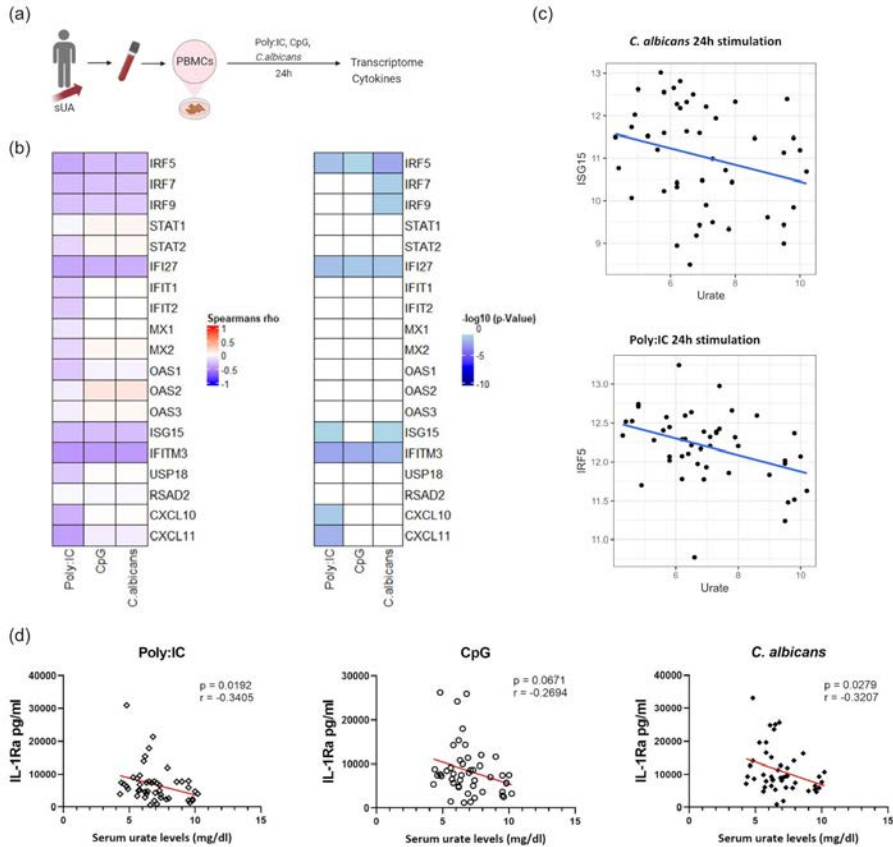


Figure 5. Serum urate levels in patients are inversely correlated with gene expression of ISGs.

Schematic representation of *in-vitro* experiments used for transcriptomic analysis (a). ComplexHeatmap for Spearman rho and p-values of serum urate levels in correlation with gene expression (variance stabilized normalized counts) of 24h treated PBMCs with Poly: IC ($n = 47$), CpG ($n = 47$) and heat-killed *Candida albicans* ($n = 46$) (b). Scatter plots of genes that inversely correlate with serum urate concentrations in 24h stimulation of PBMCs with *Candida albicans* ($r = -0.3755$, $p = 0.0093$) and Poly: IC ($r = -0.3715$, $p = 0.0101$) - gene expression on the y-axis as variance stabilized normalized counts and on the x-axis serum urate levels in mg/dL along with the fitted linear regression line in blue (c). Correlation of serum urate levels with IL-1Ra cytokine production in 24h treated PBMCs with PBMCs Poly: IC, CpG and heat-killed *Candida albicans* (d).

Discussion

This study evaluated the expression of ISGs by assessing the transcriptomes of human primary cells following exposure to soluble urate. The downregulation of IFN1-related pathways was observed in PBMCs of patients with gout treated *in vitro* with soluble urate at concentrations 12.5 and 50 mg/dL and restimulated with LPS. The analysis of differentially expressed genes and TFs in urate-treated monocytes from healthy volunteers confirmed inhibition of the IFN1 signalling pathways. Treatment with urate resulted in lower levels of phosphorylated STAT1 upon subsequent restimulation with LPS+MSU. Previous studies described that *in vitro* exposure of human monocytes with urate results in elevated IL-1 β and reduced IL-1Ra [9]. However, the addition of IFN- β *in vitro* did not rescue the pro-inflammatory effects of urate pre-treatment. These results suggest that the priming effect of urate is probably not driven by IFN1 signalling. Alternatively, it could account for another potential harmful consequence of cell exposure to urate. Interestingly, we identified an inverse relationship between the concentrations of circulating serum urate in patients and the expression of ISGs following *in vitro* stimulation of human PBMCs with fungal and viral ligands. The observed IFN1 downregulation at *in vivo*-relevant serum urate concentrations carries noteworthy implications for our understanding of how urate may influence the immune response to microbial infections.

In response to infection with various pathogens, cells like macrophages or dendritic cells produce IFN1, a key component of innate immune responses that bridge the transition to adaptive immunity [29]. In monocytes pre-treated with urate, previous transcriptomic studies identified downregulated genes enriched in pathways related to infection and autoimmunity, including IFN1 signalling-related genes associated with terms like "Influenza A" or "Systemic lupus erythematosus" [9]. In our study, we conducted transcriptomic analysis on human peripheral blood mononuclear cells (PBMCs) exposed initially to soluble urate and subsequently LPS-restimulated *in vitro*. The analysis of differentially expressed genes using GO Biological Processes revealed a reduction in the expression of genes annotated to the IFN1-related Gene Ontology (GO) (**Figure 1b**). Similarly, other top terms included genes involved in pathways related to complement activation, aligning with previously reported findings [9]. While the exposure of cells to a lower concentration of urate (12.5 mg/dL) did not greatly affect the overall differential gene expression (DEG) analysis, many genes within the interferon signalling

pathway still show significant down-regulation, although the effect of lower dose urate priming is smaller and implies more subtle changes (**Figure S2**). Nevertheless, GSEA identifies terms related to "interferon responses" and "viral regulation" that are associated with down-regulated gene expression similar to that observed with urate 50 mg/dL exposure (**Figure S1**). It is intriguing to note that the genes downregulated by urate priming, such as interferon-induced proteins with tetratricopeptide repeats (*IFIT1*, *IFIT2*), 2'-5'-oligoadenylate synthetases (*OAS1*, *OAS2*, *OAS3*), and interferon-induced transmembrane proteins (*IFITM3*) (**Figure 1e**), were upregulated in patients undergoing treatment with rasburicase, a urate-lowering drug [16].

Our findings were endorsed in publicly available transcriptomic data of monocytes treated with urate only (**Figure 2**), suggesting that urate might modulate interferon-related immune responses under these conditions. A recent epigenome-wide association study (EWAS) focusing on serum urate found changes in DNA methylation to causally influence serum urate concentrations. The analysis of GO Biological processes for CpG sites linked to urate reveals enrichment of pathways related to urate transport and IFN1 signalling and regulation pathways [12]. We previously showed an inverse relationship, that hyperuricemia results in genome-wide differentially methylated sites (e.g., *IFITM3*) [13]. Ultimately, further investigation is needed to understand whether urate affects DNA methylation or if alterations in DNA methylation have consequences for urate concentrations, particularly in relation to IFN1 regulation.

Urate may influence signalling pathways driven by interferons, possibly through mechanisms that inhibit STAT1 activation, as urate treatment potentially reduces STAT1 phosphorylation, which is particularly visible after stimulation with LPS+MSU (**Figure 3**). These results align with a previous report from our group showing a decrease in phosphorylated STAT3 and IL-1Ra levels upon pre-exposure to urate [30]. STAT3 homodimers can also be involved in the IFN1 signalling pathway to counterbalance the pro-inflammatory responses under certain conditions [24]. Still, activated STAT1 homodimers are predominantly associated with the IFN- γ (type II interferon) signalling pathway [31], but IFN1 can also promote IFN- γ production, which in turn activates STAT1 [31]. Additionally, the activation of STAT1 can be influenced by other cytokines such as IL-10 [32]. The observed pattern of suppressed pSTAT1 following *in vitro* urate priming is consistent with reduced activation of other TFs like *IRF5*, *IRF9*, *STAT1*, and *STAT2* (**Figure 1f**, **Figure 2d**), responsible for inducing the

transcription of ISGs [33]. Moreover, several of these TFs are downregulated by urate in a dose-dependent manner (**Figure S4**). In the PBMCs of patients with gout, Wang et al. identified differentially methylated TF motifs, such as *STAT2* and *IRF1*, that may impact gene regulation [14].

Inhibition of IFN1 promotes pro-inflammatory activation in atherosclerosis. The uptake of acetylated LDL (acLDL) by macrophages and the subsequent foam cell formation leads to a reduced type I interferon response, which is recovered after administration of exogenous IFN- β treatment [34]. Here, the stimulation of PBMCs with IFN- β in the presence of urate at 50 mg/dL (**Figure 4**) did not alter the pro-inflammatory effects of urate pre-treatment. We can still observe a reduction in IL-1Ra and induction of IL-6 and IL-1 β on LPS+MSU restimulation. This implies that the downregulation of genes in the IFN1 pathway is unlikely to be the mechanistic factor contributing to the observed proinflammatory effects of urate (**Figure 4**). Alternatively, it might represent a potentially detrimental consequence of prior exposure to elevated urate concentrations that could impact susceptibility to infections.

This potential link between elevated urate levels and increased infection risk is underscored by the presence of a pro-inflammatory state related to hyperuricemia, leading to the hypothesis that patients with gout may have an enhanced susceptibility to infections. Several studies show an association between hyperuricemia or gout and poor responses to Sars-CoV-2 infection [35] [36] or pneumonia [37]. High serum urate concentrations were associated with an increased risk of composite outcome and mechanical ventilation in COVID-19 [35]. On the other hand, other studies propose that low urate concentrations can independently predict a worsened outcome of COVID-19 in patients with severe and critical forms of the disease [38]. In patients hospitalized with SARS-CoV-2 infection, there is a drastic decrease in serum urate concentrations, especially in severe cases requiring mechanical ventilation, which is restored upon discharge [39]. Oxidative stress during the resolution of inflammatory processes could explain the urate consumption, given urate's antioxidant effect in scavenging free radicals to mitigate oxidative damage [40]. However, most of these studies do not include serum urate concentrations before infection or admission, and the impact of urate concentration changes in the context of COVID-19 remains unclear. Interestingly, in one study, a history of hyperuricemia was significantly linked to COVID-19 severity in a Japanese cohort [41]. In PBMCs of patients with gout, the expression of ISGs like Interferon Regulatory Factor 5 (*IRF5*), Interferon

Alpha Inducible Protein 27 (*IFI27*), and Interferon Induced Transmembrane Protein 3 (*IFITM3*), shows a negative correlation with circulating serum urate concentrations when triggered with Poly: IC, CpG and *C. albicans* (**Figure 5b,c**), consistent with our *in vitro* findings. However, this may indicate a wider effect of urate on ISG expression, extending beyond merely viral stimulation responses.

Another aspect of significant relevance is the downregulated IL-1Ra cytokine production at these circulating urate concentrations. The downregulation of IL1Ra in response to urate exposure is supported by *in vitro* evidence [18]. The induction of IL-1Ra production by IFN- β (**Figure 4b**) aligns with previous evidence [29]. Still, the long-lasting effect of urate remains unaffected by this short-term induction of IL-1Ra, implying a transient impact of IFN1 but a lasting effect in response to urate. Following TLR stimulation, IL-1Ra also exhibits a negative relationship with serum urate levels (**Figure 5d**), reinforcing the *in vitro* findings of IL-1Ra downregulation [9] within the context of circulating urate concentrations. This is an important aspect, since in circulation, a systemic increase of anti-inflammatory IL-1Ra may occur as a result of systemic increase of pro-inflammatory mediators. Plasma levels of IL-1Ra have been reported to positively correlate with urate levels [42]. Based on our observations, we could not establish a clear interaction between these pathways, as they seem to be independent of each other in terms of regulation by urate and this needs further investigation. However, despite not being mechanistically connected, both ISGs and IL-1Ra exhibit a parallel decrease in response to urate.

This study shows a distinct transcriptional shift in human myeloid cells exposed to soluble urate characterized by downregulation of genes involved in IFN1 regulation, viral and bacterial replication-related processes, and complement activation. While these observations were particularly pronounced *in vitro* when exposing immune cells to high urate concentrations, they remain consistent when using lower concentrations. Importantly, these results have been validated in stimulated PBMCs from patients with varying serum urate concentrations. This observed effect seems to be soluble urate-specific since transcriptome analysis of MSU crystals treated macrophages did not impact genes belonging to IFN1 or IRFs [15].

While this study provides valuable insights into soluble urate *in vitro*, it is critical to acknowledge certain limitations. Our results on urate-exposed PBMCs were further examined in a publicly available transcriptomic dataset on

urate-treated monocytes. While these results may not be entirely comparable, there is significant overlap in many of the top terms identified in the pathway analysis. Next, we only investigated the effect of IFN- β , while the impact of IFN- α and other interferons (IFN- γ) remains unexplored. Protein concentration analysis of pSTAT1 was restricted due to a limited number of available samples. Monitoring infections in a cohort of patients with hyperuricemia and gout was not possible, which could have added valuable insights to our findings. To expand the relevance of this study, further studies should focus on evaluating IFN1 changes before and after urate-lowering therapy in patients to better understand the significance of urate modification not only in infection-related immune responses but also in broader scopes.

Conclusion

The present study found that urate-treated human PBMCs and monocytes show downregulation of the IFN1 signalling pathway, supported by diminished STAT1 phosphorylation. Given that inducing the IFN1 pathway with IFN- β did not reverse the pro-inflammatory effect of urate, this is unlikely to play a role in the inflammatory priming due to urate. However, this suggests that elevated urate pre-exposure could negatively impact immune responses to viral stimuli. Indeed, in patients with hyperuricemia, high serum urate concentrations are inversely correlated with *in vitro* responses to both viral and fungal stimulations. This correlation supports an impaired IFN1 signalling and, consequently, may render individuals more susceptible to microbial infections.

Ethics approval and consent to participate

In vitro experiments were approved by the Ethical Committee of the „Iuliu Hațieganu” University of Medicine and Pharmacy, Cluj-Napoca (approval no. 425/2016) and by the Ethical Committee of the Radboud University Medical Center (no. NL32357.091.10; registration number 2010/104). All participants provided written informed consent before inclusion. All experiments were conducted according to the principles of the Declaration of Helsinki.

Acknowledgments

This work was supported by a Competitiveness Operational Programme grant of the Romanian Ministry of European Funds (P_37_762, MySMIS 103587).

References

- [1] Bardin T, Richette P. Definition of hyperuricemia and gouty conditions. *Curr Opin Rheumatol*. 2014;26(2):186–91.
- [2] Kuwabara M, Niwa K, Ohtahara A, Hamada T, Miyazaki S, Mizuta E, et al. Prevalence and complications of hypouricemia in a general population: A largescale cross-sectional study in Japan. *PLoS One*. 2017;12(4):1–13.
- [3] Dalbeth N, Choi HK, Joosten LAB, Khanna PP, Matsuo H, Perez-Ruiz F, et al. Gout. *Nat Rev Dis Prim*. 2019;5(1).
- [4] Joosten LAB, Crişan TO, Bjornstad P, Johnson RJ. Asymptomatic hyperuricaemia: a silent activator of the innate immune system. *Nat Rev Rheumatol*. 2020;16(2):75–86.
- [5] Grayson PC, Young Kim S, Lavalley M, Choi HK. Hyperuricemia and incident hypertension: A systematic review and meta-analysis. *Arthritis Care Res*. 2011;63(1):102–10.
- [6] Johnson RJ, Nakagawa T, Sanchez-Lozada LG, Shafiu M, Sundaram S, Le M, et al. Sugar, uric acid, and the etiology of diabetes and obesity. *Diabetes*. 2013;62(10):3307–15.
- [7] Lv Q, Meng X-F, He F-F, Chen S, Su H, Xiong J, et al. High Serum Uric Acid and Increased Risk of Type 2 Diabetes: A Systemic Review and Meta-Analysis of Prospective Cohort Studies. *PLoS One*. 2013;8(2):e56864.
- [8] Crişan TO, Cleophas MCP, Oosting M, Lemmers H, Toenhake-Dijkstra H, Netea MG, et al. Soluble uric acid primes TLR-induced proinflammatory cytokine production by human primary cells via inhibition of IL-1Ra. *Ann Rheum Dis*. 2016;75(4):755–62.
- [9] Crişan TO, Cleophas MCP, Novakovic B, Erler K, van de Veerdonk FL, Stunnenberg HG, et al. Uric acid priming in human monocytes is driven by the AKT-PRAS40 autophagy pathway. *Proc Natl Acad Sci [Internet]*. 2017;114(21):5485–90.
- [10] Köttgen A, Albrecht E, Teumer A, Vitart V, Krumsiek J, Hundertmark C, et al. Genome-wide association analyses identify 18 new loci associated with serum urate concentrations. *Nat Genet*. 2013;45(2):145–54.
- [11] Li L, Zhang Y, Zeng C. Update on the epidemiology, genetics, and therapeutic options of hyperuricemia. *Am J Transl Res*. 2020;12(7):3167–81.
- [12] Tin A, Schlosser P, Matias-Garcia PR, Thio CHL, Joehanes R, Liu H, et al. Epigenome-wide association study of serum urate reveals insights into urate co-regulation and the SLC2A9 locus. *Nat Commun*. 2021;12(1):1–18.
- [13] Badii M, Gaal OI, Cleophas MC, Klück V, Davar R, Habibi E, et al. Urate-induced epigenetic modifications in myeloid cells. *Arthritis Res Ther*. 2021;23(1):1–11.
- [14] Wang Z, Zhao Y, Phipps-Green A, Liu-Bryan R, Ceponis A, Boyle DL, et al. Differential DNA Methylation of Networked Signaling, Transcriptional, Innate and Adaptive Immunity, and Osteoclastogenesis Genes and Pathways in Gout. *Arthritis Rheumatol*. 2020; 72(5):802–814.
- [15] Cobo I, Cheng A, Murillo-Saich J, Coras R, Torres A, Abe Y, et al. Monosodium urate crystals regulate a unique JNK-dependent macrophage metabolic and inflammatory response. *Cell Rep*. 2022;38(10):110489.
- [16] Tanaka T, Milaneschi Y, Zhang Y, Becker KG, Zukley L, Ferrucci L. A double blind placebo controlled randomized trial of the effect of acute uric acid changes on inflammatory markers in humans: A pilot study. *PLoS One*. 2017; 7;12(8):e0181100.
- [17] Stetson DB, Medzhitov R. Type I Interferons in Host Defense. *Immunity*. 2006;25(3):373–81.

- [18] McNab F, Mayer-Barber K, Sher A, Wack A, O'Garra A. Type I interferons in infectious disease. *Nat Rev Immunol*. 2015;15(2):87–103.
- [19] Okahira S, Nishikawa F, Nishikawa S, Akazawa T, Seya T, Matsumoto M. Interferon- β induction through toll-like receptor 3 depends on double-stranded RNA structure. *DNA Cell Biol*. 2005; 24(10):614–23.
- [20] Fitzgerald KA, Rowe DC, Barnes BJ, Caffrey DR, Visintin A, Latz E, et al. LPS-TLR4 signaling to IRF-3/7 and NF- κ B involves the toll adapters TRAM and TRIF. *J Exp Med*. 2003; 198(7):1043–55.
- [21] Saitoh SI, Abe F, Kanno A, Tanimura N, Mori Saitoh Y, Fukui R, et al. TLR7 mediated viral recognition results in focal type i interferon secretion by dendritic cells. *Nat Commun*. 2017; 17;8(1):1592.
- [22] Yang K, Puel A, Zhang S, Eidenschenk C, Ku CL, Casrouge A, et al. Human TLR-7-, -8-, and -9-mediated induction of IFN- α/β and - λ Is IRAK-4 dependent and redundant for protective immunity to viruses. *Immunity*. 2005; 23(5):465–78.
- [23] Stark GR, Darnell JE. The JAK-STAT Pathway at Twenty. *Immunity*. 2012; 36(4):503–514.
- [24] Ivashkiv LB, Donlin LT. Regulation of type i interferon responses. *Nat Rev Immunol*. 2014;14(1):36–49.
- [25] Jenkins JK, Arend WP. Interleukin 1 receptor antagonist production in human monocytes is induced by IL-1 α , IL-3, IL-4 and GM-CSF. *Cytokine*. 1993;5(5):407–15.
- [26] Tilg H, Mier JW, Vogel W, Aulitzky WE, Wiedermann CJ, Vannier E, et al. Induction of circulating IL-1 receptor antagonist by IFN treatment. *J Immunol*. 1993;150(10):4687–92.
- [27] Guarda G, Braun M, Staehli F, Tardivel A, Mattmann C, Förster I, et al. Type I Interferon Inhibits Interleukin-1 Production and Inflammasome Activation. *Immunity*. 2011; 34(2):213–223.
- [28] Castiglia V, Piersigilli A, Ebner F, Janos M, Goldmann O, Damböck U, et al. Type i Interferon Signaling Prevents IL-1 β -Driven Lethal Systemic Hyperinflammation during Invasive Bacterial Infection of Soft Tissue. *Cell Host Microbe*. 2016;19(3):375–87.
- [29] Mayer-Barber KD, Yan B. Clash of the Cytokine Titans: Counter-regulation of interleukin-1 and type i interferon-mediated inflammatory responses. *Cell Mol Immunol*. 2017;14(1):22–35.
- [30] Badii M, Klück V, Gaal O, Cabău G, Hotea I, Nica V, et al. Regulation of SOCS3-STAT3 in urate-induced cytokine production in human myeloid cells. *Joint Bone Spine*. 2024;91(3):105698.
- [31] Platanias LC. Mechanisms of type-I- and type-II-interferon-mediated signalling. *Nat Rev Immunol*. 2005;5(5):375–86.
- [32] Rahimi AAR, Gee K, Mishra S, Lim W, Kumar A. STAT-1 mediates the stimulatory effect of IL-10 on CD14 expression in human monocytic cells. *J Immunol*. 2005 Jun;174(12):7823–32.
- [33] Yoneyama M, Suhara W, Fukuhara Y, Sato M, Ozato K, Fujita T. Autocrine amplification of type I interferon gene expression mediated by interferon stimulated gene factor 3 (ISGF3). *J Biochem*. 1996;120(1):160–9.
- [34] Willemsen L, Chen H-J, van Roomen CPAA, Griffith GR, Siebeler R, Neele AE, et al. Monocyte and Macrophage Lipid Accumulation Results in Down-Regulated Type-I Interferon Responses. *Front Cardiovasc Med*. 2022;9:829877.
- [35] Chen B, Lu C, Gu HQ, Li Y, Zhang G, Lio J, et al. Serum Uric Acid Concentrations and Risk of Adverse Outcomes in Patients With COVID-19. *Front Endocrinol (Lausanne)*. 2021; 12:633767.
- [36] Topless RK, Gaffo A, Stamp LK, Robinson PC, Dalbeth N, Merriman TR. Gout and the risk of COVID-19 diagnosis and death in the UK Biobank: a population-based study. *Lancet Rheumatol*. 2022;4(4):e274–81.

- [37] Spaetgens B, De Vries F, Driessen JHM, Leufkens HG, Souverein PC, Boonen A, et al. Risk of infections in patients with gout: A population-based cohort study. *Sci Rep.* 2017;7(1):1429.
- [38] Li G, Wu X, Zhou C liang, Wang Y ming, Song B, Cheng X bin, et al. Uric acid as a prognostic factor and critical marker of COVID-19. *Sci Rep.* 2021;11(1):1-9.
- [39] Dufour I, Werion A, Belkhir L, Wisniewska A, Perrot M, De Greef J, et al. Serum uric acid, disease severity and outcomes in COVID-19. *Crit Care.* 2021;25(1):212.
- [40] Harrold LR, Etzel CJ, Gibofsky A, Kremer JM, Pillinger MH, Saag KG, et al. Sex differences in gout characteristics: Tailoring care for women and men. *BMC Musculoskelet Disord.* 2017;18(1):108.
- [41] Fukushima T, Chubachi S, Namkoong H, Otake S, Nakagawara K, Tanaka H, et al. U-shaped association between abnormal serum uric acid levels and COVID-19 severity: reports from the Japan COVID-19 Task Force. *Int J Infect Dis.* 2022;122:747-54.
- [42] Ruggiero C, Cherubini A, Ble A, Bos AJG, Maggio M, Dixit VD, et al. Uric acid and inflammatory markers. *Eur Heart J.* 2006;27(10):1174-81.

Supplementary material

Materials and methods

Participants

Participants for the study were recruited from the Rheumatology Department of the Iuliu Hațieganu University of Medicine and Pharmacy, Cluj-Napoca, Romania. The individuals involved in the study consisted of (i) patients with diagnosed gout from the HINT Project* (n=52, serum urate mg/dL median (IQR) 6.60 (5.65, 7.80), out of which 81% (n=42) were men and 19% (n=10) were women) and (ii) healthy volunteers for the *in vitro* validation experiments. Inclusion of individuals in the gout group was based on at least one clinically diagnosed gout flare and either proven presence of MSU crystals in the synovial fluid or a score of at least 8 according to the American College of Rheumatology / European League Against Rheumatism (ACR/EULAR). Approval for the current study was granted by the Ethical Committee of the „Iuliu Hațieganu” University of Medicine and Pharmacy, Cluj-Napoca (approval no. 425/2016).

For the experiments shown in Figure 3, blood was collected from Dutch healthy volunteers, approved by the Ethical Committee of the Radboud University Medical Center (no. NL32357.091.10; registration number 2010/104).

Before being included in the study, all participants provided written informed consent. Peripheral blood was drawn from the cubital vein on EDTA tubes under sterile conditions. The experiments were in accordance with the Declaration of Helsinki.

*The current study uses transcriptomic data generated by the HINT Project (Hyperuricemia-induced Inflammation: Targeting the central role of uric acid in rheumatic and cardiovascular diseases, ID P 37 762; MySMIS 103587) implemented in Cluj-Napoca Romania at the Iuliu Hațieganu University of Medicine and Pharmacy. The study aimed to describe inflammation associated with gout and urate using a systems biology approach, and therefore, relatively large datasets were available to assess differences in gene expression relevant for type I IFN pathway exploration.

Cell preparation and culture conditions

PBMCs were isolated using Ficoll-Paque (GE Healthcare) density gradient centrifugation and washed 3 times with phosphate-buffered saline (PBS) at

4°C. Cells were counted by Coulter Counter method and the number was adjusted to 10×10^6 PBMCs/ mL in Dutch Modified RPMI 1640 medium (Sigma-Aldrich) supplemented with 50 µg/mL gentamycin (Sigma-Aldrich), 2 mM GlutaMAX (Gibco) and 1 mM pyruvate (Gibco). Cells were plated in either an F-bottom 96-well plate for urate-priming experiments (see below) and a U-bottom 96-well plate for the direct 24h stimulations at 5×10^5 PBMCs in a volume of 50µL per well.

All cells were incubated in a Galay 170 R incubator (Eppendorf) at 37 °C with 5%CO₂. Each condition was performed in replicate wells at the stated concentrations of stimuli in a final volume of 200µL. At the end of the experiments, supernatants were pooled before measurement and stored at -20°C until performing ELISA.

To assess gene expression changes/cytokine responses to urate exposure *in vitro*, PBMCs were treated with soluble urate 12.5 and 50 mg/dL and RPMI medium for negative control. Urate was solubilized using a pre-warmed RPMI medium and filtered by a 0.2 µm filter. Urate concentrations were chosen based on previous studies [1]. Afterwards, the culture medium was removed, and the urate was washed away with warm PBS. The priming effect in the remaining adherent cells was investigated by stimulation with LPS (10ng/mL) or LPS (10ng/mL) + MSU (300ug/mL) for an additional 24h. All urate-priming experiments were supplemented with 10% serum. Uric acid and LPS (*E. coli* serotype 055:b5), suitable for cell culture, were purchased from Sigma. LPS was ultra-purified before cell culture experiments as follows: LPS was mixed with triethylamine, sodium deoxycholate, and a warm phenol:water solution to separate phases and isolate LPS through centrifugation. The process includes re-extraction to maximize yield, followed by dialysis to remove impurities and ethanol-based precipitation to purify LPS. Finally, the LPS is dried, tested for purity, and stored at -20°C. MSU crystals were prepared as previously described [2]. For further gene expression assessment with RNA-sequencing, stimulated cells were stored at -80 °C in TRIzol Reagent (Invitrogen).

The urate-priming protocol usually involves a 24h pre-treatment with urate, followed by an additional 24h restimulation with pattern receptor agonists to enable robust changes in proinflammatory cytokine responses. During the 24h urate treatment alone (often referred to as « priming »), there is no production of IL-1β and IL-6, however, there is a significant basal reduction of IL-1Ra, which persists even after restimulation. This indicates a silent effect of urate pre-exposure, that primes the cells toward an excessive proinflammatory state upon subsequent stimulation [3].

To assess the effect of IFN- β (from R&D Systems, Minneapolis) on primary PBMCs from healthy donors, the cells were stimulated for 24h with soluble urate (50 mg/dL), IFN- β (100 IU / ml), urate + IFN- β and RPMI medium for control. Afterwards, the medium was removed and the cells were restimulated for an additional 24h with LPS (10ng/mL) + MSU (300ug/mL). These experiments employed both patients with gout from the HINT Project and healthy volunteers for the validation experiments.

Primary PBMCs isolated from patients with gout were stimulated for 24h with several TLR ligands: Poly: IC (InvivoGen) (10 ug/mL), CpG (InvivoGen) (1 ug/mL), and heat-killed *C.albicans* (10^6 col/mL).

Cytokine measurements

Cytokine measurements were performed in supernatants collected at 24h and 48h using enzyme-linked immunosorbent assay with ELISA kits for IL-1 β , IL-1Ra, and IL-6 according to the manufacturer's instructions (R&D Systems, Minneapolis). The absorbance at 450 nm was measured with Synergy HTX Multi mode reader from Bio-Teck. The lowest range of detection was 39 pg/mL for IL-1 β ; 390 pg/mL for IL-1Ra and 94 pg/mL for IL-6. Samples were diluted before assay 10-fold for IL-1 β and IL-1Ra and 20-fold for IL-6.

Intracellular phospho-STAT1 expression

To assess the effect of urate on STAT1 expression, PBMCs from healthy volunteers were primed 24h with urate 50 mg/dL and restimulated 4h with LPS 10 ng/mL + MSU (300ug/mL). The cells were detached by being placed on ice for 30 minutes and further fixed and permeabilized with Cytofix/Cytoperm solution (eBioscience) according to the manufacturer's recommendations. Cells were then resuspended in a staining mix for extracellular markers (as detailed in **Table S9**) and incubated for 20 minutes at room temperature (RT) in the dark. For intracellular staining with pSTAT1 antibody (PE anti-STAT1 Phospho (Ser727) Antibody, Biolegend), the cells were incubated for 30 minutes on ice in the dark. Data acquisition was performed on the CytoFlex flow cytometer (FC500 flow cytometer Beckman Coulter).

The identification and selection of monocytic cell populations were carried out using a series of gating steps. Initially, forward and side scatters were employed to isolate cells from aggregates and debris and refine their granularity. Next, the CD45+ marker was used to identify granulocytes. Within the CD45+ population, subsequent gating on CD3- cells was used to

select non-T cells. Monocytes and macrophages were then selected based on positive HLA-DR among the CD3⁺ population. Phosphorylated STAT1 levels were assessed within HLA-DR⁺ cells. Further gating within the HLA-DR⁺ population allowed for the differentiation of monocyte subsets into classical, intermediate, and non-classical.

Transcriptomic profiling

PBMCs (n=52) were exposed for 24h *in vitro* to RPMI medium (control), a high (50 mg/dL) or a low (12.5 mg/dL) concentration of urate solubilized in RPMI, followed by stimulation with LPS 10 ng/mL for an additional 24h. PBMCs (n=47 for Poly: IC and CpG and n=46 for *C. albicans*) were treated for 24h *in vitro* with various TLR ligands.

Samples were stored at -80 °C in TRIzol reagent (Invitrogen) and later sent to BGI for commercial RNA-Seq analysis (Beijing Genomics Institute, Beijing, China). The integrity of the RNA was evaluated using Agilent 2100 Bioanalyzer.

The sequencing was performed with the DNBseq technology. Raw data was generated by removing reads mapped to rRNAs. Clean reads were generated using SOAPnuke software (v.1.5.2) by removing reads with adaptors, reads with unknown bases >10%, and low-quality reads, defined as reads with a quality score less than 15 in over 50% bases. Clean reads were mapped to UniGenes using Bowtie2 and read counts were estimated with RSEM (v.1.2.12).

Primary human monocytes (n=4) were treated for 20h *in vitro* with high concentrations of urate (50 mg/mL) solubilized in RPMI and RPMI medium (control) and the publicly available data [1] was used for analysis.

Statistical analysis

The statistical analysis and graphical visualization were performed using GraphPad version 9.0 (GraphPad Software, La Jolla California USA) and R version 4.2.2 (R Foundation for Statistical Computing, Vienna, Austria. URL <https://www.R-project.org/>). Considering data distribution, statistical evaluation was performed using One-Way ANOVA or Kruskal-Wallis when testing for at least 3 groups, Student t-test or Mann-Whitney, when comparing 2 groups, and Spearman's or Pearson's correlation. Values of P <0.05 were considered statistically significant and multiple testing correction was applied when needed.

For the transcriptome data, after obtaining the raw read values – normalization, quality control, and identification of differentially expressed genes (DEGs) were performed using the Bioconductor package DESeq2 (Version: DESeq2_1.24.0) [4]. Samples with highly abnormal normalized count values (± 3 Standard Deviations on PC1 or PC2) were excluded before proceeding. Expression levels of individual genes were examined by obtaining normalized counts (vst function in the DESeq package). The sequencing was performed in 2 different runs, without separating the sample pairs, therefore for an accurate graphical representation (Figure 1E), a batch adjustment was performed using the limma package v3.46 [5]. After normalization, the samples were paired in the design formula and different conditions were compared. Pathway enrichment analysis using GO Biological Processes (GOBP) and Gene Set Enrichment Analysis (GSEA) was performed [6] on the differentially expressed genes. Libraries that were used to perform the functional enrichment analysis include DOSE (v_3.22.1) and clusterProfiler (v_4.4.4) [7]. The transcription factor enrichment analysis and the graphical representation of the results were performed with ChIP-X Enrichment Analysis Version 3 (ChEA3) [8], which is available online. Schematic representations were made using Biorender.

Supplementary figures and tables

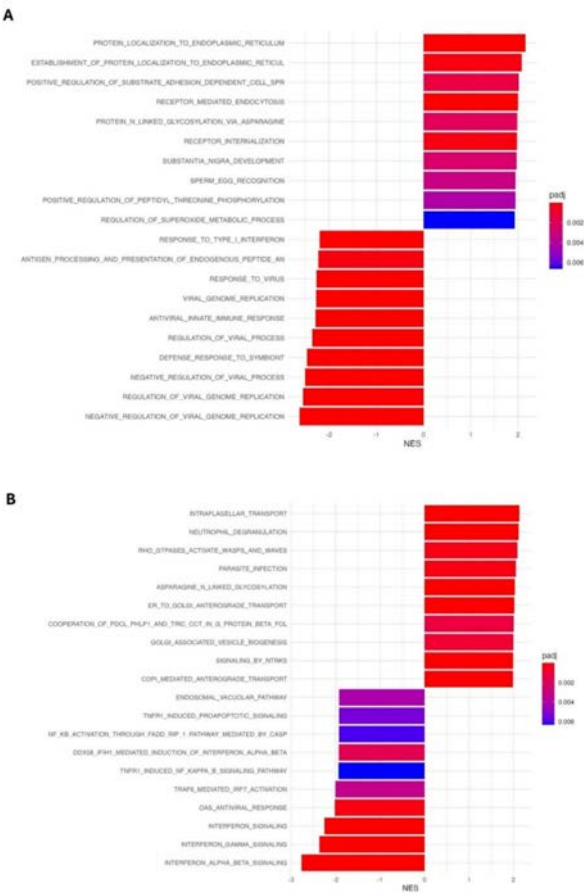


Figure S1. Pathway analysis of PBMCs primed with urate 12.5 mg/dL and restimulated with LPS 10 ng/mL. GSEA GO Biological Processes (A); GSEA Reactome (B).

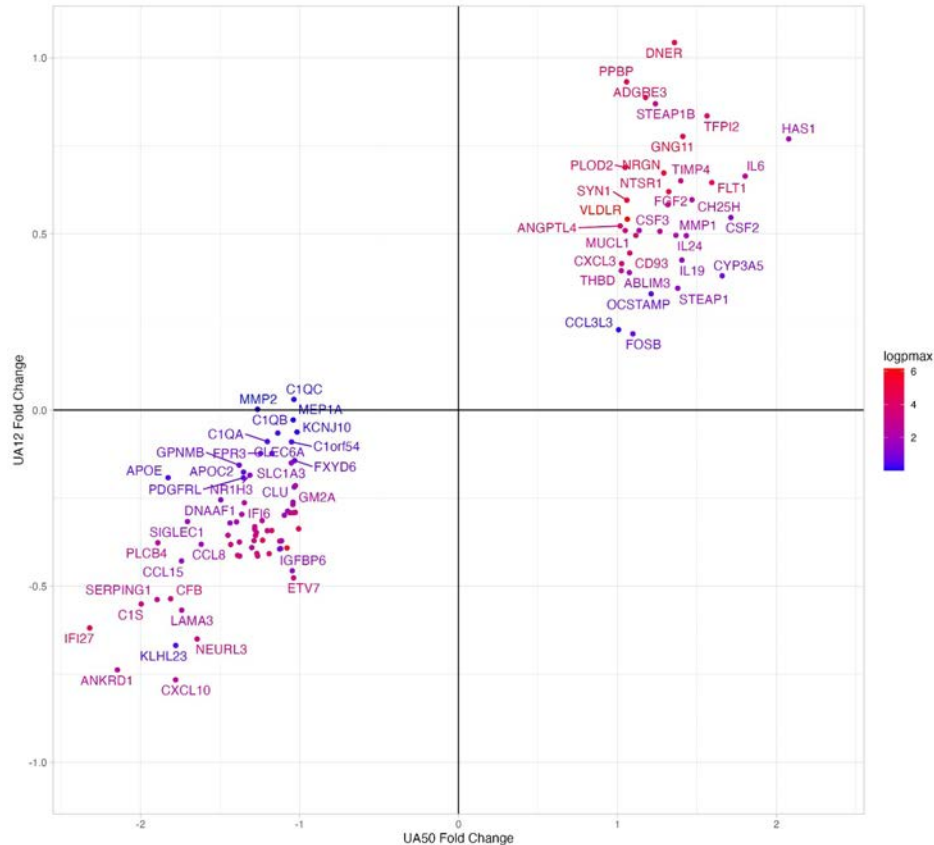


Figure S2. Comparison of Fold changes in gene expression in PBMCs treated with urate at concentrations of 50 mg/mL and 12.5 mg/mL, followed by restimulation with LPS (10 ng/mL).

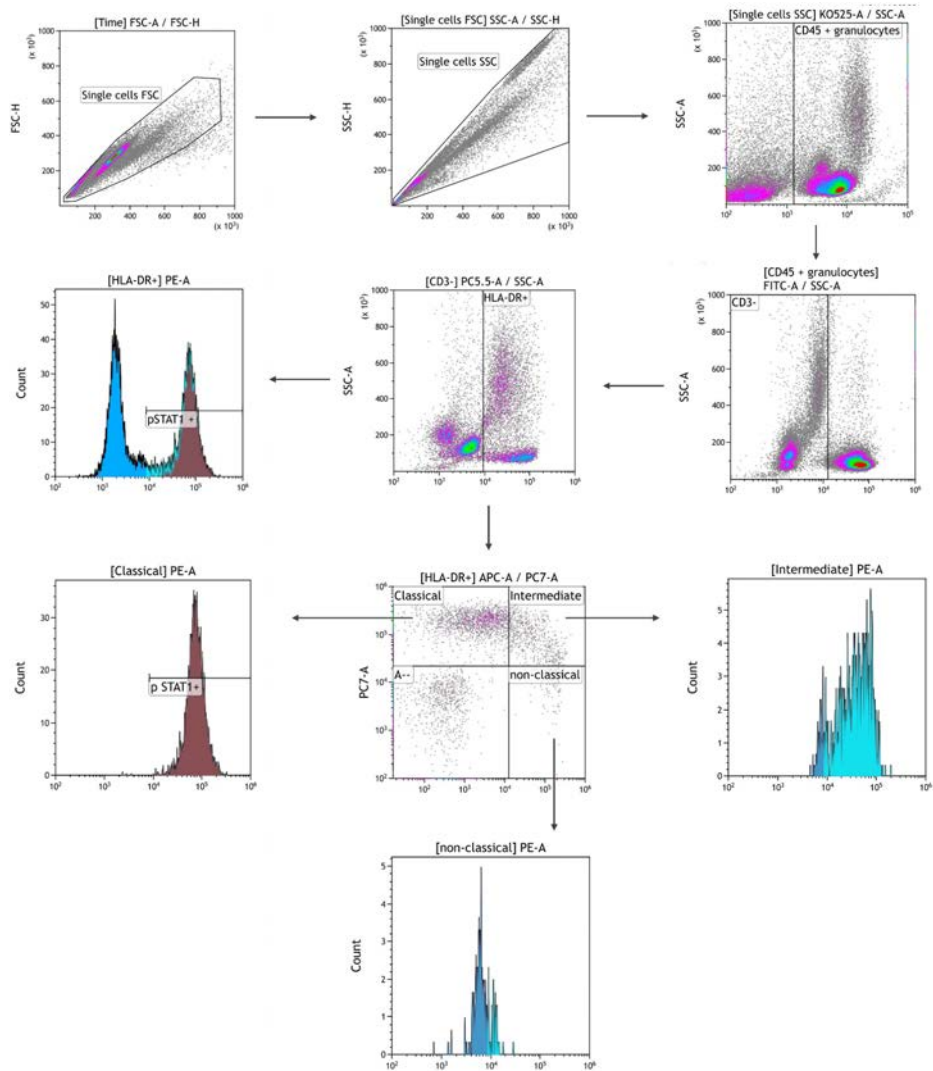


Figure S3. Flow cytometry gating strategy used to define STAT1⁺ monocytic populations in urate primed and LPS+MSU restimulated PMBCs.

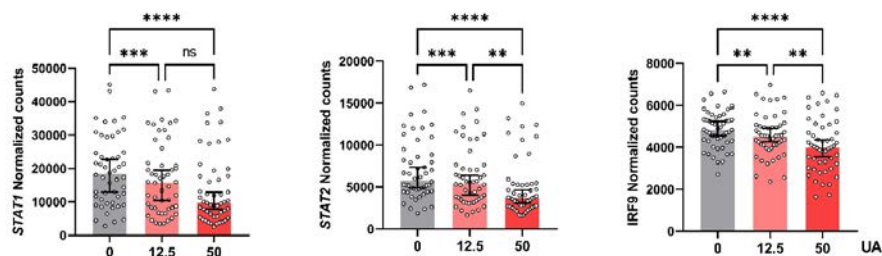


Figure S4. Gene expression of STAT1, STAT2 and IRF93 (forming ISGF3 complex), is down-regulated upon in vitro urate 50 mg/dL priming and LPS 10 ng/mL restimulation of human PBMCs (D) (Friedman test with Dunn's multiple comparisons test; Data presented as Median with 95% CI

Table S1. Differential expression analysis in urate 50 mg/dL and LPS restimulated human PBMCs compared to control conditions. Top 20 most DOWN / UP -regulated genes

Gene Id	Name	Symbol	baseMean	log2 Fold Change	pvalue	adjusted pvalue
6373	C-X-C Motif Chemokine Ligand 11	CXCL11	67,72958984	-2,32310664	6,28E-14	1,69E-12
3429	Interferon Alpha Inducible Protein 27	IFI27	742,5852431	-2,320818552	4,72E-36	1,17E-32
27063	Ankyrin Repeat Domain 1	ANKRD1	139,2877856	-2,146450405	1,01E-21	1,14E-19
26471	Nuclear Protein 1, Transcriptional Regulator	NUPR1	9,290358388	-2,093145081	6,50E-13	1,44E-11
716	Complement C1s	C1S	472,1249464	-1,996557931	7,15E-32	1,18E-28
710	Serpin Family G Member 1	SERPING1	2988,62289	-1,89625086	3,70E-24	6,48E-22
5332	Phospholipase C Beta 4	PLCB4	61,68007347	-1,881908331	1,01E-29	6,82E-27
348	Apolipoprotein E	APOE	747,0477161	-1,827149587	2,89E-25	6,15E-23
629	Complement Factor B	CFB	7507,859476	-1,811228048	7,38E-30	5,49E-27
3627	C-X-C Motif Chemokine Ligand 10	CXCL10	486,5872602	-1,780199867	4,38E-12	8,54E-11
151230	Kelch Like Family Member 23	KLHL23	16,78871261	-1,779322421	0,018740398	0,0483573
6359	C-C Motif Chemokine Ligand 15	CCL15	27,3223101	-1,747055941	4,07E-14	1,14E-12
3909	Laminin Subunit Alpha 3	LAMA3	247,4947872	-1,741816303	1,64E-16	7,11E-15
6614	Sialic Acid Binding Ig Like Lectin 1	SIGLEC1	10849,95486	-1,705401768	6,51E-21	6,33E-19
8820	HESX Homeobox 1	HESX1	20,28683829	-1,649379706	1,41E-15	5,19E-14
93082	Neutralized E3 Ubiquitin Protein Ligase 3	NEURL3	327,6132589	-1,644577388	3,30E-19	2,35E-17
6355	C-C Motif Chemokine Ligand 8	CCL8	18600,97695	-1,619227174	1,76E-19	1,31E-17
123872	Dynein Axonemal Assembly Factor 1	DNAAF1	63,22727159	-1,498172846	9,06E-21	8,64E-19
3957	Galectin 2	LGALS2	21,09663678	-1,479782845	3,96E-08	4,02E-07
3434	Interferon Induced Protein With Tetratricopeptide Repeats 1	IFIT1	2752,77054	-1,450666747	3,57E-19	2,49E-17

Table S1. Continued

Gene Id	Name	Symbol	baseMean	log2 Fold Change	pvalue	adjusted pvalue
2247	Fibroblast Growth Factor 2	FGF2	254,8559642	1,317752633	9,72E-17	4,45E-15
4923	Neurotensin Receptor 1	NTSR1	201,9212395	1,322980623	2,84E-22	3,52E-20
92737	Delta/Notch Like EGF Repeat Containing	DNER	242,8223676	1,358774863	6,70E-16	2,60E-14
11009	Interleukin 24	IL24	4813,36963	1,368002366	5,53E-12	1,07E-10
26872	STEAP Family Member 1	STEAP1	57,46928698	1,380621218	1,01E-20	9,48E-19
7079	TIMP Metallopeptidase Inhibitor 4	TIMP4	29,61702015	1,39971946	3,60E-17	1,77E-15
29949	Interleukin 19	IL19	127,2343122	1,405340328	3,25E-11	5,50E-10
2791	G Protein Subunit Gamma 11	GNG11	114,1070303	1,4116615	2,73E-21	2,84E-19
4312	Matrix Metallopeptidase 1	MMP1	1458,87432	1,433135431	3,70E-17	1,80E-15
9023	Cholesterol 25-Hydroxylase	CH25H	103,1867449	1,469095328	3,28E-14	9,36E-13
7980	Tissue Factor Pathway Inhibitor 2	TFPI2	974,2771238	1,563623594	7,10E-14	1,88E-12
2321	Fms Related Receptor Tyrosine Kinase 1	FLT1	1882,350824	1,59378335	1,21E-22	1,65E-20
1577	Cytochrome P450 Family 3 Subfamily A Member 5	CYP3A5	77,12611361	1,659074067	4,86E-14	1,34E-12
1437	Colony Stimulating Factor 2	CSF2	120,4372535	1,713685798	1,10E-10	1,69E-09
3569	Interleukin 6	IL6	13807,78261	1,80394611	1,80E-12	3,72E-11
4314	Matrix Metallopeptidase 3	MMP3	27,32364836	1,919006857	6,12E-11	9,87E-10
4319	Matrix Metallopeptidase 10	MMP10	10,56435485	1,992939273	1,03E-11	1,91E-10
3036	Hyaluronan Synthase 1	HAS1	231,2726792	2,077618253	1,02E-16	4,63E-15
6318	Serpin Family B Member 4	SERPINB4	26,05640209	2,343918218	6,08E-14	1,65E-12
8293	Small EDRK-Rich Factor 1A	SERF1A	34,53572237	4,402794807	0,003597784	0,011718385

Table S2. GO terms and p values associated with Biological Processes enrichment analysis for DOWN-regulated genes with urate 50 mg/dL treatment and LPS restimulation in human PBMCs (Top 20 terms).

GO ID	Description	GeneRatio	BgRatio	pvalue	p.adjust	qvalue	geneID	Count
GO:0006956	complement activation	10/84	38/13317	2,35072E-14	4,59096E-11	3,64485E-11	C1S/SERPING1/CFB/C1R/C2/A2M/C1QA/C1QB/C1QC/CLU	10
GO:0006958	complement activation, classical pathway	8/84	26/13317	2,53861E-12	2,10942E-09	1,67471E-09	C1S/SERPING1/C1R/C2/C1QA/C1QB/C1QC/CLU	8
GO:0009615	response to virus	18/84	343/13317	3,24027E-12	2,10942E-09	1,67471E-09	IFI27/CXCL10/CCL8/IFIT1/RSAD2/IFITM3/IFI6/ISG15/IFIT3/IFIT2/OAS1/OAS3/MX1/MX2/HERC5/OAS2/CLU/IFI44	18
GO:0006959	humoral immune response	13/84	153/13317	1,12725E-11	5,50381E-09	4,37E-09	CXCL11/C1S/SERPING1/CFB/CXCL10/C1R/C2/A2M/CAMP/C1QA/C1QB/C1QC/CLU	13
GO:0051607	defense response to virus	15/84	257/13317	5,76156E-11	1,98135E-08	1,57303E-08	IFI27/CXCL10/IFIT1/RSAD2/IFITM3/IFI6/ISG15/IFIT3/IFIT2/OAS1/OAS3/MX1/MX2/HERC5/OAS2	15
GO:0140546	defense response to symbiont	15/84	258/13317	6,0871E-11	1,98135E-08	1,57303E-08	IFI27/CXCL10/IFIT1/RSAD2/IFITM3/IFI6/ISG15/IFIT3/IFIT2/OAS1/OAS3/MX1/MX2/HERC5/OAS2	15
GO:0002455	humoral immune response mediated by circulating immunoglobulin	8/84	39/13317	9,35725E-11	2,61067E-08	2,07267E-08	C1S/SERPING1/C1R/C2/C1QA/C1QB/C1QC/CLU	8
GO:0034340	response to type I interferon	9/84	62/13317	1,57545E-10	3,84606E-08	3,05347E-08	IFI27/IFIT1/USP18/IFITM3/ISG15/OAS1/OAS3/MX1/OAS2	9

Table S2. Continued

GO ID	Description	GeneRatio	BgRatio	pvalue	p.adjust	qvalue	geneID	Count
GO:0045071	negative regulation of viral genome replication	8/84	53/13317	1,25532E-09	2,72404E-07	2,16267E-07	IFIT1/RSAD2/IFITM3/ISG15/OAS1/OAS3/MX1/OAS2	8
GO:0048525	negative regulation of viral process	9/84	79/13317	1,46584E-09	2,86278E-07	2,27282E-07	IFIT1/RSAD2/IFITM3/ISG15/OAS1/LY6E/OAS3/MX1/OAS2	9
GO:0071357	cellular response to type I interferon	8/84	56/13317	1,98139E-09	3,45794E-07	2,74533E-07	IFI27/IFIT1/USP18/IFITM3/ISG15/OAS1/OAS3/OAS2	8
GO:0019058	viral life cycle	14/84	281/13317	2,12469E-09	3,45794E-07	2,74533E-07	IFI27/AP0E/SIGLEC1/CCL8/IFIT1/RSAD2/IFITM3/ISG15/OAS1/LY6E/CD80/OAS3/MX1/OAS2	14
GO:0019079	viral genome replication	10/84	125/13317	5,67047E-09	8,51879E-07	6,76324E-07	IFI27/CCL8/IFIT1/RSAD2/IFITM3/ISG15/OAS1/OAS3/MX1/OAS2	10
GO:0050778	positive regulation of immune response	16/84	447/13317	1,55767E-08	2,17295E-06	1,72515E-06	C1S/SERPING1/CFB/IL18/RSAD2/CD80/C1R/FPR3/C2/A2M/C1QA/ID01/CLEC6A/C1QB/C1QC/CLU	16
GO:0019221	cytokine-mediated signaling pathway	15/84	412/13317	3,71927E-08	4,84249E-06	3,84455E-06	CXCL11/IFI27/CXCL10/CCL15/CCL8/USP18/XCR1/IL18/IFITM3/NR1H3/ISG15/OAS1/OAS3/MX1/OAS2	15
GO:0002683	negative regulation of immune system process	14/84	354/13317	4,00893E-08	4,84559E-06	3,84701E-06	SERPING1/USP18/GPNMB/NR1H3/ISG15/OAS1/LRRC32/CD80/A2M/OAS3/ID01/FOXF1/MDK/C1QC	14
GO:0060337	type I interferon signaling pathway	7/84	54/13317	4,29515E-08	4,84559E-06	3,84701E-06	IFI27/USP18/IFITM3/ISG15/OAS1/OAS3/OAS2	7

Table S2. Continued

GO ID	Description	GeneRatio	BgRatio	pvalue	p.adjust	qvalue	genelD	Count
GO:0009617	response to bacterium	16/84	482/13317	4,46598E-08	4,84559E-06	3,84701E-06	CXCL11/ANKRD1/CXCL10/IL18/ CMPK2/NR1H3/ISG15/OAS1/ CD80/C2/CAMP/OAS3/IDO1/ FABP4/OAS2/IFI44	16
GO:0045069	regulation of viral genome replication	8/84	83/13317	4,7954E-08	4,92917E-06	3,91337E-06	IFIT1/RSAD2/IFITM3/ISG15/OAS1/ OAS3/MX1/OAS2	8
GO:1903900	regulation of viral life cycle	9/84	122/13317	6,97861E-08	6,81462E-06	5,41026E-06	IFIT1/RSAD2/IFITM3/ISG15/ OAS1/LY6E/OAS3/MX1/OAS2	9

Table S3. GO terms and p values associated with Biological Processes enrichment analysis for UP-regulated genes with urate 50 mg/dL treatment and LPS restimulation in human PBMCs (Top 20 terms).

GO ID	Description	GeneRatio	BgRatio	pvalue	p.adjust	qvalue	geneID	Count
GO:0032496	response to lipopolysaccharide	8/41	281/13317	1,85729E-06	0,001779017	0,001464988	THBD/CXCL3/PPBP/CSF3/IL24/TIMP4/CSF2/IL6	8
GO:0002237	response to molecule of bacterial origin	8/41	296/13317	2,73695E-06	0,001779017	0,001464988	THBD/CXCL3/PPBP/CSF3/IL24/TIMP4/CSF2/IL6	8
GO:0042531	positive regulation of tyrosine phosphorylation of STAT protein	4/41	47/13317	1,25323E-05	0,004524811	0,003726099	IL20/IL24/CSF2/IL6	4
GO:0060326	cell chemotaxis	7/41	269/13317	1,58549E-05	0,004524811	0,003726099	CCL3L3/CXCL3/PPBP/FGF2/CH25H/FLT1/IL6	7
GO:0022617	extracellular matrix disassembly	4/41	51/13317	1,74031E-05	0,004524811	0,003726099	MMP1/IL6/MMP3/MMP10	4
GO:0071222	cellular response to lipopolysaccharide	6/41	191/13317	2,38293E-05	0,004879967	0,004018564	CXCL3/PPBP/CSF3/IL24/CSF2/IL6	6
GO:0042509	regulation of tyrosine phosphorylation of STAT protein	4/41	58/13317	2,90902E-05	0,004879967	0,004018564	IL20/IL24/CSF2/IL6	4
GO:0071219	cellular response to molecule of bacterial origin	6/41	199/13317	3,00306E-05	0,004879967	0,004018564	CXCL3/PPBP/CSF3/IL24/CSF2/IL6	6
GO:0007260	tyrosine phosphorylation of STAT protein	4/41	61/13317	3,55435E-05	0,005004542	0,004121149	IL20/IL24/CSF2/IL6	4
GO:0030595	leukocyte chemotaxis	6/41	208/13317	3,84965E-05	0,005004542	0,004121149	CCL3L3/CXCL3/PPBP/CH25H/FLT1/IL6	6

Table S3. Continued

GO ID	Description	GeneRatio	BgRatio	pvalue	p.adjust	qvalue	geneID	Count
GO:0071216	cellular response to biotic stimulus	6/41	226/13317	6,11692E-05	0,007229087	0,005953021	CXCL3/PPBP/CSF3/IL24/CSF2/IL6	6
GO:0032963	collagen metabolic process	4/41	76/13317	8,45197E-05	0,008680178	0,007147968	MMP1/IL6/MMP3/MMP10	4
GO:0009617	response to bacterium	8/41	482/13317	9,25965E-05	0,008680178	0,007147968	THBD/CXCL3/PPBP/CSF3/IL24/TIMP4/CSF2/IL6	8
GO:0050731	positive regulation of peptidyl-tyrosine phosphorylation	5/41	153/13317	0,000100648	0,008680178	0,007147968	IL20/CSF3/IL24/CSF2/IL6	5
GO:0006935	chemotaxis	8/41	490/13317	0,000103849	0,008680178	0,007147968	CCL3L3/CXCL3/PPBP/ECSCR/FGF2/CH25H/FLT1/IL6	8
GO:0042330	taxis	8/41	492/13317	0,000106833	0,008680178	0,007147968	CCL3L3/CXCL3/PPBP/ECSCR/FGF2/CH25H/FLT1/IL6	8
GO:0030574	collagen catabolic process	3/41	34/13317	0,000151693	0,011600037	0,009552419	MMP1/MMP3/MMP10	3
GO:0097529	myeloid leukocyte migration	5/41	197/13317	0,000327377	0,023069054	0,018996945	CCL3L3/CXCL3/PPBP/FLT1/IL6	5
GO:0018108	peptidyl-tyrosine phosphorylation	6/41	309/13317	0,000337163	0,023069054	0,018996945	IL20/CSF3/IL24/FLT1/CSF2/IL6	6
GO:0018212	peptidyl-tyrosine modification	6/41	312/13317	0,000355034	0,023077187	0,019003643	IL20/CSF3/IL24/FLT1/CSF2/IL6	6

Table S4. GO terms and p values associated with Gene Set Enrichment Analysis (GSEA) for DOWN-regulated genes with urate 50 mg/dL treatment and LPS restimulation in human PBMCs (Top 20 terms).

GO ID	Description	setSize	enrichmentScore	NES	pvalue	p.adjust	qvalue	rank
GO:0045071	negative regulation of viral genome replication	53	-0,829531073	-2,40817	1E-10	8,54667E-08	7,9E-08	1057
GO:0045069	regulation of viral genome replication	83	-0,778272553	-2,38393	1E-10	8,54667E-08	7,9E-08	1057
GO:0019079	viral genome replication	125	-0,72753971	-2,36759	1E-10	8,54667E-08	7,9E-08	1076
GO:0051607	defense response to virus	257	-0,670493733	-2,35041	1E-10	8,54667E-08	7,9E-08	1744
GO:0140546	defense response to symbiont	258	-0,669353264	-2,35034	1E-10	8,54667E-08	7,9E-08	1744
GO:1903900	regulation of viral life cycle	122	-0,693621849	-2,25222	1E-10	8,54667E-08	7,9E-08	942
GO:0009615	response to virus	343	-0,622293729	-2,22272	1E-10	8,54667E-08	7,9E-08	1744
GO:0050792	regulation of viral process	141	-0,674581191	-2,21759	1E-10	8,54667E-08	7,9E-08	2008
GO:0019058	viral life cycle	281	-0,597337614	-2,0995	1E-10	8,54667E-08	7,9E-08	2008
GO:0045087	innate immune response	657	-0,557402404	-2,07245	1E-10	8,54667E-08	7,9E-08	1744
GO:0016032	viral process	376	-0,550950063	-1,98305	1E-10	8,54667E-08	7,9E-08	1945
GO:0050776	regulation of immune response	719	-0,48858783	-1,82622	1E-10	8,54667E-08	7,9E-08	1894
GO:0048525	negative regulation of viral process	79	-0,740204835	-2,25831	2,61608E-10	2,06388E-07	1,91E-07	1057
GO:0002250	adaptive immune response	393	-0,520029814	-1,87413	3,06245E-10	2,24346E-07	2,07E-07	1733
GO:0002831	regulation of response to biotic stimulus	320	-0,533230544	-1,89429	1,0801E-09	7,38502E-07	6,83E-07	1740
GO:0034097	response to cytokine	782	-0,440764585	-1,65339	1,59744E-09	1,02396E-06	9,47E-07	1775
GO:0002684	positive regulation of immune system process	736	-0,444623827	-1,66333	1,94539E-09	1,17364E-06	1,09E-06	1744
GO:0071357	cellular response to type I interferon	56	-0,770051221	-2,24193	3,07469E-09	1,65969E-06	1,53E-06	812
GO:0022613	ribonucleoprotein complex biogenesis	402	0,439859596	1,855451	2,99866E-09	1,65969E-06	1,53E-06	4531
GO:0002460	adaptive immune response based on somatic recombination of immune receptors built from immunoglobulin superfamily domains	269	-0,551549181	-1,93684	5,38058E-09	2,75916E-06	2,55E-06	1733
GO:0006956	complement activation	38	-0,82052763	-2,22646	8,91095E-09	4,35194E-06	4,02E-06	448

Table S4. Continued

GO ID	Description	setSize	enrichmentScore	NES	pvalue	p.adjust	qvalue	rank
GO:0050778	positive regulation of immune response	447	-0,484245155	-1,75673	9,59639E-09	4,47366E-06	4,14E-06	2339
GO:0042254	ribosome biogenesis	292	0,473889542	1,933214	1,28195E-08	5,71639E-06	5,29E-06	4910
GO:0048002	antigen processing and presentation of peptide antigen	59	-0,753524101	-2,21027	1,88752E-08	8,066E-06	7,46E-06	1197
GO:0019724	B cell mediated immunity	132	-0,629236599	-2,06259	2,02465E-08	8,30593E-06	7,68E-06	1329
GO:0002478	antigen processing and presentation of exogenous peptide antigen	37	-0,820459549	-2,21728	2,51269E-08	9,9116E-06	9,17E-06	1197
GO:0006958	complement activation, classical pathway	26	-0,870519764	-2,2153	2,668E-08	1,01345E-05	9,37E-06	448
GO:0071345	cellular response to cytokine stimulus	700	-0,437610073	-1,63367	3,78988E-08	1,38818E-05	1,28E-05	1775
GO:0016064	immunoglobulin mediated immune response	129	-0,628892404	-2,05654	4,10265E-08	1,45092E-05	1,34E-05	1329
GO:0002253	activation of immune response	277	-0,525705357	-1,84869	5,2869E-08	1,80742E-05	1,67E-05	1301
GO:0060337	type I interferon signaling pathway	54	-0,751860364	-2,18583	5,71E-08	1,88908E-05	1,75E-05	812
GO:0002495	antigen processing and presentation of peptide antigen via MHC class II	33	-0,824275001	-2,19879	6,49669E-08	2,08219E-05	1,93E-05	1197
GO:0035456	response to interferon-beta	29	-0,845393938	-2,1916	7,70365E-08	2,3942E-05	2,21E-05	866
GO:0002252	immune effector process	510	-0,462513328	-1,69361	8,89301E-08	2,68255E-05	2,48E-05	1619
GO:0034340	response to type I interferon	62	-0,722933747	-2,13229	1,3382E-07	3,9213E-05	3,63E-05	812
GO:0019886	antigen processing and presentation of exogenous peptide antigen via MHC class II	29	-0,837047246	-2,16996	2,05708E-07	5,86039E-05	5,42E-05	1197
GO:0035455	response to interferon-alpha	20	-0,880319964	-2,12405	3,19723E-07	8,86238E-05	8,2E-05	657
GO:0002683	negative regulation of immune system process	354	-0,484319646	-1,73671	4,51811E-07	0,000118815	0,00011	1158
GO:0002764	immune response-regulating signaling pathway	379	-0,473176489	-1,70602	4,43884E-07	0,000118815	0,00011	2620
GO:0044403	biological process involved in symbiotic interaction	239	-0,520218938	-1,81174	5,24782E-07	0,000134554	0,000124	1619

Table S5. Transcription Factor (TF) sorted according to their MeanRank. Top 10 TFs

Rank	TF	Mean Rank	Overlapping Genes	Library
1	STAT1	4.333	43	Literature ChIP-seq,9;ARCHS4 Coexpression,4;ENCODE ChIP-seq,2;Enrichr Queries,6;ReMap ChIP-seq,2;GTEx Coexpression,3
2	STAT2	9.4	33	ARCHS4 Coexpression,5;ENCODE ChIP-seq,1;Enrichr Queries,8;ReMap ChIP-seq,1;GTEx Coexpression,32
3	NR1H3	9.8	37	Literature ChIP-seq,8;ARCHS4 Coexpression,14;Enrichr Queries,13;ReMap ChIP-seq,9;GTEx Coexpression,5
4	BATF3	10.0	26	ARCHS4 Coexpression,10;Enrichr Queries,18;GTEx Coexpression,2
5		12.67	27	ARCHS4 Coexpression,6;Enrichr Queries,21;GTEx Coexpression,11
6	IRF9	13.0	31	ARCHS4 Coexpression,19;Enrichr Queries,7;ReMap ChIP-seq,4;GTEx Coexpression,22
7	ETV3L	20.33	21	ARCHS4 Coexpression,24;Enrichr Queries,23;GTEx Coexpression,14
8	IRF5	25.33	22	ARCHS4 Coexpression,17;Enrichr Queries,31;GTEx Coexpression,28
9	IRF7	26.33	28	ARCHS4 Coexpression,8;Enrichr Queries,4;GTEx Coexpression,67
10	EGR2	41.33	22	ARCHS4 Coexpression,43;Enrichr Queries,36;GTEx Coexpression,45

Table S6. Differential expression analysis in urate 12.5 mg/dL and LPS restimulated human PBMCs compared to control conditions. Top 20 most DOWN / UP-regulated genes

GeneID	Name	Symbol	baseMean	log2FoldChange	pvalue	adjusted pvalue
6373	C-X-C Motif Chemokine Ligand 11	CXCL11	76,80621661	-0,791227509	6,93E-05	0,001541205
3627	C-X-C Motif Chemokine Ligand 10	CXCL10	537,9571013	-0,76543793	0,000167	0,002885418
27063	Ankyrin Repeat Domain 1	ANKRD1	166,4613639	-0,737061936	0,000108	0,002079544
93082	Neutralized E3 Ubiquitin Protein Ligase 3	NEURL3	346,0006906	-0,649601864	7,55E-06	0,000324351
3429	Interferon Alpha Inducible Protein 27	IFI27	850,1254311	-0,618321034	5,56E-07	5,56E-05
4283	C-X-C Motif Chemokine Ligand 9	CXCL9	271,2149444	-0,569386774	0,007612	0,043584098
3909	Laminin Subunit Alpha 3	LAMA3	251,1338919	-0,567803704	0,000305	0,004460872
716	Complement C1s	C1S	565,8356845	-0,550290645	1,12E-05	0,000416306
710	Serpin Family G Member 1	SERPING1	3314,869589	-0,537505864	7,13E-05	0,001571376
629	Complement Factor B	CFB	7806,740689	-0,535450291	7,33E-06	0,000319879
574016	CLLU1 Antisense RNA 1	CLLU1-AS1	66,55037586	-0,532246733	0,000162	0,002799893
79370	Apoptosis Facilitator Bcl-2-Like Protein 14	BCL2L14	205,6709599	-0,503348423	2,12E-06	0,000130525
144455	E2F Transcription Factor 7	E2F7	32,86348792	-0,487296549	0,000146	0,002594755
162517	F-Box Protein 39	FBXO39	14,79912395	-0,480928417	2,12E-05	0,000657633
51513	ETS Variant Transcription Factor 7	ETV7	366,403705	-0,476148979	1,00E-05	0,000390589
3489	Insulin Like Growth Factor Binding Protein 6	IGFBP6	77,00092222	-0,455981201	0,005635	0,035408879
24141	Lysosomal Associated Membrane Protein Family Member 5	LAMP5	87,27418505	-0,439505471	0,002729	0,02182168
6359	C-C Motif Chemokine Ligand 15	CCL15	31,83724403	-0,428078463	0,004117	0,028849129
160365	C-Type Lectin Like 1, Pseudogene	CLECL1P	17,86239681	-0,424748134	7,91E-05	0,001690304
91543	Radical S-Adenosyl Methionine Domain Containing 2	RSAD2	5378,367535	-0,414141449	1,26E-05	0,000449508

Table S6. Continued

GenId	Name	Symbol	baseMean	log2FoldChange	pvalue	adjusted pvalue
6853	Synapsin I	SYN1	212,7382312	0,595819591	8,51E-09	4,99E-06
9023	Cholesterol 25-Hydroxylase	CH25H	70,35513298	0,597034504	0,000133	0,00241269
152273	FYVE, RhoGEF And PH Domain Containing 5	FGD5	35,99725398	0,614096128	3,96E-08	1,16E-05
7850	Interleukin 1 Receptor Type 2	IL1R2	167,9604163	0,614134632	0,001277	0,012747364
4923	Neurotensin Receptor 1	NTSR1	182,2067784	0,619857914	4,36E-08	1,23E-05
57413	Transmembrane And Immunoglobulin Domain Containing 3	TMIGD3	70,42062435	0,628882488	2,10E-09	2,29E-06
2321	Fms Related Receptor Tyrosine Kinase 1	FLT1	1461,394579	0,645805729	1,11E-07	2,10E-05
8685	Macrophage Receptor With Collagenous Structure	MARCO	6123,534878	0,649088397	4,84E-10	1,09E-06
7079	TIMP Metalloproteinase Inhibitor 4	TIMP4	25,00413364	0,650723978	9,05E-06	0,000363296
3569	Interleukin 6	IL6	11692,55779	0,663998319	8,00E-05	0,001694575
4900	Neurogranin	NRGN	205,9887326	0,673042979	5,98E-09	4,24E-06
5352	Procollagen-Lysine,2-Oxoglutarate 5-Dioxygenase 2	PLOD2	22,8557778	0,688779476	5,98E-07	5,82E-05
6696	Secreted Phosphoprotein 1	SPP1	5393,303345	0,757749412	1,70E-08	7,63E-06
3036	Hyaluronan Synthase 1	HAS1	184,5336996	0,769762888	0,001105	0,011417728
2791	G Protein Subunit Gamma 11	GNG11	95,68891832	0,776786623	7,10E-09	4,35E-06
7980	Tissue Factor Pathway Inhibitor 2	TFPI2	958,1310678	0,835096507	8,07E-07	6,98E-05
256227	STEAP Family Member 1B	STEAP1B	40,73450977	0,869541639	6,33E-05	0,001446954
84658	Adhesion G Protein-Coupled Receptor E3	ADGRE3	273,8462531	0,887422429	1,91E-07	2,87E-05
5473	Pro-Platelet Basic Protein	PPBP	33829,81097	0,931677975	8,05E-08	1,78E-05
92737	Delta/Notch Like EGF Repeat Containing	DNER	274,0494388	1,043198024	2,30E-08	9,39E-06

Table S7. GO terms and p values associated with Gene Set Enrichment Analysis (GSEA) using REACTOME for DOWN-regulated genes with urate 12.5 mg/dL treatment and LPS restimulation in human PBMCs (Top 20 terms).

pathway	pval	padj	log2err	ES	NES	size
INTERFERON_ALPHA_BETA_SIGNALING	3,08E-18	2,59E-15	1,105337	-0,80373	-2,76781	63
INTERFERON_GAMMA_SIGNALING	3,58E-11	6,70E-09	0,851339	-0,64637	-2,36647	88
INTERFERON_SIGNALING	6,05E-16	2,55E-13	1,02767	-0,54047	-2,25338	242
OAS_ANTIVIRAL_RESPONSE	2,95E-06	0,000184	0,627257	-0,93619	-2,01928	9
TRAF6_MEDIATED_IRF7_ACTIVATION	0,000103	0,003275	0,538434	-0,78259	-2,00576	16
TNFR1_INDUCED_NF_KAPPA_B_SIGNALING_PATHWAY	0,000274	0,006313	0,498493	-0,64656	-1,93759	32
DDX58_IFIH1_MEDIATED_INDUCION_OF_INTERFERON_ALPHA_BETA	4,47E-05	0,001711	0,557332	-0,55294	-1,93005	67
NF_KB_ACTIVATION_THROUGH_FADD_RIP_1_PATHWAY_MEDIATED_BY_CASPASE_8_AND_10	0,000249	0,006001	0,498493	-0,80466	-1,9251	13
TNFR1_INDUCED_PROAPOPTOTIC_SIGNALING	0,000215	0,005415	0,518848	-0,68665	-1,92297	24
ENDOSOMAL_VACUOLAR_PATHWAY	0,000146	0,004188	0,518848	-0,84709	-1,92209	11
COPI_MEDIATED_ANTEROGRADE_TRANSPORT	4,49E-07	3,98E-05	0,674963	0,595899	1,989277	88
SIGNALING_BY_NTRKS	1,55E-07	1,64E-05	0,690132	0,573728	1,990088	114
GOLGI_ASSOCIATED_VESICLE_BIOGENESIS	1,56E-05	0,00082	0,57561	0,648325	1,996454	52
COOPERATION_OF_PDCL_PHLIP1_AND_TRIC_CCT_IN_G_PROTEIN_BETA_FOLDING	2,41E-05	0,001128	0,57561	0,737108	2,00343	28
ER_TO_GOLGI_ANTEROGRADE_TRANSPORT	1,60E-08	2,25E-06	0,733762	0,567674	2,019379	137
ASPARAGINE_N_LINKED_GLYCOSYLATION	6,88E-12	1,93E-09	0,887075	0,52946	2,030801	273
PARASITE_INFECTION	2,86E-06	0,000184	0,627257	0,657789	2,054359	57
RHO_GTPASES_ACTIVATE_WASPS_AND_WAVES	4,46E-06	0,000268	0,610527	0,730246	2,088282	35
NEUTROPHIL_DEGRANULATION	8,15E-20	1,37E-16	1,151221	0,531913	2,116962	446
INTRAFLAGELLAR_TRANSPORT	2,82E-07	2,64E-05	0,674963	0,708156	2,133198	47

Table S8. GO terms and p values associated with Gene Set Enrichment Analysis (GSEA) using GO BP for DOWN-regulated genes with urate 12.5 mg/dL treatment and LPS restimulation in human PBMCs (Top 20 terms).

pathway	pval	padj	log2err	ES	NES	size
NEGATIVE_REGULATION_OF_VIRAL_GENOME_REPLICATION	7,18E-14	6,85E-11	0,954542	-0,7922	-2,62793	51
REGULATION_OF_VIRAL_GENOME_REPLICATION	6,58E-14	6,85E-11	0,954542	-0,7101	-2,5539	80
NEGATIVE_REGULATION_OF_VIRAL_PROCESS	3,20E-12	1,75E-09	0,898671	-0,70121	-2,5119	78
DEFENSE_RESPONSE_TO_SYMBIONT	5,43E-23	4,14E-19	1,237897	-0,58228	-2,46979	286
REGULATION_OF_VIRAL_PROCESS	7,53E-13	4,79E-10	0,921426	-0,59858	-2,35685	143
ANTIVIRAL_INNATE_IMMUNE_RESPONSE	7,57E-08	1,48E-05	0,704976	-0,70418	-2,28995	45
VIRAL_GENOME_REPLICATION	5,31E-11	2,25E-08	0,851339	-0,59062	-2,27498	122
RESPONSE_TO_VIRUS	8,98E-21	2,28E-17	1,177893	-0,5216	-2,26918	368
ANTIGEN_PROCESSING_AND_PRESENTATION_OF_ENDOGENOUS_PEPTIDE_ANTIGEN	1,65E-06	0,000174	0,643552	-0,82339	-2,22831	20
RESPONSE_TO_TYPE_I_INTERFERON	8,19E-08	1,52E-05	0,704976	-0,63172	-2,20288	68
REGULATION_OF_SUPEROXIDE_METABOLIC_PROCESS	0,000179	0,006652	0,518848	0,725525	1,930881	24
POSITIVE_REGULATION_OF_PEPTIDYL_THREONINE_PHOSPHORYLATION	0,000103	0,00427	0,538434	0,738252	1,943764	23
SPERM_EGG_RECOGNITION	6,84E-05	0,003201	0,538434	0,74824	1,945195	22
SUBSTANTIA_NIGRA_DEVELOPMENT	4,69E-05	0,002453	0,557332	0,679319	1,968687	36
RECEPTOR_INTERNALIZATION	2,00E-06	0,000203	0,627257	0,584151	1,97647	90
PROTEIN_N_LINKED_GLYCOSYLATION_VIA_ASPARAGINE	3,45E-05	0,001937	0,557332	0,762669	1,982706	22
RECEPTOR_MEDIATED_ENDOCYTOSIS	2,65E-09	7,22E-07	0,774939	0,535611	1,998941	197
POSITIVE_REGULATION_OF_SUBSTRATE_ADHESION_DEPENDENT_CELL_SPREADING	2,07E-05	0,001329	0,57561	0,701783	2,015147	35
ESTABLISHMENT_OF_PROTEIN_LOCALIZATION_TO_ENDOPLASMIC_RETICULUM	1,90E-06	0,000198	0,643552	0,709968	2,075976	38
PROTEIN_LOCALIZATION_TO_ENDOPLASMIC_RETICULUM	1,44E-07	2,34E-05	0,690132	0,67792	2,157524	60

Table S9. GO terms and p values associated with Biological Processes enrichment analysis for down-regulated genes with urate 50 mg/dL treatment alone in human monocytes (Top 20 terms).

GO ID	Description	GeneRatio	BgRatio	pvalue	p.adjust	qvalue	geneID
GO:0050792	regulation of viral process	26/271	145/14230	2,70273E-18	9,43793E-15	7,78386E-15	CD4/CD74/EIF2AK2/OAS1/OAS3/OAS2/IFIH1/STAT1/CXCR4/APOBEC3A/TRIM22/IFITM3/GSN/IFIT5/MX1/LY6E/IFI16/AXL/CD28/PARP10/CITA/IFIT1/ISG15/PLSCR1/HLA-DRB1/APOBEC3C
GO:1903900	regulation of viral life cycle	24/271	126/14230	1,31668E-17	2,29892E-14	1,89602E-14	CD4/CD74/EIF2AK2/OAS1/OAS3/OAS2/IFIH1/APOBEC3A/TRIM22/IFITM3/GSN/IFIT5/MX1/LY6E/IFI16/AXL/CD28/PARP10/CITA/IFIT1/ISG15/PLSCR1/HLA-DRB1/APOBEC3C
GO:0048525	negative regulation of viral process	19/271	81/14230	5,79011E-16	6,73968E-13	5,5585E-13	EIF2AK2/OAS1/OAS3/OAS2/IFIH1/STAT1/APOBEC3A/IFITM3/GSN/IFIT5/MX1/LY6E/IFI16/PARP10/CITA/IFIT1/ISG15/PLSCR1/APOBEC3C
GO:0051607	defense response to virus	30/271	254/14230	1,02162E-15	7,95202E-13	6,55837E-13	EIF2AK2/OAS1/TLR8/DDX58/DHX58/OAS3/OAS2/IFIH1/STAT1/IFIT3/IFIT2/IFI6/FGL2/APOBEC3A/TRIM22/DDX60/IFI44L/PARP9/HERC5/IFITM3/IFIT5/MOV10/MX1/IFI16/MX2/IFIT1/ISG15/PLSCR1/TLR7/APOBEC3C
GO:0140546	defense response to symbiont	30/271	255/14230	1,13861E-15	7,95202E-13	6,55837E-13	EIF2AK2/OAS1/TLR8/DDX58/DHX58/OAS3/OAS2/IFIH1/STAT1/IFIT3/IFIT2/IFI6/FGL2/APOBEC3A/TRIM22/DDX60/IFI44L/PARP9/HERC5/IFITM3/IFIT5/MOV10/MX1/IFI16/MX2/IFIT1/ISG15/PLSCR1/TLR7/APOBEC3C

Table S9. Continued

GO ID	Description	GeneRatio	BgRatio	pvalue	p.adjust	qvalue	geneID
GO:0009615	response to virus	34/271	341/14230	1,98044E-15	1,15262E-12	9,50612E-13	EIF2AK2/OAS1/TLR8/HSPB1/DDX58/ DHX58/OAS3/OAS2/IFIH1/STAT1/ STMN1/IFIT3/IFIT2/CXCR4/IFI6/FGL2/ APOBEC3A/TRIM22/DDX60/IFI44L/ IFI44/PARP9/HERC5/IFITM3/IFIT5/ MOV10/MX1/IFI16/MX2/IFIT1/ISG15/ PLSCR1/TLR7/APOBEC3C
GO:0002495	antigen processing and presentation of peptide antigen via MHC class II	13/271	31/14230	4,94226E-15	2,4168E-12	1,99324E-12	CD74/TREM2/LGMN/MARCHF1/ HLA-DQB1/HLA-DRB1/HLA-DQA1/ HLA-DRB5/HLA-DMA/HLA-DRA/HLA- DPB1/HLA-DPA1/HLA-DMB
GO:0048002	antigen processing and presentation of peptide antigen	16/271	57/14230	5,53677E-15	2,4168E-12	1,99324E-12	HFE/CD74/TREM2/LGMN/CLEC4A/ MARCHF1/ACE/HLA-DQB1/HLA- DRB1/HLA-DQA1/HLA-DRB5/HLA- DMA/HLA-DRA/HLA-DPB1/HLA- DPA1/HLA-DMB
GO:0002504	antigen processing and presentation of peptide or polysaccharide antigen via MHC class II	13/271	33/14230	1,32755E-14	5,1509E-12	4,24817E-12	CD74/TREM2/LGMN/MARCHF1/ HLA-DQB1/HLA-DRB1/HLA-DQA1/ HLA-DRB5/HLA-DMA/HLA-DRA/HLA- DPB1/HLA-DPA1/HLA-DMB
GO:0045071	negative regulation of viral genome replication	15/271	54/14230	4,75512E-14	1,66049E-11	1,36947E-11	EIF2AK2/OAS1/OAS3/OAS2/IFIH1/ APOBEC3A/IFITM3/IFIT5/MX1/ IFI16/PARP10/IFIT1/ISG15/PLSCR1/ APOBEC3C
GO:0019882	antigen processing and presentation	18/271	99/14230	3,90387E-13	1,2393E-10	1,0221E-10	HFE/CD74/TREM2/LGMN/CLEC4A/ FGL2/MARCHF1/CD1D/ACE/HLA- DQB1/HLA-DRB1/HLA-DQA1/HLA- DRB5/HLA-DMA/HLA-DRA/HLA- DPB1/HLA-DPA1/HLA-DMB

Table S9. Continued

GO ID	Description	GeneRatio	BgRatio	pvalue	p.adjust	qvalue	geneID
GO:0002399	MHC class II protein complex assembly	9/271	14/14230	5,3191E-13	1,42879E-10	1,17838E-10	HLA-DQB1/HLA-DRB1/HLA-DQA1/HLA-DRB5/HLA-DMA/HLA-DRA/HLA-DPB1/HLA-DPA1/HLA-DMB
GO:0002503	peptide antigen assembly with MHC class II protein complex	9/271	14/14230	5,3191E-13	1,42879E-10	1,17838E-10	HLA-DQB1/HLA-DRB1/HLA-DQA1/HLA-DRB5/HLA-DMA/HLA-DRA/HLA-DPB1/HLA-DPA1/HLA-DMB
GO:0019884	antigen processing and presentation of exogenous antigen	13/271	43/14230	7,14851E-13	1,78304E-10	1,47055E-10	CD74/LGMN/CLEC4A/CD1D/HLA-DQB1/HLA-DRB1/HLA-DQA1/HLA-DRB5/HLA-DMA/HLA-DRA/HLA-DPB1/HLA-DPA1/HLA-DMB
GO:0019886	antigen processing and presentation of exogenous peptide antigen via MHC class II	11/271	27/14230	9,71815E-13	2,20256E-10	1,81654E-10	CD74/LGMN/HLA-DQB1/HLA-DRB1/HLA-DQA1/HLA-DRB5/HLA-DMA/HLA-DRA/HLA-DPB1/HLA-DPA1/HLA-DMB
GO:0002478	antigen processing and presentation of exogenous peptide antigen	12/271	35/14230	1,00919E-12	2,20256E-10	1,81654E-10	CD74/LGMN/CLEC4A/HLA-DQB1/HLA-DRB1/HLA-DQA1/HLA-DRB5/HLA-DMA/HLA-DRA/HLA-DPB1/HLA-DPA1/HLA-DMB
GO:0045069	regulation of viral genome replication	16/271	83/14230	3,17524E-12	6,52231E-10	5,37922E-10	EIF2AK2/OAS1/OAS3/OAS2/IFIH1/APOBEC3A/IFITM3/IFIT5/MX1/IFI16/CD28/PARP10/IFIT1/ISG15/PLSCR1/APOBEC3C
GO:0019058	viral life cycle	27/271	287/14230	7,29463E-12	1,41516E-09	1,16714E-09	CD4/CD74/EIF2AK2/SIGLEC1/OAS1/OAS3/OAS2/IFIH1/CXCR4/APOBEC3A/APOE/TRIM22/IFITM3/GSN/IFIT5/MX1/LY6E/IFI16/AXL/CD28/PARP10/CIITA/IFIT1/ISG15/PLSCR1/HLA-DRB1/APOBEC3C

Table S9. Continued

GO ID	Description	GeneRatio	BgRatio	pvalue	p.adjust	qvalue	geneID
GO:0002396	MHC protein complex assembly	9/271	18/14230	1,20827E-11	2,05542E-09	1,69519E-09	HLA-DQB1/HLA-DRB1/HLA-DQA1/ HLA-DRB5/HLA-DMA/HLA-DRA/HLA-DPB1/HLA-DPA1/HLA-DMB
GO:0002501	peptide antigen assembly with MHC protein complex	9/271	18/14230	1,20827E-11	2,05542E-09	1,69519E-09	HLA-DQB1/HLA-DRB1/HLA-DQA1/ HLA-DRB5/HLA-DMA/HLA-DRA/HLA-DPB1/HLA-DPA1/HLA-DMB

Table S10. Transcription Factor (TF) sorted according to their MeanRank. Top 10 TFs

Rank	TF	Mean Rank	Overlapping Genes	Library
1	TFEC	4.667	100	ARCHS4 Coexpression,2;Enrichr Queries,11;GTEx Coexpression,1
2	IRF8	8.5	91	Literature ChIP-seq,4;ARCHS4 Coexpression,7;Enrichr Queries,15;GTEx Coexpression,8
3	SP140	11.67	82	ARCHS4 Coexpression,15;Enrichr Queries,5;GTEx Coexpression,15
4	SP100	11.67	79	ARCHS4 Coexpression,21;Enrichr Queries,7;GTEx Coexpression,7
5	IRF7	12.0	77	ARCHS4 Coexpression,9;Enrichr Queries,2;GTEx Coexpression,25
6	BATF3	12.67	74	ARCHS4 Coexpression,18;Enrichr Queries,18;GTEx Coexpression,2
7	IRF5	13.67	85	ARCHS4 Coexpression,10;Enrichr Queries,17;GTEx Coexpression,14
8	STAT1	15.83	117	Literature ChIP-seq,59;ARCHS4 Coexpression,4;ENCODE ChIP-seq,2;Enrichr Queries,6;ReMap ChIP-seq,2;GTEx Coexpression,22
9	BATF2	16.0	75	ARCHS4 Coexpression,17;Enrichr Queries,10;GTEx Coexpression,21
10	IRF9	16.0	101	ARCHS4 Coexpression,16;Enrichr Queries,8;ReMap ChIP-seq,37;GTEx Coexpression,3

Table S11. Markers used in flow cytometry

Extracellular markers	Fluorochrome	Clone
CD14 (mono)	Pe.cy7	61D3
CD16 (mono)	APC	B73.1
CD3 (Tcells)	FITC	UCHT1
HLA-DR	PC5	-
CD45	BV510	-
Intracellular markers	Fluorochrome	Clone
Phospho STAT1	PE	A17012

Table S12. Correlation between serum urate levels (median (IQR) 6.60 (5.65, 7.80)) and normalized counts of ISGs in response to 24h stimulation with Poly: IC, CpG, and *C. albicans*.

Urate correlations	Poly: IC		CpG		<i>C. albicans</i>	
	Spearman rho	p-value	Spearman rho	p-value	Spearman rho	p-value
<i>IRF5</i>	-0,3715	0,0101	-0,2919	0,0465	-0,2919	0,0018
<i>IRF7</i>	-0,2865	0,0509	-0,2544	0,0844	-0,2544	0,0263
<i>IRF9</i>	-0,2651	0,0717	-0,2236	0,1309	-0,2236	0,0248
<i>STAT1</i>	-0,0374	0,8031	0,0507	0,7352	0,0507	0,2399
<i>STAT2</i>	-0,1777	0,2321	0,0437	0,7704	0,0437	0,0819
<i>IFI27</i>	-0,3755	0,0093	-0,3447	0,0176	-0,3447	0,0154
<i>IFIT1</i>	-0,2152	0,1463	0,0130	0,9311	0,0130	0,2504
<i>IFIT2</i>	-0,2257	0,1272	-0,0082	0,9566	-0,0082	0,1797
<i>MX1</i>	-0,1096	0,4632	-0,0055	0,9708	-0,0055	0,2644
<i>MX2</i>	-0,1683	0,2580	0,0437	0,7707	0,0437	0,2499
<i>OAS1</i>	-0,2355	0,1111	-0,0630	0,6738	-0,0630	0,1675
<i>OAS2</i>	-0,0743	0,6195	0,1249	0,4027	0,1249	0,2494
<i>OAS3</i>	-0,0824	0,5817	0,0427	0,7754	0,0427	0,1672
<i>ISG15</i>	-0,2964	0,0431	-0,2763	0,0601	-0,2763	0,0468
<i>IFITM3</i>	-0,4491	0,0015	-0,4361	0,0022	-0,4361	0,0053
<i>USP18</i>	-0,2224	0,1330	0,0232	0,8770	0,0232	0,2065
<i>RSAD2</i>	-0,0334	0,8234	-0,0356	0,8124	-0,0356	0,1562
<i>CXCL10</i>	-0,3409	0,0190	0,0151	0,9198	0,0151	0,1048
<i>CXCL11</i>	-0,4184	0,0034	-0,0757	0,6130	-0,0757	0,0944

References

- [1] Crişan TO, Cleophas MCP, Novakovic B, et al. Uric acid priming in human monocytes is driven by the AKT-PRAS40 autophagy pathway. *Proc Natl Acad Sci* 2017; 114:5485–5490.
- [2] Joosten LAB, Netea MG, Mylona E, et al. Engagement of fatty acids with toll-like receptor 2 drives interleukin-1 β production via the ASC/caspase 1 pathway in monosodium urate monohydrate crystal-induced gouty arthritis. *Arthritis Rheum* 2010; 62:3237–3248.
- [3] Crişan TO, Cleophas MCP, Oosting M, et al. Soluble uric acid primes TLR-induced proinflammatory cytokine production by human primary cells via inhibition of IL-1Ra. *Ann Rheum Dis* 2016; 75:755–762.
- [4] Love MI, Huber W, Anders S. Moderated estimation of fold change and dispersion for RNA-seq data with DESeq2. *Genome Biol* 2014; 15:1–21.
- [5] Ritchie ME, Phipson B, Wu D, et al. Limma powers differential expression analyses for RNA-sequencing and microarray studies. *Nucleic Acids Res* 2015; 43:e47.
- [6] Subramanian A, Tamayo P, Mootha VK, et al. Gene set enrichment analysis: A knowledge-based approach for interpreting genome-wide expression profiles. *Proc Natl Acad Sci U S A* 2005; 102:15545–15550.
- [7] Yu G, Wang LG, Han Y, et al. ClusterProfiler: An R package for comparing biological themes among gene clusters. *Omi A J Integr Biol* 2012; 16:284–287.
- [8] Keenan AB, Torre D, Lachmann A, et al. ChEA3: transcription factor enrichment analysis by orthogonal omics integration. *Nucleic Acids Res* 2019; 47:W212–W224.



CHAPTER 5

Sex-specific differences in cytokine levels in patients with gout compared to controls

Medeea Badii*, Orsolya I. Gaal*, Ioana Hotea, Valentin Nica, Andreea M. Mirea, Dragoş Mărginean, HINT Consortium, Cristina Pamfil, Simona Rednic, Radu A. Popp, Tania O. Crişan# and Leo A.B. Joosten#

*These authors contributed equally to this work

#These authors share senior authorship

Gout, Urate, and Crystal Deposition Disease. 2024; 2(2):133-143.

Summary

Gout, an inflammatory disease orchestrated by interleukin-1 β activation and release, is more prevalent in men. The clinical profiles of patients with gout report differences by sex. This study aims to investigate sex-specific cytokine profiles in circulation and in stimulated peripheral blood mononuclear cells (PBMCs) of patients with gout and controls. Participants included in the gout group met the criteria of the American College of Rheumatology/European League Against Rheumatism (ACR/EULAR). The control group included individuals with varying levels of serum urate and absence of gout. PBMCs were stimulated *in vitro* for 24 h with various TLR ligands. Cytokines were determined in culture supernatants and plasma. Plasma IL-1Ra and high-sensitivity C-reactive protein (hsCRP) were higher in men with gout compared to men without gout whereas no significant differences in circulating cytokines were observed in women. PBMCs of patients with gout showed higher cytokine production of IL-1 β , IL-1Ra, and TNF- α following 24 h stimulation, predominantly observed in women. We identified sex-specific cytokine production in gout in response to *in vitro* stimulation. While men with gout had higher levels of circulating cytokines, stimulated PBMCs of women with gout show an enhanced capacity for cytokine production. These data may suggest potentially different regulatory mechanisms of inflammation in men and women with gout.

Introduction

Gout is an inflammatory disease driven by innate immune mechanisms around interleukin-1 β activation and release [1,2]. Since gout is more prevalent in men compared to women, it has mostly been considered a condition that impacts men [3]. Still, clinical profiles of patients with gout are reported to differ by sex: older age, higher prevalence of comorbidities, use of diuretics have been reported more in women [4], and high consumption of alcohol, especially beer, in men [5]. Women report greater disease severity, which affects their daily activities, despite their better adherence to dietary modifications and receiving the same treatment as men [5,6]. These differences could result in bias in clinical care since a study shows that women receive medical advice for disease management less often than men [6].

Men are more frequently and severely affected by infectious diseases [7], while autoimmune diseases predominantly affect women [8]. Initial explanations for sexual dimorphism in immunity have first centered around the differences in the levels of sex hormones or the different compositions of sex chromosomes. The role of sex hormones in regulating immune responses has been extensively studied [9], and it shows that their levels correlate with immune circulating mediators [10]. Furthermore, a study showing differences in LPS-induced cytokine responses in the immune cells of pre-pubescent males and females suggests that sex hormones alone cannot completely account for the distinct immune responses observed in females and males [11]. In SARS-CoV-2 infection, female sex hormones interact with the oestrogen receptors to inhibit immune responses, indicating a potential protective role for oestrogens; moreover, women over the age of 55 present an increased mortality rate [12]. Some studies propose that sex chromosomes also contribute to the observed sexual dimorphism, as many genes on the X chromosome are linked to the regulation of immune system functions [13]. A possible regulatory mechanism for sex-specific immune responses might involve microRNA since the X chromosome is known to contain 10% of the microRNA (miRNA) in the human genome as compared to 2% miRNA on the Y chromosome [14]. When stimulated with TLR-specific ligands, monocytes of men show higher cytokine production compared to women or individuals with Klinefelter syndrome XXY, suggesting that regulation of sex-specific immune responses may be dependent on the X-linked genes [15].

Additional evidence from in vitro studies reveals that stimulation of peripheral blood mononuclear cells (PBMCs) of healthy individuals results in increased

monocyte-derived cytokine responses in men [16]. In individuals with metabolic syndrome, men exhibit higher levels of various circulating pro-inflammatory markers such as IL-6 and leptin, while women present lower levels of anti-inflammatory adiponectin [17]. In vitro stimulation of PBMCs from men with metabolic syndrome shows an enhanced capacity for cytokine production [17]. While these sex-specific immune differences cannot be explained by hormonal differences alone, they are greatly impacted by age [16,17]. Overall, men present an elevated immune response as indicated by a comprehensive meta-analysis that looked at cytokine production upon LPS stimulation in 15 study populations. Interestingly, these changes are not age-dependent nor disease-dependent [18]. Under stress-related conditions, such as exposure to cortisol stimulation, men exhibit higher levels of proinflammatory cytokines, whereas women tend to have a shift towards higher levels of anti-inflammatory mediators [19].

The objective of this study is to gain insight into the immune responses of patients with gout and controls by examining sex-specific cytokine profiles in both circulation and stimulated peripheral blood mononuclear cells (PBMCs).

Materials and methods

Participants

Participants for this study were recruited from the Rheumatology Department of the Iuliu Hațieganu University of Medicine and Pharmacy, Cluj-Napoca, Romania. The enrolled patients are part of a larger study, the HINT Project (Hyperuricemia-induced Inflammation: Targeting the central role of uric acid in rheumatic and cardiovascular diseases, ID P 37 762; MySMIS 103587) implemented in Cluj-Napoca Romania at the Iuliu Hațieganu University of Medicine and Pharmacy. All participants gave written informed consent before being included in this study. The study participants consisted of patients with diagnosed gout and individuals without gout. Peripheral blood was drawn from the cubital vein on EDTA tubes under sterile conditions. Approval for the current study was granted by the Ethical Committee of the "Iuliu Hațieganu" University of Medicine and Pharmacy, Cluj-Napoca (approval no. 425/2016). Individuals were included in the gout group if they had experienced at least, one clinically diagnosed gout flare and had either confirmed the presence of MSU crystals in their synovial fluid or a score of at least 8 according to the American College of Rheumatology/European League Against Rheumatism (ACR/EULAR).

Throughout the sections of this report, we employ the terms 'women' and 'men' to refer to participants of female and male biological sex, respectively. This distinction is deliberate and aimed at clearly distinguishing the context in which we are discussing sex and gender.

Cell Preparation and Culture Conditions

PBMCs were obtained through density gradient centrifugation using Ficoll-Paque (GE Healthcare, Chicago, IL, USA) and subsequently washed 3 times with phosphate-buffered saline (PBS, Sigma, St. Louis, MO, USA) at 4 °C. PBMCs were counted by the Coulter Counter method (Multisizer 4e Beckman Coulter, Brea, CA, USA). Cells were plated in a round-bottom 96-well plate (Greiner Bio-One, Kremsmünster, Austria) at 5×10^5 PBMCs in a volume of 50 μ L per well with Dutch Modified RPMI 1640 medium (Sigma) supplemented with 50 μ g/mL gentamycin (Sigma), 2 mM GlutaMAX (Gibco, Waltham, MA USA), and 1 mM pyruvate (Gibco).

PBMCs isolated from patients and controls were treated for 24 h with the following stimuli in two separate experiments using round-bottom plates: first experiment—C16 (200 μ M palmitate conjugated with human albumin), C16 + MSU (monosodium urate) crystals (300 μ g/mL) and RPMI + albumin for negative control; second experiment—LPS (lipopolysaccharide) high dose (0.1 μ g/mL), LPS low dose (0.001 μ g/mL), LPS low dose + MSU crystals (300 μ g/mL), PHA (10 μ g/mL; Phytohaemagglutinin InvivoGen, San Diego, CA, USA), Poly: IC (10 μ g/mL; InvivoGen), CpG (1 μ g/mL; InvivoGen), heat-killed *Candida albicans* (10^6 col/mL), *Staphylococcus aureus* (10^6 col/mL), *Escherichia coli* (10^6 col/mL), *Borrelia burgdorferi* (10^6 col/mL), *Mycobacterium tuberculosis* lysate (5 μ g/mL) and RPMI for negative control for IL-1 β and basal level measurements for IL-1Ra. All stimuli were prepared prior to conducting the experiments, aliquoted, and stored at -20 °C. Replicate wells were used for each experimental condition at the stated concentrations in a total volume of 200 μ L. The supernatants were pooled before being stored at -20 °C until the ELISA measurements were performed. All cells were incubated in a Galay 170 R incubator (Eppendorf, Hamburg, Germany) at 37 °C with 5% CO₂.

LPS (*E. coli* serotype 055:b5; Sigma), suitable for cell culture, was ultra-purified before cell culture experiments. MSU crystals were prepared as previously described [20] and sonicated before being added to the cell culture.

Cytokine Measurements

Supernatants collected at 24 h were used for cytokine measurement using enzyme-linked immunosorbent assay with commercial ELISA kits for IL-1 β , IL-1Ra, and TNF according to the manufacturer's instructions (R&D Systems, Minneapolis, MN, USA). The absorbance at 450 nm was measured with Synergy HTX Multi-mode reader from Bio-Tek. The lowest range of detection was 39 pg/mL for IL-1 β , 390 pg/mL for IL-1Ra and 78 pg/mL for TNF. Samples were diluted before assay 10-fold for IL-1 β and IL-1Ra and 5-fold for TNF. EDTA Plasma IL-1Ra and hsCRP were diluted prior assay and measured following the manufacturer's instructions (Quantikine ELISA Kit, R&D Systems, Minneapolis, MN, USA). The lowest range of detection was 0.3105 μ g/mL for hsCRP and 31.2 pg/mL for IL-1Ra. For the circulating markers and cytokines produced following PBMC stimulation, any measurement falling below or exceeding the detection limit was adjusted to the corresponding detection limit. In the analysis of in vitro cytokine production, samples measuring IL-1 β levels exceeding twice the value of the lowest standard, equivalent to 78 pg/mL, were excluded from the dataset, to account for potential contamination. This exclusion criterion was applied across all cytokines for the corresponding sample.

Statistical Analysis

The statistical analysis was performed using R (R Foundation for Statistical Computing, Vienna, Austria) software (4.2.2 and 4.2.3 versions) with R Studio IDE (as an integrated development environment). Considering data distribution, statistical evaluation was performed using Student's t-test or Mann-Whitney and values of $p < 0.05$ were considered statistically significant. Pearson's Chi-squared test was applied to categorical data.

For the in vitro cytokine production analysis, a linear model was created using the 'lm' function in R. The model was run 3 times: for all data with sex and age as covariates, and separately for women and men, disregarding the correction factor for "sex".

Model1 = $\log(\text{cytokine_production}) \sim \text{Group} + \text{Age} + \text{Sex}$ for ALL in the case of gout vs. non-gout

Model2 = $\log(\text{cytokine_production}) \sim \text{Group} + \text{Age}$ in the case of female/male

Results

Characteristics of Patients with Gout and Healthy Controls

Table 1 illustrates the total number of patients recruited within the HINT study. The prevalence of gout was 19% in women and 81% in men, while a larger percentage (68%) were women in the group without gout. Pearson's Chi-squared test finds evidence of an association between group and sex that is statistically significant ($p < 0.001$). In addition, our results indicate that gout is more prevalent in men compared to women by approximately 3– 4:1 and this is in accordance with what has been reported in the literature [21]. Both groups were similar in terms of age (IQR = 63, $p = 0.3$). Serum urate levels were significantly higher in the gout group compared to patients without gout ($p < 0.001$). Body mass index (BMI) was higher in patients with gout ($p = 0.03$).

Table 1. Baseline characteristics of the gout and control cohorts in all patients included. 1n (%); Median (IQR); 2Pearson's Chi-squared test or Wilcoxon rank sum test; Unknown accounts for missing information.

Characteristic	n	Gout, n = 299 ¹	No_Gout, n = 480 ¹	p-value ²
Sex	777			<0.001
F (female)		56 (19%)	324 (68%)	
M (male)		243 (81%)	154 (32%)	
Unknown		0	2	
Age (years)	763	63 (55, 69)	63 (57, 70)	0.3
Unknown		5	11	
Urate (mg/dL)	762	7.10 (5.70, 8.69)	6.10 (4.70, 7.60)	<0.001
Unknown		7	10	
BMI	743	30.0 (26.8, 33.2)	28.6 (26.2, 32.3)	0.003
Unknown		8	28	

When analyzing the data divided by sex, we observed that patients with gout, whether they were women or men, did not significantly differ from their respective control groups in terms of age. In patients affected by gout, it was notable that women tended to be older than men (Figure 1B). Furthermore, both women and men with gout displayed elevated serum urate levels compared to their control counterparts (Figure 1A), although interestingly, within the gout group, there were no substantial differences in urate levels between men and women (Figure 1B). Moreover, among patients with gout, women exhibited a higher body mass index (BMI) than men (Figure 1B), and

a higher frequency for comorbidities type 2 diabetes, hypertension, or liver steatosis (Figure 1C). However, when analyzing the data by sex, both women and men with gout had higher BMIs compared to the corresponding controls without gout (Figure 1A).

Sex-Specific Cytokine Production upon 24 h In Vitro Stimulation of PBMCs

After filtering out the samples that measured IL-1 β in RPMI above 78 mg/dL, had missing information on age, sex, and serum urate, the dataset for *in vitro* cytokine production analysis included data from two experiments: the first experiment included a total number of $n = 134$ patients with gout (28 women and 106 men) and $n = 227$ patients without gout (154 women and 73 men); the second included a total number of $n = 131$ patients with gout (25 women and 106 men) and $n = 224$ patients without gout (150 women and 74 men). The bar plot illustrates the distribution per-centages of women and men within the groups (Figure 2A). Summary statistics for the baseline characteristics of this participant subset are available in the Supplementary Material and reflect the characteristics of the larger dataset.

To gain a deeper understanding of the inflammatory aspects of gout, we conducted an analysis examining the association between *in vitro* cytokine production (IL-1 β , IL-1Ra, TNF) in response to several stimuli based on a linear regression model. Age and sex were included as co-variates since it is well documented in the literature that they can impact the immune system.

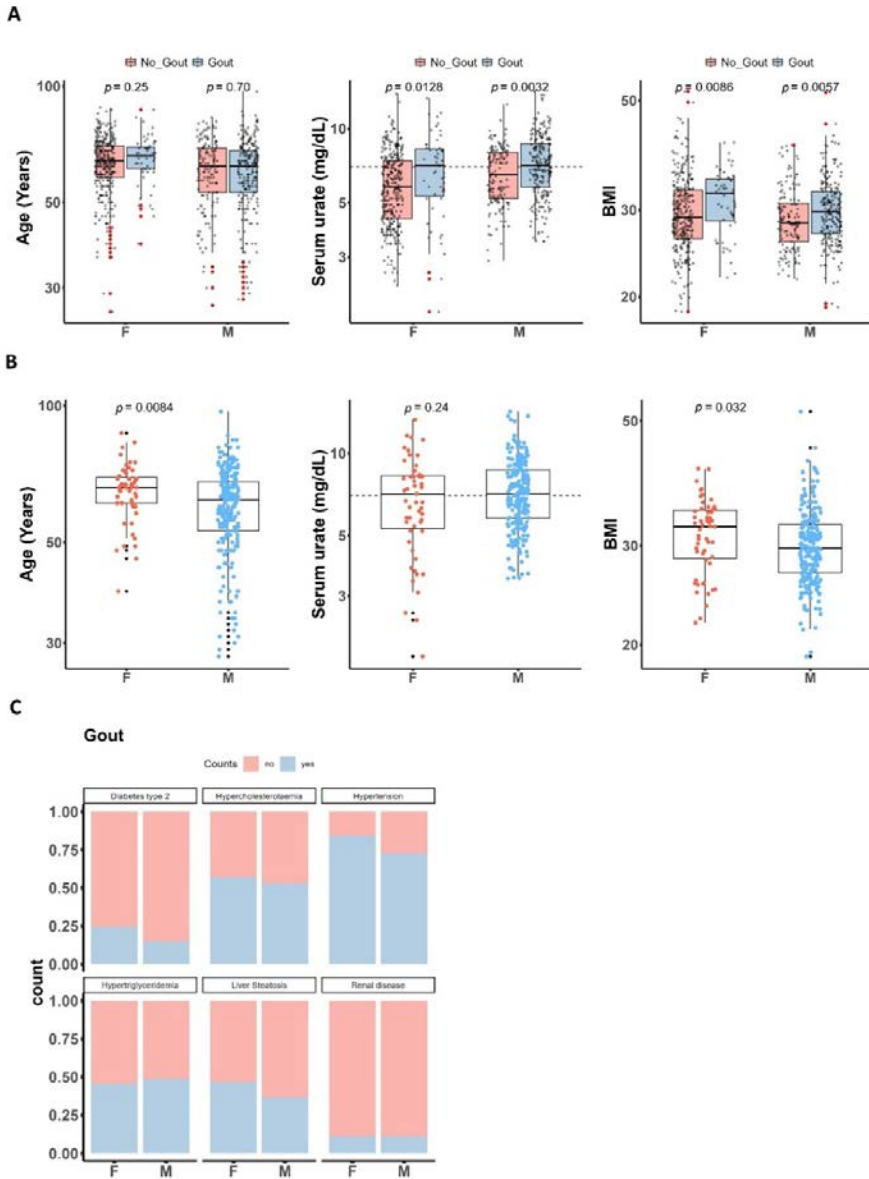


Figure 1. Baseline characteristics. (A) Box plots split into women (F) and men (M) with and without gout. (B) Box plots of only patients with gout split into women (F) and men (M). Unpaired two-sample Wilcoxon test (also known as Wilcoxon rank sum test or Mann-Whitney test); outliers' samples are indicated by the red (A) and black (B) dots. (C) Comorbidities distribution in patients with gout split by sex.

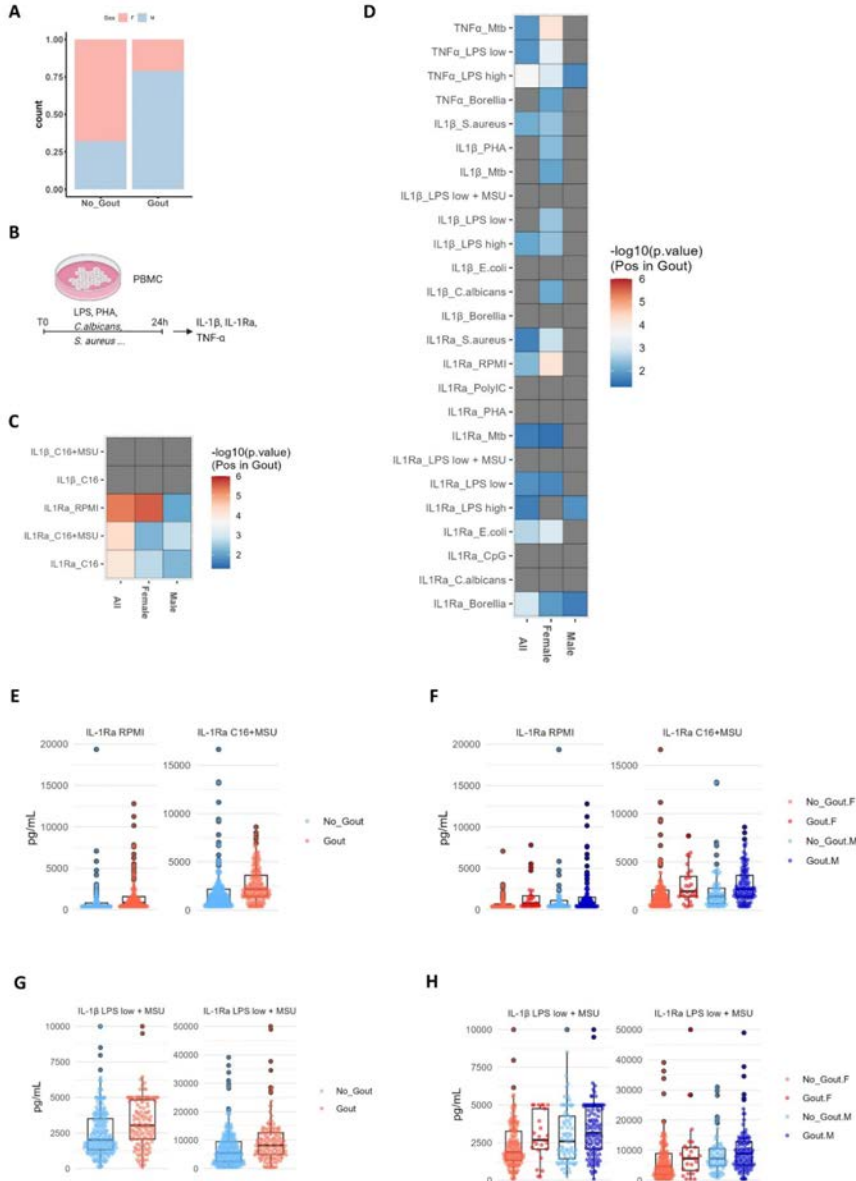


Figure 2. Association of cytokine production in PBMCs and sex in patients with and without gout.

(A) Percentage of women (F) and men (M) in both groups. (B) Experimental design. (C,D) p-values of association between gout and cytokine levels in all patients or split by sex. In all patients, age and sex have been added as co-variables, rather when split by sex, only age was added as a covariate. All p-values were calculated using linear regression and cytokine data were log transformed. Grey colour belongs to non-significant p-values (>0.05). (E,F) Sample distribution example of basal IL-1Ra levels (RPMI) and in stimulation with C16 and MSU in all patients or split by sex. (G,H) Sample distribution of IL-1 β and IL-1Ra levels after stimulation with LPS low dose and MSU in all patients or split by sex; On the y-axis, values are presented without commas for numbers exceeding four digits.

When the analysis was stratified by sex, age was the only covariate added. The overall findings indicate a significant association between gout and increased cytokine production, even after adjusting for age and sex (Figure 2C,D). Despite not reaching statistical significance after adjusting for age and sex, there is an observable trend of increased production of IL-1 β and IL-1Ra in response to stimulation with MSU crystals and TLR agonists such as LPS (Figure 2G,H, Supplementary Figures S3 and S4). Box plots showing sample distribution for all stimuli and samples have been included in the Supplementary Material. We observed significant positive associations predominantly in women with gout for all the cytokines after adjusting for age, irrespective of the stimuli used (Figure 2C,D).

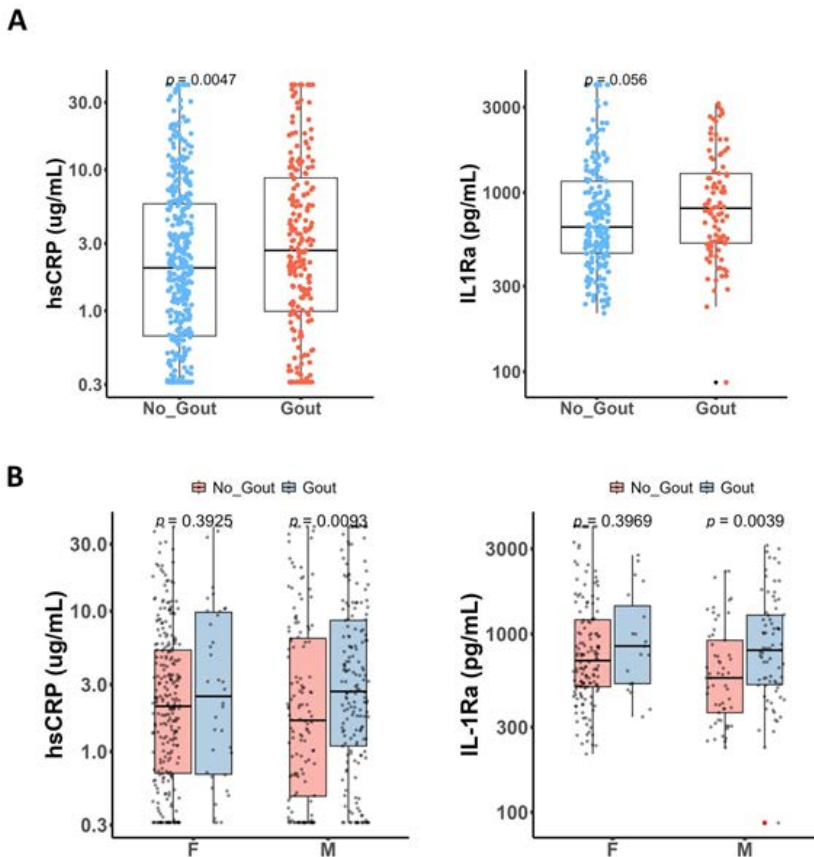


Figure 3. Circulating markers. (A) Box plots for high-sensitive CRP and plasma IL-1Ra for patients with and without gout. (B) Box plots split into women (F) and men (M). Unpaired two-sample Wilcoxon test (also known as Wilcoxon rank sum test or Mann-Whitney test); Black (A) and red (B) dots mark outlier samples.

Circulating Markers Are Elevated in Men with Gout

When looking at high-sensitive CRP in circulation, patients with gout show elevated levels, with a significant increase observed only in men with gout. Among women with gout, the levels of high-sensitive CRP were comparable to those in the control group. In the case of plasma IL-1Ra, a trend toward higher levels was observed in patients with gout, which became significant in men with gout, after stratifying by sex (Figure 3A,B).

Discussion

The impact of sex is often overlooked in research studies as it is commonly seen as a confounder that can skew results. Studies on aging are starting to explore the potential biological differences between men and women [22,23], which could result in distinct outcomes in terms of disease states or infections [24]. Gout, an inflammatory disease associated with IL-1 β activation and higher prevalence in men compared to women, displays distinct clinical profiles based on sex. This study explores sex-specific cytokine production in response to TLR in vitro stimulation in patients with gout. PBMCs from patients with gout show increased IL-1 β , IL-1Ra, and TNF production upon 24 h stimulation, particularly in women. On the other hand, men with gout had elevated levels of plasma IL-1Ra and high-sensitive CRP, but no significant differences in circulating cytokines were observed in women. In the gout group, women were older and had a slightly higher BMI compared to men and presented with comorbidities more often.

Gout can develop even at a younger age in men [25], while it is relatively rare in premenopausal women [26]. In our study, we observed that women with gout tend to be of older age than men with gout (Figure 1), findings that are supported by the literature [5]. Overall, patients with gout showed markedly higher serum urate concentrations when compared with control subjects, patients without gout but with either normal or elevated serum urate (referred to as normo- or hyperuricemic individuals). Most often, men with gout present higher levels of serum urate compared to women [27]. Notably, there was no difference in serum urate between men and women with gout in our group. The BMI measurements in women with gout were significantly higher compared to men with gout (Figure 1), in line with the association between excess adiposity and an increased risk of gout in women [28]. In a study following 534 healthy individuals exposed to various stimuli, the analysis reveals that factors like age

and sex significantly influence cytokine production but remain unaffected by smoking and body mass index (BMI) [16].

Men and women may have different baseline levels of certain immune cells which could result in differences in their immune system responses. A study on immune changes among individuals aged 50 and older observed over the course of a year that men and women had different cell populations, with women having more CD4⁺ T cells and men more CD8⁺ T cells [29]. Furthermore, compared to men, PBMCs of women may exhibit a lower percentage of natural killer (NK) cells, and a higher percentage of plasma cells [30]. Neutrophils are essential in clearing microorganisms but switch to a proinflammatory phenotype in several autoimmune diseases. Type 1 interferon pathway is up-regulated in neutrophils from healthy women, through a mechanism that involves estradiol-dependent maturation. Neutrophils isolated from women and primed in vitro with IFN- α show increased proinflammation on restimulation with viral-like ligands, suggesting possible hyperresponsiveness to danger signals [31]. The interferon signature was also detected in monocytes of post-menopausal women presenting low-grade inflammation, defined as hsCRP above 3 $\mu\text{g/mL}$ [32]. In our study, we found increased innate cytokine production predominantly in stimulated PBMCs of women with gout (Figure 2), suggesting women may mount more robust inflammatory responses to infections. While this could be beneficial to resolution of an infection, it may also contribute to exacerbation of symptoms. Within the dataset of the UK Biobank cohort, it was observed that women diagnosed with gout presented increased susceptibility to COVID-19-related mortality [33]. Healthy men showed increased cytokine capacity in response to in vitro stimulation in both PBMCs and whole blood, particularly of immune innate cytokines [16]. In addition, PBMCs from men with metabolic syndrome display an enhanced capacity for cytokine production as well. Circulating markers reveal that men with metabolic syndrome had elevated levels of several pro-inflammatory markers such as IL-6 and leptin, while women with metabolic syndrome showed lower levels of anti-inflammatory adiponectin [17]. In our study, men with gout show increased levels of pro-inflammatory hsCRP and anti-inflammatory IL-1Ra (Figure 3). These findings may suggest an interplay of inflammatory factors in male gout patients, where heightened inflammation as indicated by hsCRP is potentially counteracted by an increase in the anti-inflammatory IL-1Ra.

We recognize the need for caution when drawing robust conclusions solely based on the group with a smaller sample size. To enhance the credibility of

our findings, further research is warranted to replicate and validate these observations, ideally with more balanced sex distributions among the groups. Additionally, we acknowledge that only sex and age have been considered in the analysis. However, it is important to recognize that other factors like lifestyle, medication use, hormones, or underlying health conditions in patients with gout may also impact cytokine production. Given the substantial amount of missing data in various clinical variables, our model incorporated only age and sex as covariates. In this sense, it is important that these results are further investigated in relation to other datasets as well. Moreover, regarding in vitro production of IL-1 β , some samples were measured at the upper limit of the standard curve, which could potentially mask significant differences between groups.

Conclusion

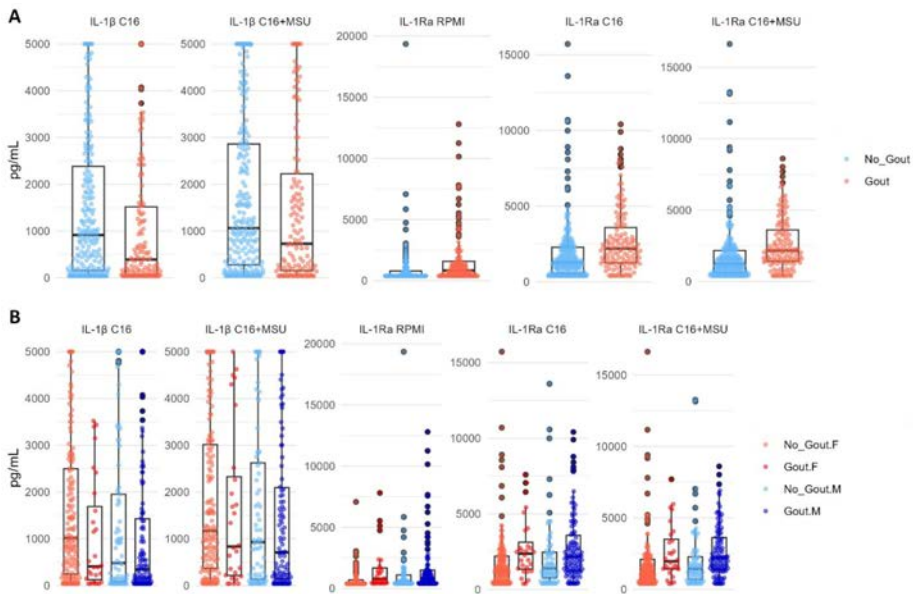
The elevated cytokine production in women with gout following stimulation suggests a potentially more robust immune response in this subgroup. On the other hand, the elevated levels of IL-1Ra and hsCRP in men with gout highlight the presence of systemic inflammation. These results possibly underline distinct immune responses between men and women with gout. Further functional studies will help elucidate some of the mechanistic links between cytokine dysregulation and gout pathogenesis. Omics techniques, like RNA sequencing, could advance our understanding of the pathways involved and complex interplay between cytokine production and sex in gout pathogenesis, with the ultimate goal of improving patient care and establishing a base for future therapeutic strategies.

References

- [1] Martinon F, Pétrilli V, Mayor A, et al. Gout-associated uric acid crystals activate the NALP3 inflammasome. *Nature* 2006; 440: 237–241.
- [2] So A, Dumusc A, Nasi S. The role of IL-1 in gout: From bench to bedside. *Rheumatology* 2018; 57: i12–i19.
- [3] Zhu Y, Pandya BJ, Choi HK. Prevalence of gout and hyperuricemia in the US general population: The National Health and Nutrition Examination Survey 2007–2008. *Arthritis Rheum* 2011; 63: 3136–41.
- [4] Te Kampe R, Janssen M, van Durme C, et al. Sex differences in the clinical profile among patients with gout: Cross-sectional analyses of an observational study. *J Rheumatol* 2021; 48: 286–92.
- [5] Harrold LR, Etzel CJ, Gibofsky A, et al. Sex differences in gout characteristics: Tailoring care for women and men. *BMC Musculoskelet Disord* 2017; 18:108.
- [6] Bergsten U, Dehlin M, Klingberg E, et al. Gender differences in illness perceptions and disease management in patients with gout, results from a questionnaire study in Western Sweden. *BMC Musculoskelet Disord* 2023; 24: 300.
- [7] Van Lunzen J, Altfeld M. Sex differences in infectious diseases-common but neglected. *J Infect Dis* 2014; 209: 79–80.
- [8] Angum F, Khan T, Kaler J, et al. The Prevalence of Autoimmune Disorders in Women: A Narrative Review. *Cureus* 2020; 12: e8094.
- [9] Klein SL, Flanagan KL. Sex differences in immune responses. *Nat Rev Immunol* 2016; 16: 626–38.
- [10] Verthelyi D, Klinman DM. Sex hormone levels correlate with the activity of cytokine-secreting cells in vivo. *Immunology* 2000; 100: 384–90.
- [11] Casimir GJ, Heldenbergh F, Hanssens L, et al. Gender differences and inflammation: An in vitro model of blood cells stimulation in prepubescent children. *J Inflamm* 2010; 7: 28.
- [12] Li F, Boon ACM, Michelson AP, et al. Estrogen hormone is an essential sex factor inhibiting inflammation and immune response in COVID-19. *Sci Rep* 2022; 12: 9462.
- [13] Schurz H, Salie M, Tromp G, et al. The X chromosome and sex-specific effects in infectious disease susceptibility. *Hum Genom* 2019; 13: 2.
- [14] Pinheiro I, Dejager L, Libert C. X-chromosome-located microRNAs in immunity: Might they explain male/female differences?: The X chromosome-genomic context may affect X-located miRNAs and downstream signaling, thereby contributing to the enhanced immune response of females. *BioEssays* 2011; 33: 791–802.
- [15] Lefèvre N, Corazza F, Valsamis J, et al. The number of X chromosomes influences inflammatory cytokine production following Toll-like receptor stimulation. *Front Immunol* 2019; 10: 1052.
- [16] Ter Horst R, Jaeger M, Smeekens SP, et al. Host and Environmental Factors Influencing Individual Human Cytokine Responses. *Cell* 2016; 167: 1111–1124.e13.
- [17] Ter Horst R, van den Munckhof ICL, Schraa K, et al. Sex-specific regulation of inflammation and metabolic syndrome in obesity. *Arterioscler Thromb Vasc Biol* 2020; 40: 1787–800.
- [18] Beenakker KGM, Westendorp RGJ, de Craen AJM, et al. Men Have a Stronger Monocyte-Derived Cytokine Production Response upon Stimulation with the Gram-Negative Stimulus Lipopolysaccharide than Women: A Pooled Analysis Including 15 Study Populations. *J Innate Immun* 2020; 12: 142–153.

- [19] Da Pozzo E, Giacomelli C, Cavallini C, et al. Cytokine secretion responsiveness of lymphomonocytes following cortisol cell exposure: Sex differences. *PLoS ONE* 2018; 13: e0200924.
- [20] Joosten LA, Netea MG, Mylona E, et al. Engagement of fatty acids with toll-like receptor 2 drives interleukin-1 β production via the ASC/caspase 1 pathway in monosodium urate monohydrate crystal-induced gouty arthritis. *Arthritis Rheum* 2010; 62: 3237–48.
- [21] Singh JA, Gaffo A. Gout epidemiology and comorbidities. *Semin. Arthritis Rheum* 2020; 50: S11–S16.
- [22] Hägg S, Jylhävä J. Sex differences in biological aging with a focus on human studies. *eLife* 2021; 10: e63425.
- [23] Márquez EJ, Chung CH, Marches R, et al. Sexual-dimorphism in human immune system aging. *Nat. Commun* 2020; 11: 751.
- [24] Bongen E, Lucian H, Khatri A, et al. Sex Differences in the Blood Transcriptome Identify Robust Changes in Immune Cell Proportions with Aging and Influenza Infection. *Cell Rep* 2019; 29: 1961–1973.e4.
- [25] Evans PL, Prior JA, Belcher J, et al. Gender-specific risk factors for gout: A systematic review of cohort studies. *Adv Rheumatol* 2019; 59: 24.
- [26] Patel AV, Gaffo AL. Managing Gout in Women: Current Perspectives. *J. Inflamm. Res.* 2022, 15, 1591–8.
- [27] Tin A, Marten J, Halperin Kuhns VL, et al. Target genes, variants, tissues and transcriptional pathways influencing human serum urate levels. *Nat Genet* 2019; 51: 1459–74.
- [28] McCormick N, Yokose C, Lu N, et al. Impact of adiposity on risk of female gout among those genetically predisposed: Sex-specific prospective cohort study findings over >32 years. *Ann Rheum Dis* 2022; 81: 556–63.
- [29] Lakshmikanth T, Muhammad SA, Olin A, et al. Human Immune System Variation during 1 Year. *Cell Rep* 2020; 32: 107923.
- [30] Huang Z, Chen B, Liu X, et al. Effects of sex and aging on the immune cell landscape as assessed by single-cell transcriptomic analysis. *Proc Natl Acad Sci USA* 2021; 118: e2023216118.
- [31] Gupta S, Nakabo S, Blanco LP, et al. Sex differences in neutrophil biology modulate response to type I interferons and immunometabolism. *Proc Natl Acad Sci USA* 2020; 117: 16481–91.
- [32] So J, Tai AK, Lichtenstein AH, et al. Sexual dimorphism of monocyte transcriptome in individuals with chronic low-grade inflammation. *Biol Sex Differ* 2021; 12: 43.
- [33] Topless RK, Gaffo A, Stamp LK, et al. Gout and the risk of COVID-19 diagnosis and death in the UK Biobank: A population-based study. *Lancet Rheumatol* 2022; 4: e274–e281.

SUPPLEMENTARY MATERIAL



Supplementary Figure 1. Box plots showing distribution of cytokine levels in PBMCs from patients with and without gout (A) and split by sex (B) that were stimulated in vitro for 24 h with C16 and C16+MSU.

Supplementary Table 1. Baseline characteristics of the gout and control cohorts in all patients included for experiment 1.

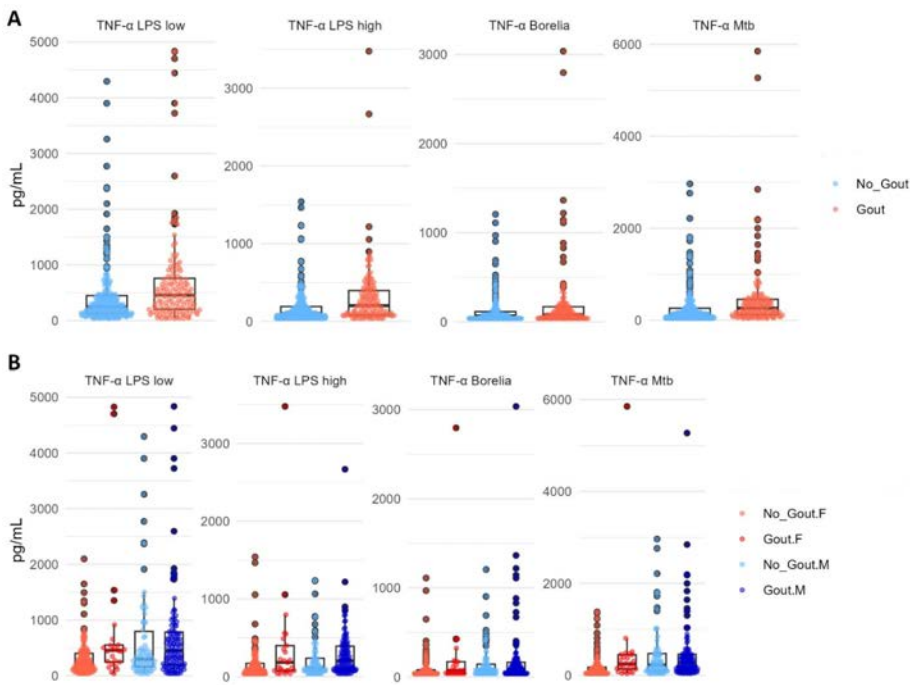
Characteristic	<i>n</i>	No_Gout, <i>n</i> = 227 ¹	Gout, <i>n</i> = 134 ¹	<i>p</i> -value ²
Sex	361			<0.001
F		154 (68%)	28 (21%)	
M		73 (32%)	106 (79%)	
Age (years)	361	61 (53, 69)	62 (54, 68)	0.8
BMI	354	28.7 (26.2, 32.0)	29.7 (26.7, 33.1)	0.035
Unknown		6	1	
Urate (mg/dL)	361	5.30 (4.30, 6.30)	6.70 (5.53, 8.10)	<0.001

¹*n* (%); Median (IQR); ²Pearson's Chi-squared test; Wilcoxon rank sum test

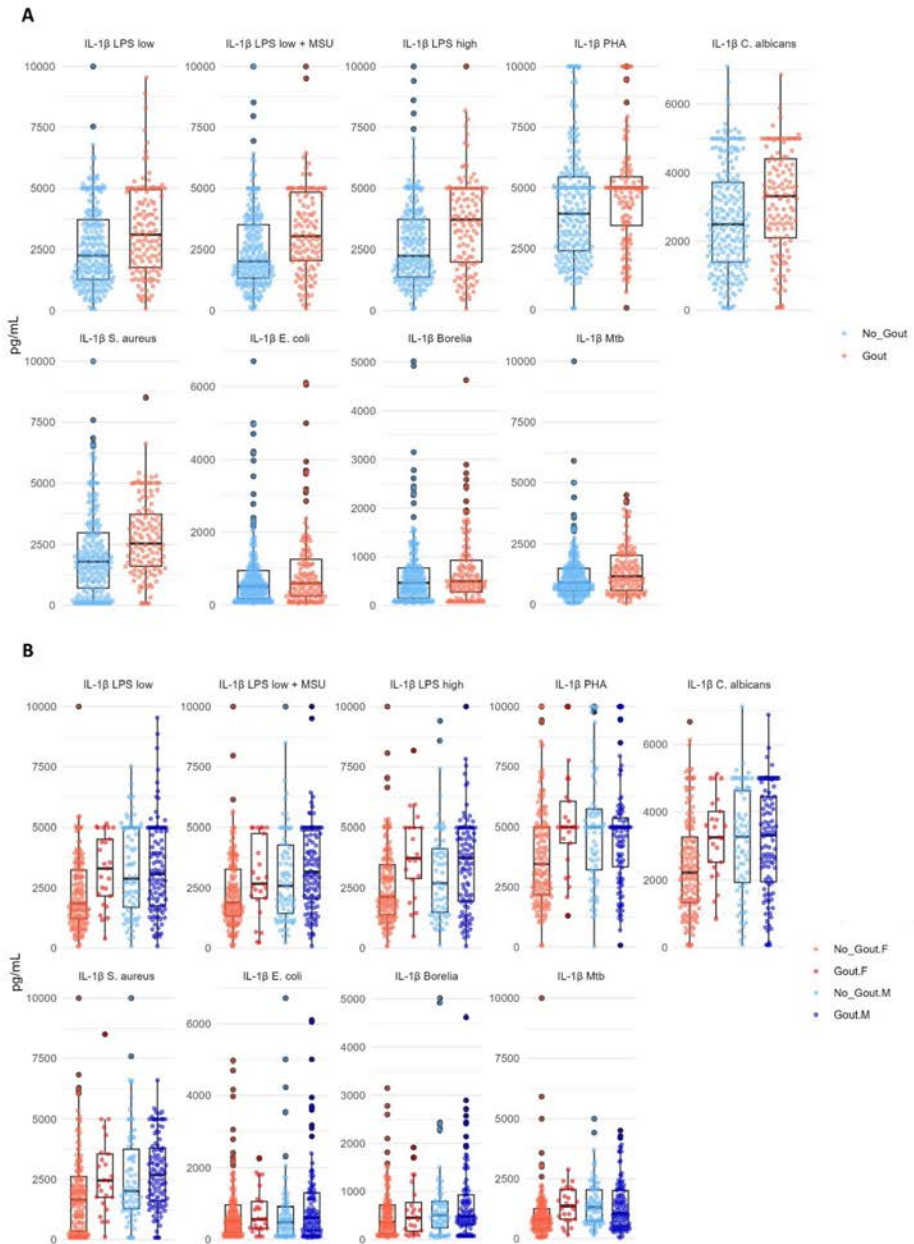
Supplementary Table 2. Baseline characteristics only for the gout patients included for experiment 1.

Characteristic	n	F, n = 28 ¹	M, n = 106 ¹	p-value ²
Age (years)	134	66 (62, 70)	60 (51, 66)	0.002
BMI	133	30.6 (28.0, 34.0)	29.4 (26.7, 32.3)	0.4
Unknown		0	1	
Urate (mg/dL)	134	6.60 (5.50, 7.55)	6.80 (5.53, 8.45)	0.2

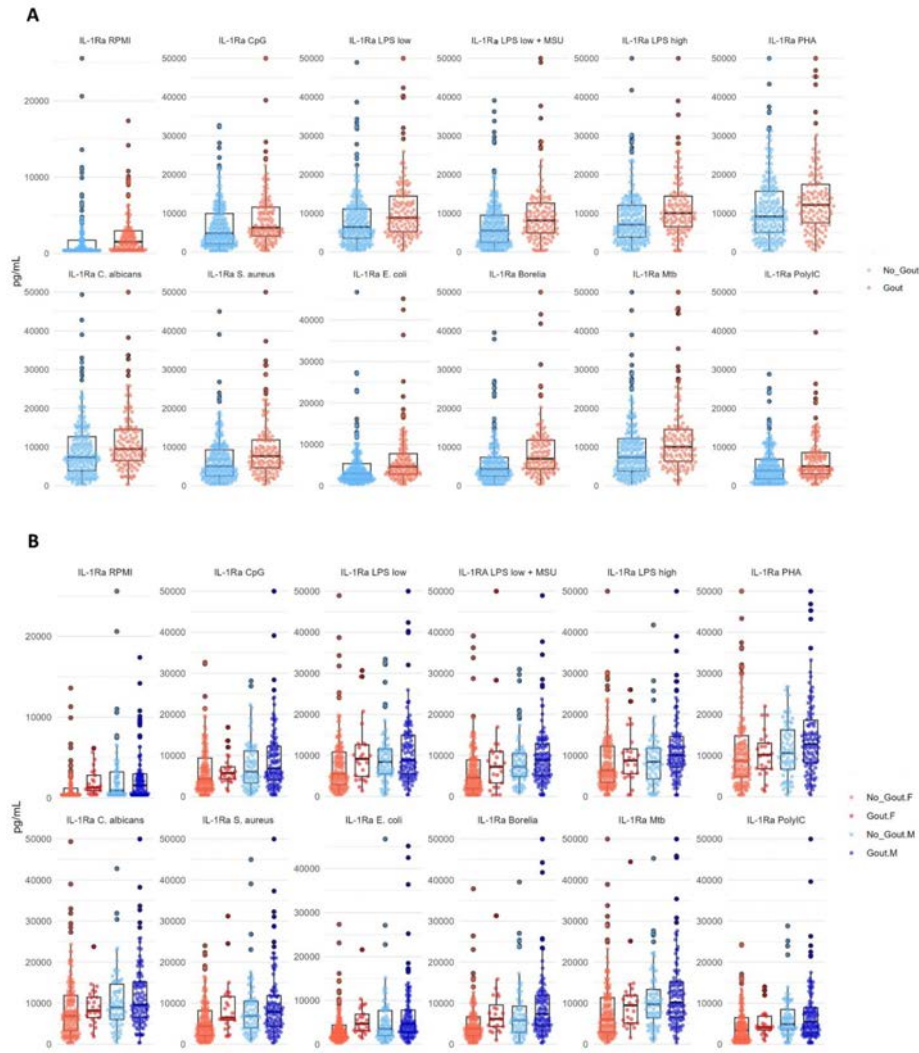
¹Median (IQR); ²Wilcoxon rank sum test



Supplementary Figure 2. Box plots showing distribution of TNF-α levels in PBMCs from patients with and without gout (A) and split by sex (B) that were stimulated in vitro for 24 h.



Supplementary Figure 3. Box plots showing distribution of IL-1 β levels in PBMCs from patients with and without gout (A) and split by sex (B) that were stimulated in vitro for 24 h.



Supplementary Figure 4. Box plots showing distribution of IL-1Ra levels in PBMCs from patients with and without gout (A) and split by sex (B) that were stimulated in vitro for 24 h.

Supplementary Table 3. Baseline characteristics of the gout and control cohorts in all patients included for experiment 2.

Characteristic	<i>n</i>	No_Gout, <i>n</i> = 224 ¹	Gout, <i>n</i> = 131 ¹	<i>p</i> -value ²
Sex	355			<0.001
F		150 (67%)	25 (19%)	
M		74 (33%)	106 (81%)	
Age (years)	355	61 (53, 68)	63 (55, 68)	0.4
BMI	345	28.4 (25.9, 31.6)	30.1 (27.1, 33.2)	0.002
Unknown		10	0	
Urate (mg/dL)	355	5.20 (4.28, 6.20)	6.70 (5.60, 8.15)	<0.001

¹*n* (%); Median (IQR); ²Pearson's Chi-squared test; Wilcoxon rank sum test

Supplementary Table 4. Baseline characteristics only for the gout patients included for experiment 2.

Characteristic	<i>n</i>	F, <i>n</i> = 25 ¹	M, <i>n</i> = 106 ¹	<i>p</i> -value ²
Age (years)	131	66 (62, 71)	61 (52, 67)	0.006
BMI	131	30.9 (29.1, 34.9)	29.8 (26.9, 32.6)	0.15
Urate (mg/dL)	131	6.60 (5.60, 7.50)	6.80 (5.63, 8.70)	0.2

¹Median (IQR); ²Wilcoxon rank sum test

CHAPTER 6

Trained immunity and inflammation in rheumatic diseases

Medeea Badii*, Orsolya Gaal*, Radu A. Popp¹, Tania O. Crişan#, Leo A.B. Joosten#

*These authors contributed equally to this work

#These authors share senior authorship

Joint Bone Spine. 2022;89(4):105364.

Summary

Rheumatic diseases include a variety of autoimmune and autoinflammatory conditions that are characterized by musculoskeletal involvement and systemic disease. Both innate and adaptive immunity can contribute to the complex inflammatory processes that take part in the pathogenesis of these debilitating disorders. Over the past decade, studies have led to a paradigm-shift around the concept of immune memory, generating the knowledge that cells of the innate immune system can develop a *de facto* memory mediated by epigenetic reprogramming and metabolic changes (trained immunity). Here we provide an overview of current data that describes features of trained immunity in rheumatic diseases. We link evidence on inflammatory mediators and cytokine production, immunometabolism and epigenetic regulation of immunological programs, and outline the fact that trained immunity could play mechanistic roles in rheumatic diseases such as gout, rheumatoid arthritis, systemic lupus erythematosus or systemic sclerosis. This review describes recent findings in several important rheumatic disorders and emphasizes changes in the functional program of innate immune cells that are reminiscent of a trained immune phenotype. Further assessment of trained immunity in rheumatic disease can provide targetable mechanisms that could potentially alter the disease symptomatology and evolution.

Introduction

Innate immune memory has been increasingly studied over the past decade. Features of immunological memory have been described in organisms that lack an adaptive immune system, such as plants or invertebrates, raising the hypothesis that innate immune memory is also present in vertebrates [1]. Studies in mammals have pointed out to a cross-protection between infections with different pathogens that is mediated by the activation of nonspecific innate immune mechanisms [1]. In humans, epidemiological studies have demonstrated beneficial effects of vaccines, such as Bacillus-Calmette-Guérin (BCG), measles, or oral polio vaccine against infections with pathogens other than the ones targeted by the vaccine itself [1]. In the last decade, the study of innate immune memory has been significantly moved forward as the concept of "trained immunity" was proposed by Netea *et al.* [2]. Trained immunity is currently defined as the long-term adaptation of myeloid cells, natural killer (NK) cells, and innate lymphoid cells (ILCs), mediated by metabolic rewiring and epigenetic reprogramming that follow an encounter with inflammatory triggers, infections or vaccinations. This functional reprogramming leads to an increased innate immune response to subsequent challenges [1][2].

Trained immunity is initiated in response to Pathogen-associated molecular patterns (PAMPs) or Damage-associated molecular patterns (DAMPs). DAMPs are endogenous molecules capable of inducing inflammatory responses under sterile conditions by modulation of inflammatory gene expression and inflammasome activation. Interleukin 6 [1], TNF- α [3] but also members of the IL-1 family such as interleukin 1 beta (IL-1 β) [4], are among the proinflammatory cytokines involved in the immune responses of trained cells. We can note an increase in cytokine production when human monocytes are primed or trained *in-vitro* with microbial stimuli (such as beta-glucan or BCG) [5], but also with endogenous molecules such as oxidized low-density lipoprotein (oxLDL) [6], oxidized phospholipids (oxPAPC) [7], or urate [8]. These stimuli bind to Pattern Recognition Receptors (PRRs) on myeloid cells leading to the release of effector molecules and subsequent increased response to second stimulation (Figure 1) [1]. The increase in proinflammatory cytokines such as IL-6, and IL-1 β is present up to 3 months post-BCG vaccination in humans [9]. But how does this memory persist in time, considering that, in humans, both the non-classical and classical monocytes are short-lived? [11]. It is now known that the innate immune memory is formed and maintained at the level of myeloid progenitor cells in the bone marrow [9] [10].

Innate immune memory, as opposed to adaptive memory, is a consequence of the functional adaptation of innate immune cells induced by epigenetic changes, such as alterations of chromatin marks, and by modifications in cellular metabolism, including a shift towards increased glycolysis and decreased oxidative phosphorylation (Figure 1). Histone modifications accumulate in response to training in monocytes, such as H3K4me3 at gene promoters, or H3K4me1 and H3K27ac at enhancer regions, and some of them persist even after the initial stimuli have been removed (e.g. H3K4me1) [11]. More recently, the inhibition of lysine methyltransferase G9a in BCG-trained monocytes resulted in a decrease of H3K9me2 marks at the promoters of pro-inflammatory genes, emphasizing the potential role of H3K9me2 in trained immunity [12].

Another hallmark of trained innate immune cells is metabolic rewiring. Pro-inflammatory cytokines or PRR ligands promote different metabolic pathways in monocytes and modulate the mammalian target of rapamycin (mTOR), which is a central metabolic regulator of immunity. Classical induction of trained immunity by beta-glucan leads to a shift of cellular metabolism from oxidative phosphorylation (OXPHOS) towards aerobic glycolysis via the mTOR/HIF1a/Akt pathway [13]. LPS-derived macrophages express a strong glycolysis signature known as the Warburg effect, associated with increased pro-inflammatory cytokine production. Mannose, natural C-2 epimer of glucose, prevents LPS-induced macrophage activation by impairing *IL1B* gene expression and therefore attenuating inflammation. Such effect results from inhibition of glucose metabolism and suppression of succinate-mediated HIF-1 α activation [14]. Along with increased glycolysis, beta-glucan-trained monocytes display an increased activity of the cholesterol synthesis pathway and elevated mevalonate, which in turn amplifies the inflammatory response through an IGF1R-mTOR mediated pathway [15]. Treatment with fumarate, a TCA (tricarboxylic acid) cycle metabolite, leads to increased TNF- α production upon LPS stimulation in monocytes, along with ultrastructural changes of the mitochondria and elevated membrane potential that could propose mitochondrial activation. [3]. Moreover, itaconate, a metabolite that can alter the TCA cycle, contributes to immune tolerance and has been associated with the prevention of immunopathology during *Mycobacterium tuberculosis* infection [16]. Taken together, these processes indicate that cells displaying a trained innate immune phenotype show alterations in the cellular metabolism and that metabolic changes can directly impact the immune response of the cell.

As mentioned above, trained immunity can have a beneficial role when referring to cross-protection in the case of infection with various pathogens, but it can also

contribute to the worsening of autoimmune or autoinflammatory diseases by contributing to chronic inflammation. We posit that trained immunity is a process that takes place in cells of patients with autoinflammatory or autoimmune rheumatic diseases, potentially predisposing to persistent inflammation and exacerbation of symptoms (Figure 2). An extensive review of the literature is beyond the scope of this report, as it has been elaborated in more detail elsewhere [17], instead we focus here on recent studies that contribute to our knowledge on epigenetic and metabolic changes in innate immune cells revealing the potential roles of innate immune training in several rheumatic disorders.

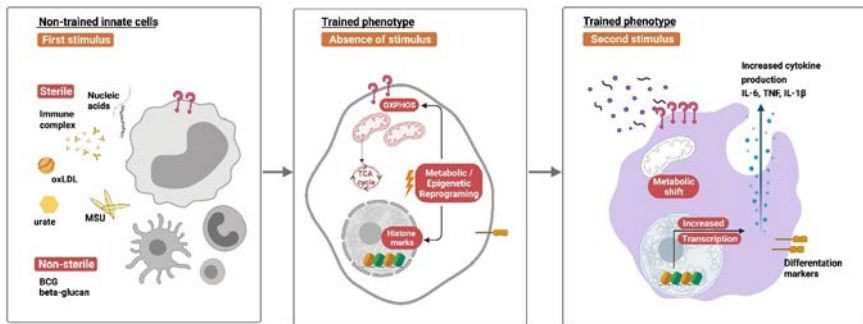


Figure 1. Schematic representation of innate immune memory development. Upon a first encounter of innate immune cells with a Pathogen Associated Molecular Pattern (e.g., BCG, beta-glucan)/or Damage Associated Molecule Pattern (e.g., urate, oxLDL, immune complexes), the down-stream signalling via Pattern Recognition Receptors (PRRs) promotes metabolic changes (e.g., altered glycolysis or OXPHOS) and epigenetic modifications (e.g., histone modifications, DNA methylation) which persist after the initial triggers have been removed. Consequently, on a subsequent stimulation, the cells exhibit faster and stronger inflammatory responses facilitated by the pre-existent epigenetic marks which allow for increased gene expression, giving rise to hyper-inflammatory responses.

Gout

Gout is a chronic inflammatory arthritis generally affecting middle-aged men and the elderly population caused by monosodium urate (MSU) crystal deposition and inflammation within joints and periarticular structures. The MSU crystals form when serum urate concentrations surpass the solubility threshold, leading to precipitation into needle-shaped crystals. Serum urate above physiological levels (0.36 mmol/l or 6 mg/dL), is defined as hyperuricemia [18] [19]. The IL-1 family members play an important role in gout, particularly IL-1 β released by MSU-stimulated monocytes and macrophages which further contribute to the pathogenesis of the flares. MSU crystals trigger gout flares by activating the NLRP3 inflammasome [20]. The

gout flare is characterized by secretion of pro-inflammatory cytokines such as IL-1 β by the resident macrophages, neutrophilic infiltration in the synovial tissue and fluid, redness and swelling in the affected area [21]. In contrast, IL-1Ra has a counterbalancing role, binding to IL-1 receptor type 1 and competitively inhibiting further IL-1 β signalling [22].

MSU crystals are an important characteristic of gout pathogenesis and act as DAMPS to activate the NLRP3 inflammasome. The elevated levels of IL-1 β and increased expression of NLRP3 inflammasome in response to MSU stimulation in macrophages are accompanied by a GLUT1-mediated glucose uptake and a cellular metabolic shift towards upregulated glycolysis [23]. Recently, it has been shown that soluble urate can also activate the inflammasome [24], while other investigations argue that the precipitation of urate into crystals is required for the activation of NLRP3 [25]. In addition, inflammasome-independent effects of MSU were also reported in macrophages, and this was shown to be mediated by JNK phosphorylation and subsequent translocation of the transcription factor JUN to gene regions that regulate inflammation and metabolism [26].

Another described DAMP that might contribute to the gout pathogenesis is the cold-inducible RNA-binding protein (CIRP), which, through the priming of the NLRP3 inflammasome in neutrophils, leads to an increase of cleaved IL-1 β levels after a subsequent stimulation with MSU crystals [27].

Notably, *in-vitro* treatment of human monocytes with soluble urate primes the cells to a production of increased IL-1 β , and decreased IL-1Ra following a subsequent LPS stimulation, and this effect on cytokine production is observed at the level of gene transcription. These changes are mediated by activation of the AKT-PRAS40 pathway and inhibition of autophagy, which leads to IL-1 mediated inflammation [28]. This facilitated state of IL-1 β production is long lived, and the imprinting seems to be mediated by epigenetic reprogramming, because inhibitors of histone methyl transferases abolished the "reprogramming" effect of urate [29]. Moreover, in human monocytes, urate treatment resulted in enrichment of histone modifications H3K4me3 and H3K27ac at promoters of genes such as *MED24*, *CSF3*, *TAF1C*, *DNAAF1*, and downregulation at *APOE* promoter. In addition, the assessment of whole blood DNA of hyperuricemic individuals revealed several differentially methylated regions in comparison to normouricemic individuals (e.g. *HLA-G*, *IFITM3*, *PRKAB2*), suggesting that urate induced inflammatory responses might be epigenetically regulated [8].

When monocytes of gout patients were investigated for DNA methylation, results revealed differentially methylated sites associated with IL-1 β signalling and with gouty inflammation, suggesting that DNA methylation might be an important regulator of cytokine production in monocytes. [30]. In addition, PBMCs of gout patients show differentially methylated regions in known gout risk genes (e.g., *SLC2A9*, *ABCC9*), together with transcription factors that have enriched motifs for genes involved in osteoclast and T helper cell differentiation (e.g. (*NFATC2*, *MEF2C*), indicating that epigenetic changes might take place in both innate and adaptive immunity pathways. [31]. Long non-coding RNAs are emerging as novel biomarkers in various disorders, and a first such study performed on samples from gout patients reveals differentially expressed lnc-RNAs in acute and intercritical phase that associated with inflammatory markers in these patients [32].

The altered cytokine profile observed in immune cells, both at protein and gene level, along with the epigenetic changes, enforce the hypothesis that trained immunity might be present in myeloid cells of patients with gout.

Rheumatoid arthritis (RA)

Rheumatoid arthritis (RA), a chronic systemic autoimmune disease which primarily affects women, is defined by persistent synovial inflammation in small diarthrodial joints, progressive cartilage and bone destruction along with autoantibody production [33]. The cause of cartilage and bone destruction present in RA is mainly caused by macrophages via the production of cytokines and chemokines and by the regulation of osteoclast activity [34]. The role of the innate immune system is gaining much attention in the development of RA, and indications that innate immune memory could be relevant to this disease have been observed.

Cytokines play a crucial role in the pathogenesis of the disorder, with TNF or IL-6 having an important role in the induction of osteoclasts, which may contribute to joint destruction [35]; IL-1 β is proven to have stimulatory effects on osteoclastogenesis [36], which can be accompanied by initiation of synovial cell proliferation and matrix metalloproteinase induction by chondrocytes, together contributing to bone destruction [37]. The presence of autoantibodies is another important hallmark of RA. Extracellular vesicles, like microparticles (MP), can form immune complexes with autoantibodies (MP-IC) and further promote the proinflammatory differentiation of macrophages to an M1-like profile while supporting B-cell survival [38]. In vitro data on

monocyte-derived macrophages from patients with RA and healthy controls in the presence of MP-IC shows a more proinflammatory M1-like phenotype which could not be completely reversed by IL-4 treatment [38].

Monocytes from RA patients seem to be more prone to metabolic reprogramming with LPS for sustained induction of pro-inflammatory responses. The cells display significantly higher baseline OCR, maximal respiratory capacity and ATP synthesis compared to LPS-activated healthy monocytes [39]. Enhanced glycolysis, as indicated by high concentrations of lactate and distinctly low concentrations of glucose, is observed in the inflamed joint of patients with RA [40]. These metabolic changes are suggestive of a trained immunity phenotype.

Epigenetic modifications, such as histone acetylation was shown to be involved in the regulation of chemokine C-C motif ligand 2 (CCL2), also known as monocyte chemoattractant protein-1 (MCP1), associated with disease activity in RA. LPS-stimulated THP-1 cells show increased histone acetylation of H3 and H4 in the CCL2 promoter region [41]. While analysing PBMCs from patients with RA, the gene expression of activation marker histone variant H3.3 encoded by *H3F3A* was increased in patients with RA in comparison with healthy controls [42]. In addition, there is also evidence of hypomethylation at the TNF- α promoter in CD4⁺T-cells along with differential expression of 3 cytokines (IL-21, IL-34 and RANKL). Although most DNA methylation changes are seen in T-cells, monocytes also have some differentially methylated genes in RA [43].

Surprisingly however, TNF has been recently reported to also be able to serve as a critical downregulator of CD14⁺ monocyte differentiation into osteoclasts in homeostatic conditions [44]. TNF inhibited osteoclastogenesis and was associated to a reduction in H3K4me3 enrichment at the promoter region of RANK-L, which plays a key role in the osteoclast formation and activity [44]. At the same time, a population of circulating non-monocyte osteoclast precursors were epigenetically preconditioned to neglect TNF-mediated signalling (32, 40). Interestingly, monocytes from a subset of patients with active RA were shown to have altered epigenetic states which made them resistant to the homeostatic pathway of TNF-dependent inhibition of osteoclast differentiation. This suggests that previous epigenetic processes could aggravate erosive processes in different subsets of patients and that alternative mechanisms may be at play in the progression of RA. The cause of such initial epigenetic reprogramming is yet unknown but addressing the

possibility of trained immunity occurring and contributing to the pathogenesis and response to therapy in RA is worthwhile.

Systemic Lupus Erythematosus (SLE)

SLE is a complex autoimmune disease affecting females more frequently than males, characterized by over-production of autoantibodies, multi-organ involvement and extreme variability in patient phenotype. The main cause remains elusive and to date there is not a cure available, but innate immune cells are described to be involved in the pathogenesis of the disease. CD16⁺ monocytes play an important role in the pathogenesis of SLE and exhibit a proinflammatory phenotype with elevated CD80, CD86, HLA-DR, and CX3CR1 expression on the cell surface. This cell subset is enriched in SLE and has an exacerbated capacity to promote CD4⁺ T cell polarization into a Th17 phenotype. CD16⁺ monocytes can also drive CD19⁺ B cells to differentiate into plasma B cells and regulatory B cells with more Ig production [45]. Transcriptomic assessment of hematopoietic stem and progenitor cells (HSPC) in mice and patients with SLE revealed a strong myeloid signature which correlated to transcriptional activation of cytokines and chemokines [46]. This indicates that priming of the immune cells in SLE could already happen in the bone marrow in a similar manner as seen in trained immunity scenarios [46].

The type 1 interferon (IFN1) gene signature is one of the hallmarks of SLE [47]. Moreover, prior exposure to IFN α results in enhanced IFN α -producing capacity of monocytes [48]. TNF is important in the pathogenesis of SLE and crosstalk signalling between TNF and IFN1 can reshape the chromatin in order to work as an “integration node” that regulates transcriptional output and reprograms the inflammatory responses induced by TLR4 ligands. On the one hand, TNF extensively reprogrammed human macrophages in response to LPS tolerization and almost abolished TLR4 signalling in these cells. On the other hand, IFN1 effectively ended TNF-induced cross-tolerance by priming chromatin to enable strong transcriptional responses to weak signals and to prevent the silencing of T cell genes. This suggests that IFN1 is able to regulate chromatin at distinct sets of genes that encode for inflammatory mediators, in addition to canonical ISGs [49].

The role of IgG-immune complexes (IC) has widely been described in SLE but the mechanisms by which they trigger organ inflammation have long remained unresolved. Jing C. *et al* have found that stimulation of monocyte-derived-macrophages and of kidney macrophages during antibody-mediated nephritis

with IgG-ICs results in a altered cell metabolism with elevated glycolysis and reduced OXPHOS and fatty acid metabolism. This shift is mediated by the HIF1 α /mTOR pathway, necessary for the induction of ROS production and proinflammatory mediators such as IL-1 β and PG2E. Furthermore, glycolysis inhibition with 2-Deoxy-D-glucose significantly diminished tissue inflammation, underlining its therapeutic potential in treating in lupus nephritis [50]. This immunometabolic profile is reminiscent of the metabolic shift observed in cells trained with β -glucan [51]. In addition to this, T cells and neutrophils in patients with SLE manifest increased levels of reactive oxygen species (ROS) and inhibiting mitochondrial ROS (mtROS) and oxidative stress can mitigate certain aspects of autoimmune disease and organ damage in lupus-predisposed mice [52]. Role of NET formation by neutrophils in sterile inflammation remains largely unresolved, but the mitochondria might play an important role in the generation of NETs via ROS production and release of oxidized mtDNA [53].

Several studies have focused on epigenetic modification such as DNA methylation to answer the question on how certain genes are regulated in SLE. Whole-genome transcription and DNA methylation analysis of peripheral blood mononuclear cells identified differential gene regulation in pathways involving IFN, TLR, accompanied by abnormal DNA methylation and elevated cytokine production (e.g. IL-17A, IP-10, bFGF, TNF, IL-6, IL-15, GM-CSF, IL-1Ra, IL-5, and IL-12p70) in SLE patients compared to healthy individuals [54]. Also, in a paediatric SLE (pSLE) genome-wide DNA methylation analysis, the DNAm signature comprised 21 CpG sites that point to differential loss of DNAm across the major immune cell lineages of pSLE patients. Epigenetic reprogramming of type I interferon-related genes is a widespread phenomenon in blood cells of pSLE patients, which can occur in the haematopoietic stem cells [55]. Furthermore, H3K4me3 is a major chromatin mark regulating gene transcription and histone modifications in SLE across different cell types. Differential H3K4me3 enrichment was observed in monocytes at promoters and enhancers of genes related to inflammatory response such as CCL2, CCL7, CCR1, CXCR1, IL-1R1, and TRIM1 and TNF signalling.

Finally, transcriptomic profiling in patients with the disease reveals no differences when comparing active and inactive SLE. These results suggest that immune cells from inactive SLE patients maintain a transcriptomic profile resembling that of active SLE, despite favorable treatment [56]. Based on

these results, it is tempting to speculate that these effects could be mediated by persistent epigenetic changes in trained immune cells.

Sjögren syndrome

Primary Sjögren syndrome (pSS) is a chronic autoimmune disease, most commonly present in middle aged women, associated with lymphocytic infiltration or immune complex deposition at exocrine glands, causing dryness of mucosal surfaces [57]. pSS often accompanies other systemic autoimmune diseases such as RA or SLE.

Several reports indicate that pSS patients depict elevated levels of cytokines, such as IL-6, IL-7, IL-18, IL-22 produced by epithelial cells, and TNF or IFN- γ generated by regulatory B cells [58]. The secretion of proinflammatory cytokines in pSS was recently shown to be induced by epithelial cell-derived apoptotic particles which carry autoantigens and adjuvant nucleic acids [59]. These apoptotic particles are considered danger signals that stimulate plasmacytoid dendritic cells (pDCs) via TLR-7 and TLR-9, favouring the autoantibody production and autoinflammation [59]. Additionally, the NLRP3 inflammasome activation by monocytes in pSS patients is triggered due to build-up of proinflammatory cell free-DNA from pyroptotic macrophages in the blood circulation and the further infiltration into salivary gland tissues [60]. STAT1 phosphorylation following IFN- γ stimulation of PBMCs of pSS patients is significantly enhanced compared to controls, suggesting an important role for STAT1-mediated gene responses in patients with pSS [61]. Moreover, the expression of *SOCS1* and *SOCS3* mRNA is increased in pSS patients, indicating increased sensitivity of immune cells from patients with pSS to STAT1-activating signals, partly explaining the IFN signature observed in pSS [62].

Epigenetic modifications, such as DNA methylation, play an important role in the pathological process of the disease [63]. IFN1 inducible genes *IFI44L*, *MX1*, *PAARP9*, *EPSTI1* and *IFITM1* are among the genes that are hypomethylated in circulating monocytes isolated from patients with pSS [63]. In addition, miRNAs were also associated to pSS by suppressing the TGF β signalling pathway [64]. TGF β 1 plays an important role in the induction of fibrotic processes via the activation of the SMAD signalling pathway and it is observed to be an essential component in the transition phase from salivary gland inflammation to salivary gland fibrosis [64]. Yet, mir-146a is one of the miRNAs discovered to have higher expression in mouse primary macrophages, dendritic cells and neutrophils in the presence of TLR agonists, besides having

a role in macrophage activation and control of proinflammatory cytokine production. In line with this, it is reported as being overexpressed in PBMCs from pSS patients and proven to activate the IL23/IL23R signalling pathway and promote Th17 cell differentiation *in vitro* [65].

These observations provide clues that epigenetic regulation in response to inflammatory triggers could alter the inflammatory signalling and contribute to the deregulation of immune processes in pSS. Albeit coincidental, these findings suggest that the study of innate immune training in both circulating and epithelial cells would be an interesting future research step in pSS.

Systemic sclerosis (SSc)

SSc is an autoimmune connective tissue disease consisting in immune dysfunction, fibrosis and vasculopathy, ultimately leading to multi-system involvement [66].

Innate immune cells play a major role in SSc pathophysiology, with mononuclear inflammatory cells infiltrating the perivascular and dermal areas at a very early stage of the disease [67]. Moreover, macrophages are presented as modulators of fibroblast activation as well as drivers of fibrosis. Interestingly, TGF β , IL-6, and CCL2 are elevated in SSc macrophages and cannot be further induced by LPS under basal conditions. The basal release and synthesis of IL-6 in macrophages of patients with SSc drives STAT3 phosphorylation and immune activation [68].

Stimuli initiating inflammatory responses in SSc are still the subject of research. Microparticles released from activated platelets are abundant in the blood of patients with SSc and express the damage-associated molecular pattern (DAMP) HMGB1 [69]. HMGB1 promotes fibrosis while coordinating the actions of monocytes and neutrophils in deep vein thrombosis, sustaining the vasculopathy associated to the disease [69]. Another DAMP proposed lately in the literature is the tenascin-C, an endogenous TLR4 ligand with a likely pathogenetic role in SSc, being an essential promoter of tissue fibrosis [70]. Skin biopsies of SSc patients reveals tenascin-C as a highly upregulated matricellular protein associated with both TLR4 and IL-6 expression and the deposition of this protein might contribute to the progression of skin and lung fibrosis [70].

The effects of trained immunity in SSc inflammation and fibrosis were addressed in murine models and in co-culture models of macrophage-(HOCI)-fibroblasts using macrophages previously trained with BCG or low dose

LPS. Depending on initial stimulus, trained macrophages exhibited different immunomodulatory properties *in vitro* and *in vivo*: training with BCG promoted T and B cell activation along with cytokine production and subsequent fibrosis, whereas low dose LPS promoted tolerance and diminished the fibro-inflammatory phenotype [67]. This indicates that trained immunity can be therapeutically targeted in SSc and also that trained immunity stimuli that are not directly related to the SSc pathogenesis could aggravate or dampen the inflammation and fibrosis observed in SSc.

Similarly to SLE or pSS, there is a strong type I IFN signature in SSc as well. Type I IFN pathway is dysfunctional at the epigenetic level in SSc patients, being associated to a hypomethylation status and upregulation of type I IFN-associated genes *IFI44L*, *IFITM1*, *EIF2AK2*, *MX1*, and *PARP9* both in CD4+ and CD8+ T cells [71]. Recently, it has been shown that IFN β stimulation induces epigenetic changes (acquisition of chromatin marks such as altered histone H3.3 and H3K36 trimethylation) and transcriptional memory at interferon inducible genes *Mx1*, *Ifit1*, *Oas1a* granting faster and prominent transcription upon restimulation in mouse embryonic fibroblasts (MEFs) and bone marrow (BM)-derived macrophages. [72]. The deregulation of the IFN response in SSc monocytes is maintained by altered epigenetic factors as well as by upregulation of the long non-coding RNA (lncRNA) NRIR [73]. 886 lncRNAs with an altered expression were recently described in SSc monocytes, from which PSMB8-AS1 is involved in the secretion of IL-6 and TNF, linking it to monocyte dysregulation [74]. Variations in histone marks H3K4me3 and H3K27ac, were also described at IFN inducible genes contributing to the complex epigenetic landscape that controls the type I IFN pathway in SSc [75]. Moreover, transcriptome analysis of monocyte-derived macrophages of patients with SSc show enrichment of genes involved in increased metabolic rates (glycolysis, hypoxia and mammalian target of rapamycin (mTOR) signalling), all of which being linked with a proinflammatory activation profile [76].

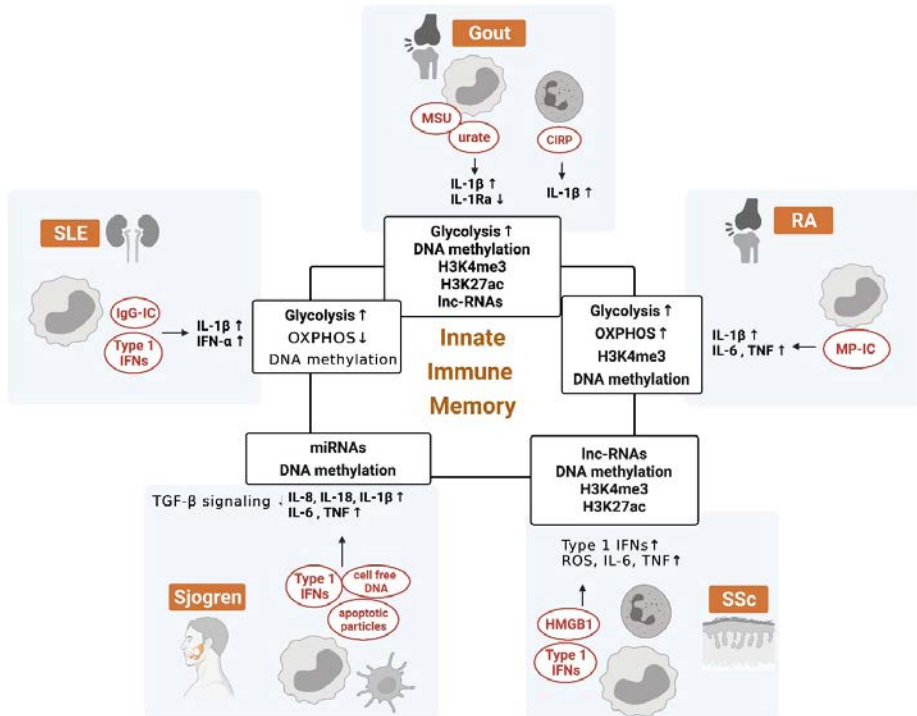
Based on all evidence at the level of epigenetic profile, and considering the indications of immunometabolic changes, trained immunity might play a role in the pathogenesis and progression of SSc and holds promise for targeted immunotherapies.

Conclusions

The incidence of auto-inflammatory and auto-immune diseases is expected to increase in the near future, especially in developed and industrialized countries, highlighting the importance of finding novel therapeutic approaches in which trained immunity might constitute a relevant target. In this review, we present recent findings supporting the concept that trained immunity may be present in several autoinflammatory and autoimmune rheumatic diseases (Figure 2) and that it could contribute to the induction, maintenance, or even worsening of the symptoms. The main characteristics of innate immune memory are epigenetic modifications, altered cellular metabolism along with higher cytokine production. Here we provide an overview of recent findings which suggest that these trained immunity features are observed in rheumatic diseases, nevertheless, further studies are required to establish the precise mechanisms that underlie these processes in each of these examples. In addition to this, trained immunity may be an inflammatory process which can predispose individuals with rheumatic diseases to chronic secondary pathologies, such as atherosclerosis and cardiovascular disease risk in patients with RA or SLE, associated comorbidities like metabolic syndrome in gout or risk of lymphoma in pSS. Together, these results underpin the possible involvement of trained immunity in rheumatic diseases and their long-term complications and open new avenues for targetable mechanistic discoveries.

> Figure 2. Potential mediators of innate immune memory in rheumatic disorders. Innate immune memory formation follows through epigenetic and metabolic rewiring of the myeloid cells. Certain endogenous or exogenous stimuli initiate inflammatory responses and alterations in the metabolic pathways (e.g., enhanced glycolysis) or changes in the epigenetic blueprint (e.g., hyper/hypo methylation of DNA regions, histone modifications) that will further affect how the cells respond (e.g., increased transcription of inflammatory genes) contributing to the induction, maintenance, or even worsening of the symptoms in rheumatic disorders. In gout, MSU-treated macrophages reveal a GLUT1-mediated glucose uptake and subsequent enhanced glycolysis to promote IL-1 β production. Additionally, soluble urate primes circulating monocytes towards an elevated production of IL-1 β and reduced IL-1Ra. Hyperuricemia correlated with changes in DNA methylation patterns or differential enrichment of histone modifications H3K4me3 and H3K27ac at promoters of genes. Moreover, the NLRP3 inflammasome in neutrophils of gout patients could be primed by the cold-inducible RNA-binding protein (CIRP) to produce increased levels of IL-1 β on a later stimulation with MSU crystals. PBMCs of gout patients show differential expression of several lncRNAs. In RA, common increased pro-inflammatory mediators are IL-6, TNF and IL-1 β . The elevated cytokine responses could be attributed to an altered epigenetic landscape such as histone modifications (H3K4me3) at the promoter region of RANK-L in monocytes. Immune complexes MP-IC can drive monocytes towards a M1-like phenotype

differentiation with increased IL-1 β , IL-6 and TNF production. LPS-stimulated monocytes from RA patients display altered cellular metabolism, in particular increased glycolysis and OXPHOS. Genes in RA might be differentially expressed via DNA methylation. The type 1 interferon (IFN1) gene signature is one of the hallmarks of SLE in myeloid cells and DNA methylation is a possible epigenetic mechanism by which these genes are regulated. Additionally, overproduction of autoantibodies and further immune complex formation stimulate monocyte-derived-macrophages and kidney macrophages to results in an altered cell metabolism along with elevated levels of pro-inflammatory mediators such as IL-1 β or IFN- α . In primary Sjögren syndrome (pSS), apoptotic particles stimulate dendritic cells to support autoinflammation by production of IL-6, TNF and IL-8. Additionally, cell free-DNA present in the serum of pSS patients primes the NLRP3 inflammasome of monocytes for increased IL-1 β and IL-18 (ref52). miRNAs were found associated to pSS by suppressing the TGF β signalling pathway. IFN1 genes in pSS might be regulated by DNA methylation. HMGB1, released from activated platelets of patients with SSc, promotes fibrosis while modulating the activity of monocytes and neutrophils to maintain the vasculopathy associated with the disease (increased pro-inflammatory cytokines, increased ROS). Changes in histone marks H3K4me3 and H3K27ac, lncRNAs and DNA methylation could explain how IFN1 genes are regulated in patients with SSc.



(Abbreviations: CIRP, Cold-inducible RNA-binding protein; IgG-IC, IgG immune complex; HMGB1, High Mobility Group Box 1; IL-1 β , Interleukin 1 beta; IL-1Ra, Interleukin 1 receptor antagonist; IL-6, Interleukin 6; IFN- α , Interferon alpha; NETs, Neutrophil extracellular traps; OXPHOS, Oxidative phosphorylation; RA, Rheumatoid arthritis; ROS, Reactive oxygen species; SLE, Systemic Lupus Erythematosus; SSc, Systemic Sclerosis; TNF, Tumor Necrosis Factor; TGF- β , Transforming growth factor beta)

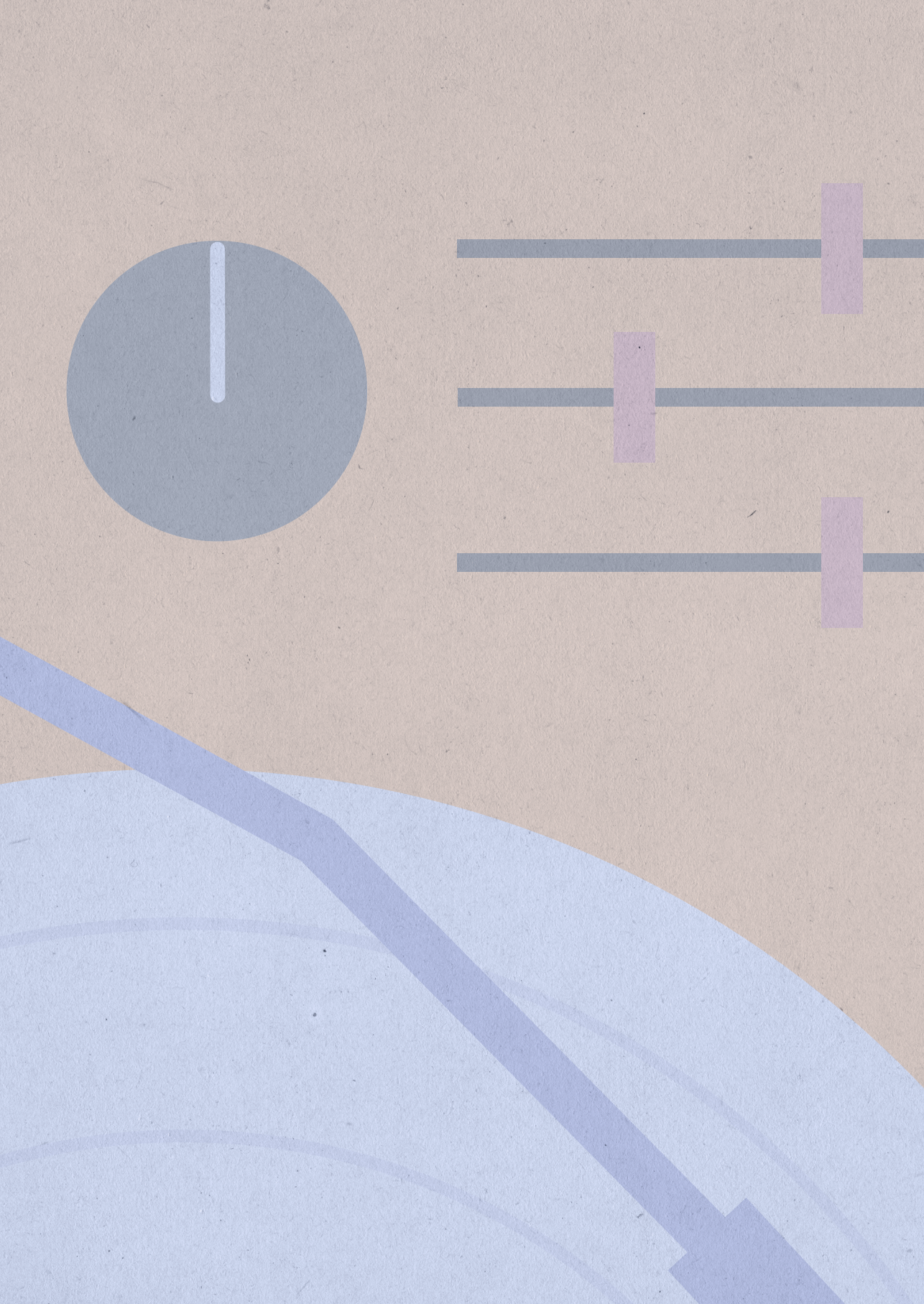
References

- [1] Netea MG, Domínguez-Andrés J, Barreiro LB, et al. Defining trained immunity and its role in health and disease. *Nat Rev Immunol* 2020; 20: 375–88.
- [2] Netea MG, Quintin J, Van Der Meer JWM. Trained immunity: A memory for innate host defense. *Cell Host Microbe* 2011; 9: 355–61.
- [3] Pérez-Hernández CA, Kern CC, Butkeviciute E, et al. Mitochondrial Signature in Human Monocytes and Resistance to Infection in *C. elegans* During Fumarate-Induced Innate Immune Training. *Front Immunol* 2020; 11: 1751.
- [4] Moorlag SJCFM, Röring RJ, Joosten LAB, Netea MG. The role of the interleukin-1 family in trained immunity. *Immunol Rev* 2018; 281: 28–39.
- [5] Moorlag SJCFM, Khan N, Novakovic B, et al. β -Glucan Induces Protective Trained Immunity against *Mycobacterium tuberculosis* Infection: A Key Role for IL-1. *Cell Rep* 2020; 31: 107634.
- [6] Groh LA, Ferreira A V, Helder L, et al. oxLDL-Induced Trained Immunity Is Dependent on Mitochondrial Metabolic Reprogramming. *Immunometabolism* 2021; 3: e210025.
- [7] Di Gioia M, Spreafico R, Springstead JR, et al. Endogenous oxidized phospholipids reprogram cellular metabolism and boost hyperinflammation. *Nat Immunol* 2020; 21: 42–53.
- [8] Badii M, Gaal OI, Cleophas MC, et al. Urate-induced epigenetic modifications in myeloid cells. *Arthritis Res Ther* 2021; 23: 1–11.
- [9] Cirovic B, de Bree LCJ, Groh L, et al. BCG Vaccination in Humans Elicits Trained Immunity via the Hematopoietic Progenitor Compartment. *Cell Host Microbe* 2020; 28: 322;34.e5.
- [10] Mitroulis I, Ruppova K, Wang B, et al. Modulation of Myelopoiesis Progenitors Is an Integral Component of Trained Immunity. *Cell* 2018; 172: 147;61.e12.
- [11] Fanucchi S, Domínguez-Andrés J, Joosten LAB, Netea MG, Mhlanga MM. The Intersection of Epigenetics and Metabolism in Trained Immunity. *Immunity* 2021; 54: 32–43.
- [12] Mourits VP, van Puffelen JH, Novakovic B, et al. Lysine methyltransferase G9a is an important modulator of trained immunity. *Clin Transl Immunol* 2021; 10: e1253.
- [13] Arts RJW, Carvalho A, La Rocca C, et al. Immunometabolic Pathways in BCG-Induced Trained Immunity. *Cell Rep* 2016; 17: 2562–71.
- [14] Torretta S, Scagliola A, Ricci L, et al. D-mannose suppresses macrophage IL-1 β production. *Nat Commun* 2020; 11: 1–12.
- [15] Bekkering S, Arts RJW, Novakovic B, et al. Metabolic Induction of Trained Immunity through the Mevalonate Pathway. *Cell* 2018; 172: 135;46.e9.
- [16] Domínguez-Andrés J, Novakovic B, Li Y, et al. The Itaconate Pathway Is a Central Regulatory Node Linking Innate Immune Tolerance and Trained Immunity. *Cell Metab* 2019; 29: 211;20.e5.
- [17] Arts RJW, Joosten LAB, Netea MG. The potential role of trained immunity in autoimmune and autoinflammatory disorders. *Front Immunol* 2018; 9: 6–9.
- [18] Bardin T, Richette P. Definition of hyperuricemia and gouty conditions. *Curr Opin Rheumatol* 2014; 26: 186–91.
- [19] Bardin T. Hyperuricemia starts at 360 micromoles (6mg/dL). *Joint Bone Spine* 2015; 82: 141–3.
- [20] Dalbeth N, Merriman TR, Stamp LK. Gout. *The Lancet* 2016; 388: 2039–52.
- [21] Dalbeth N, Choi HK, Joosten LAB, et al. Gout. *Nat Rev Dis Primers* 2019; 5: 69.
- [22] Klück V, Liu R, Joosten LAB. The role of interleukin-1 family members in hyperuricemia and gout. *Joint Bone Spine* 2021; 88: 105092.

- [23] Renaudin F, Orliaguet L, Castelli F, et al. Gout and pseudo-gout-related crystals promote GLUT1-mediated glycolysis that governs NLRP3 and interleukin-1 β activation on macrophages. *Ann Rheum Dis* 2020; 79: 1506–14.
- [24] Braga TT, Forni MF, Correa-Costa M, et al. Soluble Uric Acid Activates the NLRP3 Inflammasome. *Sci Rep* 2017; 7: 1–14.
- [25] Alberts BM, Barber JS, Sacre SM, et al. Precipitation of soluble uric acid is necessary for in Vitro activation of the NLRP3 inflammasome in primary human monocytes. *J Rheumatol* 2019; 46: 1141–50.
- [26] Cobo I, Cheng A, Murillo-saich J, et al. Monosodium Urate Crystals regulate a unique JNK-dependent macrophage metabolic and inflammatory response. *Cell Rep* 2022; 38:110489.
- [27] Fujita Y, Yago T, Matsumoto H, et al. Cold-inducible RNA-binding protein (CIRP) potentiates uric acid-induced IL-1 β production. *Arthritis Res Ther* 2021; 23: 1–9.
- [28] Crişan TO, Cleophas MCP, Oosting M, et al. Soluble uric acid primes TLR-induced proinflammatory cytokine production by human primary cells via inhibition of IL-1Ra. *Ann Rheum Dis* 2016; 75: 755–62.
- [29] Crişan TO, Cleophas MCP, Novakovic B, et al. Uric acid priming in human monocytes is driven by the AKT-PRAS40 autophagy pathway. *Proc Natl Acad Sci U S A* 2017; 114: 5485–5490.
- [30] Tseng CC, Liao WT, Wong MC, et al. Cell lineage-specific methylome and genome alterations in gout. *Aging (Albany NY)* 2021; 13: 3843–63.
- [31] Wang Z, Zhao Y, Phipps-Green A, et al. Differential DNA Methylation of Networked Signaling, Transcriptional, Innate and Adaptive Immunity, and Osteoclastogenesis Genes and Pathways in Gout. *Arthritis Rheumatol* 2020; 72: 802–14.
- [32] Qing YF, Zheng JX, Tang YP, et al. LncRNAs Landscape in the patients of primary gout by microarray analysis. *PLoS One* 2021; 16: 1–17.
- [33] Sparks JA. Rheumatoid arthritis. *Ann Intern Med* 2019; 170: ITC1–ITC15.
- [34] Horwood NJ. Macrophage Polarization and Bone Formation: A review. *Clin Rev Allergy Immunol* 2016; 51: 79–86.
- [35] Yokota K, Sato K, Miyazaki T, et al. Characterization and Function of Tumor Necrosis Factor and Interleukin-6-Induced Osteoclasts in Rheumatoid Arthritis. *Arthritis Rheumatol* 2021; 73:1145–54.
- [36] Shiratori T, Kyumoto-Nakamura Y, Kukita A, et al. IL-1 β Induces Pathologically Activated Osteoclasts Bearing Extremely High Levels of Resorbing Activity: A Possible Pathological Subpopulation of Osteoclasts, Accompanied by Suppressed Expression of Kindlin-3 and Talin-1. *J Immunol* 2018; 200: 218–28.
- [37] Dayer JM. The pivotal role of interleukin-1 in the clinical manifestations of rheumatoid arthritis. *Rheumatology* 2003; 42: 3–10.
- [38] Burbano C, Villar-Vesga J, Vásquez G, et al. Proinflammatory differentiation of macrophages through microparticles that form immune complexes leads to T-and B-cell activation in systemic autoimmune diseases. *Front Immunol* 2019; 10: 1–18.
- [39] McGarry T, Hanlon MM, Marzaioli V, et al. Rheumatoid arthritis CD14+ monocytes display metabolic and inflammatory dysfunction, a phenotype that precedes clinical manifestation of disease. *Clin Transl Immunol* 2021; 10: 1–18.

- [40] Qiu J, Wu B, Goodman SB, et al. Metabolic Control of Autoimmunity and Tissue Inflammation in Rheumatoid Arthritis. *Front Immunol* 2021; 12: 1–17.
- [41] Lin YC, Lin YC, Huang MY, et al. Tumor necrosis factor- α inhibitors suppress CCL2 chemokine in monocytes via epigenetic modification. *Mol Immunol* 2017; 83: 82–91.
- [42] Asadipour M, Hassan-Zadeh V, Aryaeian N, Shahram F, Mahmoudi M. Histone variants expression in peripheral blood mononuclear cells of patients with rheumatoid arthritis. *Int J Rheum Dis* 2018; 21: 1831–7.
- [43] Pitaksalee R, Burska AN, Ajaib S, et al. Differential CpG DNA methylation in peripheral naïve CD4+ T-cells in early rheumatoid arthritis patients. *Clin Epigenetics* 2020; 12: 1–16.
- [44] Ansalone C, Cole J, Chilaka S, et al. TNF is a homeostatic regulator of distinct epigenetically primed human osteoclast precursors. *Ann Rheum Dis* 2021; 80: 748–57.
- [45] Zhu H, Hu F, Sun X, et al. CD16+ monocyte subset was enriched and functionally exacerbated in driving T-cell activation and B-cell response in systemic lupus erythematosus. *Front Immunol* 2016; 7: 1–15.
- [46] Grigoriou M, Banos A, Filia A, et al. Transcriptome reprogramming and myeloid skewing in haematopoietic stem and progenitor cells in systemic lupus erythematosus. *Ann Rheum Dis* 2019; 242–53.
- [47] Herrada AA, Escobedo N, Iruretagoyena M, et al. Innate immune cells' contribution to systemic lupus erythematosus. *Front Immunol* 2019; 10: 1–9.
- [48] Murayama G, Chiba A, Kuga T, et al. Inhibition of mTOR suppresses IFN α production and the STING pathway in monocytes from systemic lupus erythematosus patients. *Rheumatol (United Kingdom)* 2020; 59: 2992–3002.
- [49] Park SH, Kang K, Giannopoulou E, et al. Type I interferons and the cytokine TNF cooperatively reprogram the macrophage epigenome to promote inflammatory activation. *Nat Immunol* 2017; 18: 1104–16.
- [50] Jing C, Castro-Dopico T, Richoz N, et al. Macrophage metabolic reprogramming presents a therapeutic target in lupus nephritis. *Proc Natl Acad Sci U S A* 2020; 117: 15160–71.
- [51] Kumar V, Giamarellos-bourboulis EJ, Martens JHA, et al. mTOR/HIF1 α -mediated aerobic glycolysis as metabolic basis for trained immunity. *Science* 2014; 345: 1–18.
- [52] Fortner KA, Blanco LP, Buskiewicz I, et al. Targeting mitochondrial oxidative stress with MitoQ reduces NET formation and kidney disease in lupus-prone MRL- lpr mice. *Lupus Sci Med* 2020; 7: e000387.
- [53] Lood C, Blanco LP, Purmalek MM, et al. Neutrophil extracellular traps enriched in oxidized mitochondrial DNA are interferogenic and contribute to lupus-like disease. *Nat Med* 2016; 22: 146–53.
- [54] Zhu H, Mi W, Luo H, et al. Whole-genome transcription and DNA methylation analysis of peripheral blood mononuclear cells identified aberrant gene regulation pathways in systemic lupus erythematosus. *Arthritis Res Ther* 2016; 18: 1–17.
- [55] Yeung KS, Lee TL, Mok MY, et al. Cell lineage-specific genome-wide DNA methylation analysis of patients with paediatric-onset systemic lupus erythematosus. *Epigenetics* 2019; 14: 341–51.
- [56] Panousis NI, Bertsias GK, Ongen H, et al. Combined genetic and transcriptome analysis of patients with SLE: distinct, targetable signatures for susceptibility and severity. *Ann Rheum Dis* 2019; 78: 1079–89.
- [57] Brito-Zerón P, Baldini C, Bootsma H, et al. Sjögren syndrome. *Nat Rev Dis Prim* 2016; 2: 1–20.

- [58] Srivastava A, Makarenkova HP. Innate immunity and biological therapies for the treatment of sjögren's syndrome. *Int J Mol Sci* 2020; 21: 1–45.
- [59] Ainola M, Porola P, Takakubo Y, et al. Activation of plasmacytoid dendritic cells by apoptotic particles – mechanism for the loss of immunological tolerance in Sjögren's syndrome. *Clin Exp Immunol* 2018; 191: 301–10.
- [60] Vakrakou AG, Boiu S, Ziakas PD, et al. Systemic activation of NLRP3 inflammasome in patients with severe primary Sjögren's syndrome fueled by inflammagenic DNA accumulations. *J Autoimmun* 2018; 91: 23;33.
- [61] Pertovaara M, Silvennoinen O, Isomäki P. Cytokine-induced STAT1 activation is increased in patients with primary Sjögren's syndrome. *Clin Immunol* 2016; 165: 60–7.
- [62] Yoshimoto K, Suzuki K, Takei E, Ikeda Y, Takeuchi T. Elevated expression of BAFF receptor, BR3, on monocytes correlates with B cell activation and clinical features of patients with primary Sjögren's syndrome. *Arthritis Res Ther* 2020; 22: 1–10.
- [63] Luo X, Peng Y, Chen Y-Y, et al. Genome-wide DNA methylation patterns in monocytes derived from patients with primary Sjogren syndrome. *Chin Med J (Engl)* 2021; 134: 1310–6.
- [64] Sisto M, Lorusso L, Ingravallo G, et al. The TGF- β 1 signaling pathway as an attractive target in the fibrosis pathogenesis of Sjögren's syndrome. *Mediators Inflamm* 2018; 2018: 5–7.
- [65] Wang X, Xin S, Wang Y, et al. MicroRNA-146a-5p enhances T helper 17 cell differentiation via decreasing a disintegrin and metalloprotease 17 level in primary sjögren's syndrome. *Bioengineered* 2021; 12: 310;24.
- [66] Wells AU. Systemic sclerosis. *ERS Monogr* 2019; 2019: 90–105.
- [67] Jeljeli M, Riccio LGC, Doridot L, et al. Trained immunity modulates inflammation-induced fibrosis. *Nat Commun* 2019; 10: 1–15.
- [68] Bhandari R, Ball MS, Martyanov V, et al. Profibrotic Activation of Human Macrophages in Systemic Sclerosis. *Arthritis Rheumatol* 2020; 72: 116;9.
- [69] Maugeri N, Capobianco A, Rovere-Querini P, et al. Platelet microparticles sustain autophagy-associated activation of neutrophils in systemic sclerosis. *Sci Transl Med* 2018; 10: eaa03089.
- [70] Bhattacharyya S, Wang W, Morales-Nebreda L, et al. Tenascin-C drives persistence of organ fibrosis. *Nat Commun* 2016; 7: 1–14.
- [71] Ding W, Pu W, Wang L, et al. Genome-Wide DNA Methylation Analysis in Systemic Sclerosis Reveals Hypomethylation of IFN-Associated Genes in CD4+ and CD8+ T Cells. *J Invest Dermatol* 2018; 138: 1069–77.
- [72] Kamada R, Yang W, Zhang Y, et al. Interferon stimulation creates chromatin marks and establishes transcriptional memory. *Proc Natl Acad Sci U S A* 2018; 115: E9162;71.
- [73] Mariotti B, Servaas NH, Rossato M, et al. The long non-coding RNA NRIR drives IFN-Response in monocytes: Implication for systemic sclerosis. *Front Immunol* 2019; 10: 1–16.
- [74] Servaas NH, Mariotti B, van der Kroef M, et al. Characterization of long non-coding rnas in systemic sclerosis monocytes: A potential role for psmb8-as1 in altered cytokine secretion. *Int J Mol Sci* 2021; 22: 4365.
- [75] Van Der Kroef M, Castellucci M, Mokry M, et al. Histone modifications underlie monocyte dysregulation in patients with systemic sclerosis, underlining the treatment potential of epigenetic targeting. *Ann Rheum Dis* 2019; 78: 529–38.
- [76] Moreno-Moral A, Bagnati M, Koturan S, et al. Changes in macrophage transcriptome associate with systemic sclerosis and mediate GSDMA contribution to disease risk. *Ann Rheum Dis* 2018; 77: 596–601.



CHAPTER 7

Summary, general discussion,
and perspectives

Summary

Hyperuricemia arises from elevated concentrations of serum urate and is recognized for its involvement in the onset of gout, but also its contribution to cardiovascular and metabolic diseases [1]. After surpassing the solubility threshold, urate can precipitate and form monosodium urate (MSU) crystals in joints and surrounding tissues. In gout, MSU crystals can trigger acute flares and, if not properly managed, may accumulate in formations called tophi, which can lead to destruction in the adjacent bone [2]. High concentrations of urate, whether soluble or crystallized, play an important role in the initiation of pro-inflammatory states. While urate has been acknowledged for its antioxidant properties in the past, more recently, it has been demonstrated that urate exhibits pro-oxidant and proinflammatory characteristics [3]. Recent findings indicate that soluble urate can prime human monocytes *in vitro*, resulting in heightened immune responses when faced with a second challenge [4]. A growing number of studies underline the capacity of the innate immune system to establish immune memory (termed "trained immunity") to protect against infections. Under sterile conditions, a dysregulated trained immunity program can contribute to disease states. This phenomenon could be explained by the epigenetic and metabolic changes that the cells of the innate immune cells experience as they develop and adapt to respond to immunological triggers [5]. However, there is still much to learn about the functions of urate in the serum and how it contributes to inflammatory processes within human subjects.

This aim of this thesis was to explore whether elevated concentrations of soluble uric acid (hyperuricemia) can induce epigenetic and transcriptional reprogramming within innate immune cells and investigate potential mechanisms underlying the hyperinflammatory state characterized by the shift in cytokine production (e.g. increased IL-1 β and reduced IL-1Ra).

The scope of this thesis has been directed toward exploring the inflammation associated with hyperuricemia and gout. The first study (Chapter 2) confirms that *in vitro* urate-priming of the peripheral blood mononuclear cells (PBMCs) results in a shift in cytokine production, characterized by increased production of pro-inflammatory IL-1 β and IL-6, and decreased production of anti-inflammatory IL-1Ra. Importantly, the cytokine production *in vitro* was persistent even after allowing a resting period. Histone modifications and DNA methylation variation were observed in response to urate exposure. The pro-inflammatory effects were mitigated when methylation was pharmacologically

inhibited in mice *in vivo*. These findings suggest that epigenetic alterations in myeloid cells induced by urate priming could potentially be targeted for therapeutic interventions in gout.

The role of the suppressor of cytokine signalling 3 (SOCS3) in inflammation induced by urate was explored next in Chapter 3, following its identification as having differentially methylated regions in the previous study. The results indicate that urate-priming of immune cells results in increased pro-inflammatory and reduced anti-inflammatory cytokine production, along with altered SOCS3 expression and phosphorylation of STAT3 upon a subsequent stimulation. SOCS3 and phosphorylated STAT3 may play a role in urate-induced inflammation, since the urate priming proinflammatory effect was not observed in PBMCs of patients with continuously activated STAT3. Modulation of SOCS3 in response to urate in monocytes could not be explained by DNA methylation modifications in an *in vitro* setting with a 24-hour treatment period.

In parallel, urate-priming resulted in suppressed type 1 interferon-related signalling pathways in human mononuclear cells of patients with gout and decreased phosphorylated STAT1 as described in Chapter 4. Moreover, an inverse relationship was observed between the expression of interferon-stimulated genes (ISGs) and IL-1Ra cytokine production in stimulated PBMCs, correlating with serum urate concentrations in these patients. These findings might suggest a potential link between deficient IFN1 signalling and increased susceptibility to viral infections.

In Chapter 6, sex-specific variations in cytokine production have been identified among patients with gout, emphasizing potential distinct mechanisms that may regulate inflammation in men and women with gout.

Finally, the recent literature on trained immunity in gout and other rheumatic conditions has been reviewed in Chapter 7, emphasizing its potential involvement in initiating, sustaining, and exacerbating the symptoms, as well as potentially predisposing individuals to additional pathologies.

The following section offers an overview of the findings presented in the previous chapters, situating them within the context of current literature in the field (summarized in Figure 1).

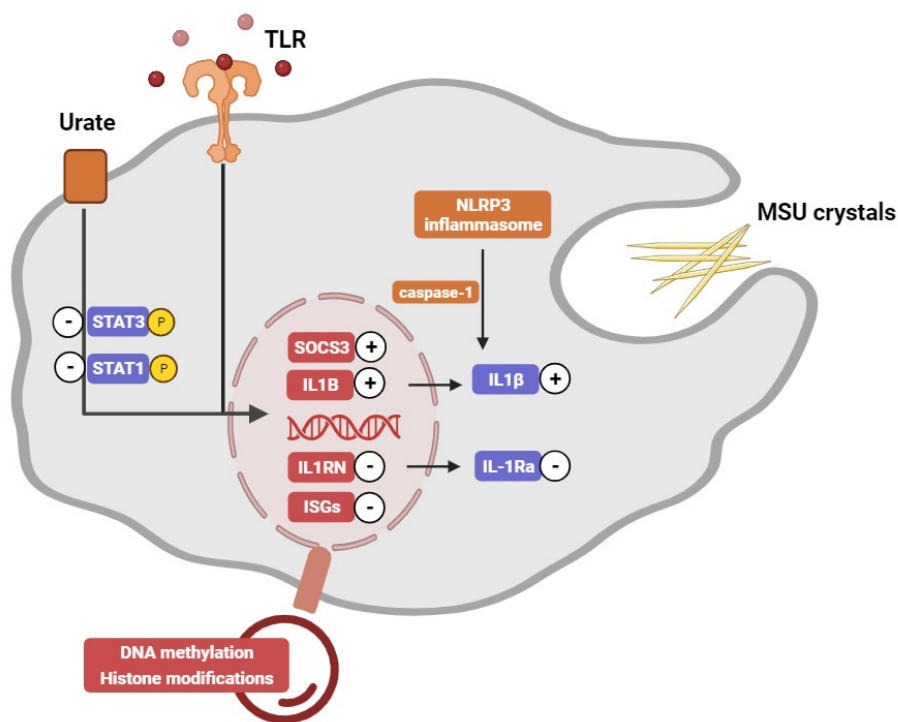


Figure 1. Schematic representation of data described in the thesis and outlined in this chapter. Please refer to the chapters for comprehensive clarifications. **IL1B/IL-1β** – Interleukin 1 beta, **IL1RN/IL-1Ra** – Interleukin-1 receptor antagonist, **ISGs** – Interferon stimulated genes, **MSU** – monosodium urate, **P** – Phosphate, **SOCS3** – Suppressor Of Cytokine Signalling 3, **STAT1** – Signal transducer and activator of transcription 1, **STAT3** – Signal transducer and activator of transcription 3, **TLR** – Toll-Like Receptor.

Discussion

Chapter 1 of this thesis gives a brief overview of inflammation induced by elevated urate concentrations and how it affects gout and other conditions. Additionally, it delves into the metabolic and epigenetic changes associated with innate immune memory following exposure to both soluble and crystal forms of urate. High concentration of urate in the bloodstream are clinically defined as hyperuricemia. Gout is an inflammatory arthritis caused by the deposition of monosodium urate (MSU) crystals in joints and soft tissues. The formation of monosodium urate crystals is a result of the crystallization of urate, which occurs when the concentration of urate in the blood surpasses

its solubility limit. The presence of MSU crystals triggers an inflammatory response, leading to the characteristic symptoms of gout, such as joint pain, swelling, and redness [6]. MSU crystals act as damage-associated molecular patterns (DAMPs) in gout by activating the NLRP3 inflammasome complex in the tissue-resident macrophages to drive the production of Interleukin-1 β (IL-1 β). Additionally, the engagement of toll-like receptors (TLR) agonists such as fatty acids, and the subsequent enhancement of inflammasome activation by MSU crystals establish the link between the metabolic changes preceding a gout attack and the subsequential inflammatory flare in the joints of affected patients [7]. Furthermore, it has been demonstrated that elevated soluble urate concentrations also have proinflammatory effects on immune on non-immune cells [4]. This chapter describes the role and effects of urate on immune cells, both soluble and in its crystal form, in humans. We provide base evidence for several mechanisms of inflammation in hyperuricemia and gout, that may have implications for other health issues and introduce the concept of innate immune memory as a result of urate exposure.

In **Chapter 2**, in order to gain a deeper understanding of the long-term effects of urate, we start by investigating the epigenetic-mediated innate immune memory associated with persistent elevated urate exposure, a key metabolite in gout pathogenesis. As previously described, *in vitro* urate priming results in a dose-dependent cytokine production on a subsequent stimulation in the absence of urate, characterized by increased IL-1 β and reduced IL-1Ra production [4], mediated partially by the AKT-pathway and inhibition of autophagy [8]. In PBMCs of patients with gout, Wang *et al.*, identifies differentially methylated regions at known gout-risk genes and TF-gene networks in leukocytes [9]. We hypothesized that urate could prime or train the monocytes to induce immunological memory through alterations in the epigenome. We found that treatment with elevated urate concentrations leads to an increase in the pro-inflammatory response in both *in vitro* and in mice, and this effect could be reversed using broad-spectrum methylation inhibitors. Furthermore, it is worth noting that differential cytokine production persisted even after introducing a resting time of up to 5 days between exposure to urate and subsequent TLR restimulation, a phenomenon reminiscent of trained immunity [10]. Several agents, like β -glucan (exogenous) or oxidized cholesterol (endogenous) induce a sustained state of immunological memory (referred to as “trained immunity”) in cells of the innate immune system, like monocytes and macrophages, through mechanisms that involve epigenetic rewiring [11]. In addition, epigenetic alterations, including

histone modifications and differential DNA methylation, were observed in individuals with hyperuricemia, indicating the potential of targeting epigenetic changes in myeloid cells as a future therapeutic strategy for gout. Histone modifications, through their direct effect on the chromatin structure and transcription factor recruitment, impact gene expression. Two histone marks of actively transcribed genes, H3K4me3 and H3K27ac, both of which play an important role in innate immune memory [12], did not show extensive modifications in the context of the whole genome in response to soluble urate exposure. Nevertheless, within the datasets of histone modifications, several target genes that hold significance in the context of urate-mediated effects, including *IL1* genes that encode for pro-inflammatory cytokines, were found enriched at H3K27ac. The clinical profile of patients with type 2 diabetes who present with wounds often show elevated serum urate concentrations. The assessment of wound macrophages of patients with type 2 diabetes reveals decreased Setdb2, a histone methyltransferase of H3K9 associated with gene inactivation. Concurrently, there is an upregulation of IL-1 β and TNF production. The reduction in the suppression activity of certain genes may affect the inflammatory response and, consequently, healing processes due to an altered epigenetic regulation. Interestingly, the increase in xanthine oxidase (XO) suggests that Setdb2 may even play a role in regulating the urate production [13]. We further explored the DNA methylation patterns associated with hyperuricemia among people of New Zealand Māori ancestry. The risk of developing hyperuricemia and gout is up to 3 times higher in the Māori population compared to individuals of European descent and this may be linked to genetic factors such as genetic polymorphisms that raise serum urate [14]. Even without considering dietary factors, ancient Māori skeletons discovered before the Western culture showed evidence of gout [15]. Following whole blood DNA methylation analysis, we identified an increased number of differentially methylated probes and differentially methylated regions in individuals with hyperuricemia compared to normouricemic controls. Most differentially methylated regions belonged to genes encoding for proteins involved in the regulation of cellular metabolism (PRKAB2), autoimmunity (HLA-G), and defense against viral infections (IFITM3). On the other hand, another whole blood DNA methylation analysis (EWAS) shows the opposite, that changes in DNA methylation, notably CpGs in the *SLC1A9* gene that encodes for a urate transporter, directly affect urate concentrations, suggesting that epigenetic dysregulation may contribute to hyperuricemia and gout pathogenesis [16].

Chapter 3 expands on the findings that PBMCs pre-treated with urate show increased pro-inflammatory IL-1 β and reduced anti-inflammatory IL-1Ra production upon LPS re-stimulation to include individuals with hyperuricemia and patients with gout. Additionally, the study aimed to decipher the underlying molecular mechanisms that are responsible for or contribute to uric acid priming in human monocytes. *In vitro*, urate-priming of myeloid cells triggers the transcription of *SOCS3*. Suppressors of Cytokine Signalling (SOCS) proteins. SOCS proteins known as JAK-STAT signalling inhibitors and provide negative feedback mechanisms to regulate the balance between pro-inflammatory and anti-inflammatory cytokine levels. By binding to JAK kinases directly via the kinase inhibitory region (KIR), SOCS3 controls cytokine production by suppressing STAT3 activation induced by cytokines that form complexes with the glycoprotein 130 (gp130) IL-6 receptor subunit [17]. Other stimuli such as LPS or monosodium urate crystals also upregulate the expression of several SOCS proteins [18]. SOCS3 holds an essential role for the well development of an organism and is expressed by both immune and non-immune cells. This is demonstrated by the fact that mice deficient in *Socs3*, which results in hyperactivation of *Stat3*, do not survive beyond the perinatal period [19]. In mice with IL-1-induced inflammatory arthritis, the absence of SOCS3 resulted in joint inflammation, marked by extensive neutrophil infiltration in the synovium and increased pro-inflammatory cytokine production [20]. Osteoclasts, cells that resorb the bone, also appeared in increased numbers in the arthritic knee joints of SOCS3-deficient mice, further contributing to bone destruction. This may be in relation to elevated IL-17 production, which is associated with osteoclastogenesis [20]. SOCS proteins, especially SOCS1-3, have been studied about rheumatoid arthritis as well, where they are believed to either limit inflammatory processes [21] or facilitate disease progression through their altered expression [22]. Inducing CIS3/SOCS3 to target the IL-6-gp130-JAK-STAT3 pathway could offer a novel approach to treating rheumatoid arthritis, aiming to mitigate the severity and reduce joint swelling in experimental mouse models [23]. An experimental model for collagen-induced arthritis disease has also demonstrated a protective role for SOCS3 in mitigating inflammation via down-regulation of Tyro3, Axl, and Mer (TAM) receptors, negative regulators of TLRs and type I interferon signalling [24]. In gout, SOCS proteins are involved in modulating the pathways driven by IL-1 β [25]. IL-1 β has the capacity to induce SOCS3 expression [26], rendering it a promising candidate for addressing inflammation in gouty arthritis, especially considering a recent study that proposed a potential role for SOCS3 in resolving gout flares [27]. The majority of the time, gout flares resolve by themselves,

and this spontaneous resolution was associated with the rapid induction of several anti-inflammatory factors, including transforming growth factor beta 1 (TGFβ1), IL-1Ra, IL-10, and soluble TNF receptors. In addition, the induction of CIS and SOCS3, has also been associated with the spontaneous resolution of acute gouty arthritis [25]. When compared to intercritical gout remission and controls, PBMCs from patients with advanced gout remission show increased *SOCS3* expression in both monocyte and lymphocyte populations (monocytes, CD4+T cells, and B cells), which may be connected to the resolution of systemic inflammation [28]. In our study, urate treatment results in the upregulation of *SOCS3* with a subsequent suppression of phosphorylated STAT3 and a corresponding reduction in IL-1Ra production, suggesting a possible pro-inflammatory impact in this context. Under certain conditions, STAT3 can promote the transcription of *IL1RN* (IL-1Ra) in monocytes by binding to specific DNA sequences in the promoter region [29]. We observed that PBMCs from patients positive for the *JAK2 V617F* somatic mutation showed no change in IL-1β and IL-6 levels when primed with urate, indicating a possible role for STAT3 in urate-induced inflammation. In **Chapter 2**, we noted distinct DNA methylation patterns at three adjacent CG sites within the *SOCS3* gene region in the whole blood of hyperuricemic individuals when compared to normouricemic controls. However, these variations were lost after accounting for adjustments related to cell-type composition. While different cell types have distinct methylation patterns and adjusting for cell-type composition is important for revealing accurate differentially methylated probes and regions, during inflammatory states the dynamic of cell populations can change. Computational deconvolution using a reference methylation profile which was generated at baseline condition may not accurately reflect the cell types in the analyzed samples, making the interpretation of the biological findings more intricate. Providing an analysis before and after cell-type composition may be useful. In the present study, we found no significant whole genome changes regarding DNA methylation in *SOCS3* in the context of a pure monocyte population treated *in vitro* with soluble urate alone. It is important to consider that these findings may be influenced by potential limitations related to the sample size and the duration of urate treatment - 24h - both of which may not fully mirror the complex *in vivo* scenarios in patients.

Chapter 4 further delves into exploring the mechanism underlying urate priming. In this sense, several cell culture models are used to explore differential gene expression by RNA-Sequencing together with cytokine production. The analysis of differentially expressed genes and transcription

factor enrichment in urate-treated human PBMCs reveals that the type 1 interferon (IFN1) signalling pathway is downregulated. This is confirmed in monocytes treated with urate in a publicly available dataset [8]. The downregulation of IFN1 is further supported by the observation of diminished STAT1 activity in monocytes exposed to urate. In **Chapter 3**, we show that urate-priming results in the reduction of phosphorylated STAT3 as well. It is known that in addition to STAT1 and STAT2, the interferon- α/β receptor (IFNAR) also activates homodimers of STAT3 as parts of the canonical IFN1 signalling pathway to negatively regulate STAT-dependent gene induction and dampen inflammation [30]. IFN1 have demonstrated a complex role in the immune responses, which also includes limiting the production of IL-1 β and inducing IL-1Ra production, possibly by cross-talk between signalling pathways [31]. Additionally, IFN1 may impact the activation of the inflammasome complexes, influencing the release of mature IL-1 β [32]. While a direct connection between IFN1 and gout has not been well-established, IFN1 might modulate the related immune responses by impacting IL-1 production [33].

In the '80, A. Weinberger and J. Pinkhas first hypothesized that type 1 interferons are among the cytokines that mediate inflammation in acute gouty arthritis by facilitating MSU crystals uptake by the macrophages present in the joint lining [34]. It was only recently discovered that urate crystals engage the C-type lectin receptor (a PRR) Clec12A and amplify the type 1 interferon pathway triggered by cytosolic RNA, thus favouring the transcription of Interferon Inducible Genes (ISGs) [35]. Yet, the involvement of soluble urate in the type 1 interferon pathway is less defined. In our study, we observed that inducing the type 1 interferon pathway with IFN- β in the presence of urate did not alter the pro-inflammatory effects of urate, suggesting that the downregulation of the IFN1 signalling pathway is unlikely to be part of the mechanism behind urate-priming. Still, several recent studies have pointed to associations between urate and type 1 interferons. In patients with gout, DNA methylation in PBMCs identified changes in transcription factors (TFs) with a role in interferon signalling (*STAT2*, *IRF1*) [9]. In patients with intercritical gout and proven MSU crystal deposition, increased expression levels of several ISGs (*IRF1*, *IRF7*, *IFI16*, *STAT1*) were observed, potentially adding to the inflammatory response at this stage [28]. Several enriched pathways involve type 1 interferons in a whole blood DNA methylation EWAS urate study and the authors propose that alterations in DNA methylation patterns affect serum urate concentrations directly [16]. As demonstrated in **Chapter 2**, whole blood DNA methylation analysis of individuals with hyperuricemia shows, among others, differentially

methyated regions at *IFITM3*, suggesting that urate might modulate the type 1 interferon pathway. The current study demonstrates that high serum urate levels *in vivo* inversely correlate with the response to *in vitro* stimulations with Poly: IC, CpG, and *Candida albicans*. Many recent investigations demonstrate a link between hyperuricemia or gout and suboptimal responses to Sars-Cov2 infection [36] [37]. Nonetheless, it is important to note that these urate effects may be specific to the soluble form since monosodium urate (MSU) crystals do not induce changes in the genes encoding for type 1 interferons [18]. These findings support the notion of a deficient IFN1 signalling pathway when exposed to elevated urate concentrations, implying that pre-exposure to urate may have a detrimental effect on the response to stimulations that rely on ISG induction, potentially increasing susceptibility to microbial infections.

Chapter 6 explores the distinct pro-inflammatory response of stimulated PBMCs of patients with gout, focusing on differences related to sex. Gout is an inflammatory condition driven by innate immune mechanisms centered on the activation and release of IL-1 β . Epidemiological studies show that women affected by gout are generally older, have a higher BMI, and have more comorbidities [38] compared to men with gout, and this aligns with the observations in our cohort. Risk factors such as renal disease or the use of diuretics (which can decrease renal UA excretion) are more often observed in women [39] [38]. Still, men commonly have higher concentrations of serum urate [40].

This study demonstrates that patients with gout show increased *in vitro* cytokine production compared to non-gout controls. *In vitro* stimulated PBMCs from men indicate a higher capacity for cytokine production and elevated levels of various pro-inflammatory markers [41]. In the current study, men with gout have higher circulating cytokine concentrations, while it is the women with gout who display increased *in vitro* cytokine production capacity. Hormonal changes alone cannot fully account for these observed immune differences, however, generally sex and age appear to be significant contributors to this variation [42].

In pre-menopausal women, gout is rare [43], but increased serum urate concentrations have been linked also to reproductive disorders such as polycystic ovary syndrome (PCOS) and endometriosis through mechanisms that involve inflammation, oxidative stress, and mitochondrial

dysfunction [44]. A significant association has been observed between infertility and serum urate levels in women. However interesting, the concentration of urate to which significant associations were found was 4.4 mg/dL, which falls below the threshold for clinically defined hyperuricemia [45]. In men with hyperuricemia, low sperm count is associated with high serum urate concentrations, possibly through a mechanism that alters hormone levels [46]. These studies indicate that urate can even impact fertility in both women and men.

Given that clinical profiles of patients with gout and hyperuricemia vary between men and women, it becomes essential to investigate the possible distinct regulatory mechanisms in inflammation in both sexes, rather than treating sex only as a covariate for biological variation. Furthermore, the consequences of elevated serum urate concentrations extend beyond gout, affecting both men and women in different ways.

Finally, in **Chapter 7**, the recent literature was reviewed to explore the concept of innate immune memory, examining its possible involvement in gout and hyperuricemia and extending these insights to other rheumatic diseases. Rheumatic diseases, marked by musculoskeletal and systemic involvement, cover a diverse range of autoimmune and autoinflammatory conditions, where the intricate inflammatory processes leading to these debilitating disorders involve contributions from both innate and adaptive immunity [47]. Recent research has brought about a significant shift in our understanding of immune memory, revealing that cells of the innate immune system can acquire a form of immunological memory through epigenetic reprogramming and metabolic changes, known as "trained immunity" [48]. It was first noted in studies of the BCG vaccination which demonstrated that these cellular changes result in an enhanced innate immune response to later challenges [49]. While the concept of trained immunity emerged to support a role for the innate immune cells in enhancing immune defense through the development of immunological memory, trained immunity has been reported to contribute to disease pathogenesis in various conditions such as atherosclerosis, and autoinflammatory disorders [11]. Here, we highlight trained immunity features in rheumatic disorders like gout, rheumatoid arthritis, systemic lupus erythematosus, or systemic sclerosis and discuss their possible mechanistic involvement in the disease pathogenesis. Gout is an autoinflammatory disease triggered by monosodium urate (MSU) crystal depositions within joints and surrounding tissues. IL-1 β is the central

cytokine involved and its secretion by the tissue-resident macrophages is dependent on the activation of NLRP3 inflammasome [2]. We underline that in addition to MSU crystals, soluble urate can also activate the innate immune system, contributing to immune programming and inflammation in gout [50]. Increased IL-1 β production in response to MSU crystal stimulation results in a cellular metabolic shift towards upregulated glycolysis [51]. Interestingly, increased glycolysis promotes inflammasome activation [52]. Moreover, MSU crystal-stimulated macrophages show enrichment for pathways involving cellular metabolism [53]. This could constitute a possible mechanism adding to sustained inflammation in gout. Soluble urate primes the innate immune cells to increase IL-1 β and reduced IL-1Ra production by activation of the AKT-PRAS40 pathway and inhibition of autophagy, processes that may be mediated via epigenetic changes [8]. These findings support effects reminiscent of trained immunity phenotype for both soluble and crystal forms of urate. Epigenetic dysregulation can affect the patterns of gene expression linked to inflammation and immune responses, which are significant factors in the aetiology of hyperuricemia and gout. This knowledge may help identify new targets for treatment or create strategies to alter epigenetic markers in order to reduce inflammation and immune system dysregulation associated with gout and hyperuricemia.

Future prospectives

Although the role of the crystalized form of urate is well known in gout, soluble urate remains the subject of ongoing research, particularly when considering its link to many comorbidities. Individuals with asymptomatic hyperuricemia face higher risks of developing hypertension, chronic kidney disease, obesity, metabolic syndrome, fatty liver disease, and diabetes mellitus. Additionally, a growing body of evidence underlines that hyperuricemia acts as pro-inflammatory factor.

This thesis presents a novel and comprehensive approach to understanding the mechanisms and effects of urate exposure in vitro treated myeloid cells and in patients with hyperuricemia and gout. It includes multiple layers of analysis, such as DNA methylation, cytokine production, and transcriptomic data, adding to the existing research on urate priming.

Building upon previous studies, this thesis extends the understanding of urate priming and further shows a persistence of urate's effects after an initial exposure and its capacity to induce immune innate memory. It was previously demonstrated that urate priming results in a shift in cytokine production, with increased proinflammatory and decreased anti-inflammatory cytokine production, and this process is mediated by mechanisms involving the AKT and PRAS40 phosphorylation and mTOR activation [8]. We were able to further extend the effects of urate priming in samples from hyperuricemic and gout patients and show that this was accompanied by an increased SOCS3 expression and downregulated STAT3 phosphorylation. We observed the effect of soluble urate on many biological pathways, including the downregulation of type 1 interferons and STAT1 phosphorylation. Moreover, STAT3 is known for the induction of SOCS3 but also for the regulation of type 1 interferons activity under certain conditions.

DNA methylation patterns observed in both hyperuricemic individuals and monocytes treated *in vitro* with soluble urate offer valuable insight into the epigenetic modifications induced by urate and how it may impact on gene regulation. We have shown that DNA methylation profiles are different in hyperuricemic people. This has been shown in relatively small sample size and conducting a DNA methylation study with larger cohorts of hyperuricemic individuals and patients with gout, while also separating by sex, will complete the findings in this thesis. However, the current results establish a foundation for evidence on different immune responses between women and men with gout, particularly in cytokine production. Further investigation on multi-omics approaches is needed, as this will add additional layers of information to characterize urate driven inflammation.

The transcriptomic data obtained from human PBMCs exposed to urate *in vitro* enabled the examination of transcriptional changes induced by urate and its correlation with cytokine production. The present understanding of urate priming is further enhanced by the large number of samples that comprise both transcriptomic and cytokine data and that allowed us to draw robust conclusions. Our understanding of the mechanisms governing urate-induced inflammation remains incomplete as these pathways are also modulated by numerous additional factors. Future studies of immune priming long-non-coding RNAs (lncRNAs) provide promising ground to enrich our knowledge by identifying possible topological domains that are associated during urate exposure that will enable deeper insight into how gene expression, and

subsequently, cytokine production is regulated following urate exposure. Innate immune memory relies on long non-coding RNAs (lncRNA) that serve as scaffolds for chromatin regulation and are key molecules in inducing and maintaining the robustness of gene transcription [54].

These findings underscore the pro-inflammatory effect of soluble urate, extending its significance beyond gout, and emphasize the necessity for future research involving larger patient cohorts. Moreover, studies that explore the effect of urate lowering therapy on reducing the innate immune memory status of myeloid cells should be initiated.

References

- [1] Crisan TO, Netea MG, Joosten LAB. Innate immune memory: Implications for host responses to damage-associated molecular patterns. *Eur J Immunol* 2016; 46: 817–28.
- [2] Dalbeth N, Choi HK, Joosten LAB, et al. Gout. *Nat Rev Dis Primers*. 2019;5(1):69.
- [3] Sautin YY, Johnson RJ. Uric acid: The oxidant-antioxidant paradox. In: *Nucleosides, Nucleotides and Nucleic Acids* 2008; 27(6):608–19.
- [4] Crişan TO, Cleophas MCP, Oosting M, et al. Soluble uric acid primes TLR-induced proinflammatory cytokine production by human primary cells via inhibition of IL-1Ra. *Ann Rheum Dis* 2016; 75: 755–62.
- [5] Netea MG, van der Meer JWM. Trained Immunity: An Ancient Way of Remembering. *Cell Host Microbe* 2017; 21: 297–300.
- [6] Martillo MA, Nazzari L, Crittenden DB. The crystallization of monosodium urate. *Curr Rheumatol Rep* 2014; 16: 1–13.
- [7] Joosten LAB, Netea MG, Mylona E, et al. Engagement of fatty acids with toll-like receptor 2 drives interleukin-1 β production via the ASC/caspase 1 pathway in monosodium urate monohydrate crystal-induced gouty arthritis. *Arthritis Rheum* 2010; 62: 3237–48.
- [8] Crişan TO, Cleophas MCP, Novakovic B, et al. Uric acid priming in human monocytes is driven by the AKT–PRAS40 autophagy pathway. *Proc Natl Acad Sci* 2017; 114: 5485–5490.
- [9] Wang Z, Zhao Y, Phipps-Green A, et al. Differential DNA Methylation of Networked Signaling, Transcriptional, Innate and Adaptive Immunity, and Osteoclastogenesis Genes and Pathways in Gout. *Arthritis Rheumatol* 2020; 72(5):802–14.
- [10] Netea MG, Joosten LAB, Latz E, et al. Trained immunity: A program of innate immune memory in health and disease. *Science* 2016; 352(6284):aaf1098.
- [11] Netea MG, Domínguez-Andrés J, Barreiro LB, et al. Defining trained immunity and its role in health and disease. *Nat Rev Immunol* 2020; 20: 375–88.
- [12] Fanucchi S, Domínguez-Andrés J, Joosten LAB, et al. The Intersection of Epigenetics and Metabolism in Trained Immunity. *Immunity* 2021; 54: 32–43.
- [13] Kimball AS, Davis FM, denDekker A, et al. The Histone Methyltransferase Setdb2 Modulates Macrophage Phenotype and Uric Acid Production in Diabetic Wound Repair. *Immunity* 2019; 51: 258–271.e5.
- [14] Zaka R, Williams CJ. New developments in the epidemiology and genetics of gout. *Curr Rheumatol Rep* 2006; 8: 215–23.
- [15] Johnson RJ, Sánchez-Lozada LG, Nakagawa T, et al. Do thrifty genes exist? Revisiting uricase. *Obesity* 2022; 30: 1917–26.
- [16] Tin A, Schlosser P, Matias-Garcia PR, et al. Epigenome-wide association study of serum urate reveals insights into urate co-regulation and the SLC2A9 locus. *Nat Commun* 2021; 12: 1–18.
- [17] Schmitz J, Weissenbach M, Haan S, et al. SOCS3 exerts its inhibitory function on interleukin-6 signal transduction through the SHP2 recruitment site of gp130. *J Biol Chem* 2000; 275(17):12848–56.
- [18] Cobo I, Cheng A, Murillo-Saich J, et al. Monosodium urate crystals regulate a unique JNK-dependent macrophage metabolic and inflammatory response. *Cell Rep* 2022; 38: 110489.
- [19] Carow B, Rottenberg ME. SOCS3, a major regulator of infection and inflammation. *Front Immunol* 2014; 5: 1–13.

- [20] Wong PKK, Egan PJ, Croker BA, et al. SOCS-3 negatively regulates innate and adaptive immune mechanisms in acute IL-1-dependent inflammatory arthritis. *J Clin Invest* 2006; 116: 1571–81.
- [21] Ivashkiv LB, Tassiulas I. Can SOCS make arthritis better? *J Clin Invest* 2003; 111: 795–7.
- [22] Isomäki P, Alanärrä T, Isohanni P, et al. The expression of SOCS is altered in rheumatoid arthritis. *Rheumatology* 2007; 46: 1538–46.
- [23] Shouda T, Yoshida T, Hanada T, et al. Induction of the cytokine signal regulator SOCS3/CIS3 as a therapeutic strategy for treating inflammatory arthritis. *J Clin Invest* 2001; 108: 1781–8.
- [24] Van Den Brand BT, Abdollahi-Roodsaz S, Vermeij EA, et al. Therapeutic efficacy of Tyro3, Axl, and Mer tyrosine kinase agonists in collagen-induced arthritis. *Arthritis Rheum* 2013; 65: 671–80.
- [25] Chen YH, Hsieh SC, Chen WY, et al. Spontaneous resolution of acute gouty arthritis is associated with rapid induction of the anti-inflammatory factors TGF β 1, IL-10 and soluble TNF receptors and the intracellular cytokine negative regulators CIS and SOCS3. *Ann Rheum Dis* 2011; 70: 1655–63.
- [26] Tengesdal IW, Dinarello A, Powers NE, et al. Tumor NLRP3-Derived IL-1 β Drives the IL-6/STAT3 Axis Resulting in Sustained MDSC-Mediated Immunosuppression. *Front Immunol* 2021; 12: 1–11.
- [27] Orji OC, López-Domínguez MB, Sandoval-Plata G, et al. Upregulated expression of FFAR2 and SOCS3 genes is associated with Gout. *Rheumatology* 2022; 1–7.
- [28] Gu H, Yu H, Qin L, et al. MSU crystal deposition contributes to inflammation and immune responses in gout remission. *Cell Rep* 2023; 42: 113139.
- [29] Tamassia N, Castellucci M, Rossato M, et al. Uncovering an IL-10-dependent NF-KB recruitment to the IL-1 α promoter that is impaired in STAT3 functionally defective patients. *FASEB J* 2010; 24(5):1365–75.
- [30] Ivashkiv LB, Donlin LT. Regulation of type I interferon responses. *Nat Rev Immunol* 2014; 14: 36–49.
- [31] Man SM, Kanneganti TD. Type I Interferon Keeps IL-1 β in Check. *Cell Host Microbe* 2016; 19: 272–4.
- [32] Ludigs K, Parfenov V, Pasquier RAD, et al. Type I IFN-mediated regulation of IL-1 production in inflammatory disorders. *Cell Mol Life Sci* 2012; 69: 3395–418.
- [33] Mayer-Barber KD, Yan B. Clash of the Cytokine Titans: Counter-regulation of interleukin-1 and type I interferon-mediated inflammatory responses. *Cell Mol Immunol* 2017; 14: 22–35.
- [34] Hypotheses M. 6: 781–784, 1980. 1980; 781–4.
- [35] Li K, Neumann K, Duhan V, et al. The uric acid crystal receptor Clec12A potentiates type I interferon responses. *Proc Natl Acad Sci U S A* 2019; 116: 18544–9.
- [36] Topless RK, Gaffo A, Stamp LK, et al. Gout and the risk of COVID-19 diagnosis and death in the UK Biobank: a population-based study. *Lancet Rheumatol* 2022; 4: e274–e281.
- [37] Chen B, Lu C, Gu HQ, et al. Serum Uric Acid Concentrations and Risk of Adverse Outcomes in Patients With COVID-19. *Front Endocrinol (Lausanne)* 2021; 12: 1–8.
- [38] te Kampe R, Janssen M, van Durme C, et al. Sex differences in the clinical profile among patients with gout: Cross-sectional analyses of an observational study. *J Rheumatol* 2021; 48: 286–92.
- [39] Harrold LR, Yood RA, Mikuls TR, et al. Sex differences in gout epidemiology: Evaluation and treatment. *Ann Rheum Dis* 2006; 65: 1368–72.

- [40] Browne LD, Jaouimaa FZ, Walsh C, et al. Serum uric acid and mortality thresholds among men and women in the Irish health system: A cohort study. *Eur J Intern Med* 2021; 84: 46–55.
- [41] ter Horst R, Jaeger M, Smeekens SP, et al. Host and Environmental Factors Influencing Individual Human Cytokine Responses. *Cell* 2016; 167: 1111–1124.e13.
- [42] ter Horst R, van den Munckhof ICL, Schraa K, et al. Sex-specific regulation of inflammation and metabolic syndrome in obesity. *Arterioscler Thromb Vasc Biol* 2020; 40: 1787–800.
- [43] Patel A V., Gaffo AL. Managing Gout in Women: Current Perspectives. *J Inflamm Res* 2022; 15: 1591–8.
- [44] Hu J, Xu W, Yang H, et al. Uric acid participating in female reproductive disorders: a review. *Reprod Biol Endocrinol* 2021; 19: 1–11.
- [45] Hong X, Zhao F, Wang W, et al. Elevated serum uric acid is associated with infertility in women living in America. *Sci Rep* 2023; 13: 1–8.
- [46] Ma J, Han R, Cui T, et al. Effects of high serum uric acid levels on oxidative stress levels and semen parameters in male infertile patients. *Medicine (Baltimore)*. 2022;101(3):e28442.
- [47] Theofilopoulos AN, Gonzalez-Quintial R, Lawson BR, et al. Sensors of the innate immune system: Their link to rheumatic diseases. *Nat Rev Rheumatol* 2010; 6: 146–56.
- [48] Netea MG, Quintin J, Van Der Meer JWM. Trained immunity: A memory for innate host defense. *Cell Host Microbe* 2011; 9: 355–61.
- [49] Arts RJW, Moorlag SJCFM, Novakovic B, et al. BCG Vaccination Protects against Experimental Viral Infection in Humans through the Induction of Cytokines Associated with Trained Immunity. *Cell Host Microbe* 2018; 23: 89–100.e5.
- [50] Cabău G, Crişan TO, Klück V, et al. Urate-induced immune programming: Consequences for gouty arthritis and hyperuricemia. *Immunol Rev* 2020; 294: 92–105.
- [51] Renaudin F, Orliaguet L, Castelli F, et al. Gout and pseudo-gout-related crystals promote GLUT1-mediated glycolysis that governs NLRP3 and interleukin-1 β activation on macrophages. *Ann Rheum Dis* 2020; 79: 1506–14.
- [52] Chou WC, Rampanelli E, Li X, et al. Impact of intracellular innate immune receptors on immunometabolism. *Cell Mol Immunol* 2022; 19: 337–51.
- [53] Cobo I, Cheng A, Murillo-saich J, et al. Monosodium urate crystals regulate a unique JNK-dependent macrophage metabolic and inflammatory response. *Cell Rep*. 2022;38(10):110489.
- [54] Fanucchi S, Mhlanga MM. Lnc-ing Trained Immunity to Chromatin Architecture. *Front Cell Dev Biol* 2019; 7: 1–7.

APPENDICES

Summary in English

Nederlandse samenvatting

List of publications

Curriculum vitae

Portfolio

Research data management

Acknowledgements

Summary in English

Uric acid is the end product that results from the metabolic breakdown of purines in the liver. In the bloodstream, at physiological pH, uric acid is present in its ionized form as urate. Hyperuricemia arises from elevated concentrations of serum urate and is recognized for its involvement in the onset of gout, but also its contribution to cardiovascular and metabolic diseases. Hyperuricemia can develop from either overproduction or underexcretion and is typically asymptomatic. Humans and higher primates have lost the function of the enzyme uricase which metabolizes urate to allantoin, a water-soluble compound that is easier to excrete. After surpassing the solubility threshold, urate can precipitate and form monosodium urate (MSU) crystals in joints and surrounding tissues. In gout, MSU crystals can lead to acute flares, and if not properly managed, can even accumulate in formations called tophi. The acute flares are initiated by the activation of the NLRP3 inflammasome and subsequent release of interleukin-1 beta (IL-1 β). Gout is one of the oldest described rheumatic diseases and affects approximately 1% of the world's population, reaching up to 2.5-3.9% prevalence in developed countries. Gout is often accompanied by other health issues like cardiovascular, metabolic syndrome, and kidney disease.

High concentrations of urate, whether soluble or crystallized, play an important role in the initiation of pro-inflammatory states. While soluble urate has been acknowledged for its antioxidant properties in the past, more recently, it has been demonstrated that urate exhibits pro-oxidant and proinflammatory characteristics. Recent findings indicate that soluble urate can prime human monocytes *in vitro*, resulting in heightened immune responses when faced with a second challenge. A growing number of studies underline the capacity of the innate immune system to establish immune memory (termed "trained immunity") to protect against infections. This phenomenon could be explained by the epigenetic and metabolic changes that the cells of the innate immune cells experience as they develop and adapt to respond to immunological triggers. However, there is still much to learn about the functions of urate in the serum and how it contributes to inflammatory processes within the body.

This thesis aims to explore if elevated concentrations of soluble urate (hyperuricemia) can induce epigenetic and transcriptional reprogramming within innate immune cells and investigate potential mechanisms underlying the hyperinflammatory state characterized by the shift in cytokine production (increased IL-1 β and reduced interleukin-1 Receptor antagonist, IL-1Ra).

In **Chapter 2**, I investigate the impact of urate exposure on the production of proinflammatory cytokines in human cells at the epigenetic level. As described previously, I confirm that *in vitro* urate-priming of the immune cells results in a shift in cytokine production, characterized by increased production of pro-inflammatory IL-1 β and decreased production of anti-inflammatory IL-1Ra. The current findings show that these effects persist even after removing urate and allowing the cells to rest. Furthermore, these effects can be reversed upon pharmacological inhibition of methylation *in vivo* in mice. I hypothesized that urate priming induces innate immune memory, and we investigated whether urate treatment can trigger epigenetic reprogramming in myeloid cells. Based on previous evidence linking metabolic stimuli to epigenetic changes, DNA methylation status was assessed in 76 New Zealand Māori individuals with varying levels of serum urate. In addition, two histone mark candidates were explored through ChIP-sequencing (H3K4me3 and H3K27ac) in urate-primed monocytes. These findings suggest that both mechanisms of epigenetic regulation may be associated with urate exposure, providing potential new targets for further investigation into gout and urate-induced inflammation.

In **Chapter 3**, I further investigate the mechanisms associated with urate-induced inflammation *in vitro*, employing an immunological, transcriptomic, and epigenetic approach to investigate the role of the suppressor of cytokine signalling 3 (SOCS3) in urate-induced inflammation, using both healthy donors and patients. It has previously been shown *in vitro* that urate priming facilitates IL-1 β production in peripheral blood mononuclear cells (PBMCs) and that a mechanism for the amplification of IL-1 β consists in the downregulation of IL-1 receptor antagonist (IL-1Ra). In the present study, I extend these findings to individuals with hyperuricemia and patients with gout. I further show that *in vitro* urate priming would result in higher levels of SOCS3 due to the suppression of phosphorylated STAT3, accompanied by a reduction in IL-1Ra cytokine production. The observed shift in elevated SOCS3 and reduced pSTAT3 could play a role in urate-induced hyperinflammation since urate priming had no effect on PBMCs from patients with constitutively activated STAT3.

In **Chapter 4**, I assess the modulation of the type 1 interferon pathway by urate priming in human myeloid cells. To this end, I analyse the type I interferon-related genes in the transcriptome of human primary cells in response to soluble urate *in vitro* and in correlation to serum urate levels in patients. The results indicate that urate priming downregulates genes in the type 1

interferon-related pathways in both human monocytes and PBMCs. However, stimulation of PBMCs with IFN- β does not rescue the pro-inflammatory effects of urate. Interestingly, an inverse correlation was observed between serum urate levels and stimulations both in vivo and in vitro. These findings suggest that downregulation of IFN1 is most likely not the driving mechanism behind urate priming, but nevertheless, these results support a deficient IFN1 signalling, which could potentially lead to an increased vulnerability to viral infections in patients with hyperuricemia.

In **Chapter 5**, I investigate the distinct pro-inflammatory response of stimulated PBMCs of patients with gout, focusing on differences between sexes. Gout, an inflammatory disease, is primarily driven by innate immune processes that involve the activation and release of IL-1 β . Epidemiological research has shown sex-based differences in gout manifestations. Here, I show that patients with gout have increased cytokine production compared to controls. Particularly, men with gout have higher circulating cytokine levels, whereas women with gout exhibit a greater capacity for cytokine production in vitro compared to controls.

In **Chapter 6**, I delve into recent literature to examine the role of innate immune memory in gout and hyperuricemia and its potential implications for other rheumatic diseases. These diseases, characterized by musculoskeletal and systemic symptoms, cover various autoimmune and autoinflammatory conditions. The complex inflammatory mechanisms underlying these debilitating disorders result from interactions between the innate and adaptive immune systems. Furthermore, the cells of the innate immune system can develop a type of immunological memory through epigenetic reprogramming and metabolic changes, termed also "trained immunity". In this chapter, I explore how trained immunity manifests in gout and other rheumatic diseases, and I discuss its potential mechanistic role in the pathogenesis of these diseases.

While the role of crystalized uric acid in gout is well established, the soluble form remains a focus of ongoing research, particularly due to its association to many comorbidities like cardiovascular and metabolic diseases. The findings in the present thesis highlight the pro-inflammatory effect of soluble urate, emphasizing its importance beyond just gout.

Nederlandse samenvatting

Urinezuur is het eindproduct dat ontstaat uit de metabole afbraak van purines in de lever. In de bloedbaan is urinezuur bij fysiologische pH aanwezig in zijn geïoniseerde vorm: uraat. Hyperurikemie ontstaat door verhoogde concentraties serum uraat en staat bekend om zijn betrokkenheid bij het ontstaan van jicht, maar ook om zijn bijdrage aan cardiovasculaire en metabole ziekten. Hyperurikemie kan zich ontwikkelen door overproductie of verminderde uitscheiding en is meestal asymptomatisch. Mensen en hogere primaten hebben de functie verloren van het enzym uricase, dat uraat metaboliseert tot allantoïne, een wateroplosbare verbinding die gemakkelijker uit te scheiden is. Na het overschrijden van de oplosbaarheidsdrempel kan uraat neerslaan en monosodiumuraat (MSU) kristallen vormen in gewrichten en omliggende weefsels. Bij jicht kunnen MSU-kristallen leiden tot acute aanvallen van gewrichtsontstekingen, en als ze niet goed worden beheerd, kunnen ze zich zelfs ophopen in formaties die tophi worden genoemd. De acute aanvallen worden geïnitieerd door de activatie van het NLRP3-inflammasoom en de daaropvolgende afgifte van interleukine-1 bèta (IL-1β). Jicht is een van de oudst beschreven reumatische aandoeningen en treft ongeveer 1% van de wereldbevolking, oplopend tot 2,5-3,9% prevalentie in ontwikkelde landen. Jicht gaat vaak gepaard met andere gezondheidsproblemen zoals cardiovasculaire aandoeningen, metabool syndroom en nierziekten.

Hoge concentraties uraat, of het nu oplosbaar of gekristalliseerd is, spelen een belangrijke rol bij het initiëren van inflammatie. Hoewel oplosbaar uraat in het verleden als antioxidant werd gezien, is recentelijk aangetoond dat uraat pro-oxidante en pro-inflammatoire kenmerken vertoont. Recente bevindingen wijzen erop dat oplosbaar uraat menselijke monocytten in vitro kan primen, wat resulteert in verhoogde immuunresponsen bij een tweede stimulatie. Een groeiend aantal studies benadrukt het vermogen van het aangeboren immuunsysteem om een immuungeheugen op te bouwen (genoemd "getrainde immuniteit") ter bescherming tegen infecties. Dit fenomeen kan worden verklaard door de epigenetische en metabole veranderingen die de cellen van het aangeboren immuunsysteem ondergaan terwijl ze zich ontwikkelen en aanpassen om te reageren op immunologische prikkels. Er is echter nog veel te leren over de functies van oplosbaar uraat en hoe het bijdraagt aan inflammatoire processen binnen het lichaam.

Deze scriptie heeft als doel te onderzoeken of verhoogde concentraties van oplosbaar uraat (hyperurikemie) epigenetische en transcriptionele herprogrammering binnen aangeboren immuuncellen kunnen induceren en mogelijke mechanismen te onderzoeken die ten grondslag liggen aan de hyperinflammatoire toestand, gekenmerkt door de verschuiving in cytokineproductie (verhoogde IL-1 β en verminderde IL-1Ra).

In **Hoofdstuk 2** onderzoek ik de impact van uraatsblootstelling op de productie van pro-inflammatoire cytokinen in menselijke cellen op epigenetisch niveau. Zoals eerder beschreven, bevestig ik dat in vitro uraat-priming van immuuncellen resulteert in een verschuiving in cytokineproductie, gekenmerkt door verhoogde productie van pro-inflammatoire IL-1 β en verminderde productie van anti-inflammatoire IL-1Ra. De huidige bevindingen tonen aan dat deze effecten blijven bestaan, zelfs na het verwijderen van uraat en het laten rusten van de cellen. Bovendien kunnen deze effecten worden omgekeerd door farmacologische remming van methylatie in vivo bij muizen. Ik stelde de hypothese dat uraat-priming het aangeboren immuungeheugen induceert, en we onderzochten of uraatbehandeling epigenetische herprogrammering in myeloïde cellen kan veroorzaken. Op basis van eerder bewijs dat metabolische stimuli koppelt aan epigenetische veranderingen, werd de DNA-methyleringsstatus beoordeeld bij 76 Nieuw-Zeelandse Māori-individueen met verschillende niveaus van serum uraat. Daarnaast werden twee histonmerken onderzocht via ChIP-sequencing (H3K4me3 en H3K27ac) in met uraat-geprimeerde monoccyten. Deze bevindingen suggereren dat beide mechanismen van epigenetische regulatie geassocieerd kunnen zijn met uraatsblootstelling, wat nieuwe potentiële doelen biedt voor verder onderzoek naar jicht en door uraat-geïnduceerde ontsteking.

In **Hoofdstuk 3** onderzoek ik verder de mechanismen die geassocieerd zijn met door uraat-geïnduceerde ontsteking in vitro. Hierbij maak ik gebruik van een immunologische, transcriptomische en epigenetische benadering om de rol van de suppressor van cytokinesignalering 3 (SOCS3) in door uraat-geïnduceerde ontsteking te bestuderen, met behulp van zowel gezonde donoren als patiënten. Eerder is in vitro aangetoond dat uraat-priming de productie van IL-1 β in perifere mononucleaire bloedcellen (PBMCs) bevordert en dat een mechanisme voor de amplificatie van IL-1 β bestaat uit de downregulatie van de IL-1-receptorantagonist (IL-1Ra). In de huidige studie breid ik deze bevindingen uit naar individuen met hyperurikemie en patiënten met jicht. Verder toon ik aan dat in vitro uraat-priming leidt tot hogere niveaus

van SOCS3 door de onderdrukking van gefosforyleerd STAT3, vergezeld van een vermindering in de productie van IL-1Ra. De waargenomen verschuiving met verhoogd SOCS3 en verminderd pSTAT3 zou een rol kunnen spelen in door uraat-geïnduceerde hyperinflammatie, aangezien uraat-priming geen effect had op PBMCs van patiënten met continu geactiveerd STAT3.

In **Hoofdstuk 4** beoordeel ik de modulatie van type 1 interferonen door uraat-priming in menselijke myeloïde cellen. Hiertoe analyseer ik de type I interferon-gerelateerde genen in het transcriptoom van menselijke primaire cellen als reactie op oplosbaar uraat in vitro en in correlatie met serum uraatconcentraties bij patiënten. De resultaten geven aan dat uraat-priming expressie van genen in de type 1 interferon-gerelateerde signaalwegen vermindert in zowel menselijke monocyten als PBMCs. Echter, stimulatie van PBMCs met IFN- β herstelt niet de pro-inflammatoire effecten van uraat. Interessant genoeg werd een inverse correlatie waargenomen tussen serum uraatconcentraties en stimulaties zowel in vivo als in vitro. Deze bevindingen suggereren dat downregulatie van IFN1 hoogstwaarschijnlijk niet het drijvende mechanisme is achter uraat-priming, maar desalniettemin ondersteunen deze resultaten een deficiënte IFN1-signaaloverdracht, wat mogelijk kan leiden tot een verhoogde kwetsbaarheid voor virale infecties bij patiënten met hyperurikemie.

In **Hoofdstuk 5** onderzoek ik de pro-inflammatoire respons van gestimuleerde PBMCs van patiënten met jicht, met de nadruk op verschillen tussen de seksen. Jicht, een inflammatoire ziekte, wordt primair gedreven door aangeboren immuunprocessen die de activatie en afgifte van IL-1 β omvatten. Epidemiologisch onderzoek heeft geslachtsgebonden verschillen in de manifestaties van jicht aangetoond. Hier toon ik aan dat patiënten met jicht een verhoogde cytokineproductie hebben vergeleken met controles. Met name hebben mannen met jicht hogere circulerende cytokineniveaus, terwijl vrouwen met jicht in vitro een grotere capaciteit voor cytokineproductie vertonen in vergelijking met controles.

In **Hoofdstuk 6** duik ik in recente literatuur om de rol van aangeboren immuungeheugen bij jicht en hyperurikemie te onderzoeken en de mogelijke implicaties ervan voor andere reumatische aandoeningen. Deze ziekten, gekenmerkt door musculoskeletale en systemische symptomen, omvatten verschillende auto-immun- en autoinflammatoire aandoeningen. De complexe inflammatoire mechanismen die ten grondslag liggen aan deze

slopende aandoeningen, zijn het resultaat van interacties tussen het aangeboren en adaptieve immuunsysteem. Bovendien kunnen de cellen van het aangeboren immuunsysteem een soort immunologisch geheugen ontwikkelen door epigenetische herprogrammering en metabole veranderingen, ook wel "getrainde immuniteit" genoemd. In dit hoofdstuk onderzoek ik hoe getrainde immuniteit zich manifesteert bij jicht en andere reumatische ziekten, en bespreek ik de potentiële mechanistische rol ervan in de pathogenese van deze ziekten.

Hoewel de rol van gekristalliseerd urinezuur bij jicht goed is vastgesteld, blijft de oplosbare vorm een focus van lopend onderzoek, vooral vanwege de associatie met veel comorbiditeiten zoals cardiovasculaire en metabole ziekten. De bevindingen in deze scriptie benadrukken het pro-inflammatoire effect van oplosbaar uraat, wat de relevantie ervan ook los van jicht onderstreept.

List of publications

Gaal OI, Leask M, Nica V, Cabău G, **Badii M**, Hotea I, de Graaf DM, Zhang Z, Li Y, Pamfil C, Rednic S, Merriman TR, Crişan TO, Joosten LAB. Gout-associated SNP at the IL1RN-IL1F10 region is associated with altered cytokine production in PBMCs of patients with gout and controls. *Arthritis Res Ther*. 2024;26(1):205. <https://doi.org/10.1186/s13075-024-03436-0>

Badii M, Nica V, Straton AR, Kischkel B, Gaal O, Cabău G, Klück V, Hotea I; HINT Consortium; Novakovic B, Pamfil C, Rednic S, Netea MG, Popp RA, Joosten LAB, Crişan TO. Downregulation of type I interferon signalling pathway by urate in primary human PBMCs. *Immunology*. 2024 Oct 1. Epub ahead of print. doi: 10.1111/imm.13858

Cabău, G., **Badii, M.**, Mirea, A. M., Gaal, O. I., van Emst, L., Popp, R. A., Crişan, T. O., & Joosten, L. A. B. (2024). Long-Lasting Enhanced Cytokine Responses Following SARS-CoV-2 BNT162b2 mRNA Vaccination. *Vaccines*, 12(7), 736. <https://doi.org/10.3390/vaccines12070736>

Badii M, Gaal OI, Hotea I, Nica V, Mirea AM, Mărginean D, HINT Consortium, Pamfil C, Rednic S, Popp RA, Crişan, T. O., & Joosten, L. A. B. Sex-Specific Differences in Cytokine Production Capacity in Patients with Gout Compared to Controls. *Gout, Urate, and Crystal Deposition Disease*. 2024; 2(2):133-143. <https://doi.org/10.3390/gucdd2020012>

Röring RJ, Li W, Liu R, Bruno M, Zhang B, Debisarun PA, Gaal O, **Badii M**, Klück V, Moorlag SJCFM, van de Veerdonk F, Li Y, Joosten LAB, Netea MG. Epigenetic, transcriptional, and functional characterization of myeloid cells in familial Mediterranean fever. *iScience*. 2024 Feb 29;27(4):109356. <https://doi.org/10.1016/j.isci.2024.109356>

Badii, M., Klück, V., Gaal, O., Cabău, G., Hotea, I., Nica, V., Mirea, A. M., Bojan, A., Zdrengea, M., HINT Consortium, Novakovic, B., Merriman, T. R., Liu, Z., Li, Y., Xu, C. J., Pamfil, C., Rednic, S., Popp, R. A., Crişan, T. O., & Joosten, L. A. B. (2024). Regulation of SOCS3-STAT3 in urate-induced cytokine production in human myeloid cells. *Joint bone spine*, 91(3), 105698. Advance online publication. <https://doi.org/10.1016/j.jbspin.2024.105698>

Gaal, O. I., Liu, R., Marginean, D., **Badii, M.**, Cabău, G., Hotea, I., Nica, V., Colcear, D., HINT Consortium, Pamfil, C., Merriman, T. R., Rednic, S., Popp, R. A., Crişan, T. O., & Joosten, L. A. B. (2024). GWAS-identified hyperuricemia-associated IGF1R variant rs6598541 has a limited role in urate mediated inflammation in human mononuclear cells. *Scientific reports*, 14(1), 3565. <https://doi.org/10.1038/s41598-024-53209-7>

Cabău, G., Gaal, O., **Badii, M.**, Nica, V., Mirea, A. M., Hotea, I., HINT-consortium, Pamfil, C., Popp, R. A., Netea, M. G., Rednic, S., Crișan, T. O., & Joosten, L. A. B. (2023). Hyperuricemia remodels the serum proteome toward a higher inflammatory state. *iScience*, 26(10), 107909. <https://doi.org/10.1016/j.isci.2023.107909>

Szabo, I., **Badii, M.**, Gaál, I. O., Szabo, R., Sîrbe, C., Humiță, O., Joosten, L. A. B., Crișan, T. O., & Rednic, S. (2023). Immune Profiling of Patients with Systemic Sclerosis through Targeted Proteomic Analysis. *International journal of molecular sciences*, 24(24), 17601. <https://doi.org/10.3390/ijms242417601>

Szabo, I., **Badii, M.**, Gaál, I. O., Szabo, R., Popp, R. A., Joosten, L. A. B., Crișan, T. O., & Rednic, S. (2023). Enhanced Innate and Acquired Immune Responses in Systemic Sclerosis Primary Peripheral Blood Mononuclear Cells (PBMCs). *International journal of molecular sciences*, 24(19), 14438. <https://doi.org/10.3390/ijms241914438>

Sîrbe, C., **Badii, M.**, Crișan, T. O., Bența, G., Grama, A., Joosten, L. A. B., Rednic, S., & Pop, T. L. (2023). Detection of Novel Biomarkers in Pediatric Autoimmune Hepatitis by Proteomic Profiling. *International journal of molecular sciences*, 24(8), 7479. <https://doi.org/10.3390/ijms24087479>

Badii, M., Gaal, O., Popp, R. A., Crișan, T. O., & Joosten, L. A. B. (2022). Trained immunity and inflammation in rheumatic diseases. *Joint bone spine*, 89(4), 105364. <https://doi.org/10.1016/j.jbspin.2022.105364>

Badii, M., Gaal, O. I., Cleophas, M. C., Klück, V., Davar, R., Habibi, E., Keating, S. T., Novakovic, B., Helsen, M. M., Dalbeth, N., Stamp, L. K., Macartney-Coxson, D., Phipps-Green, A. J., Stunnenberg, H. G., Dinarello, C. A., Merriman, T. R., Netea, M. G., Crișan, T. O., & Joosten, L. A. B. (2021). Urate-induced epigenetic modifications in myeloid cells. *Arthritis research & therapy*, 23(1), 202. <https://doi.org/10.1186/s13075-021-02580-1>

Mohseni, S., **Badii, M.**, Kylhammar, A., Thomsen, N. O. B., Eriksson, K. F., Malik, R. A., Rosén, I., & Dahlin, L. B. (2017). Longitudinal study of neuropathy, microangiopathy, and autophagy in sural nerve: Implications for diabetic neuropathy. *Brain and behavior*, 7(8), e00763. <https://doi.org/10.1002/brb3.763>

Curriculum Vitae



Medeea Badii was born on the 2nd of July 1990 in Botoșani, Romania. She completed her high school education at "A.T. Laurian" in Botoșani with the main subjects Mathematics – Informatics – Advanced English. In 2009, she began her undergraduate studies in Biology at the "Al. I. Cuza" University in Iași, followed by a master's in Molecular Genetics at the same institution, graduating in 2016. During 2015, she participated in the "LLP Erasmus

Placement Mobility" and conducted research on diabetic neuropathy under the supervision of Prof. Dr. Simin Mohseni at Linköping University, Sweden. In 2017, she joined the doctoral program at the "Iuliu Hatieganu" University of Medicine and Pharmacy in Cluj-Napoca, starting her PhD project under the supervision of Prof. Dr. Leo A.B. Joosten. In 2019, she began a joint PhD at the Department of Internal Medicine, Radboud UMC, supervised by Prof. Dr. Leo A.B. Joosten and Prof. Dr. Mihai G. Netea, where she also received training. During her PhD, she had the opportunity to attend and present at numerous international conferences. She published several articles on gout, as well as on other rheumatic disorders. In June 2024 she successfully defended her thesis at the UMF Cluj-Napoca. She is currently working as a postdoctoral researcher in the same group, where she focuses on gout and hyperuricemia, but also on systemic sclerosis and systemic lupus erythematosus.

Portfolio

PhD portfolio of Oana-Medeea Badii

Department: Internal Medicine
PhD period: 29/10/2019 – 31/12/2024
PhD Supervisor(s): Prof. Dr. L.A.B. Joosten, Prof. Dr. M.G. Netea
PhD Co-supervisor(s): Dr. T.O. Crişan

Training activities	Hours
Courses	2.00
• Radboudumc - Scientific integrity (2024)	40.00
• Scientific research methodology (2018)	10.00
• Notions of scientific research ethics (2018)	8.00
• European legislation in research (2018)	8.00
• Publication norms and ethics of scientific publication (2018)	16.00
• Scientific documentation (2018)	16.00
• Design and management of grants (2018)	2.00
• Poster communication - rules, solutions, tricks (2018)	4.00
• Evidence-based medicine (2018)	4.00
• Oral presentation and ppt (2018)	20.00
• Medical biotechnologies (2018)	10.00
• Handling of laboratory animals used in biomedical research (2018)	4.00
• Theoretical bases of the in vitro and in vivo experiments - cell cultures and isolated organ (2018)	4.00
• Cell cultures in experimental medicine (2018)	
Seminars	150.00
• Weekly cytokine meetings (2019-2024)	
Conferences	16.00
• European Crystal Network Workshop (2019) #	16.00
• 4th Conference on Innate Immune Memory (2019) #	8.00
• G-CAN Fifth Annual Meeting (2019) #	40.00
• ACR/ARP Annual Meeting (2019)	16.00
• European Crystal Network Workshop (2020) *	8.00
• European Crystal Network Workshop (2022) *	16.00
• Summer Conference on Innate Immune Memory (2022) *	16.00
• G-CAN Annual Meeting (2022) *	16.00
• European Crystal Network Workshop (2023) #	16.00
• G-CAN Annual Meeting (2023) *	16.00
• European Crystal Network Workshop (2024)	16.00
• G-CAN 10th Annual Meeting (2024)	
Other	10.00
• A crash course in de novo genome sequencing, assembly and downstream analyses (2023)	16.00
• Hands-on Pathogen Genomics course (2023)	
Total	524.00

Oral presentations are marked with an asterisk (*) and poster presentations are marked with a hashtag (#) following the activity name.

Research data management

Ethics and privacy

All experiments were conducted according to the principles of the Declaration of Helsinki. Informed consent was obtained from all research participants. Measures such as independent monitoring, participant anonymization (individual codes), access authorization (only within the project), and secure data storage, were implemented to ensure the data's availability, integrity, and confidentiality.

Stimulation experiments in chapter 2 were approved by the Ethical Committee of Radboud University Nijmegen (nr. 42561.091.12).

The DNA methylation study in chapter 2 was approved by the New Zealand Lower South Health and Disability Ethics Committee (MEC/05/10/130).

The animal study in chapter 2 was approved by The Institutional Animal Care and Use Committees of the University of Colorado Denver, Aurora, CO (protocol #0035).

The studies in chapters 3, 4 and 5 use data generated by the HINT Project (Hyperuricemia-induced Inflammation: Targeting the central role of uric acid in rheumatic and cardiovascular diseases, ID P 37 762; MySMIS 103587) supported by a Competitiveness Operational Program Grant of the Romanian Ministry of European Funds and implemented in Cluj-Napoca, Romania, at the "Iuliu Hațieganu" University of Medicine and Pharmacy. The medical ethical review committee of Iuliu Hațieganu University of Medicine and Pharmacy has given approval to conduct these studies (approval no. 425/2016).

Data collection and storage

Data from experimental setups performed in chapter 2 involves Dutch participants part of the 200 Functional Genomics (200FG) cohort in the Human Functional Genomics Project (<http://www.humanfunctionalgenomics.org>).

The data in chapters 3, 4 and 5 involves Romanian patients and cannot be stored outside Romania. The raw data from omics analyses is actively being used for ongoing publications by doctoral students. All data is securely stored locally on hard drives and computers within the Medical Genetics Department at the "Iuliu Hațieganu" University of Medicine and Pharmacy in Cluj-Napoca.

Additionally, paper-based records, such as lab journals, are securely kept in cabinets within the department.

The data for chapter 2, 3, 4 and 5 was generated through laboratory experiments using anonymized human and non-human material. Patient information was collected from both paper-based and electronic health records.

Data sharing

All studies are published as open access, with supplementary files available on the respective journal websites.

Data supporting this thesis can be provided upon request by contacting the following correspondence:

Tania Crisan: tania.crisan@radboudumc.nl;

Leo Joosten: leo.joosten@radboudumc.nl

Acknowledgements

I am deeply grateful for the chance I have had as a doctoral student to work under the guidance of exceptional supervisors and mentors. This thesis is not just a culmination of my own efforts but reflects the collective contributions and support of many people across various countries and continents, from whom I learned immensely.

I extend my heartfelt gratitude to my promoters, **Prof. Dr. Leo Joosten** and **Prof. Dr. Mihai Netea**.

Dear **Prof. Dr. Leo Joosten**, dear **Leo**, thank you for the opportunity to work in an inspiring scientific environment. Your unwavering support has been a cornerstone throughout these years. Thank you for sharing your scientific knowledge with me, sparking my curiosity, and teaching me how to approach complex topics with confidence. Your kindness, empathy, and humor have enriched this experience significantly. You have always led by example and gave me space to think, and this is something I aspire to follow. Your support has been particularly invaluable during challenging times when experiments did not work out as anticipated. I would always leave our meetings feeling optimistic and motivated, ready to learn from my results and use those insights to shape new ideas and directions.

Dear **Prof. Dr. Mihai Netea**, dear **Mihai**, I am immensely thankful for your mentorship; your approach to critical thinking and your ability to simplify complex questions have taught me so much. Thank you for your rigorous reviews of my manuscripts and for your thoughtful suggestions!

Dear **Prof. Dr. Cheng**, Prof. Dr. **Yang Li** and **Zhaoli**, thank you for the help with the in vitro DNA methylation and transcriptomics data analysis and I look forward to continuing our collaboration.

Dear Prof. **Dr. Tony Merriman** and **Boris Novakovic**, thank you for the help with DNA methylation study in patients, transcriptomics and gout. I appreciate you taking the time to review my manuscripts carefully and provide thoughtful feedback.

Dear **Tania**, your mentorship throughout this thesis has been truly invaluable, and I cannot thank you enough for your support in all my daily endeavours,

from our lab work to manuscript preparation. You have had a big impact on my writing, helping me become more organized and disciplined, and, in a way, you have also helped me find joy in it. From you, I learned the incredible value of a well-structured protocol and a thorough calculation sheet – tools that truly save half the work! When it came to paper rebuttals, you showed me how to navigate differing opinions, embrace rejections with a light heart, and keep pursuing what I enjoy doing. Your enthusiasm and dedication are truly contagious, and I hope to carry a spark of that same spirit with me as I move forward.

I want to extend my humble thanks to everyone involved in the HINT Consortium. Dear **Prof. Dr. Rednic, Cristina Pamfil** and **Ioana Hotea**, thank you for your valuable contributions and dedication in the clinic. **Ioana**, your organizing skills with the patient databases have set a standard I continually strive to maintain. I thank **Radu** for his support in the management of the lab and appreciate our philosophical conversations.

I express my huge appreciation to **Orsi** and **Georgiana**, with whom I share many nice memories in the lab, especially those big ELISA sessions. Whenever we travelled to conferences, thanks for letting me drag you around cities in the name of chasing that must-try dish or scoping out that hyped restaurant. A big thank you to **Valentin** and **Dragos** for their support with data analysis. **Dear Anca** and **Maria**, I appreciate our time in the lab and look forward to making more memories – and papers! Thank you for the many FG-experiments, lunches and coffees we shared. Trips to conferences and karaoke nights are some of my most treasured memories with the team! Dear **Iulia** and **Claudia**, thank you for the nice collaboration on the systemic sclerosis and systemic lupus erythematosus projects!

I thank everyone at **AIG lab** for making me feel welcome during my time there.

Dear **Viola**, I will always remember our first big ELISA together – it marked the beginning of many more that followed! Dear **Ruiqi**, thank you for the bike rides and showing me great places to eat. Dear **Brenda**, thank you for the important support with the STAT1 experiments! Dear **Jessica**, thank you for your friendship and for being such a kind soul and warm presence to be around, I always had so many laughs with you! Dear **Liesbeth**, thank you for your help with learning the CHIP protocol, I appreciate your clear explanations and calm demeanour. Dear **Helga**, thank you for your help with the puzzling

Luminex machine. Dear **Heidi** and **Trees**, thank you for your guidance in the lab and for your practical advice, which have been incredibly helpful. Dear **Gizem** and **Priya**, and dear **Ozlem**, thank you for being such wonderful office mates. I cherish the time we spent together. Dear **Colins**, thank you for your help with explaining R and statistics. To everyone, I appreciate the time spent together during lunches or Friday drinks in the afternoon at SQL, and, of course, at conferences from Nijmegen to Cluj.

Many thanks to all co-authors and collaborators in publishing the articles that are part of this thesis. I am also grateful I had the opportunity to present my work at ECN Paris and G-CAN across USA.

Dear **Prof. Dr. Simin Mohseni**, dear **Simin**, the months I spent under your guidance at Linköping University have truly shaped the way I approach academic work and research. Your kindness and cheerful energy always made me look forward to Mondays. Thank you for everything you taught me during that time—it's where I truly understood how much consistency and curiosity can pay off. Thank you for taking the time to show me the beautiful town of Vadstena and introduce me to canyoning for the first time on Sweden's stunning lakes!

My profound gratitude goes to my parents and grandparents for their support and trust in my decisions; to my friends for their never-ending encouragements. Dragă Buni, vreau să-ți mulțumesc din suflet pentru tot suportul și încurajările tale necondiționate pe parcursul acestor ani. Ești o sursă de inspirație și putere pentru mine.

Dear **George**, you have been incredibly supportive since day one. Thank you for believing in me, especially during times when I struggled to believe in myself, and for being the mirror that reflects the best in me.

I have come to understand that earning a PhD is a transformative journey that goes beyond the scientific contributions. I am thankful to everyone for their contributions to my growth, both as a scientist and as a person.

I gratefully acknowledge RadboudUMC for providing the financial support in printing this thesis.



9 789465 150543 >